Lista de lucrari

1. A new boson approach for the wobbling motion in even-odd nuclei, A. A. Raduta, C. M. Raduta and R. Poenaru, Jour. Phys. G:Nucl. Part. Phys. 48(2021)015106

2. New results about the canonical transformation for boson operators, C.M. Raduta and A. A. Raduta, Int. Jour. Mod. Phys. E, vol. 30, No3, 2150019 (2021)

3. Parity Partner Bands in ^{163}Lu: A novel approach for describing the negative parity states from a triaxial super-deformed band, R. Poenaru and A. A. Raduta, Int. Jour. Mod. Phys. E, vol 30,No 5 (2021)2150033.

4. Extensive Study of the Positive and Negative Parity Wobbling States for an Odd-Mass Triaxial Nucleus I: Energy Spectrum, R. Poenaru, A. A. Raduta, Romanian Journal of Physics 66, 308 (2021)

5. Extensive Study of the Positive and Negative Parity Wobbling States for an Odd-Mass Triaxial Nucleus II: Classical Trajectories, R. Poenaru, A. A. Raduta, Romanian Journal of Physics 66, 309 (2021)

6. Simultaneous description of wobbling and chiral properties in even-odd triaxial nuclei, C. M. Raduta , A. A. Raduta, R. Poenaru and Al.H. Raduta, submitted to Jour.Phys. G: Nucl. Part. Phys., 49 (2022) 2, 05105.

7. Double-β transition $0^+ \to 2^+$ within a fully renormalized proton-neutron quasiparticle random-phase approximation with the gauge symmetry restored, Phys. Rev C 106 044301 (2022).

8. Microscopic description of the Pygmy and Giant Dipole Resonances in even-even nuclei. Application to the isotopes ^{150,152,154,156,158,160}Gd, A. A. Raduta, C. M. Raduta and R. Poenaru, trimisa spre publicare la Physical Review C.

9. Toward a new approach for the Pygmy Dipole Resonance in even-even nuclei. Application to the isotopes ^{144,148,150,152,154}Sm, A. A. Raduta, C. M. Raduta and Al. H. Raduta, trimisa spre publicare la Journal of Physics G: Nuclear and Particle Physics.

A new boson approach for the wobbling motion in even-odd nuclei

A. A. Raduta[a),b)], C. M. Raduta [a)] and R. Poenaru [a),c)]
[a)] *Department of Theoretical Physics, Institute of Physics and Nuclear Engineering, Bucharest, POBox MG6, Romania*
[b)] *Academy of Romanian Scientists, 54 Splaiul Independentei, Bucharest 050094, Romania and*
[c)] *Doctoral School of Physics, Bucharest University,*
405 Atomistilor Str., Bucharest-Magurele, Romania

A triaxial core rotating around the middle axis, i.e. 2-axis, is cranked around the 1-axis, due to the coupling of an odd proton from a high j orbital. Using the Bargmann representation of a new and complex boson expansion of the angular momentum components, the eigenvalue equation of the model Hamiltonian acquires a Schrödinger form with a fully separated kinetic energy. From a critical angular momentum, the potential energy term exhibits three minima, two of them being degenerate. Spectra of the deepest wells reflects a chiral-like structure. Energies corresponding to the deepest and local minima respectively, are analytically expressed within a harmonic approximation. Based on a classical analysis, a phase diagram is constructed. It is also shown that the transverse wobbling mode is unstable. The wobbling frequencies corresponding to the deepest minimum are used to quantitatively describe the wobbling properties in ^{135}Pr. Both energies and e.m. transition probabilities are described.

I. INTRODUCTION

The wobbling motion consists in a precession of the total angular momentum of a triaxial system combined with an oscillation of its projection on the quantization axis around a steady position. Bohr and Mottelson described the wobbling motion within a triaxial rotor model for high spin states, where the total angular momentum almost aligns to the principal axis with the largest moment of inertia [1]. This pioneering paper was followed by a fully microscopic description due to Marshalek [2]. Since then, a large volume of experimental and theoretical results has been accumulated [3–28]. Also, the concept of wobbling motion has been extended to even-odd nuclei. Experimentally, the excited wobbling states are known in several even-odd triaxial nuclei like ^{161,163,165,167}Lu [4, 6, 7, 13, 17, 18], ^{167}Ta [19], ^{135}Pr [29–35], ^{187}Au [36], ^{133}La[37], ^{105}Pd [38] and ^{133}Ba [39].

With the time several formalisms were attempted to describe the wobbling motion in nuclei. Thus, the classical interpretation of Bohr and Mottelson was widely used by various authors in the context of interpreting the new data that meanwhile appeared [5, 9, 31, 40, 41]. The oldest and simplest boson description of the wobbling phenomenon belongs to Bohr and Mottelson [1]. More elaborate interpretations are those of Refs. [14, 15, 24], where Holstein-Primakoff [42] and Dyson [43] boson expansions were used, respectively. The semi-classical studies [16, 25–28, 33] proved to be an efficient and flexible tool for a realistic view of this phenomenon in even-odd nuclei.

The wobbling states are actually fingerprints of the triaxial structure of the nuclei, which justifies the attractive appeal of the subject. The first paper devoted to triaxial nuclei was that of Davydov and Fillipov [46]. The γ deformation of the atomic nuclei has been treated by many authors [47–51]. In Ref.[52], Davydov introduced, for the first time in the literature, a Hamiltonian appropriate for an even-odd nucleus consisting in a core and an odd particle moving in a potential coupling it to the collective core. This Hamiltonian is nowadays widely used by theoreticians. The first results reported for even-odd nuclei within a quasiparticle plus triaxial rotor framework, for the rare earth region, were given in Refs. [53–57].

The wobbling motion has a longitudinal/transverse character depending on whether the relative position of the odd-particle and the core axis with the largest MoI are parallel/perpendicular [31]. Although the concept of transverse wobbling is being used by many authors, a certain debate on whether such a wobbling motion exists or not is still standing [28, 30, 32, 41].

In the present paper we propose a new formalism based on a boson expansion of the angular momentum components. A particular case of the new expansion is a generalization of the Dyson boson representation. By using the Bargmann representation [44], the eigenvalue equation for the model Hamiltonian is brought to a Schrödinger form which, in the harmonic approximation, leads to an explicit expression for the wobbling frequency. Also, a semi-classical description is provided, which is fully consistent with the quantal treatment. Within this picture, it is proved that the transversal mode is unstable despite the fact that we assumed that the middle axis is of maximal MoI. The formalism is applied, with a positive result, to ^{135}Pr.

The project sketched above is accomplished according to the following plan. Using a new boson expansion for the angular momentum, in section II the Schrödinger equation for the model Hamiltonian is derived, while in section III, another boson expansion is obtained. The harmonic approximation is delivered in Section IV, while the classical approach is presented in Section V. In Section VI we give the analytical formulas for the electromagnetic transition probabilities. Numerical results and discussions are presented in Section VII, while the summary and the final conclusions are described in section VIII.

II. A COMPACT FORMULA FOR THE POTENTIAL ENERGY OF A PARTICLE-TRIAXIAL ROTOR HAMILTONIAN

Assuming a rigid coupling of an odd nucleon to a triaxial core, the Hamiltonian for the even-odd system may be approximated as:

$$\hat{H}_{rot} = \sum_{k=1,2,3} A_k (\hat{I}_k - \hat{j}_k)^2, \tag{2.1}$$

with $A_k = \frac{1}{2\mathcal{J}_k}$ and I standing for the total angular momentum.

For a rigid coupling of the odd proton to the triaxial core, we suppose that **j** stays in the principal plane (1,2). Also, we consider that the maximal moment of inertia (MoI) is $\mathcal{J}_2$; furthermore, we expand the linear term in I_2 as the first order of approximation:

$$\hat{I}_2 = I\left(1 - \frac{1}{2}\frac{\hat{I}_1^2 + \hat{I}_3^2}{I^2}\right). \tag{2.2}$$

Thus, the Hamiltonian acquires the form:

$$\hat{H}_{rot} = A\hat{H}' + (A_1 I^2 - A_2 j_2 I) + \sum_{k=1,2} A_k \hat{j}_k^2, \tag{2.3}$$

where the following notations have been used:

$$\begin{aligned} A &= A_2(1 - \frac{j_2}{I}) - A_1, \\ \hat{H}' &= \hat{I}_2^2 + u\hat{I}_3^2 + 2v_0\hat{I}_1, \ \text{with} \\ u &= \frac{A_3 - A_1}{A}, \ v_0 = \frac{-A_1 j_1}{A}. \end{aligned} \tag{2.4}$$

For what follows, we suppose that the MoI's are such that $1 > u > 0$.

A Hamiltonian similar to $\hat{H}'$, but describing an even-even nucleus, was studied in both semi-classical and quantal frameworks. Here we focus our attention on the quantal description. Note that $\hat{H}'$ looks like a Hamiltonian for a triaxial rotor amended with a term, which cranks the system to rotate around the one-axis. It is convenient to choose the cranking axis as quantization axis. Moreover, it is useful to express the considered Hamiltonian in terms of the raising and lowering angular momenta operators:

$$\hat{I}_\pm = \hat{I}_2 \pm i\hat{I}_3, \ \ \hat{I}_0 = \hat{I}_1. \tag{2.5}$$

In the intrinsic frame of reference, the angular momentum components satisfy the commutation relations:

$$\left[\hat{I}_-, \hat{I}_+\right] = 2\hat{I}_0, \ \ \left[\hat{I}_\mp, \hat{I}_0\right] = \mp\hat{I}_\mp. \tag{2.6}$$

In terms of the new variables, one obtains:

$$\hat{H}' = \frac{1-u}{4}\left(\hat{I}_+^2 + \hat{I}_-^2\right) + \frac{1+u}{4}\left(\hat{I}_+\hat{I}_- + \hat{I}_-\hat{I}_+\right) + 2v_0\hat{I}_0. \tag{2.7}$$

The Schrödinger equation associated to $\hat{H}'$,

$$\hat{H}'|\Psi\rangle = E|\Psi\rangle, \tag{2.8}$$

is further written in terms of the conjugate variables q and $\frac{d}{dq}$, by using the following representation for the angular momentum components:

$$\begin{aligned} \hat{I}_\mp &= i\frac{c \pm d}{k's}\left(I \mp \hat{I}_0\right), \\ \hat{I}_0 &= Icd - s\frac{d}{dq} \equiv \hat{I}_1, \end{aligned} \tag{2.9}$$

where s, c and d denote the Jacobi elliptic functions:

$$\begin{aligned} s &= sn(q,k), \ \ c = cn(q,k), \ \ d = dn(q,k), \ \ \text{with} \\ k &= \sqrt{u}, \ \ k' = \sqrt{1-k^2}, \\ q &= \int_0^\varphi \left(1 - k^2\sin^2(t)\right)^{-1/2} dt \equiv F(\varphi, k). \end{aligned} \tag{2.10}$$

The dependence of the Jacobi functions on the variable q is shown in Fig.1. Their connection with the trigonometric function is given by:

$$s = \sin\varphi, \ \ c = \cos\varphi, \ \ d = \sqrt{1 - k^2 s^2}. \tag{2.11}$$

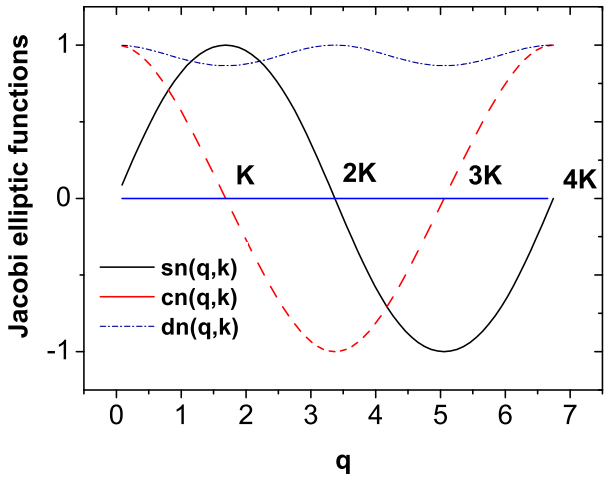

FIG. 1: (Color online) The elliptic functions sn, cn, and dn are represented as function of q, for $k = 1/2$.

Obviously, the functions s, c and d are periodic in φ, with the periods $4K, 4K$ and $2K$ respectively, where:

$$K = \frac{\pi}{2}{}_2F_1(\frac{1}{2}, \frac{1}{2}, 1; k^2). \tag{2.12}$$

The standard notation for the hyper-geometric function ${}_2F_1(\alpha, \beta, \gamma; \epsilon)$, has been used. The magnitude K is

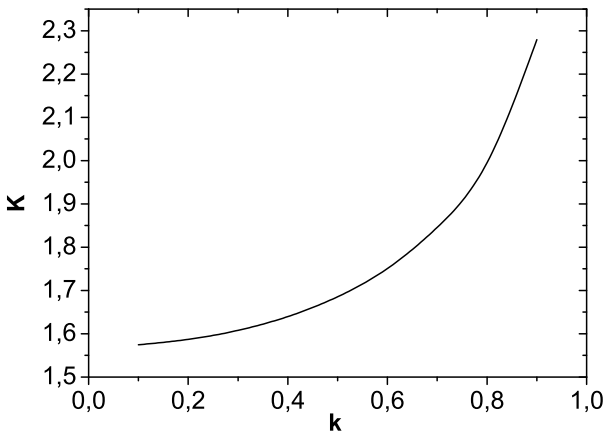

FIG. 2: (Color online) The period K given by Eq.2.12 is plotted as function of k.

plotted as function of k in Fig.2. In terms of the newly introduced conjugate coordinates, $\hat{H}'$ becomes:

$$\hat{H}' = -\frac{d^2}{dq^2} - 2v_0 s\frac{d}{dq} + I(I+1)s^2k^2 + 2v_0 cdI. \quad (2.13)$$

Changing the wave-function by the transformation:

$$|\Psi\rangle = (d - kc)^{-\frac{v_0}{k}}|\Phi\rangle, \quad (2.14)$$

the Schrödinger equation acquires a new form, where the kinetic and potential energies are separated:

$$\left[-\frac{d^2}{dq^2} + V(q)\right]|\Phi\rangle = E|\Phi\rangle. \quad (2.15)$$

The potential energy term has the expression:

$$V(q) = \left[I(I+1)k^2 + v_0^2\right]s^2 + (2I+1)v_0 cd. \quad (2.16)$$

It is worth mentioning that the transformation (2.9) preserves the commutation relations obeyed by the angular momentum components (2.6).

The shape of the potential energy term is shown in Fig. 3. Note that V(q) is invariant with respect to the transformation $q \to -q$. This leads to the fact that in the interval, for example of [-4K,4K], the potential exhibits two deep symmetric wells with degenerate minima, and three local minima in $q = 0, \pm 4K$. States inside the local minima are meta-stable, since they are tunnelling to the adjacent deep minima. The states in the deepest wells are degenerate. The shape of the potential V(q) in the interval of [0,4K] is shown in Fig.3, for a few angular momenta I. To visualize the symmetry mentioned above, we plotted V(q) in a larger interval, namely [-4K,4K]. Denoting by ψ_+ the wave function of a state in the right deepest well, and by ψ_- the function corresponding to the same energy as the former state, but the left deepest

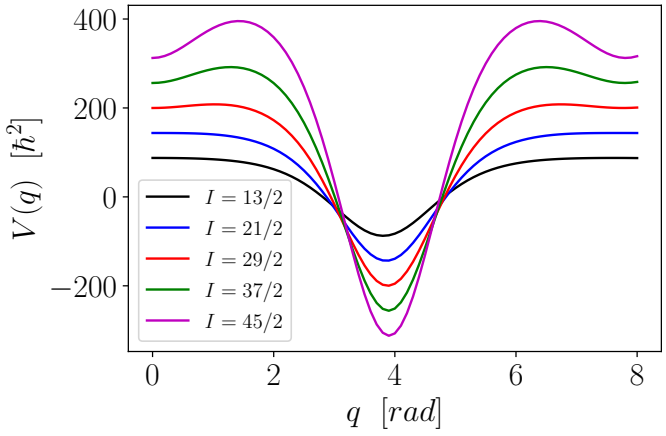

FIG. 3: (Color online) The potential energy is plotted as function of q for a particular set of values for the moment of inertia $(MoI) : \mathcal{J}_2 : \mathcal{J}_3 : \mathcal{J}_1 = 100 : 40 : 20\hbar^2 MeV^{-1}$,the odd particle angular momentum j=13/2 and $\theta = \pi/6$.

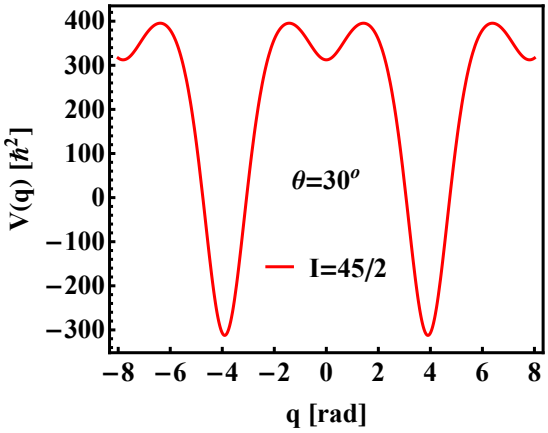

FIG. 4: (Color online) The potential energy is plotted as function of q for a particular set of values for the moment of inertia $(MoI) : \mathcal{J}_2 : \mathcal{J}_3 : \mathcal{J}_1 = 100 : 40 : 20\hbar^2 MeV^{-1}$ and $\theta = \pi/6$. Negative values for q are also included. The total angular momentum is I=45/2 and j=13/2.

minimum, they are both spread over the whole interval of [-4K,+4K]. However, the sum $\psi_+ + \psi_-$ is mainly located in the right deepest well, while the difference $\psi_+ - \psi_-$ is mainly spread inside the left deepest well.

In order to prove that the transformation (2.9) preserves the commutation relations for the angular momentum components, we need the first derivatives of the Jacobi functions:

$$\begin{aligned}
\frac{d}{dq}sn(q) &= cn(q)dn(q), \\
\frac{d}{dq}cn(q) &= -sn(q)dn(q), \\
\frac{d}{dq}dn(q) &= -k^2 sn(q)cn(q). \quad (2.17)
\end{aligned}$$

Note now that by using the Bargmann [44] mapping to

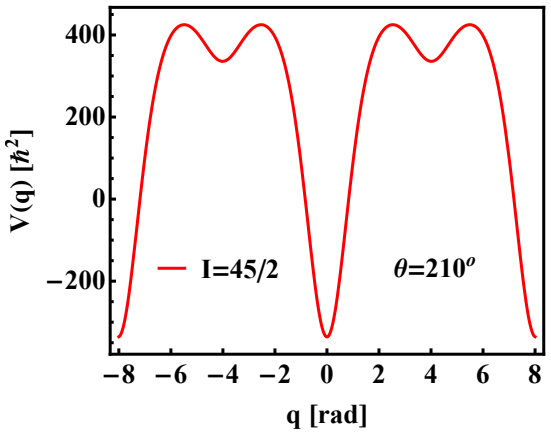

FIG. 5: (Color online) The potential energy is plotted as function of q for a particular set of values for the moment of inertia (MoI) : $\mathcal{J}_2 : \mathcal{J}_3 : \mathcal{J}_1 = 100 : 40 : 20\hbar^2 MeV^{-1}$, and $\theta = 7\pi/6$. Negative values for q are also included. The total angular momentum is I=45/2 and j=13/2.

the boson operators $b, b^\dagger$

$$q \to b^\dagger, \quad \frac{d}{dq} \to b, \tag{2.18}$$

it becomes manifest that Eq. (2.9) expresses a homeomorph mapping of the angular momentum components, i.e. the generators of a SU(2) algebra, onto a boson realization of the mentioned algebra. Indeed, within the Bargmann representation we have:

$$\begin{aligned}
\hat{I}_+ &= i\frac{c(b^\dagger) - d(b^\dagger)}{k' s(b^\dagger)} \left(I + Ic(b^\dagger)d(b^\dagger) - s(b^\dagger)b\right), \\
\hat{I}_- &= i\frac{c(b^\dagger) + d(b^\dagger)}{k' s(b^\dagger)} \left(I - Ic(b^\dagger)d(b^\dagger) + s(b^\dagger)b\right), \\
\hat{I}_0 &= Ic(b^\dagger)d(b^\dagger) - s(b^\dagger)b.
\end{aligned} \tag{2.19}$$

To our knowledge this is the first time when such a boson "expansion" shows up in the literature. Obviously, this is different from the known boson expansions proposed by Holstein-Primakoff [42], and Dyson [43]. We note that like the Dyson's, this boson representation does not preserve the hermiticity. Indeed, one can easily check that:

$$\left(\hat{I}_+\right)^+ \neq \hat{I}_- \tag{2.20}$$

Also, the boson Hamiltonian obtained from (2.13) by using he transformation (2.18), is not Hermitic. However, it may be shown [58] that it has real eigenvalues. For our further purposes it is convenient not to use the boson Hamiltonian, but rather the Schrödinger equation (2.15). We remark that in order to make the Holstein-Primakoff boson expansion tractable, the involved square root operators must be expanded in power series of $\hat{N}/I$, with $\hat{N}$ denoting the boson number operator, while I is the total angular momentum. This expansion is truncated in the second order, and moreover no contribution caused by the normal ordering of the higher order terms, is included. One remarks the fact that the whole boson series involves higher order terms in the linear momentum, which conflicts the semi-classical framework. By contradistinction, in the present case the boson Hamiltonian associated to $\hat{H}'$ is written in a normal order, and is quadratic in the linear momentum $-i\frac{d}{dq}$.

III. ANOTHER NEW BOSON EXPANSION FOR THE A.M. COMPONENTS

The case of $k = 0$ deserves a special attention. Indeed, for this value of k, one obtains:

$$q = \varphi; \quad , d = 1; \quad K = \frac{\pi}{2}, \quad k' = 1. \tag{3.1}$$

Using these simple relations in connection with Eq.(2.19), one obtains a new boson expansion for the angular momentum components in the intrinsic frame:

$$\begin{aligned}
I_+ &= i\left[-I\sin b^\dagger + (1 - \cos b^\dagger)b\right], \\
I_- &= i\left[I\sin b^\dagger + (1 + \cos b^\dagger)b\right], \\
I_0 &= I\cos b^\dagger - \left(\sin b^\dagger\right) b.
\end{aligned} \tag{3.2}$$

Again, this boson expansion is a particular case of Eq.(2.19), and different from the traditional ones mentioned above, as due to Holstein-Primakoff and Dyson. Expanding, consistently, the trigonometric functions, and keeping only the leading terms, we obtain:

$$\begin{aligned}
I_+ &= i\left[-Ib^\dagger + \frac{1}{2}(b^\dagger)^2 b\right], \\
I_- &= 2ib, \\
I_0 &= I - b^\dagger b,
\end{aligned} \tag{3.3}$$

which is just the Dyson boson expansion of the angular momentum components. Due to this result, we may assert that the boson expansions given by Eqs.(2.19), and (3.2) respectively, represent two distinct generalizations of the well known Dyson boson expansion.

IV. HARMONIC APPROXIMATION

Eq.(2.15) can be numerically solved. However, as we shall further see, there are arguments for the validity of the harmonic approximation. First, we look for the stationary point of the potential energy term. These are obtained by looking for the roots of the first derivative of $V(q)$:

$$\begin{aligned}
V'(q) &= s\left[\left(I(I+1)k^2 + v_0^2\right) 2cd - (2I+1)v_0 k'^2\right. \\
&- \left.(2I+1)v_0 2k^2 c^2\right].
\end{aligned} \tag{4.1}$$

Among the stationary points there are five minima for $q = 0, \pm 2K, \pm 4K$, respectively. As shown in Fig. 3, the minima $q = 0$, and $q = \pm 4K$ show up only for $I > 21/2$. The three minima are flat at the beginning, but their depth increases with the spin. The deepest minimum is reached at $q = \pm 2K$. Expanding the potential $V(q)$ up to the second order, in the deviation $q' = q - 2K$, one obtains the equation of a harmonic oscillator, with the spectrum:

$$E'_n = -\frac{(2I+1)^2}{2}v + \sqrt{(1+v)(u+v)(2I+1)^2 - u}\left(n + \frac{1}{2}\right), \tag{4.2}$$

where the notation $v = 2v_0/(2I+1)$ was used.

We recall now that the true Hamiltonian is $\hat{H}_{rot}$, related with $\hat{H}'$ through Eq.(2.4). Thus, the final spectrum has the expression:

$$E_n = A_1 I^2 + (2I+1)A_1 j_1 - I A_2 j_2 + \hbar\omega(n+1/2) + \sum_{i=1,2} A_i {j_i}^2. \tag{4.3}$$

where the frequency ω is defined by:

$$\begin{aligned} \omega &= \left[\left((2I+1)(A_2 - A_1 - \frac{A_2 j_2}{I}) - 2A_1 j_1\right)\right. \\ &\times \left((2I+1)(A_3 - A_1) - 2A_1 j_1\right) \\ &- \left.(A_3 - A_1)(A_2 - A_1 - \frac{A_2 j_2}{I})\right]^{1/2}. \end{aligned} \tag{4.4}$$

Following the same procedure as before, we may expand the potential around the local minimum, $q = 0$, if that exists, and keep only up to the quadratic term, we obtain the following quantal energies:

$$E_n = A_1 I^2 - (2I+1)A_1 j_1 - I A_2 j_2 + \hbar\omega'(n+1/2) + \sum_{i=1,2} A_i {j_i}^2, \tag{4.5}$$

where the new frequency has the expression:

$$\begin{aligned} \omega' &= \left[\left((2I+1)(A_2 - A_1 - \frac{A_2 j_2}{I}) + 2A_1 j_1\right)\right. \\ &\times \left((2I+1)(A_3 - A_1) + 2A_1 j_1\right) \\ &- \left.(A_3 - A_1)(A_2 - A_1 - \frac{A_2 j_2}{I})\right]^{1/2}. \end{aligned} \tag{4.6}$$

Of course, the phonon energies depend on the angle θ defining the components j_1, and j_2 of the single particle angular momentum. It is worth remarking that while the phonon energy ω defined inside the deepest well is a decreasing function, the energy of the phonon defined in the local minimum has an opposite behavior (see Fig. 6).

V. CLASSICAL DESCRIPTION

The classical picture is obtained by the diagonalization procedure, which consists in replacing the operators $\hat{I}_k$

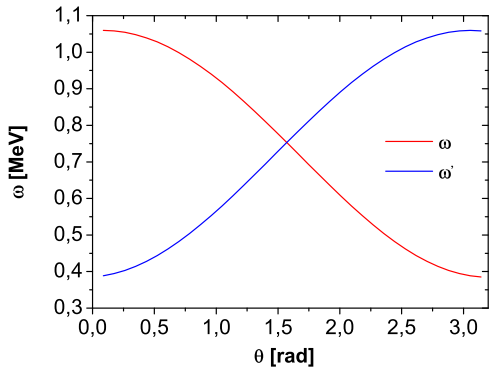

FIG. 6: (Color online) The phonon energies ω and ω' are plotted as function of θ, defining the orientation of **j** in the plane XOY, for the moments of inertia (MoI) : $\mathcal{J}_2$: $\mathcal{J}_3$: $\mathcal{J}_1 = 100 : 40 : 20\hbar^2 MeV^{-1}$.

with the classical component of the angular momentum, I_k and the algebra multiplication by:

$$[,] \to -i\{,\}, \tag{5.1}$$

with the notation $\{,\}$ for the Poisson bracket. Let us now denote by φ_k the conjugate coordinate of I_k. Thus, the classical counterpart of the Hamiltonian $\hat{H}'$ is:

$$H' = I_2^2 + uI_3^2 + 2v_0 I_1, \tag{5.2}$$

and one easily finds that:

$$\{I_k, H'\} = \dot{I}_k, \tag{5.3}$$

which leads to the following equations of motion:

$$\begin{aligned} \dot{x}_1 &= 2(1-u)x_2 x_3, \\ \dot{x}_2 &= 2(x_1 u - v_0)x_3, \\ \dot{x}_3 &= -2(x_1 - v_0)x_2, \end{aligned} \tag{5.4}$$

where, for simplicity, the notation $x_k = I_k$, k=1,2,3 has been used. Also, the symbol " $\bullet$ " is used for the time first derivative. Using the equations of motion (5.4), one proves that there are two constants of motion:

$$\begin{aligned} E &= x_2^2 + ux_3^2 + 2v_0 x_1, \\ I^2 &= x_1^2 + x_2^2 + x_3^2. \end{aligned} \tag{5.5}$$

This is a reflection of the fact that the energy, and the angular momentum are conserved. The above equation allows us to express x_2, and x_3 in terms of x_1. Making the time derivative of the first equation (5.4), and inserting the expressions of x_2, and x_3 in the resulting equation, one obtains the final equation for x_1:

$$\ddot{x}_1 + a_3 x_1^3 + a_2 x_1^2 + a_1 x_1 + a_0 = 0, \tag{5.6}$$

where the coefficients have the expressions:

$$\begin{aligned} a_3 &= 8u, \\ a_2 &= -12v_0(1+u), \\ a_1 &= 16v_0^2 - 8uI^2 + 4E(1+u), \\ a_0 &= -8v_0E + 4v_0(1+u)I^2. \end{aligned} \tag{5.7}$$

We recognize in (5.6) the differential equation for the elliptic functions of the first kind. Their explicit expressions can be obtained from the equations of motion (5.4). Indeed, from (5.5) one obtains:

$$\begin{aligned} x_2 &= (1-u)^{-1/2}\left(ux_1^2 - 2v_0x_1 + E - uI^2\right)^{1/2}, \\ x_3 &= (1-u)^{-1/2}\left(-x_1^2 + 2v_0x_1 - E + I^2\right)^{1/2}, \end{aligned} \tag{5.8}$$

and then the first equation (5.4) can be integrated with the result:

$$\begin{aligned} t - t_0 &= \int_{x_{10}}^{x_1} \frac{dx}{2\sqrt{-u(x-\alpha_1)(x-\alpha_2)(x-\alpha_3)(x-\alpha_4)}} \\ &\equiv \frac{1}{\sqrt{C}}F(\varphi,k), \end{aligned} \tag{5.9}$$

where α_1, α_2 are the roots of the equation $x_2 = 0$, while α_3, α_4, for $x_3 = 0$:

$$\begin{aligned} \alpha_{1,2} &= v_0 \pm \left[v_0^2 - u(E - I^2u)\right]^{1/2}, \\ \alpha_{3,4} &= v_0 \pm \left[v_0^2 - E + I^2)\right]^{1/2}. \end{aligned} \tag{5.10}$$

The limits for the integral (5.9) are chosen such that the integrand is a real number for any $x \in (x_{10}, x_1]$. Obviously, the integral (5.9) depends on the relative position of the poles $\alpha_i, i = 1,2,3,4$). The argument φ involved in the elliptic function is defined as:

$$\varphi = \begin{cases} \arcsin k_1, & if \text{ all } \alpha_i \text{ are real}, \\ \arctan k_1, & \text{if two } \alpha_i \text{ are complex numbers} \end{cases} \tag{5.11}$$

The explicit expressions of C, k_1^2, k^2 are given in Ref.[59]. Equation (5.9) can be reversed, and the result is a function $x_1(t)$, which is periodic, with the period

$$T = \frac{\pi}{\sqrt{C}}{}_2F_1\left(\frac{1}{2}, \frac{1}{2}, 1; k^2\right). \tag{5.12}$$

In a similar way one may find the functions $x_2(t)$, and $x_3(t)$. The set of points $(x_1(t), x_2(t), x_3(t))|_t$ defines the classical trajectory which can further be quantized. Indeed, let P_0 be an extremal point on the sphere of the radius I, to which the energy E_0 corresponds. Let us now consider the trajectory to be quantized, characterized by the energy E and surrounding P_0. Consider the calotte bordered by the chosen trajectory, whose area defines the classical action. The quantization consists in restricting the action to be an integer multiple of 2π.

$$\mathcal{L}(E) = \int \Omega = \int_{E_0}^{E}\int_0^T dE'dt' = \int_{E_0}^{E} T(E')E' = 2\pi n. \tag{5.13}$$

From here, one easily finds:

$$\frac{\partial \mathcal{L}}{\partial E} = T(E) = \frac{\partial \mathcal{L}(E)}{\partial n}\frac{\partial E}{\partial n}, \quad \frac{\partial E}{\partial n} = \frac{2\pi}{T(E)}. \tag{5.14}$$

It results that a linear dependence of E on "n" is obtained when $T(E)$ is approximated by its zero order expansion around E_0. In this case E is given by the harmonic approximation. For an even-even system the period expansion in terms of energy has been performed in Ref.[59].

Here we adopt a different procedure to obtain the harmonic motion of the even-odd system. Several situation are considered: A1) Indeed, changing the Carthesian to

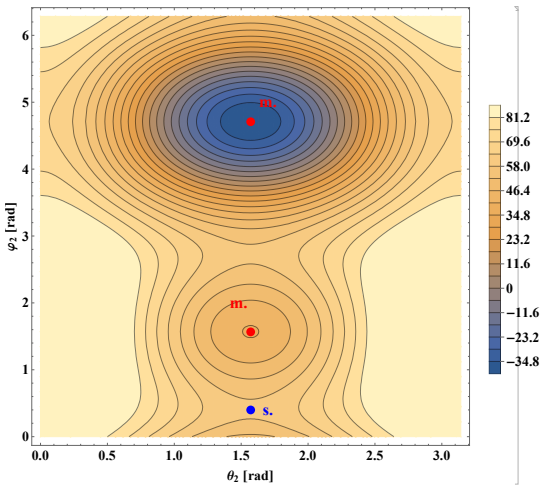

FIG. 7: (Color online) Contour plot of the case A) for I=19/2, j=11/2 and $\theta = 70^0$ of ^{135}Pr corresponding to the MoI's: $\mathcal{I}_1 : \mathcal{I}_2 : \mathcal{I}_3 = 10 : 40 : 20\hbar^2 Mev^{-1}$. The minima (m.) and the saddle points(S.) are also mentioned

the polar coordinates:

$$x_2 = I\cos\theta_2,\ x_3 = I\sin\theta_2\cos\varphi_2,\ x_1 = I\sin\theta_2\sin\varphi_2, \tag{5.15}$$

which is convenient in the case the maximal MoI corresponds to the 2-axis, the energy function H' can be expressed only in terms of the canonical conjugate coordinates (x_2, φ):

$$\begin{aligned} H' &= x_2^2\left(1 - u\cos^2\varphi_2 - \frac{v_0}{I}\sin\varphi_2\right) \\ &+ uI^2\cos^2\varphi_2 + 2v_0I\sin\varphi_2. \end{aligned} \tag{5.16}$$

The function H' has a minimum in $(x_2, \varphi_2) = (0, -\frac{\pi}{2})$. In the minimum point, the second derivatives of H' have the values:

$$\begin{aligned} \frac{\partial^2 H'}{\partial x_2^2}|_m &= 2\left(1 + \frac{v_0}{I}\right), \\ \frac{\partial^2 H'}{\partial \varphi_2^2}|_m &= 2\left(u + \frac{v_0}{I}\right)I^2. \end{aligned} \tag{5.17}$$

Also the minimal value of H' is:

$$H'|_m = -2v_0I\ . \tag{5.18}$$

Denoting by $(\bar{x}_2, \bar{\varphi}_2)$ the deviation of the current coordinates form those of the minimum point, the second order expansion of H' looks like:

$$H' = -2v_0 I + \left(1 + \frac{v_0}{I}\right)\bar{x}_2^2 + \left(u + \frac{v_0}{I}\right) I^2 \bar{\varphi}_2^2. \quad (5.19)$$

This describes a harmonic oscillator of a frequency:

$$\omega = 2\sqrt{(1+v)(u+v)I^2}, \quad (5.20)$$

with $v = \frac{v_0}{I}$. By quantization, the spectrum corresponding to H' coincides with that from (4.2), provided the approximation $I + \frac{1}{2} \approx I$ is adopted.

In the minimum point, the angular momentum components are:

$$(x_1, x_2, x_3) = (-I, 0, 0)_m, \quad (5.21)$$

while the energy is: $E_m = -2vI^2$.

A2) One may check that $(0, \frac{\pi}{2})$ is also a minimum of H', in which the angular momentum is $(I, 0, 0)$, while the energy has the expression $E_m = 2vI^2$. The second order expansion of H' is :

$$H' = 2v_0 I + (1-v)\bar{x}_2^2 + I^2(u-v)\bar{\varphi}_2^2. \quad (5.22)$$

This describes an harmonic oscillation of frequency:

$$\omega = 2\sqrt{(1-v)(u-v)I^2}. \quad (5.23)$$

This frequency coincide with the quantal frequency ω' given by Eq.(4.5), if we adopt the approximation $I + \frac{1}{2} \approx I$, which is valid for a large I.

A3) Another pair of conjugate, and stationary variables, which might be minimum for the energy function is:

$$(x_2, \varphi_2)_s = (0, \arcsin\left(\frac{v_0}{Iu}\right)). \quad (5.24)$$

To this, it corresponds the harmonic Hamiltonian;

$$H'_h = uI^2 + \frac{v_0^2}{u} + (1-u)\bar{x}_2^2 - u\left(I^2 - \frac{v_0^2}{u^2}\right)\bar{\varphi}_2^2. \quad (5.25)$$

Obviously, the mentioned stationary point is a saddle point, to which the following angular momentum corresponds: $(x_1, x_2, x_3) = (\frac{v_0}{u}, 0, \sqrt{(I^2 - \frac{v_0^2}{u^2})}_s$, with the energy of: $E_s = (u + \frac{v^2}{u})I^2$. The trajectories corresponding to the situations labelled by A1)-A3) are visualized by the contour plot given in Fig. 7. One notices that the trajectories of energies close to a minimum, surround exclusively that minimum, while due to the tunneling effect, the trajectories of large energies surround all minima.

B1) Choosing now the 3-axis as quantization axis, and the corresponding polar coordinates:

$$x_1 = I\sin\theta_3\cos\varphi_3,\ x_2 = I\sin\theta_3\sin\varphi_3,\ x_3 = I\cos\theta_3, \quad (5.26)$$

the Hamiltonian H' can be expressed in terms of the canonical conjugate variables (x_3, φ_3):

$$H' = x_3^2\left(u - \sin^2\varphi_3 - \frac{v_0}{I}\cos\varphi_3\right) + I^2\sin^2\varphi_3 + 2v_0 I\cos\varphi_3. \quad (5.27)$$

One stationary point which might be a minimum is $(x_3, \varphi_3) = (0, \pi)$. The corresponding angular momentum components are $(x_1, x_2, x_3) = (-I, 0, 0)_m$. Therefore, the angular momentum is oriented along the 1-axis. The minimum energy is $E_m = -2v_0 I$. The harmonic Hamiltonian, i.e. the second order expansion of H' around $(0, \pi)$, is:

$$H'_h = -2v_0 I + \left(u + \frac{v_0}{I}\right)\bar{x}_3^2 + I^2\left(\left(1 + \frac{v_0}{I}\right)\bar{\varphi}_3^2. \quad (5.28)$$

Although the harmonic Hamiltonian is different from that from the case A1), the two scenarios provide the same angular frequencies, but the canonical conjugate variables are interchanged.

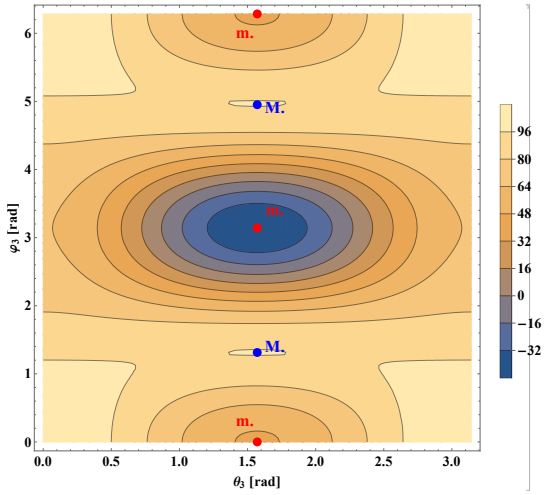

FIG. 8: (Color online)Contour plot of the case B) for I=19/2, j=11/2 and $\theta = 70^0$ of ^{135}Pr corresponding to the MoI's: $\mathcal{I}_1 : \mathcal{I}_2 : \mathcal{I}_3 = 10 : 20 : 40\hbar^2 Mev^{-1}$. The minima (m.) and maxima (M.) are also mentioned.

B2) Similarly, one shows that $(x_3, \varphi_3) = (0, 0)$ is a minimum, which results the quadratic expansion:

$$H'_h = 2v_0 I + \left(u - \frac{v_0}{I}\right)\bar{x}_3^2 + I^2\left(1 - \frac{v_0}{I}\right)\bar{\varphi}_3^2, \quad (5.29)$$

with the stationary angular momentum $((x_1, x_2, x_3) = (I, 0, 0)_m$, and the corresponding energy $E_m = 2v_0 I$. The harmonic frequency determined by H'_h:

$$\omega = 2\sqrt{(1-v)(u-v)I^2}. \quad (5.30)$$

B3) In this case, the stationary point is $(x_3, \varphi_3) = (0, \arccos\frac{v_0}{I})$, which leads to $(x_1, x_2, x_3) = (v_0, \sqrt{I^2 - v_0^2}, 0)_M$. The corresponding quadratic expansion of H' is:

$$H'_h = I^2 + v_0^2 + (u-1)\bar{x}_3^2 + (v_0^2 - I^2)\bar{\varphi}_3^2, \quad (5.31)$$

which indicates that the stationary point is a maximum point with the critical energy equal to $E_M = I^2(1+v^2)$. The trajectories determined by the circumstances specified by the cases B1)-B3) are represented in the contour plot from Fig. 8.

C1) If the maximal MoI corresponds to the 1-axis, then we choose this as quantization axis, and the polar coordinates:

$$x_1 = I\cos\theta_1,\ x_2 = I\sin\theta_1\cos\varphi_1,\ x_3 = I\sin\theta_1\sin\varphi_1. \tag{5.32}$$

The Hamiltonian becomes:

$$H' = \left(\cos^2\varphi + u\sin^2\varphi\right)\left(I^2 - x_1^2\right) + 2v_0x_1. \tag{5.33}$$

This has a stationary point in $(x_1,\varphi_1) = \left(\frac{v_0}{u},\frac{\pi}{2}\right)$. This is a saddle point for H', as suggested by the second order expansion:

$$H'_h = uI + \frac{v_0}{u} - u\bar{x}_1^2 + (1-u)\left(I^2 - \frac{v_0^2}{u^2}\right)\bar{\varphi}_1. \tag{5.34}$$

The corresponding angular momentum and energy are: $(x_1,x_2,x_3) = (\frac{v_0}{u},0,\sqrt{(I^2-\frac{v_0^2}{u^2})_s}$, and $E_s = (u+\frac{v^2}{u})I^2$.

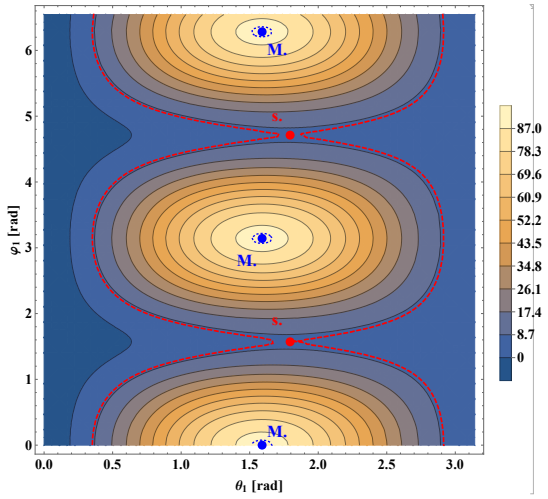

FIG. 9: (Color online) The contour plot of the case C) for I=19/2 of ^{135}Pr corresponding to the MoI's, and θ determined by the adopted fitting procedure. The maxima and saddle points are also mentioned.

C2) The stationary point $(v_0,0)$ is a maximum, with the angular momentum $(x_1,x_2,x_3) = (v_0,\sqrt{I^2-v_0^2},0)_M$, and energy $E_M = I^2+v_0^2$. The quadratic expansion around this point is:

$$H'_h = I^2 + v_0^2 - \bar{x}_1^2 + (u-1)(I^2-v_0^2)\bar{\varphi}_1^2. \tag{5.35}$$

Concluding this analysis, there are four minima, the cases A1), A2), B1), and B2), one maximum, the cases B3),C2), and one saddle point, the situations A3) and C1). The frequencies corresponding to the four minima are grouped in two pairs of degenerate frequencies, and moreover the frequency showing up in the cases A1), and B1) is equal to the one provided by the quantal description for the deepest minimum of the potential energy. The other two degenerate minima, A2) and B2), produce a frequency equal to the one showing up in the quantal description for the local minimum. In the minimum points, the total angular momentum is oriented along a principal axis,namely the 1-axis, while for the maximum and the saddle point is located in a principal plane. It is worth mentioning that in the maximum point, the angular momentum is oriented along the 2-axis to which the maximal MoI corresponds. Therefore, the transverse wobbling is unstable.

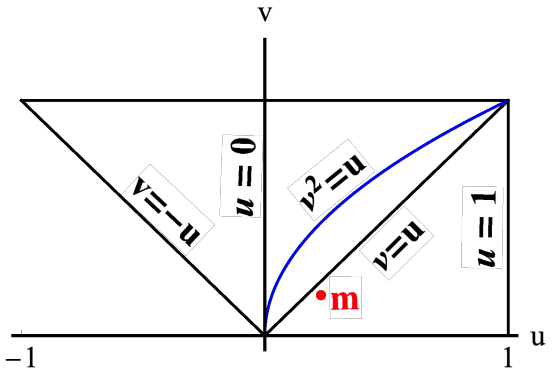

FIG. 10: (Color online) The phase diagram for I=15/2 of ^{135}Pr. Using the MoI's, and θ determined by the adopted fitting procedure, and $\theta = 150^0$, we mentioned the minimum point by a red and full circle having a lowercase m.

According to the contour plot of Fig. 9, all trajectories, determined by the conditions C1,C2), are meta-stable.

A. The phase diagram

The character of the stationary point to be minimum, maximum or saddle point is decided by the signs of the diagonal matrix elements of the Hessian: a) if all diagonal elements are positive, the stationary point is minimum; b) if all diagonal m.e. are negative, then we deal with a maximum, while c) it is a saddle point if one m.e. is positive and the other is negative. Equating the Hessian to zero, one obtains the parameters u, and v for which the critical points are degenerate. The resulting equations may be unified in a single formulae:

$$(1-u)(1-v^2)(v^2-u^2)(v^2-u) = 0. \tag{5.36}$$

The last factor in the above equation is obtained by equating the critical energies E_M, and E_s. Each factor generates a curve, called separatrice, in the parameter space spanned by (u,v). As shown in Fig. 10, the separatrices are bordering manifolds defining unique nuclear phases characterized by a specific portrait of the stationary points. Indeed, among the factors involved in

Eq.(5.36), we recognize those defining the two wobbling frequencies. On the other hand a vanishing energy defines a Goldstone mode [45] which, as a matter of fact, render evidently a phase transition.

VI. ELECTROMAGNETIC TRANSITIONS

We are interested in describing the experimental data for the electric quadrupole intra- and inter-band transitions as well as the magnetic dipole transitions. We begin with the electric transitions. Aiming at this goal, we need the wave functions describing the involved states, and the transition quadrupole operator. The wave function for an I-state is the solution of the Schrödinger equation for the given total angular momentum, I. Note that the wave function is degenerate with respect to "M", the projection of I on the x-axis, in the laboratory frame. Since the ground state is the vacuum state for the wobbling phonon operator, and moreover, in the minimum point of the constant energy surface, the a.m. projection on the one-axis of the intrinsic frame is equal to -I, it results that the K quantum number is equal to -I. Therefore the solution of the Schrödinger equation must be labelled by the mentioned quantum numbers, i.e.

$$\begin{aligned} \Psi_{IM} &= \Phi_{I,-I}|IM,-I\rangle, \text{ with} \\ |IMK\rangle &= \sqrt{\frac{2I+1}{8\pi^2}}D^I_{M,K}. \end{aligned} \tag{6.1}$$

Here we consider the first two wobbling bands as signature partner bands, the arguments being in detail given in Ref.[28]. More specifically, the spin sequence of the first band is $j+R$, for R=0,2,4,... , while for the second band the spin succession is $j+R$, with R=1,3,5,.... Note that the quadrupole inter-band transition is forbidden since, for the states mentioned above, have $\Delta K = 1$. In this case, considering the component $K = -I+1$ in one of the involved states is necessary. The quadrupole transition operator is taken as:

$$\mathcal{M}(E2;\mu) = \sqrt{\frac{5}{16\pi}}e\left(Q_{20}D^2_{\mu 0} + Q_{22}D^2_{\mu 2} + Q_{2-2}D^2_{\mu -2}\right), \tag{6.2}$$

where Q_0, and Q_2, denote the $K=0$, and $K=\pm 2$ components of the quadrupole transition operator, respectively. Note that since the intrinsic component of the wave function depends on one of the conjugate variables q, and d/dq, that is q, we must express the quadrupole operators in terms of the q variable. This will be achieved by writing Q-s in the space of angular momentum and then use the Bargmann representation of the a.m. components. Thus we have:

$$\begin{aligned} Q_0 &= \left(-\frac{1}{4}\sqrt{\frac{2}{3}}\left(\hat{I}_+\hat{I}_- + \hat{I}_-\hat{I}_+\right) + \sqrt{\frac{2}{3}}\hat{I}_1^2\right)\bar{Q}_0, \\ Q_{\pm 2} &= \frac{1}{2}\hat{I}^2_{\pm}\bar{Q}_2. \end{aligned} \tag{6.3}$$

In the next step, the a.m. components $\hat{I}_\pm$, and $\hat{I}_0$ are written in the Bargmann representation, and then the derivative coefficients expanded in the second order around the minimum point of the energy. The result is:

$$\begin{aligned} Q_0 &= \frac{1}{\sqrt{6}}\left[3\bar{q}^2\frac{d^2}{d\bar{q}^2} - 3(2I-1)\bar{q}\frac{d}{d\bar{q}}\right. \\ &+ \left. I(2I-1) - I(I-1)(1+k^2)\bar{q}^2\right], \\ Q_2 &= \frac{1}{k'^2}\left\{\left[-2+(1+k^2)\bar{q}^2\right]\frac{d^2}{d\bar{q}^2} - (2I-1)(1+k^2)\bar{q}\frac{d}{d\bar{q}}\right. \\ &- \left. I(1+k^2) + I\left[(I+1)(1+k^2) + k^2(k^2+3)\right]\bar{q}^2\right\}. \end{aligned} \tag{6.4}$$

Note that the magnitude $k(=\sqrt{u})$, defined by Eq. (2.10), depends on the angular momentum I due to u. Therefore, hereafter, we attach to it a lower index specifying this dependence. The same procedure is used for he $K+1$, and $K+2$ wave-functions:

$$\begin{aligned} &\Phi_{I,-I+1} \equiv \frac{\mathcal{N}^{(1)}_I}{\sqrt{2I}}\hat{I}_-\Phi_{I,-I} = ik_I'\frac{\mathcal{N}^{(1)}_I}{\sqrt{2I}} \\ &\times \left(-I\bar{q} + \frac{\bar{\omega}_I}{4}\bar{q}^3\right)\Phi_{I,-I}, \text{ with } \mathcal{N}^{(1)}_{\rm I} = \frac{1}{\rm k'_I}\sqrt{\frac{\bar{\omega}_{\rm I}}{\rm I}}, \\ &\Phi_{I,-I+2} \equiv \frac{\mathcal{N}^{(2)}_I}{\sqrt{4I(2I-1)}}\hat{I}^2_-\Phi_{I,-I} = \frac{-\mathcal{N}^{(2)}_I k'_I}{2\sqrt{I(2I-1)}} \\ &\times \left(-I\bar{q} + \frac{1}{2}\bar{q}^2\frac{d}{d\bar{q}}\right)^2\Phi_{I,-I}, \text{ with} \mathcal{N}^{(2)}_{\rm I} = \frac{2\bar{\omega}_{\rm I}}{\rm k'^2_I\sqrt{I(2I-1)}}. \end{aligned} \tag{6.5}$$

The state describing the oscillator vacuum is

$$\Phi_{I,-I} = C_I e^{-\frac{1}{2b_I^2}\bar{q}^2}, \tag{6.6}$$

where the norm, and the oscillator length are:

$$C_I = \sqrt{\frac{2}{\pi}}\frac{1}{b_I}, \;\; b_I^2 = \frac{\hbar}{M\bar{\omega}_I}. \tag{6.7}$$

In our case, the units system is that where $\hbar = 1$, while the mass parameter is $M = \frac{1}{2}$. Therefore

$$b_I = \sqrt{\frac{2}{\bar{\omega}_I}}, \tag{6.8}$$

where ω_I is defined by Eq.(4.2) or by (4.4), and $\bar{\omega}_I = \omega_I/A$. With the above ingredients, the m.e. of the transition operator corresponding to the intrinsic states $|\Phi_{I,-I}\rangle$ can be evaluated by integration.

However, here we propose an alternative version for the necessary matrix elements, which actually will be used in our concrete calculations. We use the expression (6.3), and evaluate by brute calculations the result of acting on the system wave function with the spherical components of **I**. The nice feature of this procedure is that any reduced m.e. has as a common factor the overlap of the

initial, and final intrinsic states. For example, for inter-band and intra-band transitions, the overlap factors are:

$$\langle\Phi_{I,-I}|\Phi_{I-1,-I+1}\rangle = \frac{2\sqrt{\bar{\omega}_I\bar{\omega}_{I-1}}}{\bar{\omega}_I+\bar{\omega}_{I-1}},$$
$$\langle\Phi_{I,-I}|\Phi_{I-2,-I+2}\rangle = \frac{2\sqrt{\bar{\omega}_I\bar{\omega}_{I-2}}}{\bar{\omega}_I+\bar{\omega}_{I-2}}. \quad (6.9)$$

We checked numerically the fact that the overlap factors are very close to unity. For this reason we approximate them to one. Thus, the matrix elements involved in the equation defining the reduced transition probabilities are analytically expressed. Note that acting with the operator $Q_{2\mu}$ on the intrinsic wave function the a.m. is preserved but the K quantum number is changed by μ units. The change of a.m. is due to the overlap factor which modifies also the K quantum number by 2 units. Due to this feature the variation ΔK for initial and final states might exceed μ. However, we should keep in mind that the tensor properties of the operator $Q_{2\mu}$ specific to the laboratory frame, are lost when one passes to the intrinsic frame. On the other hand, the intrinsic wave function does not have $K=-I$, this being fulfilled for the classical minimal energy but not within the quantal picture. However, the conservation rules as well as the Wigner-Eckart theorem hold due to the laboratory frame wave factor.

The matrix elements for the intra-band transitions are:

$$\langle\Psi_I||\mathcal{M}(E2)||\Psi_{I-2}\rangle = \sqrt{\frac{5}{16\pi}}e\left\{\bar{Q}_2\frac{1}{2}\left[C^{I\ 2\ I-2}_{I\ -2\ I-2}\right.\right.$$
$$\times\ \left(\sqrt{6(I-1)(2I-3)}+\frac{2I^2-2I+5}{\sqrt{(I-2)(2I-5)}}\right)$$
$$+\ C^{I\ 2\ I-2}_{I-4\,2\,I-2}\left(\sqrt{I(2I-1)}+\frac{2I^2-2I+5}{\sqrt{I(2I-1)}}\right)\Big]$$
$$\left.+\ \bar{Q}_0C^{I\ 2\ I-2}_{I-2\,0\,I-2}\frac{1}{\sqrt{6}}(2I^2-5I+5)\right\}, \quad (6.10)$$

while those determining the inter-band transitions have the expressions [65]:

$$\langle\Psi_I||\mathcal{M}(E2)||\Psi_{I-1}\rangle = \sqrt{\frac{5}{16\pi}}e\left\{\bar{Q}_2\frac{1}{2}\left[C^{I\ 2\ I-1}_{I-3\ 2\ I-1}\right.\right.$$
$$\times\ \left(\sqrt{I(2I-1)}+\frac{2I^2-3I+\frac{3}{2}}{\sqrt{I(2I-1)}}\right)+C^{I\ 2\ I-1}_{I\ -2\ I-2}$$
$$\times\ \left.\left(\sqrt{(I-1)(2I-3)}+\frac{2I^2-3I+\frac{3}{2}}{\sqrt{(I-1)(2I-3)}}\right)\right]$$
$$\left.+\ \bar{Q}_0C^{I\ 2\ I-1}_{I-1\,0\,I-1}\frac{1}{\sqrt{24}}\left(4I^2-6I+3\right)\right\}. \quad (6.11)$$

Furthermore, the reduced transition probabilities are readily obtained:

$$B(E2;I\to I') = \left[\langle\Psi_I||\mathcal{M}(E2)||\Psi_{I'}\rangle\right]^2. \quad (6.12)$$

The factors $\bar{Q}_0$, and $\bar{Q}_2$ have the units of e.fm$^2/\hbar^2$, and are taken as free parameters.

The magnetic dipole transition operator is:

$$\mathcal{M}(M1;\mu) = \sqrt{\frac{3}{4\pi}}\mu_N\sum_\nu\left(g_R\hat{R}_\nu+g_j\hat{j}_\nu\right)D^1_{\mu\nu},$$
$$\equiv M^{coll}_{1\mu}+M^{sp}_{1\mu}, \quad (6.13)$$

where R_ν, and j_ν are the spherical components of the core and the odd nucleon angular momenta, respectively. g_R and g_j stand for the gyromagnetic factors of the core, and the coupled odd nucleon, respectively. Also, the standard notation for the Wigner function, D^J_{MK}, and for the nuclear magneton, μ_N, are used. To calculate the collective part of the transition matrix element, we need to express the wave function describing the odd system as a Kronecker product of the core, and the odd particle wave functions:

$$|IMK\rangle = \frac{1}{2j+1}\sum_{M_R,\Omega,R}C^{R\ j\ I}_{M_R\ \Omega\ M}|RM_RK\rangle\psi_{j\Omega}. \quad (6.14)$$

By a direct manipulation, one finds:

$$\langle I||M^{coll}_1||I-1\rangle = \sqrt{\frac{3}{4\pi}}g_R\mu_N\frac{1}{2j+1}C^{I+j-1\,1\,I+j-1}_{I+j-2\,1\,I+j-1}$$
$$\times\ \left[(2I-1)(2J+2j-1)(I+j-1)(I+j)\right]^{1/2}$$
$$\times\ W(I-1,j,1,I+j;I+j-1,I), \quad (6.15)$$

where the notation $W(a,b,c,d;e,f)$ stands for the Racah coefficient.

To calculate the reduced m.e. of the single particle M1 operator we need the wave function describing the odd proton whose a.m. is placed in the plane XOY making the angle θ with the axis OX. This function is obtained by rotating around the axis 3, the function $\psi_{j,j}$ associated to the odd proton having the a.m. along the 1-axis.

$$\psi'_j = R_3(\theta)\psi_{jj}. \quad (6.16)$$

The reduced m.e. of the single particle transition operator is:

$$\langle I||M^{sp}_1||I-1\rangle = \sqrt{\frac{3}{4\pi}}g_j\mu_N$$
$$\times\ C^{I\ 1\ I-1}_{I\ -1\ -I}\langle\psi_{jj}|R^\dagger_3(\theta)j_{-1}R_3(\theta)|\psi_{jj}\rangle$$
$$=\ \frac{1}{\sqrt{2}}\langle\psi_{jj}|-\hat{j}_1\sin\theta+\hat{j}_+\frac{\cos\theta-1}{2}+\hat{j}_-\frac{\cos\theta+1}{2}|\psi_{jj}\rangle$$
$$=\ -j\sin\theta\sqrt{\frac{3}{8\pi}}\mu_Ng_jC^{I\ 1\ I-1}_{I\ -1\ -I}. \quad (6.17)$$

The gyromagnetic factors have the expressions:

$$g_R=\frac{Z}{A},\ g_j=g_l+\frac{\frac{3}{4}+j(j+1)-l(l+1)}{j(j+1)}\frac{g_s-g_l}{2}, \quad (6.18)$$

where g_l, and g_s stand for the orbital and spin free gyromagnetic factors, respectively. Finally, the magnetic dipole reduced transition probability is given by:

$$B(M1;I\to I') = \left[\langle\Psi_I||\mathcal{M}(M1)||\Psi_{I'}\rangle\right]^2. \quad (6.19)$$

VII. RESULTS

The formalism described in the previous sections was applied to ^{135}Pr. The excitation energies in three bands, conventionally called band 1 (B1), band 2 (B2), and band 3 (B3), and the electromagnetic properties of the states have been described by a simple Hamiltonian (2.1), associated to the even-even core and the odd proton, which stays in the orbital $h_{11/2}$.The core properties are simulated by a triaxial core with the moments of inertia $\mathcal{J}_k$ (k=1,2,3), considered to be free parameters, while the odd proton is rigidly coupled to the core and having the angular momentum $j = 11/2$, placed in the inertial plane (1,2), and having the polar angle θ. Thus, the approach involves four free parameters $\mathcal{J}_k$ (k=1,2,3), and θ, which were fixed by a least mean square procedure, fitting the excitation energies for the three bands.

$\mathcal{I}_1$ $[\hbar^2/MeV]$	$\mathcal{I}_2$ $[\hbar^2/MeV]$	$\mathcal{I}_3$ $[\hbar^2/MeV]$	θ [degrees]	nr. of states	r.m.s. [MeV]
89	12	48	-71	20	0.174

TABLE I: The MoI's, and the parameter θ as provided by the adopted fitting procedure.

A. Energies

The excitation energies for the first three bands are obtained from Eq.(4.3):

$$\begin{aligned} E_I^{exc;1} &= A_1 I^2 + (2I+1)A_1 j_1 - I A_2 j_2 + \omega_I/2 - E_{11/2}, \\ I &= R + j, \quad R = 0, 2, 4, ..., \\ E_I^{exc;2} &= A_1 I^2 + (2I+1)A_1 j_1 - I A_2 j_2 + \omega_I/2 - E_{11/2}, \\ I &= R + j, \quad R = 1, 3, 5, ..., \\ E_{I+1}^{exc;3} &= A_1 I^2 + (2I+1)A_1 j_1 - I A_2 j_2 + 3\omega_I/2 - E_{11/2}, \\ I &= R + j, \quad R = 1, 3, 5, ... \end{aligned} \tag{7.1}$$

As we already mentioned, the involved parameters were fixed by fitting the experimental excitation energies with those described by the above equations. The parameters yielded by the fitting procedure are listed in Table I. With the parameters thus determined, and Eq.(7.1), the excitation energies are readily obtained. They are visualized in Figs.11, 12, 13 and compared with the corresponding experimental data taken from Refs.[34, 35]. Note that in the mentioned figures the three bands are conventionally called as the first, the second and the third band, respectively. Results are compared with the experimental data [35] for the bands yrast, one phonon wobbling (TW1) and the two phonon wobbling bands (TW2), respectively. Our denomination is different from that used for the experimental bands, since in our case the second band is the signature partner band of the yrast band, while the third band is one phonon band built up on the base of the second band. From there, one sees the quality of the agreement with the data, that might be appraised by the r.m.s. of the deviation which is also given in Table I. This is slightly larger but comparable with the r.m.s.'s obtained in Refs.[40] (≈0.160MeV) and [33] (≈0.150 MeV) by different methods. We may conclude that the agreement between theoretical, and experimental results is good.

	$\frac{B(E2;I^-\to(I-1)^-)}{B(E2;I^-\to(I-2)^-)}$		$\frac{B(M1;I^-\to(I-1)^-)}{B(E2;I^-\to(I-2)^-)}$ $[\frac{\mu_N^2}{e^2b^2}]$		$\delta_{I^-\to(I-1)^-}$ [MeV.fm]	
I^π	Exp.	Th.	Exp.	Th.	Exp.	Th.
$\frac{21}{2}^-$	0.843±0.032	0.400	0.164± 0.014	0.08	-1.54± 0.09	-1.971
$\frac{25}{2}^-$	0.500±0.025	0.450	0.035± 0.009	0.056	-2.384±0.37	-2.818
$\frac{29}{2}^-$	≥0.261±0.014	0.497	≤ 0.016±0.004	0.041	-	-3.825
$\frac{33}{2}^-$	-	0.543	-	0.031	-	-5.000

TABLE II: The calculated branching ratios $B(E2)_{out}/B(E2)_{in}$, and $B(M1)_{out}/B(E2)_{in}$ as well as the mixing ratios δ are compared with the corresponding experimental data taken from Ref. [34].

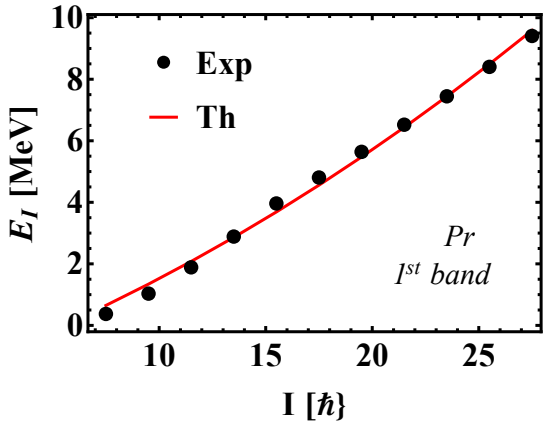

FIG. 11: (Color online) The excitation energies yielded by our calculations for the first band of ^{135}Pr, using the MoI's, and θ determined by a fitting procedure, are compared with the experimental excitation energies from the yrast band [35].

From Table I we see that the MoI's ordering predicted by our calculations is: $\mathcal{J}_1 > \mathcal{J}_3 > \mathcal{J}_2$. However, due to the adopted fitting procedure this, however, is a global result. In order to check whether this ordering holds also by using another fitting procedure, we fixed the MoI's by equating the calculated excitation energies for the lowest two states of band 1 and the second state of band 2, otherwise fixing θ to obtain a global best fit. In this way we found a set of MoI,s which reclaims a transverse wobbling regime for the odd system under consideration. Indeed, for $\theta = 140^0$, the result is $\mathcal{J}_1 = 13.53[\hbar^2/MeV]$, $\mathcal{J}_2 = 101.76[\hbar^2/MeV]$, $\mathcal{J}_3 = 52.94[\hbar^2/MeV]$. However, the overall agreement with experiment does not improve the results obtained by the initial fit method. We also plotted the potential determined by the fitted parameters

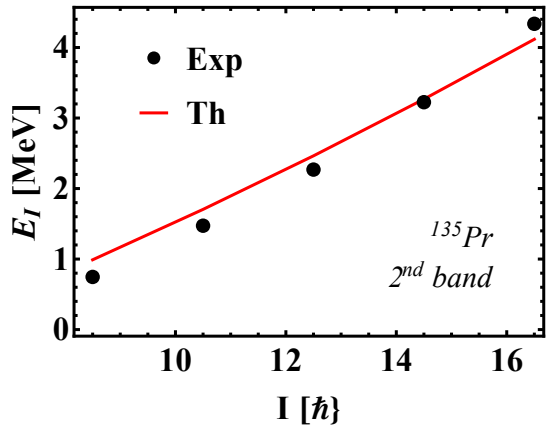

FIG. 12: (Color online) The excitation energies for the second band of ^{135}Pr, with the parameters determined as explained in the text, are compared with the experimental excitation energies from the TW1 band [35].

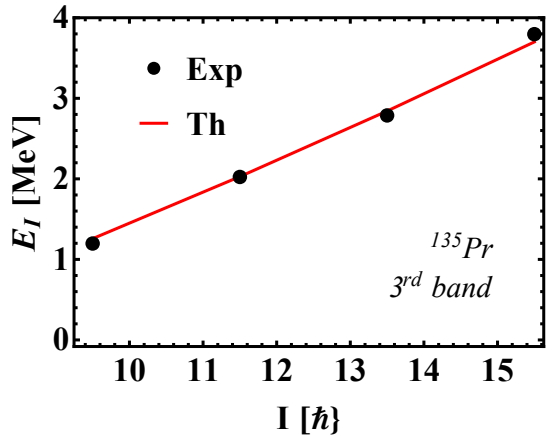

FIG. 13: (Color online) The excitation energies for the one phonon band of ^{135}Pr, with the parameters determined as explained in the text, are compared with the experimental excitation energies from the TW2 band [35].

and I=19/2. The result is of the type given in Fig.5, i.e., the deepest minimum is placed at $q = 0$. In this point $I_1 = I$, which means that the angular momentum is oriented along the one axis. Therefore, $\mathcal{J}_2$= maximal, does not necessarily mean that the rotation axis is the 2-axis. The fact that the maximal MoI established by a global fit is $\mathcal{J}_1$, indicates that for a larger angular momentum a change of MoI hierarchy takes place, and a new nuclear phase begins.

B. Comment on the chiral features of the wobbling motion

We recall that a chiral transformation brings a right-handed reference frame to a left-handed one. In the angular momentum space, the change of sign of the a.m. defines a chiral transformation. A system is invariant to a chiral transformation if its rotational energy is preserved when the sense of rotation around an axis is changed. Note that our starting Hamiltonian is a sum of two terms, one being symmetric and one antisymmetric with respect to chiral transformations.

$$\hat{H}_{rot} = \hat{H}_s + \hat{H}_a. \tag{7.2}$$

If $|\psi\rangle$ is an eigenstate for $\hat{H}_s$, and C is a chiral transformation, then $C|\psi\rangle$ is also eigenstate for $\hat{H}_s$, and corresponds to the same energy. In this case, the function $|\psi\rangle$ has the chirality equal to one, since $C|\psi\rangle = |\psi\rangle$. For $\hat{H}_a$, the above mentioned property changes to : If $|\psi\rangle$ is an eigenstate of $\hat{H}_a$ corresponding to the eigenvalue E, then $C|\psi\rangle$ is also eigenstate, but corresponding to the energy $-E$. Therefore, the eigenvalues of $\hat{H}_a$ split in two sets, one being the mirror image of the other one. This property is of a chiral nature. The eigenstates of $\hat{H}_a$ have the chirality -1 since $C|\psi\rangle = -|\psi\rangle$. The eigenstates of $\hat{H}_{rot}$ are mixtures of the two chiralities. When there are two sets of energies that are one the mirror image of the other, one says that a definite chirality is projected out [23]. In our calculation, the change of $\mathbf{I} \to -\mathbf{I}$ is achieved by changing θ to $\theta + \pi$. The a.m. dependence of the wobbling frequencies corresponding to $\theta = -71^0$, and $\theta = 109^0$ respectively, is shown in Fig. 14. The look of the potentials V, and CVC^{-1}, are shown in Figs.4 and 5 for $\theta = \pi/6$, and $\theta = 7\pi/6$ respectively, and $\mathcal{J}_2 : \mathcal{J}_3 : \mathcal{J}_1 = 100 : 40 : 20\hbar^2 MeV^{-1}$. From these two potentials we may extract the symmetric, and antisymmetric parts of V.

$$V_s = \frac{1}{2}V(\pi/6) + V(7\pi/6); \;\; V_a = \frac{1}{2}V(\pi/6) - V(7\pi/6). \tag{7.3}$$

The two potentials of definite chirality, are visualized in Fig. 15 and fig.16, respectively. A similar analysis can be performed also for the excitation energies. Indeed, Eq.(4.4) expresses explicitly the dependence of the wobbling frequency on the angle θ, which fixes the orientation of $\mathbf{j}$. Therefore, it is easy to calculate $\omega_I(\theta + \pi)$, with $\theta = -71^0$. The frequencies $\omega_I(\theta)$ and $\omega_I(\theta + \pi)$, with one being the chiral image of the other one, are plotted in Fig.14 for the yrast band. The two curves are parallel to each other, which suggests that the corresponding states have similar properties. However, they do not correspond to states of definite chirality. However, one can extract the symmetric, and antisymmetric terms of the excitation energy. Here we give the result for the yrast states:

$$\begin{aligned} &E^{exc;1}_{I,s} = A_1 I^2 + \left(\omega_I(\theta) + \omega_I(\theta+\pi)\right)/2 - E_{11/2}, \\ &I = R + j, \;\; R = 0, 2, 4, .. \\ &E^{exc;1}_{I,a} = (2I+1)A_1 j_1 - I A_2 j_2 + \left(\omega_I(\theta) - \omega_I(\theta+\pi)\right)/2, \\ &I = R + j, \;\; R = 0, 2, 4, .., \theta = -71^0. \end{aligned} \tag{7.4}$$

Since for asymmetric states, the energies $-E^{exc;1}_{I,a}$ are also eigenvalues of the antisymmetric Hamiltonian, we inter-

pret the two sets of energies $E^{exc;1}_{I,s}$, and $-E^{exc;1}_{I,a}$ as defining two bands of chirality +1, and -1, respectively. The relative energies to the head-energy of each band respectively, are plotted in Fig.17. Although the two sets of energies have different dependence on the angular momentum, one is linear (asymmetric) and the other one quadratic in a.m., the energy spacing in the two bands are close to each other, which in fact is a chiral feature of the two bands. Although we don't have enough data to conclude that the two bands are indeed of real chiral type, due to the above mentioned features, they might be, however, considered as germinos of chiral bands. Indeed, there are properties unanimously accepted, which prevent us to make a decisive statement on this matter. For a chiral band the system rotates around an axis, which doesn't belong to any of principal planes, while here the rotation axis is a principal axis. However, since in our case the Hamiltonian involves linear terms in the total angular momentum, the wobbling motion and chiral properties seem not to be disconnected.

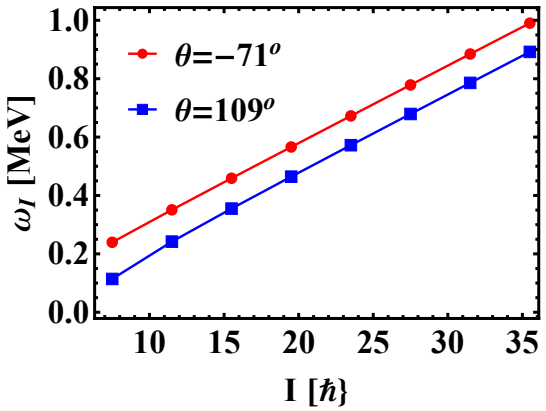

FIG. 14: (Color online) The wobbling frequencies corresponding to the angles $\theta = 109^0$, and $\theta = -71^0$, respectively.

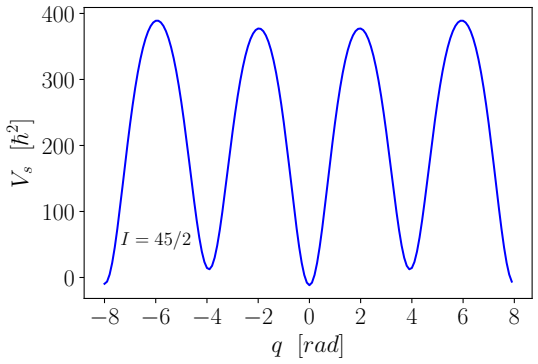

FIG. 15: (Color online) The symmetric potential, with respect to the chiral transformations, as function of q.

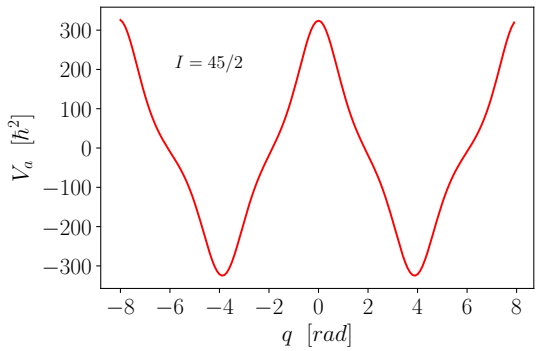

FIG. 16: (Color online) The antisymmetric potential, with respect to the chiral transformations, as function of q.

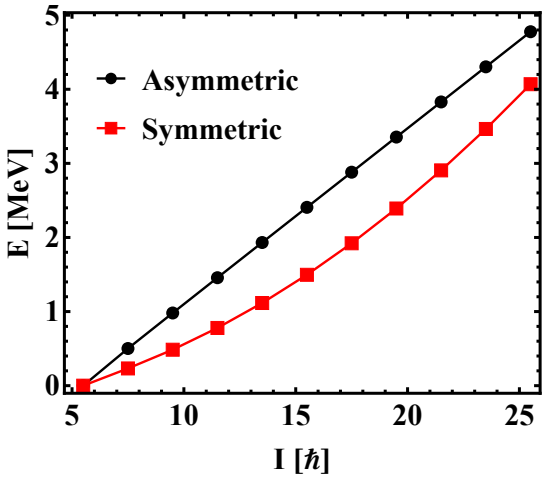

FIG. 17: (Color online)Energies of symmetric and antisymmetric states against chiral transformations, normalized to the head-energy for each band.

C. Electromagnetic transitions

The electric quadrupole reduced transition probabilities were calculated by means of Eq. (6.11), where the reduced matrix elements are those given by (6.10) for the intra-band, and (6.11), for the inter-band transitions. These expressions involve two strength parameters of the quadrupole transition operator, denoted by $\bar{Q}_0$, and $\bar{Q}_2$, respectively. These were determined by fitting two particular branching ratios which results in obtaining the values: $\bar{Q}_0 = -28.86\ e.fm^2/\hbar^2$, and $\bar{Q}_2 = 131.11\ e.fm^2/\hbar^2$. Note that the initial and final wavefunctions were determined by the energy calculations, which in fact connect the e.m. transitions to the structure of the model Hamiltonian. The results are given in Table II, where the available corresponding experimental data [34] are also listed. One notices a reasonable good agreement between the results of our calculations, and the experimental data. The increasing function of the a.m. for the ratio $B(E)_{out}/B(E)_{in}$ is well reproduced. Also, the sign of the mixing ratio, and the

increasing behavior with I, are also consistent with the data, although the magnitudes of the experimental data exceed the calculated values by a factor of about 3.

VIII. CONCLUSIONS

The formalism developed in the previous sections may be summarized as follows. A new boson expansion is proposed to describe the wobbling motion in even-odd nuclei. The used Hamiltonian has a simple structure obtained from that describing the even-even core, i.e., a triaxial rotor, by replacing the core angular momentum $\mathbf{R}$ with $\mathbf{I}-\mathbf{j}$, where $\mathbf{I}$ and $\mathbf{j}$ denote the total and odd particle angular momenta, respectively. The coupling term, describing the motion of the odd nucleon in a deformed mean field generated by the core [52] is ignored, since the odd particle is rigidly coupled to the core, and thereby does not affect the excitation energy spectrum for the odd system. The model Hamiltonian is written in a boson space by using for angular momentum an "elliptic boson expansion". Subsequently, the Bargmann representation is employed, and the eigenvalue equation of the initial model Hamiltonian is brought to a Schrödinger equation form, where the kinetic and potential energy terms are fully separated. The potential is angular momentum dependent, and exhibits several minima, and maxima. Expanding, successively, the potential around the deepest and the local minima, one arrives at two distinct expressions for the wobbling frequency. These results are also obtained within a classical picture, where the phase diagram is constructed for a particular value of I (=15/2). The frequency associated to the deepest minimum is used to describe the energies of the three bands seen in ^{135}Pr. Due to the presence of linear terms, a possible chiral behavior for the odd system is expected. One succeeds to build up states of a definite chirality. However, it is hard to call the resulting bands as twin bands, although some embryos of them are present. The electromagnetic reduced transition probabilities are calculated by using for the quadrupole transition operator a quadratic form in the angular momentum. Results for the branching ratios $B(E2)_{out}/B(E2)_{in}$, and $B(M1)_{out}/B(E2)_{in}$, as well as for the mixing ratios δ, are compared with the available data. One concludes that the agreement with experimental data for both energies, and e.m. transitions is reasonable good. It is pointed out that, although we started with the hypothesis that the maximal MoI is that of the 2-axis, the fitting procedure yielded as maximal MoI that of the 1-axis. There is a two fold reason causing that:a) the renormalization of the MoI, due to the linear terms in angular momentum and b) the Coriolis interaction simulated by the term proportional to I_1. At classical level, one showed that the transverse wobbling motion is unstable.

We may assert that the results of the present paper confirm the importance of the boson expansion concept, which was widely used in different contexts of theoretical nuclear physics [61–64].

Concluding, the present formalism provides an interesting tool to investigate the theoretical aspects of the wobbling motion in even-odd nuclei and to describe the existent data in a realistic fashion.

Acknowledgment. This work was supported by the Romanian Ministry of Research and Innovation through the project PN19060101/2019

[1] A. Bohr and B. Mottelson, *Nuclear Structure* (Benjamin, Reading, MA, 1975), Vol. II, Ch. 4.
[2] E. R. Marshalek, Nucl. Phys. **A 331**, 429, (1979).
[3] S. W. Odegard, *et al.*, Phys. Rev. Lett. **86**, 5866, (2001).
[4] D. R. Jensen *et al.*, Nucl. Phys. **A 703**, 3, (2002).
[5] I. Hamamoto *et al.* Acta. Phys. Pol. **B32**, 2545, (2001).
[6] G. Schoenwasser *et al.*, Phys. Lett. **B 552**,9, (2003).
[7] H. Amro *et al.*, Phys. Lett. **B 553**, 197, (2003).
[8] A. Görgen et al., Phys. Rev **C 69**, 031301(R), (2004).
[9] I. Hamamoto, Phys. Rev. **C 65**, 044305, (2002).
[10] M. Matsuzaki, Y. R. Shimizu, K. Matsuyanagi, Phys. Rev. **C 65**, 041303(R), (2002); Yoshifumi R. Shimizu, Masayuki Matsuzaki and Kenichi Matsuyanagi,arXiv:nucl-th/0404063v1, 22 Apr. 2004.
[11] I. Hamamoto and G. B. Hagemann, Phys. Rev. **C 67**, 014319, (2003).
[12] D. R. Jensen *et al.*, Eur. Phys. J. **A 19**, 173, (2004).
[13] G. B. Hagemann, Eur. Phys. J. **A 20**, 183, (2004).
[14] K. Tanabe and K. Sugawara-Tanabe, Phys. Rev. **C73**, 034305, (2006).
[15] Makito Oi, Phys. Lett. **B 634**, 30 (2006).
[16] A. A. Raduta, R. Budaca and C. M. Raduta, Phys. Rev. C, **76**, 064309,(2007).
[17] P. Bringel *et al.* Eur. Phys. J. **A 24**, 167, (2005).
[18] G. B. Hagemann *et al.*, Phys. Rev. Lett. 86, 5866 (2001).
[19] D. J. Hartley *et al.*, Phys. Rev. **C 80**, 041304(R), (2009).
[20] R.F. Casten, E. A. McCutchan, N. V. Zamfir, C. W. Beausuang and Jing-ye Zhang, Phys. Rev. **C 67**, 064306, (2003).
[21] D. Almehed, R. G. Nazmitdinov and F. Dönau, Phys. Scr. **T125**, 139, (2006).
[22] I. N. Mikhailov and D. Janssen, Phys. Lett. **72B**, 303, (1978).
[23] A. A. Raduta, Progress in Particle and Nuclear Physics 90, 241, (2016).
[24] M.Badea and A. A. Raduta, Rev. Roum. Phys. 21 , 743, (1979).
[25] A. A. Raduta, R. Poenaru and L. Gr. Ixaru, Phys. Rev. C **96**, 054320, (2017).
[26] A. A. Raduta, R. Poenaru and Al. H. Raduta, J. Phys. G: Nucl. Part. Phys. **45** 105104 (2018).
[27] A. A. Raduta, R Poenaru and C M Raduta, J. Phys. G: Nucl. Part. Phys. **47**,025101 (2020).
[28] A. A. Raduta, R Poenaru and C M Raduta, Phys. Rev. C **101**, 014302 (2020).
[29] Kosai Tanabe and Kazuko Sugawara Tanabe, Phys. Rev.

C **95**, 064315, (2017).
[30] Kosai Tanabe and Kazuko Sugawara Tanabe, Phys. Rev. C **97**,069802 (2018).
[31] S. Frauendorf and F. Donau, Phys. Rev. C **89**,014322, (2014).
[32] S. Frauendorf, Phys. Rev. **C97**, 069801 (2018).
[33] R. Budaca, Phys. Rev. C **97**, 024302, (2018).
[34] J. T. Matta *et al.*, Phys. Rev. Lett. **114**, 082501 (2015).
[35] N. Sensharma *et al.*,Phys. Lett. B **792**, 170 (2019).
[36] N. Sensharma *et al.*,Phys. Rev. Lett. **124**, 052501 (2020).
[37] S. Biswas *et al.*,European Physical Journal A, 5, 12856 (2019).
[38] J. Timar *et al.*, Phys. Rev. Lett. **122**, 062501 (2019).
[39] K. Rojeeta Devi, Proc. of the DAE Symp. on Nucl. Phys. 62, 308 (2017).
[40] Q.P.Chen,S. Q. Zhang and J. Meng, Phys. Rev. **C 94**, 054308 (2016).
[41] E. A. Lawrie, O, Shirinda and C. M. Petrache, Phys. Rev. C **101**, 034306 (2020).
[42] T. Holstein and H. Primakoff, Phys. Rev. **58**, 1098 (1940).
[43] T. F. Dyson, Phys. Rev. **102**,1217 (1958).
[44] V. Bargmann, Rev. Mod. Phys. **34**, 829(1962).
[45] J. Goldstone, Nuovo Cimento **19**, 154 (1961).
[46] A.S. Davydov and G.F. Filippov, Nucl. Phys. **8**, 788, (1958).
[47] L. Wilets and M. Jean, Phys. Rev. **102**, 788 (1956).
[48] J. Meyer-ter-Vehn, Nucl. Phys. **A249**, 111, 141, (1975).
[49] D. Bonatsos, D. Lenis, D. Petrellis and P. A. Terziev, Phys. Lett. **B 588** 172,(2004).
[50] D. Bonatsos, D. Lenis, D. Petrellis, P. A. Terziev and I. Yigitoglu, Phys. Lett. **B 621**, 102, (2005).
[51] A. A. Raduta, *et al.*, Nucl. Phys. **A 819**, 46 (2009).
[52] A.C. Davydov, *Teoria atomnova yadra*, Moscva, 1958 (in russian), chapters 19,20.
[53] H. Toki and Amand Faessler, Nucl. Phys. **A 253**, 231 (1975).
[54] H. Toki and Amand Faessler, Z. Physik **A 276**, 35 (1976).
[55] H. Toki and Amand Faessler, Phys. Lett. **B 63**, 121 (1976).
[56] H. Toki, K. Neergard, P. Vogel, and Amand Faessler, Nucl. Phys. **A 279**, 1 (1977).
[57] H. Toki, H. L. Yadav, A. Faessler, Phys. Lett. **B 66**, 310 (1977).
[58] T. Oguchi, Progr. Th. Phys, **25**,721 (1961).
[59] A. Gheorghe, A. A. Raduta, V. Ceausescu, Nucl. Phys. A 637, 201, (1998).
[60] M. E. Rose, *Elementary Theory of Angular Momentum* (Wiley, New York, 1957).
[61] D. Janssen, F. Donau, S. Frauendorf and R. V. Jolos, Nucl. Phys. **A 172**, 145 (1971).
[62] V. Ceausescu, A. A. Raduta, Prog. Th. Phys. **52** (3), 903 (1974)
[63] A.A.Raduta, A.Faessler and S.Stoica. Nucl.Phys.A 534, 149, (1991).
[64] A. Klein and E. R. Marshalek, Rev. Mod. Phys. **63**, 375 (1991).
[65] The convention of Rose [60] for the reduced matrix elements has been used

New results about the canonical transformation for boson operators

C. M. Raduta [a] and A. A. Raduta[a),b)]
[a] *Department of Theoretical Physics, Institute of Physics and Nuclear Engineering, Bucharest, POBox MG6, Romania and*
[b] *Academy of Romanian Scientists, 54 Splaiul Independentei, Bucharest 050094, Romania*

The Bogoliubov transformation for a monopole boson induces an unitary transformation connecting the Fock spaces of initial and correlated bosons. Here we provide a very simple method for deriving the analytical expression for the overlap matrix of the basis states generating the two boson spaces.

I. INTRODUCTION

The boson operators are widely used in various branches of Physics. In particular, Nuclear Physics benefited of this concept in many respects. Thus, in the many body theories the particle-hole or particle-particle operator are approximated with bosons which results in having by far a more tractable method, known under the name of the Random Phase Approximation (RPA)[1]. Going beyond RPA, one has been introduced the concept of the boson expansion method where pairs of fermion operators are replaced by boson series, afterwards truncated such that their algebra be conserved [2–4]. Concerning phenomenological methods, all of them are using in a way or another bosons as a device for tackling various physical problems. To give only a few examples we mention the Interacting Boson Approximation [5, 6], the Coherent State Model [7], the boson description of the triaxial rotor [8–10]. In some of the mentioned cases, for simplicity reasons, the model boson Hamiltonian is truncated at second order. To treat this form, in order to get rid of the cross terms, which raise convergence difficulties, one uses a canonical transformation defining new bosons in terms of which the dangerous terms do not show up. To each type of bosons, initial or transformed, one associates a basis generating two boson spaces, respectively. Long time ago, the unitary transformation connecting the mentioned bases was analytically expressed [11–13].

The solution provided in the quoted references deals either with a single boson or with a boson carrying a nonvanishing momentum. For a many body system the subject becomes more complex. Indeed, the connection of the RPA vacuum state and the BCS wave-function, if the phonon excitations are performed by a coherent linear combination of two quasi-particle and two quasi-hole operators, or of the RPA ground state and the Hartree-Fock vacuum, when the collective states are particle-hole excitations of the HF ground state, is derived by solving iteratively a nonlinear system of equations. We restrict our consideration to a monopole boson, on base of which the boson representation of the angular momenta involved in a triaxial rotor Hamiltonian is built up. In literature, four types of such representation are known: a) Holstein-Primakoff [14]; b) Dyson [15] c)Bargmann [16] and d) Raduta [17]. Each of these boson representations provides a realistic description of the wobbling motion in medium and heavy nuclei [8–10, 17].

The present paper provides an analytical expression for the above mentioned unitary transformation, by a distinct method, which seems to be simpler than the previous solutions. To touch this goal we organized the paper as follow. In section 2 we treat a second order boson Hamiltonian H, through the Bogoliubov (B) transformation. In section 3 we use the Bargmann representation, where the eigenvalue equation for H is transformed into a Schrödinger equation for a harmonic oscillator, whose wave-function belongs to the correlated boson basis. Going back to the boson picture the matrix, we are looking for, is readily obtained. A short summary of the procedure is presented in section 4.

II. THE BOSON HAMILTONIAN

Here we aim at finding the eigenstates and corresponding eigenvalues of the following boson Hamiltonian:

$$H = \epsilon b^\dagger b - X(b^{\dagger 2} + b^2), \tag{2.1}$$

where $b^\dagger$ and b are boson operator,i.e. obey the commutation relation:

$$\left[b, b^\dagger\right] = 1. \tag{2.2}$$

The properties of H are studied within the boson space generated by the basis:

$$|k\rangle = \frac{b^{\dagger k}}{\sqrt{k!}}|0\rangle, k = 1, 2, 3, ... \tag{2.3}$$

with $|0\rangle$ denoting the vacuum state for the boson operators, obeying the equation $b|0\rangle = 0$. The boson operator satisfy the equations of motion:

$$\begin{aligned}\left[H, b^\dagger\right] &= \epsilon b^\dagger - 2Xb,\\ [H, b] &= -\epsilon b + 2Xb^\dagger.\end{aligned} \tag{2.4}$$

Since the equations of motion are linear in the boson operators, one can define the linear combination

$$\tilde{b}^\dagger = Ub^\dagger - Vb, \tag{2.5}$$

such that the following equations hold:

$$\left[H, \tilde{b}^\dagger\right] = \omega\tilde{b}^\dagger, \quad \left[\tilde{b}, \tilde{b}^\dagger\right] = 1. \tag{2.6}$$

These equations assert that the new operators are also of boson type and moreover, in terms of the new operators the Hamiltonian is harmonic. The first equation (2.6) provides a homogeneous system of equations, for the amplitudes U and V, whose compatibility condition leads to the following expression for the energy ω:

$$\omega = \epsilon\sqrt{1-4\kappa^2}, \;\; \text{with} \;\; \kappa = \frac{\mathrm{X}}{\epsilon}. \tag{2.7}$$

Noticeable the fact that the defined excitation energy ω exists if $|\kappa| \leq 1/2$. For $\epsilon = \pm 2X$ the solution is vanishing which results a critical value for a phase transition [18]. The system becomes unstable for $X > \frac{1}{2}\epsilon$ or $X < -\frac{1}{2}\epsilon$. As for the unknowns U and V, they are determined up to a multiplicative constant to be fixed by the normalization equation given by the second equation (2.6):

$$U^2 - V^2 = 1. \tag{2.8}$$

The result for U and V is :

$$\begin{pmatrix} U^2 \\ V^2 \end{pmatrix} = \frac{1}{2}\left(\pm 1 + \frac{1}{\sqrt{1-4\kappa^2}}\right). \tag{2.9}$$

To the newly defined boson operators, one associates the basis states:

$$|\tilde{m}\rangle = \frac{\tilde{b}^{\dagger m}}{\sqrt{m!}}|\tilde{0}\rangle, \;\; \tilde{b}|\tilde{0}\rangle = 0. \tag{2.10}$$

The goal of the present paper is to provide an analytical expression for the overlap matrix:

$$G_{mn} = \langle m|\tilde{n}\rangle. \tag{2.11}$$

This objective will be accomplished in the next section. Note that the transformation (2.5) can be written in an alternative form:

$$\begin{aligned}\tilde{b}^\dagger &= Tb^\dagger T^\dagger = Ub^\dagger - Vb,\\ \tilde{b} &= TbT^\dagger = Ub - Vb^\dagger, \;\; \text{with}\\ T &= e^S, \;\; S = \frac{1}{2}y(b^{\dagger 2} - b^2), \;\; \text{and}\\ U &= \cosh y, \;\; V = \sinh y.\end{aligned} \tag{2.12}$$

The transformation (2.5) can be reversed, and thus H can be expressed in terms of the new boson operators. The result is:

$$H = -\frac{1}{2}(\epsilon - \omega) + \omega\tilde{b}^\dagger\tilde{b}. \tag{2.13}$$

Note that in terms of the new bosons, the cross term $\tilde{b}^{\dagger 2} + b^2$ does not show up. The transformation (2.5) is known under the name of the Bogoliubov transformation.

We may ask ourself, why we don't consider also the linear term in the bosons, $b^\dagger, b$. The answer is yes we could do that, but the corresponding Hamiltonian can be brought to the form (2.13) by the simple transformation $b^\dagger \to a^\dagger + c, b \to a + c$ with c a real number determined such that the hew Hamiltonian does not comprise linear terms in the new bosons $a^\dagger, a$. The transformation mentioned above is known under the name of *the boson deformation*.

III. AN ALTERNATIVE TREATMENT OF H

For what follows it is useful to introduce the Bargmann representation for the boson $b^\dagger$ and b, through the mapping

$$b^\dagger \to x, \;\; b \to \frac{d}{dx}, \tag{3.1}$$

where x denotes a real variable. Thus, the eigenvalue equation associated to H becomes a differential equation:

$$\epsilon x \frac{d\Psi}{dx} - X\frac{d^2\Psi}{dx^2} - Xx^2\Psi = E\Psi. \tag{3.2}$$

By a suitable change of function:

$$\Psi = e^{\frac{x^2}{4\kappa}}\Phi, \tag{3.3}$$

one gets rid of the first order derivative term and (3.2) acquires the Schrödinger form:

$$-\frac{1}{2m}\frac{d^2\Phi}{dx^2} + \frac{m\omega^2}{2}x^2\Phi = (E + \frac{\epsilon}{2})\Phi, \tag{3.4}$$

where

$$m = \frac{1}{2V}, \tag{3.5}$$

and the unit system of $\hbar = c = 1$ has been used. We recognize in Eq. (3.4), the Schrödinger equation for a linear oscillator of mass m and frequency ω. The oscillator energies are:

$$E_n + \frac{\epsilon}{2} = \omega(n + \frac{1}{2}), n = 0, 1, 2, ... \tag{3.6}$$

By comparison, one finds out that these are just the eigenvalues of H, derived in the previous section. Correspondingly, the eigenfunction $|\tilde{n}\rangle$ coincides with the function:

$$\begin{aligned} \Psi_n &= C_n H_n(\frac{x}{r}) \exp\left[\left(-\frac{1}{2}m\omega + \frac{1}{4\kappa}\right)x^2\right] \\ &= C_n H_n(\frac{x}{r}) \exp\left[V^2\frac{x^2}{r^2}\right]. \end{aligned} \tag{3.7}$$

Here H_n denotes the Hermite polynomial of rank n, C_n is the normalization factor, while r stands for the oscillator length defined by:

$$r^2 = \frac{1}{m\omega} = 2UV. \tag{3.8}$$

One can check that:

$$-\frac{1}{2}m\omega + \frac{1}{4\kappa} = \frac{V^2}{r^2}. \tag{3.9}$$

Using the analytical expression for the Hermite polynomial and the Taylor expansion for the exponential function one obtains:

$$|\tilde{n}\rangle = C_n \sum_{m,p} \frac{(-1)^{\frac{n-p}{2}} n! 2^p V^{m-p} (\frac{x}{r})^m}{(\frac{n-p}{2})! p! (\frac{m-p}{2})!}. \tag{3.10}$$

The constant C_n can be determined either by brute calculations, restricting the norm of $|\tilde{n}\rangle$ be equal to unity or by the more elegant procedure described in Appendix A. Using the result from there, (A.8), and the obvious relation

$$\langle 0|\tilde{n}\rangle = \frac{(-1)^{\frac{n}{2}}}{\frac{n}{2}!} C_n = \frac{T_{0,n}}{\sqrt{n!}}, \tag{3.11}$$

one arrives at:

$$C_n = \frac{V^{\frac{n}{2}} U^{-\frac{m+1}{2}}}{2^{\frac{n}{2}}\sqrt{n!}}. \tag{3.12}$$

We recall that we use the Bargmann representation and therefore the vacuum state normalized to unity is $|0\rangle = 1$ and $|m\rangle = \frac{b^{\dagger m}}{\sqrt{m!}}|0\rangle$. Multiplying, to the left, the equation (3.10) with $|m\rangle$, and replacing C_n with the expression just obtained, we get:

$$\langle m|\tilde{n}\rangle = \sqrt{m!n!}U^{-\frac{m+n+1}{2}} \sum_p \frac{(-1)^{\frac{m-p}{2}} \left(\frac{V}{2}\right)^{\frac{m+n}{2}-p}}{\left(\frac{m-p}{2}\right)! \left(\frac{n-p}{2}\right)! p!}. \tag{3.13}$$

Obviously, the summation index p is subject to the restrictions:

$$m - p = even, \;\; n - p = even, \;\; p \leq \min\{m, n\}. \tag{3.14}$$

Moreover, $|m - n| = even$.

This expression (3.13) is identical to those obtained in Refs.[11–13] by different methods.

IV. SUMMARY

In the present paper we derived analytical expression for eigenvalues and eigenstates of a second order boson Hamiltonian by using two alternative methods: a)through a canonical transformation the Hamiltonian is brought to a diagonal form. The eigenstates are correlated multi-phonon states. We looked for analytical expression for the overlap matrix of correlated and non-correlated bosons. b) In the Bargmann representation the eigenvalue relation associated to H becomes the Schrödinger equation for a harmonic oscillator.The wave-function, which is a product of an exponential function and a Hermite polynomial, provides the searched overlap matrix as coefficients of the associated Taylor series. The result is identical with that previously obtained by Tanabe [11], Rashid [12] and Raduta [13] using distinct methods, respectively. These pioneers did a wonderful job and we are glad to add to the subject by providing a simpler method of getting their results.

Concluding, the main result consists in the expression (3.13) describing the mentioned overlap matrix. As mentioned already, this expression is very useful in many formalisms dealing with monopole bosons.

Acknowledgments. This work was supported by UEFISCU through the project PCE- 16/2021

V. APPENDIX A

Here we shall derive the analytical expression for the constant C_n involved in Eq. (3.10).

Let us denote by $T_{m,n}$ the matrix elements of the canonical transformation (2.12) in the basis (2.3):

$$T_{m,n}(y) = \langle 0|b^m T b^{\dagger n}|0\rangle. \tag{A.1}$$

From here, one easily obtains the iterative equations:

$$\begin{aligned} T_{0,n} &= -VT_{1,n-1}, \\ T_{1,n-1} &= U(n-1)T_{0,n-2} - VT_{0,n}. \end{aligned} \tag{A.2}$$

which leads to:

$$T_{0,n} = -\frac{V}{U}(n-1)T_{0,n-2}. \tag{A.3}$$

Applying successively this iterative relation, one finds:

$$T_{0,n} = (-\frac{V}{U})^{\frac{n}{2}} \frac{n!}{2^{\frac{n}{2}}(\frac{n}{2})!} T_{0,0}. \tag{A.4}$$

As for $T_{0,0}$ it satisfies the differential equation

$$\frac{d}{dy}T_{0,0} = T_{0,2} = -\frac{V}{2U}T_{0,0}. \tag{A.5}$$

and the initial condition:

$$T_{0,0}(0) = 1. \tag{A.6}$$

The solution is:

$$T_{0,0} = U^{-1/2}. \tag{A.7}$$

Consequently:

$$T_{0,n} = (-V)^{\frac{n}{2}} U^{-\frac{n+1}{2}} \frac{n!}{2^{\frac{n}{2}}(\frac{n}{2})!}. \tag{A.8}$$

---

[1] L. Kisslinger and R. A. Sorensen, Rev. Mod. Phys. **35**, 853 (1963).
[2] D.Jansen,F. Donau, S. Frauendorf and R. V. Jolos, Nucl. Phys. A **172**,145 (1971).
[3] V. Ceausescu and A. A. Raduta,Prog. Th. Phys.52(3), 903(1974).
[4] A. Klein and E. R. Marshalek, Rev. Mod. Phys. 63, 375 (1991).
[5] A. Arima, F. Iachello, Ann. Phys. (N.Y.) **91**, 253 (1976).
[6] A. Arima, F. Iachello, Ann. Phys. (N.Y.) **123**, 468 (1976).
[7] A. A. Raduta, *et al.*, Nucl. Phys. **A 381**,253 (1981); Phys. Lett. **B 99**, 444(1982).
[8] M. Badea and A. A. Raduta, Rev. Roum. Phys. **21**, 743 (1979).
[9] K. Tanabe and K. Sugawara-tanabe, Phys. Rev. **C 73**, 034305 (2006).
[10] Makito Oi, Phys. Lett. **B 634**, 30 (2006).
[11] K. Tanabe, J. Math. Phys. **14**, 618 (1973).
[12] M. A. Rashid, J. Math. Phys. **16**, 378 (1973).
[13] A. A. Raduta, M. Badea and E. Badralexe , J. Math. Phys. **18**, 678 (1977).
[14] T. Holstein and H. Primakoff, Phys. Rev. **58**, 1098 (1940).
[15] T. F. Dyson, Phys. Rev. **102**,1217 (1958).
[16] V. Bargmann, Rev. Mod. Phys. **34**, 829(1962).
[17] A. A. Raduta, C. M. Raduta and R. Poenaru, Jour. Phys. G: Nucl. Part. Phys.48, 015106 (2021)
[18] J. Goldstone, Nuovo Cimento **19**, 154 (1961).

Parity Partner Bands in ^{163}Lu: A novel approach for describing the negative parity states from a triaxial super-deformed band

R. Poenaru*
Doctoral School of Physics, University of Bucharest and Horia Hulubei National Institute of Nuclear Physics and Engineering, Magurele

A. A. Raduta†
Horia Hulubei National Institute of Nuclear Physics and Engineering, Magurele and Academy of Romanian Scientists, Bucharest

(Dated: February 12, 2021)

The wobbling spectrum of ^{163}Lu is described through a novel approach, starting from a triaxial rotor model within a semi-classical picture, and obtaining a new set of equations for all four rotational bands that have wobbling character. Redefining the band structure in the present model is done by adopting the concepts of Signature Partner Bands and Parity Partner Bands. Indeed, describing a wobbling spectrum in an even-odd nucleus through signature and parity quantum numbers is an inedited interpretation of the triaxial super-deformed bands.

The wobbling motion was first described by Bohr and Mottelson within a particle triaxial rotor coupling, where the rotation axis moves on a curly cone. This sort of motion is a signature of the triaxial nuclei, these being not much considered across the time. Although it was firstly predicted theoretically for even-even nuclei [1], this collective mode was also pointed out in several even-odd nuclei, with ^{163}Lu being considered the best *wobbler*, mainly due to its relatively rich spectrum: four triaxial super-deformed bands $TSD_{1,2,3,4}$. The TSD_1 is interpreted as the ground state - yrast - band, while the other three as wobbling multi-phonon excited bands [2, 3]. The common view on these bands is that the alignment of the odd-proton angular momentum, $i_{13/2}$ drives the system to very large stable deformation. In the meantime, several neighboring odd-nuclei were identified as wobblers i. e. , ^{161,165,167}Lu [3–7, 10],,and recently the nuclei ^{135}Pr [8, 9], ^{167}Ta [10, 11], ^{187}Au [12], ^{130}Ba[13], ^{105}Pd [14], ^{127}Xe [15], and ^{183}Au [16].

In a previous work [18, 19], a successful description of the wobbling phenomenon in ^{163}Lu was achieved. Therein, the calculations were based on a particle-triaxial rotor system, that was semi-classically treated. The band structure was obtained in terms of two ground state bands (TSD1 and TSD2) of different signatures, given by coupling an odd $j = i_{13/2}$ proton to a core with angular momenta R=0,2,4,6,. . and R=1,3,5,. . . . , respectively, one wobbling phonon excitation of the TSD2 band, $n_w = 1$, TSD_3, and one ground state band obtained by coupling a different valence nucleon, namely the $j = h_{9/2}$ to a core exhibiting an a. m. from the sequence $\mathbf{R} = 0, 2, 4, \ldots$.

Here we address the question whether the four TSD bands could be described by coupling a unique single particle state, i. e. $i_{13/2}$, to a core of a natural parity for $TSD_{1,2,3}$ and a core of negative parity and $\mathbf{R} = 1, 3, 5, \ldots$. in the case of TSD_4. Within this particle-core basis a similar Hamiltonian as in the previous paper is treated via a time dependent variational formalism. In this manner one derives the classical equations of motion for the generalized canonical coordinates.

For the sake of a self content presentation,in what follows we shall briefly introduce the necessary ingredients of the formalism.

The Hamiltonian of ^{163}Lu has a particle-rotor character and describes the interaction between an even-even triaxial core and a single nucleon that moves in the quadrupole deformed mean field generated by the core.

$$H = H_{\rm rot} + H_{\rm sp} \ . \tag{1}$$

The first term represents the triaxial rotor Hamiltonian, with the core a. m. $\mathbf{R} = \mathbf{I} - \mathbf{j}$, and the inertial parameters A_k.

$$H_{\rm rot} = \sum_{i=1,2,3} A_i \left(I_i - j_i\right)^2 , \tag{2}$$

The inertial parameters A_i are related to the moments of inertia (MoI)corresponding to the principal axes of the triaxial ellipsoid, through the equation $A_i = \frac{1}{2\mathcal{I}_i}$.

The single-particle term from Eq. 1 is defined in terms of the triaxiality parameter γ and the potential strength V. Actually this term expresses the mean field for the single particle motion, determined by a collective quadrupole and a single particle quadrupole interaction [20].

$$H_{\rm sp} = \frac{V}{j(j+1}\left[\cos\gamma\left(3j_3^2 - \mathbf{j}^2\right) - \sqrt{3}\sin\gamma\left(j_1^2 - j_2^2\right)\right] + \epsilon_j . \tag{3}$$

*Electronic address: robert.poenaru@drd.unibuc.ro
†Electronic address: raduta@nipne.ro

The term ϵ_j from Eq. 3 represents the single particle energy. The eigenvalues of interest for H are obtained on the base of a semi-classical approach. Thus, the total Hamiltonian H is dequantized through the time dependent variational equation (TDVE):

$$\delta \int_0^t \langle \Psi_{IjM}|H - i\frac{\partial}{\partial t'}|\Psi_{IjM}\rangle dt' = 0, \tag{4}$$

where the trial function is chosen as:

$$|\Psi_{Ij;M}\rangle = \mathbf{N} e^{zI_-} e^{sj_-}|IMI\rangle|jj\rangle, \tag{5}$$

with I_- and j_- denoting the lowering operators for the intrinsic angular momenta $\mathbf{I}$ and $\mathbf{j}$ respectively, while $\mathbf{N}$ is the normalization factor. $|IMI\rangle$ and $|jj\rangle$ are extremal states for the operators $\hat{I}^2, \hat{I}_3$ and $\hat{j}^2, \hat{j}_3$, respectively. We notice that the trial function is a mixture of components of definite K, which is consistent with the fact that for triaxial nuclei, K is not a good quantum number. The name of TSD bands is the abbreviation for triaxial superdeformed bands suggesting that the ground band head state is an isomeric state with a relative large half-life.

The variables z and s are complex functions of time and play the role of classical phase space coordinates describing the motion of the core and the odd particle, respectively:

$$z = \rho e^{i\varphi}, \;\; s = f e^{i\psi}. \tag{6}$$

Changing the variables ρ and f to r and t, respectively:

$$r = \frac{2I}{1+\rho^2}, \;\; 0 \le r \le 2I; \;\; t = \frac{2j}{1+f^2}, \;\; 0 \le t \le 2j, \tag{7}$$

the classical equations of motion acquire the canonical Hamilton form:

$$\frac{\partial \mathcal{H}}{\partial r} = \dot{\varphi}, \; \frac{\partial \mathcal{H}}{\partial \varphi} = -\dot{r}; \; \frac{\partial \mathcal{H}}{\partial t} = \dot{\psi}; \; \frac{\partial \mathcal{H}}{\partial \psi} = -\dot{t}\,. \tag{8}$$

where $\mathcal{H}$ denotes the average of H with the trial function $|\Psi_{IjM}\rangle$ and plays the role of the classical energy function. The classical energy has the expression :

$$\mathcal{H}(r,\varphi;t,\psi) = \langle \Psi_{IjM}|H|\Psi_{IjM}\rangle$$

and is minimal ($\mathcal{H}^{(I,j)}_{min}$) in the point $(\varphi, r) = (0, I); (\psi, t) = (0, j)$, when $A_1 < A_2 < A_3$. Linearizing the equations of motion around the minimum point of $\mathcal{H}$, one obtains a harmonic motion for the system, with the frequency given by the equation:

$$\Omega^4 + B\Omega^2 + C = 0, \tag{9}$$

where the coefficients B and C have the expressions:

$$-B = [(2I-1)(A_3-A_1) + 2jA_1]\,[(2I-1)(A_2-A_1) + 2jA_1] + 8A_2A_3Ij \tag{10}$$
$$+ \left[(2j-1)(A_3-A_1) + 2IA_1 + V\frac{2j-1}{j(j+1)}\sqrt{3}(\sqrt{3}\cos\gamma + \sin\gamma)\right]\left[(2j-1)(A_2-A_1) + 2IA_1 + V\frac{2j-1}{j(j+1)}2\sqrt{3}\sin\gamma\right],$$
$$C = \left\{[(2I-1)(A_3-A_1) + 2jA_1]\left[(2j-1)(A_3-A_1) + 2IA_1 + V\frac{2j-1}{j(j+1)}\sqrt{3}(\sqrt{3}\cos\gamma + \sin\gamma)\right] - 4IjA_3^2\right\}$$
$$\times \left\{[(2I-1)(A_2-A_1) + 2jA_1]\left[(2j-1)(A_2-A_1) + 2IA_1 + V\frac{2j-1}{j(j+1)}2\sqrt{3}\sin\gamma\right] - 4IjA_2^2\right\}. \tag{11}$$

Under certain restrictions for MoI's the dispersion equation (9) admits two real and positive solutions, which here after will be denoted by Ω^I_1 and Ω^I_2 for $j = i_{13/2}$and ordered as: $\Omega^I_1 < \Omega^I_2$.

Further, to the $TSD_{1,2,3,4}$ bands we associate the energies:

$$\begin{aligned}
E^{\rm TSD1}_I &= \epsilon_j + \mathcal{H}^{(I,j)}_{\rm min} + \mathcal{F}^I_{00}, \;\; I = R + j, R = 0, 2, 4, ..., \\
E^{\rm TSD2}_I &= \epsilon_{j,1} + \mathcal{H}^{(I,j)}_{\rm min} + \mathcal{F}^I_{00}, \;\; I = R + j, R = 1, 3, 5, ... \\
E^{\rm TSD3}_I &= \epsilon_j + \mathcal{H}^{(I,j)}_{\rm min} + \mathcal{F}^I_{10}, \;\; I = R + j, R = 0, 2, 4, ... \\
E^{\rm TSD4}_I &= \epsilon_{j,2} + \mathcal{H}^{(I,j)}_{\rm min} + \mathcal{F}^I_{00}, \;\; I = R + j, \; R = 1, 3, 5, ...
\end{aligned} \tag{12}$$

where $\mathcal{F}_{n_{w_1} n_{w_2}}$ is function of the wobbling frequencies

$$F^I_{n_{w_1} n_{w_1}} = (n_{w_1} + \frac{1}{2})\Omega^I_1 + (n_{w_2} + \frac{1}{2})\Omega^I_2. \tag{13}$$

while $\mathcal{H}^{(I,j)}_{min}$ is the minimal classical energy. We considered different re-normalizations for the single-particle mean field in the signature unfavored as well as in the negative parity states, which result two distinct energy shifts for the excitation energies in the TSD2 and TSD4 bands, respectively. These two quantities will be adjusted throughout the numerical calculations such that the energy spectrum is best reproduced. The phonon numbers corresponding to the four bands are listed in Table I,

where values of the parity and signatures are also shown. In a previous publication [19] one showed that the signature is a good quantum number. One can prove that parity is also a good quantum number in our formalism. Indeed, taking into account that the parity operator is a product of the complex conjugation operation and a rotation of angle π around the 2-axis ($P = e^{-i\pi J_2}C$) and acting on the trial function with the total parity operator $P_t = P_c P_{sp}$ one obtains:

$$P_t\Psi(r,\varphi;t,\psi) = \Psi(r,\varphi+\pi;t,\psi+\pi). \quad (14)$$

On the other hand the energy function is invariant at changing the angles with π:

$$\mathcal{H}(r,\varphi+\pi;t,\psi+\pi) = \mathcal{H}(r,\varphi;t,\psi). \quad (15)$$

This induces the fact that the functions Ψ and its image through P_t are linear dependent differing by a multiplicative constant of modulus equal to unity. Thus,

$$\Psi(r,\varphi+\pi;t,\psi+\pi) = \pm\Psi(r,\varphi;t,\psi). \quad (16)$$

The above result is a reflection of the fact that the triaxial rotor admits eigenfunctions of negative parity. Indeed, let r_k ,k=0,1,2,3 be the eigenvlues of the four elements of the group D_2: $\mathcal{E}, e^{-i\pi R_1}, e^{-i\pi R_2}, e^{-i\pi R_3}$ with $\mathcal{E}$ denoting the unity rotation. The eigenfunctions of the rotor Hamiltonian being at a time eigenfunctions for the D_2 elements form irreducible representation of the group, with the eigenvalues (r_0, r_1, r_2, r_3). Two of these irrep-s have negative parity. These are: $(1,-1,-1,1)$ and $(1,1,-1,-1)$.

The spin sequences for the TSD bands are shown in Table II.

Band	n_{w_1}	n_{w_2}	π	α
TSD1	0	0	+1	+1/2
TSD2	0	0	+1	-1/2
TSD3	1	0	+1	+1/2
TSD4	0	0	-1	-1/2

TABLE I: The wobbling phonon numbers, parities and signatures assigned for the triaxial bands in ^{163}Lu within the model.

Band	j	**R**-sequence	**I**-sequence
TSD1	$i_{13/2}$	$0,2,4,\ldots$	$13/2, 17/2, 21/2, \ldots$
TSD2	$i_{13/2}$	$1,3,5,\ldots$	$27/2, 31/2, 35/2, \ldots$
TSD3	$i_{13/2}$	$0,2,4,\ldots$	$33/2, 37/2, 41/2, \ldots$
TSD4	$i_{13/2}$	$1,3,5,\ldots$	$47/2, 51/2, 55/2, \ldots$

TABLE II: The spin sequences that belong to the wobbling spectrum of ^{163}Lu, where j is the $i_{13/2}$-odd proton.

In what follows it is worth analyzing the dependence of the classical energy function on the Cartesian coordinates $x_k = I_k,\ k = 1,2,3$:

$$x_1 = I\sin\theta\cos\varphi\ , x_2 = I\sin\theta\sin\varphi\ , x_3 = I\cos\theta. \quad (17)$$

In polar coordinates the classical energy function reads:

$$\begin{aligned}\mathcal{H} &= I\left(I-\frac{1}{2}\right)\sin^2\theta\left(A_1\cos^2\varphi + A_2\sin^2\varphi - A_3\right) - \\ &- 2A_1Ij\sin\theta + T_{rot} + T_{sp}\ , \end{aligned} \quad (18)$$

where the last two terms are independent of the coordinates and have the forms:

$$T_{rot} = \frac{I}{2}(A_1+A_2) + A_3I^2\ , \quad (19)$$

$$T_{sp} = \frac{j}{2}(A_2+A_3) + A_1j^2 - V\frac{2j-1}{j+1}\sin\left(\gamma+\frac{\pi}{6}\right)\ . \quad (20)$$

In obtaining this expression the single particle terms were considered in the minimum point.

The classical energy admits two constants of motion: the system energy and the total angular momentum. Therefore, the classical trajectories are determined by intersecting the surfaces describing the two constants of motion, that are an ellipsoid and a sphere, respectively:

$$\begin{aligned} E =& \left(1-\frac{1}{2I}\right)A_1x_1^2 + \left(1-\frac{1}{2I}\right)A_2x_2^2 \\ &+ \left[\left(1-\frac{1}{2I}\right)A_3 + A_1\frac{j}{I}\right]x_3^2 \\ &+ T_{rot} + T_{sp} - I\left(I-\frac{1}{2}\right)A_3 - 2A_1Ij, \\ I^2 =& x_1^2 + x_2^2 + x_3^3. \end{aligned} \quad (21)$$

For a given total angular momentum and a given set of MoI's one can solve the above equations by expressing two unknowns in term of the third one and thus, classical trajectories of an wobbling character are obtained.

We now proceed at discussing the numerical results. As already mentioned the application is made for ^{163}Lu, since this is the only isotope exhibiting both positive and negative parity bands and thus one can check the validity of our proposed formalism. By using the expressions 12, a least squares fitting procedure was used for finding the parameter set $\mathcal{P} = (\mathcal{I}_1, \mathcal{I}_2, \mathcal{I}_3, \gamma, V)$. The found values of $\mathcal{P}$, are shown in Table III,leading to a RMS value of $\approx$ 79 keV, which is much better than that obtained through a different approach [19], where the r. m. s. is $\approx 240keV$. Keep in mind that the fitting procedure was done simultaneously for all four bands,contrary to Ref. [19]) where a separate parameter set for TSD4 was used, invoking a different polarization effect of the core, due to the particle-core interaction. Concerning the single particle energies, the unfavored states as well

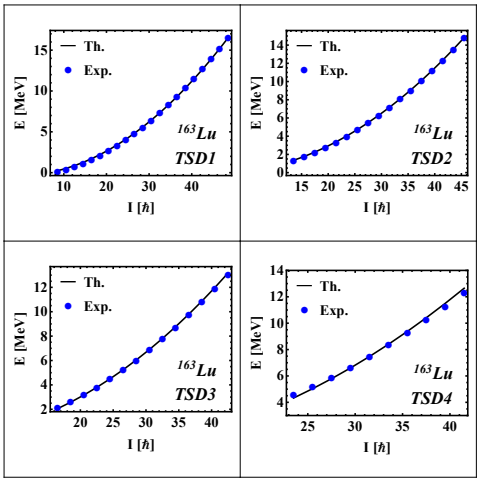

FIG. 1: The excitation energies for the bands TSD1, TSD2, TSD3, and TSD4.

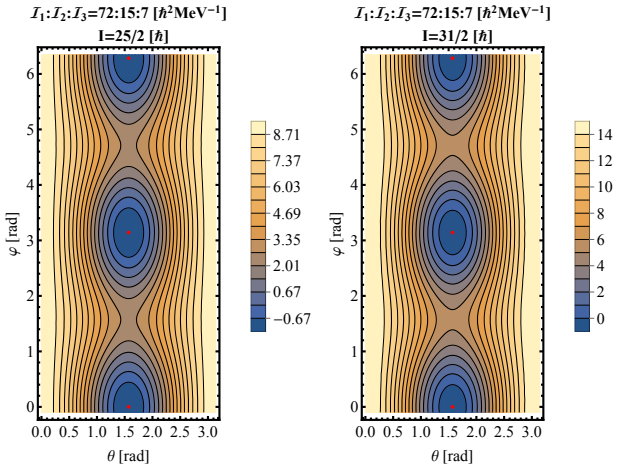

FIG. 2: A contour plot with the energy function $\mathcal{H}$ for TSD1 and TSD2. The parameter set $\mathcal{P}$ was used for the numerical calculations.

as the negative parity states induce a correction for the mean field with the quantities: $\epsilon_{j,1} - \epsilon_j = 0.3MeV$ and $\epsilon_{j,2} - \epsilon_j = 0.6$ MeV respectively. Results of our calculations are compared with the corresponding data in Fig. 1, where one remarks a very good agreement of the two sets of energies. Remarkable the fact that the difference $E_I^{\mathrm{TSD4}} - E_I^{\mathrm{TSD2}} \approx 300keV$, which suggests that the states of the same a. m. from the TSD2 and TSD4 bands might emerge through the parity projection from a sole function without space reflection symmetry. In our case, this is caused by the fact that the wobbling frequency is parity independent. In this context these bands are parity partners as defined in Refs. [24–27]

$\mathcal{I}_1$ [$\hbar^2$/MeV]	$\mathcal{I}_2$ [$\hbar^2$/MeV]	$\mathcal{I}_3$ [$\hbar^2$/MeV]	γ [deg.]	V [MeV]
72	15	7	22	2. 1

TABLE III: The parameter set $\mathcal{P}$ that was determined by a fitting procedure of the excitation energies of ^{163}Lu.

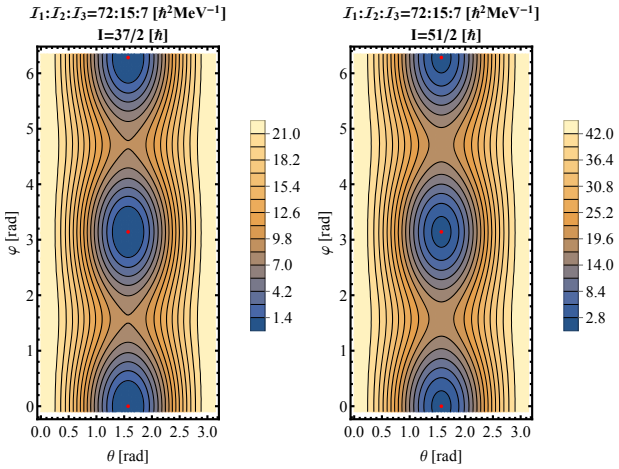

FIG. 3: A contour plot with the energy function $\mathcal{H}$ for TSD3 and TSD4. The parameter set $\mathcal{P}$ was used for the numerical calculations.

In terms of the stability of the wobbling motion with respect to the total angular momentum, several contour plots were plotted, using the obtained parameter set $\mathcal{P}$ with the help of Eq. 18. For each band, a spin close to the band head of each sequence was chosen. Due to the obtained MOI ordering, the surfaces have minimum points indicated by the red dots for each figure. Results can be seen in Figs. 2,3. The four figures have many similarities suggesting common collective properties, but also differences caused by the fact that minima have different depths. The common feature consists of that the equi-energy curves surround a sole minimum for low energy while for higher energies the trajectories go around all minima, the lack of localization indicating an unstable picture.

Finally we are interested in finding out the dependence of the classical trajectories on angular momenta as well as on energies. Indeed, when the model Hamiltonian is diagonalized for a given I, a set of $2I + 1$ energies are obtained. Therefore, it makes sense to study the trajectory change at increasing the energy. Trajectories are represented as the manifold given by intersecting the surfaces corresponding to the two constants of motion. The first energy in each row corresponds to the real excitation energy for that particular spin state, the second one represents the point at which the ellipsoid touches the sphere at the equator, which marks a nuclear phase transition - while the third one is the trajectory of the system at energies sufficiently large that the system changes its wobbling regime. For low energies, one notices two distinct trajectories having as rotation axes the 1-axis and -1-axis, respectively. As energy increases the two trajectories approaches each other which results a tilted rotation axis for each of trajectories, the rotation axes being dis-aligned. Note that this picture is fully consis-

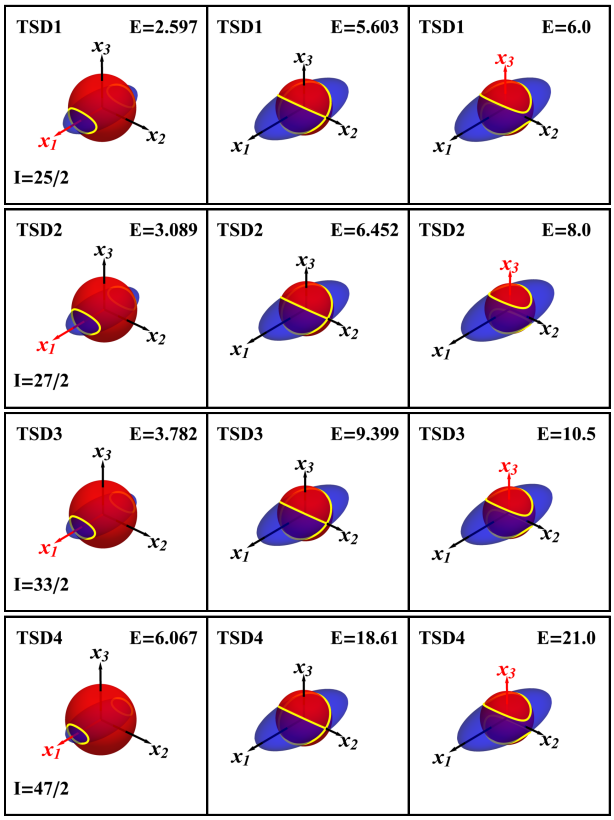

FIG. 4: The nuclear trajectory of the system for a spin state belonging to each of the four TSD bands of ^{163}Lu. Intersection line marked with yellow color represents the actual orbits.

tent with that of Ref. [28]. When the two trajectories intersect each other, the trajectories surround both minima. Increasing the energy even more one arrives again at two trajectories regime but with different rotation axes which become close to the 3-axis. This reflects another phase transition for the system.

The results of our investigation can be summarized as follows. Despite the fact that TSD4 is of an opposite parity than the lower bands, the four bands are described by coupling a sole single particle of positive parity to the core states of positive parity for $TSD_{1,2,3}$ and negative parity for TSD_4. The core is not changing, which results in having a unique set of MoI-s but the mean field for the valence nucleon is modified for unfavored signature as well as for the negative parity bands. The contour plots for one representative state from each band, shows a similar structure but different depths and reaching the unstable regimes at different energies. The system's trajectories corresponding to the four bands, obtained by intersecting the surfaces associated to the two constants of motion, the energy and the a. m. , indicate that for low energy the rotation axes are the 1-axis and -1-axis defining two disjoint trajectories, while for higher energy the rotation axes are tilted toward the 3-axis. There are signals that TSD_2 and TSD_4 are parity partner bands. Likewise the bands TSD_1 and TSD_2 are signature partner bands. The e. m. properties of these bands have been successfully described in Ref. [19]. Obviously, the results from the quoted paper are valid also here.

Concluding, the present model is a successful tool for accurately describing the wobbling spectrum of ^{163}Lu, but also for understanding the rotational motion of the nuclear system with respect to its total spin.

Acknowledgments. This work was supported by UEFISCU through the project PCE- PN3/2021

[1] A. Bohr and B. Mottelson, *Nuclear Structure* (Benjamin, Reading, MA, 1975), Vol. II, Ch. 4.
[2] ,S. W. Ødegård, *et al.* , Phs. Rev. Lett. **86** 5866, (2001).
[3] D. R. Jensen *et al.* , Nucl. Phys. **A 703**, 3, (2002).
[4] G. Schoenwasser *et al.* , Phys. Lett. **B 552**,9, (2003).
[5] H. Amro *et al.* , Phys. Lett. **B 553**, 197, (2003).
[6] G. B. Hagemann, Eur. Phys. J. **A 20**, 183, (2004).
[7] G. B. Hagemann *et al.* , Phys. Rev. Lett. 86, 5866 (2001).
[8] J. T. Matta *et al.* , Phys. Rev. Lett. **114**, 082501 (2015).
[9] N. Sensharma, *et al.* ,Phys. Lett. B,**792** (2019).
[10] P. Bringel *et al.* Eur. Phys. J. **A 24**, 167, (2005).
[11] D. J. Hartley *et al.* , Phys. Rev. **C 80**, 041304(R), (2009).
[12] N. Sensharma, *et al.* , Phys. Rev. Lett. **124**, 052501 (2020).
[13] Q. B. Chen, S. Frauendorf and C. M. Petrache, Phys. Rev. C **100**, 061301(R) (2019).
[14] J. Timar *et al.* , Phys. Rev. Lett. **122**, 062501 (2019).
[15] S. Chakraborty *et al.* ,Phys. Lett. B, **811** , 135854 (2020).
[16] S. Nandi,*et al.* ,Phys. Rev. Lett. **125** 132501 (2020).
[17] S. Frauendorf and F. Dönau Phys. Rev. C **89**, 014322 (2014).
[18] A. A. Raduta, R. Poenaru, R and C. M. Raduta Jour. Phys. G:Nucl. Part. Phys. **47**,025101 (2020).
[19] A. A. Raduta, R. Poenaru, R and C. M. Raduta, Phys. Rev. C **101**, 014302,(2020).
[20] A. C. Davydov, *Teoria atomnova yadra*, Moscva, 1958 (in russian), chapters 19,20.
[21] A. A. Raduta, Prog. Part. Nucl. Phys. **90, 241 (2016**.
[22] A. A. Raduta, R. Poenaru, and L. Gr. Ixaru, Phys. Rev. C **96**, 054320, (2017).
[23] R. Budaca, Phys. Rev. C **97** 069801 (2018).
[24] R. R. Chasman, Phys. Lett. B **96**,7,(1980).
[25] A. A. Raduta, Al. H. Raduta and Amand Faessler, Phys. Ref. C **55**, 1747, 91997).
[26] A. A. Raduta, D. Ionescu and Amnd Faessler, Phys. Rev. C **65**, 233 (2002).
[27] A. A. Raduta, Al. H. Raduta and C. M. Raduta, Phys. Rev. C **74** 044312 (2006).
[28] E. A. Lawrie, O, Shirinda and C. M. Petrache, Phys. Rev. C **101**, 034306 (2020).

Extensive Study of the Wobbling Properties in ^{163}Lu for the Positive and Negative Parity States

R. Poenaru *[1,2] and A. A. Raduta †[2,3]

[1]Doctoral School of Physics, University of Bucharest, Romania
[2]*Horia Hulubei* National Institute for Physics and Nuclear Engineering, Măgurele-Bucharest, Romania
[3]Academy of Romanian Scientists, Bucharest, Romania

April 8, 2021

Abstract

A new interpretation of the wobbling structure in ^{163}Lu is developed. Four wobbling bands are experimentally known in this isotope, where three are wobbling phonon excitations $TSD_{2,3,4}$, and the ground state band, which is TSD_1. In this work, a particle-triaxial rotor coupling is considered in a product space of single-particle and collective core states. The single-particle states describe a $j = i_{13/2}$ proton, while the core states characterize the triaxial rotor and are either of positive parity, when the bands $TSD_{1,2,3}$ are concerned or of negative parity for the TSD_4 band. There are five free parameters, three moments of inertia, the strength of the particle-core interaction, and the γ deformation. A very good description of all 62 experimental states is obtained, with a mean square error of about 80 keV. The system's stability dependence on energy is appraised in terms of a contour plot of the surface energy, while the dependence of classical trajectories on angular momentum as well as on energy is discussed by showing the intersections between the surfaces associated with the two constants of motion, i.e., the energy and the total angular momentum. This analysis suggests three different nuclear phases that emerge. The newly obtained features evidenced in the present work enrich the knowledge about the wobbling properties of ^{163}Lu.

1 Introduction

Triaxiality in nuclei has become an interesting topic for physicists over the years, mainly due to the large number of characteristics that become apparent from these kinds of shapes but also for its great challenge of measuring it experimentally. Moreover, stable triaxial shapes are of rare occurrence across the chart of nuclides [1], since the predominant character of nuclei is either spherical or axially symmetric. Over the last two decades, it has been shown that triaxiality plays a crucial role in measurements of important quantities like separation energies of the nucleons [1], and also fission barriers in heavy nuclei [2], however, concrete evidence of triaxiality in nuclei was still missing or under investigation. Tremendous work was given in finding a clear signature for non-axially symmetric shapes: effects such as anomalous signature splitting [3], signature inversion [4], and staggering of γ bands [5] were pointed out, but only recently two clear fingerprints of nuclear triaxiality have emerged in the literature, based on both experimental and theoretical findings. Indeed, the phenomena of *chiral symmetry breaking* [6] and that of *wobbling motion* (W.M.) [7] are considered as unique characteristics of nuclear triaxiality.

Chirality consists of the existence of a pair of chiral twin bands with an identical structure and almost similar energies. These bands are expected to appear due to the coupling of valence nucleons and the collective mode of rotation that could drive the total spin away from any of the three principal planes, giving rise to both left-handed and right-handed orientation of the angular momentum vectors [6]. A rigorous study of all the nuclei with chiral bands was done by Xiong and Wang [8], where reportedly a total of 59 chiral doublet bands in 47 such nuclei are confirmed. As a matter of fact, 8 of these nuclei have multiple chiral doublets. Several other studies were developed over the years, giving rise to new theoretical frameworks that accurately describe this phenomenon [9–14].

On the other hand, the experimental observations regarding wobbling motion have been quite rare, even though this kind of collective motion has been theoretically predicted almost 50 years ago by Bohr and Mottelson [7] when they were investigating the rotational modes of a triaxial nucleus employing a Triaxial Rotor Model

*E-mail: robert.poenaru@drd.unibuc.ro
†E-mail: raduta@nipne.ro

(TRM). Therein, it was shown that for a triaxial rotor, the main rotational motion is around the axis with the largest moment of inertia (MOI), as it is energetically the most favorable. This mode is quantum-mechanically disturbed by the rotation around the other two axes, since rotation around any of the three principal axes of the system are possible, due to the anisotropy between the MOIs (that is $\mathcal{I}_1 \neq \mathcal{I}_2 \neq \mathcal{I}_3$). Naturally, the description of the energy spectra and electromagnetic transitions between the rotational states of these wobbling nuclei (also known as *wobblers*) are considered to be the main characteristics that are put to the test by a theoretical investigation. The overall agreement between experimental results and the theoretically obtained data serves as an indicator for the quality of the model used to describe the wobbling picture. Regarding the experimental results for the known wobblers, this will be discussed in the next section, together with an overview of the recent progress made for the theoretical description of this type of nuclear motion.

The present work aims at extending the knowledge of the wobbling characteristics in an even-odd nucleus, which will be done by studying the energy spectrum of ^{163}Lu in a semi-classical approach, where the rotational states are described through a set of classical equations. In contradistinction with previous work, [15], in this formalism, all four wobbling bands are described by the same *core-quasiparticle alignment*, making thus the description of the wobbling motion consistent. A remarking feature for the current research is the introduction of the concept of *parity partner bands* - concerning the states from TSD_2 and TSD_4 bands - which will be discussed throughout the paper. Additionally, by studying the geometry of the triaxial rotor and that of the total angular momentum, some interesting characteristics of the wobbling motion will be pointed out.

This paper is organized as follows. In Section 2, a few theoretical aspects of WM will be mentioned, indicating some key points that the current study shall consider analyzing. Also in Section 2, experimental observations regarding WM in even-even and even-odd nuclei are presented, concluding the introductory part of the study. Following Section 3, a synopsis of the recent reinterpretation on the wobbling band structure for ^{163}Lu as described in [15] will be made. This will be the *core-idea* that serves as the foundation of the newly developed model introduced here. A direct comparison between this approach and the one from [15] is sketched, pointing out the improved features of the former. The theoretical formalism and the analytical formulas will be presented in Section 4. Experimental results concerning the wobbling spectrum of ^{163}Lu will be compared with the newly obtained data in Section 5. Finally, an outlook and conclusions are given in Section 6.

2 Wobbling motion in nuclei - experimental & theoretical overview

W.M. can be viewed as the quantum analogue for the motion of the asymmetric top, whose rotation around the axis with the largest MOI is energetically the most favored. A uniform rotation about this axis will have the lowest energy for a given angular momentum (spin). As the energy increases, this axis will start to precess with a harmonic type of oscillation about the space-fixed angular momentum vector, giving rise to a family of wobbling bands, each characterized by a wobbling phonon number n_w. The resulting quantal spectrum will be a sequence of rotational $\Delta I = 2$ bands, with an alternating signature number for each wobbling excitation. According to [7], it is possible to obtain the wobbling spectrum of any triaxial rigid rotor, by using the information related to its angular momentum I, moments of inertia $\mathcal{I}_{1,2,3}$, rotational frequency $\omega_{\rm rot}$, wobbling frequency $\omega_{\rm wob}$ as follows:

$$E_{\rm rot} = \sum_i \left(\frac{\hbar^2}{2\mathcal{I}_k}\right) I_k^2 \approx \frac{\hbar^2}{2\mathcal{I}_1} I(I+1) + \hbar\omega_{\rm wob}\left(n_w + \frac{1}{2}\right) \ , \tag{1}$$

with $\omega_{\rm wob}$ given by the following expression:

$$\hbar\omega_{\rm wob} = \hbar\omega_{\rm rot}\sqrt{\frac{(\mathcal{I}_1 - \mathcal{I}_2)(\mathcal{I}_1 - \mathcal{I}_3)}{\mathcal{I}_2\mathcal{I}_3}} \ , \tag{2}$$

where the rotational frequency of the rigid rotor is given by $\hbar\omega_{\rm rot} = \frac{\hbar I^2}{\mathcal{I}_1}$. In Eq. 1, the approximation of very large MOI along 1-axis is considered (i.e., $\mathcal{I}_1 >> \mathcal{I}_2, \mathcal{I}_3$), and $I(I+1) = I_1^2 + I_2^2 + I_3^2$. One can see that the wobbling motion is expressed as a 1-dimensional vibration with only one variable, since the energy of the zero-point fluctuation is $\frac{\hbar\omega_{\rm wob}}{2}$ [16].

Just for an illustrative purpose, Figure 1 shows a theoretical spectrum for the wobbling bands within a triaxial rigid rotor. The family of wobbling bands is obtained from a set of three moments of inertia (along the three principal axes), a given angular momentum, and increasing wobbling phonon numbers ($n_w = 0, 1, \dots$). Moreover, in Figure 1, the tilting of the angular momentum away from the rotational axis is sketched, where the tilt increases with the increase in the wobbling excitation. In a given sequence of wobbling bands, both the intra-band $\Delta I = 2$ as well as inter-band $\Delta I = 1$ transitions have a strong $E2$ collective character.

It is important to mention that the wobbling spectrum described by Eq. 1 and graphically represented in Figure 1 was firstly predicted for an even-even triaxial nucleus [7]. This predicted wobbling mode has not been

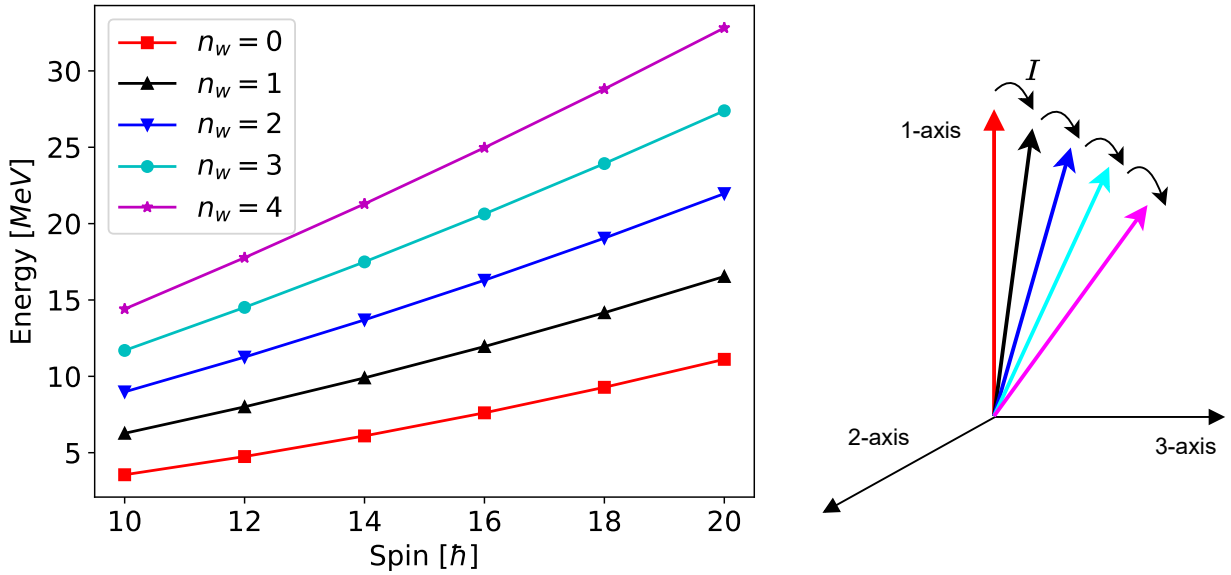

Figure 1: Family of wobbling bands for a simple triaxial rotor (left-side). Tilting of the angular momentum vector away from the rotational axis with an increase in spin (right-side). This schematic representation was done for an arbitrary set of MOIs $\mathcal{I}_1 : \mathcal{I}_2 : \mathcal{I}_3 = 25 : 5 : 2$.

experimentally confirmed yet. However, the first experimental evidence for wobbling excitations in nuclei was for an even-odd nucleus, namely ^{163}Lu, where a single one-phonon wobbling band was measured initially [17], followed by two additional wobbling bands discovered one year later [18,19].

2.1 Experimental findings

After the first discovery of wobbling bands in ^{163}Lu ($Z = 71$), an entire series of even-odd isotopes with $A \approx 160$ were experimentally confirmed as *wobblers*: ^{161}Lu, ^{165}Lu, ^{167}Lu, and ^{167}Ta. In these nuclei, the wobbling mode appears due to the coupling of a valence nucleon (the so-called $\pi(i_{13/2})$ intruder) to a triaxial core, driving the entire nuclear system up to large deformation ($\epsilon \approx 0.4$) [20].

With time, several nuclei in which WM occurs were also found in regions of smaller A. Indeed, two isotopes with $A \approx 130$: ^{133}La [21] and ^{135}Pr [22, 23] were identified as having wobbling bands which emerge from the coupling of a triaxial even-even core with the $\pi(h_{11/2})$ nucleon for ^{135}Pr, and an additional pair of positive parity quasi-protons for ^{133}La. In the case of ^{133}La, the system is characterized as a longitudinal wobbler (it is in fact the first nucleus in which the longitudinal wobbling regime has been experimentally identified), while ^{135}Pr has a transverse wobbling regime. In both cases, the resulting coupling has a deformation $\epsilon = 0.16$ [21,22], which is smaller than the deformation in the heavier nuclei from the $A \approx 160$ region. A third nucleus that also lies in this mass region was confirmed very recently by Chakraborty et. al. in [24], namely the odd-A ^{127}Xe, where a total of four wobbling bands have been reported by the team (two yrast bands, and two excited phonon bands with $n_w = 1$ and $n_w = 2$). It is also suggested that ^{131}Ba could exhibit transverse wobbling [25] due to the alignment of a quasiparticle with hole-like character (the $h_{11/2}$ neutron), but in order to support this interpretation, the connecting transitions must show predominant $E2$ character.

Some additional progress was made in the $A \approx 100$ mass region, with experimental evidence for ^{105}Pd with two such bands that are built on a $\nu(h_{11/2})$ configuration, the first one so far in which a valence neutron couples to the triaxial core [26]. The resulting configuration drives the nuclear system up to deformation $\epsilon \approx 0.26$ and a transverse wobbling behavior.

The heaviest nuclei known so far in which WM has been experimentally observed are the isotopes $Z = 79$ with $A = 183$ [27] and $A = 187$ [28], respectively. However, for the case of ^{187}Au, there is an ongoing investigation [29] whether the two wobbling bands ($n_w = 0$ and $n_w = 1$) are bands with wobbling character, or if they are of magnetic nature (which would exclude the wobbling phonon interpretation). The nucleus ^{183}Au has probably the most interesting wobbling behavior, due to the appearance of both increasing and decreasing parts of the wobbling energy as a function of angular momentum, for states belonging to the same band (see Figure 5 from [27]). The experimental evidence for this nucleus shows that the positive parity band behave as a TW (despite the increasing behavior) due to the geometry of the coupling of the odd quasiparticle. This has important implications which will be discussed later on. For now, it is important to remember that there are cases where some transverse wobblers could be increasing functions of angular momentum, in the low-spin regions.

Regarding the wobbling motion for the even-even nuclei (behavior that was described in Figure 1), the experimental results are fragmentary, with scarce or unclear evidence on this collective behavior. However, some embryos of even-even wobblers have been reported in the recent years. For example, the ^{112}Ru ($Z = 44$) nucleus has three wobbling bands [30], two of them being the excited one- and two-wobbling phonon bands. Another nucleus is ^{114}Pd [31], with two excited bands of wobbling character, similar to ^{112}Ru. Indeed, for ^{112}Ru and ^{114}Pd the ground band together with the odd and even spin members of the γ-bands were interpreted as zero-(yrast), one-, and two-phonon wobbling bands. Unfortunately, since there are no data concerning the electromagnetic transitions, its wobbling character is still unclear. The even-even nucleus ^{130}Ba ($Z = 56$) [32–34] was confirmed very recently to exhibit wobbling behavior based on a two quasiparticle configuration with pair of bands with even and odd spins as zero- and one-phonon wobbling bands, respectively. What is worth noting for this case is the fact that these two bands are built on a configuration in which two aligned protons that emerge from the bottom of $h_{11/2}$ shell couple with the triaxial core. One remarks the change in nature of the wobbling motion from a purely collective form, but in the presence of two aligned quasiparticles [33], with a transverse wobbling character.

Concerning the interpretation of the energy spectrum for the wobbling motion which occurs in the nuclei that were mentioned above, it is mandatory to discuss some aspects related to its behavior with the increase in total angular momentum (nuclear spin). Thus, the concepts of *longitudinal wobblers* (LW) and *transverse wobblers* (TW) emerged from an extensive study done by Frauendorf et. al. [35] in which the team studied the possible coupling schemes that a valence nucleon can create with the triaxial core, giving rise to two possible scenarios. Based on microscopic calculations using the Quasi-Particle Triaxial Rotor (QTR) model, they showed that if the odd valence nucleon aligns its angular momentum vector $\vec{j}$ with the axis of largest MOI, the nuclear system is of longitudinal wobbling character. On the other hand, if the odd nucleon aligns its a.m. vector $\vec{j}$ with an axis perpendicular to the one with the largest MOI, then the nuclear system has a transverse wobbling character. Consequently, for LW the wobbling energy $E_{\rm wob}$ (see Eq. 3) has an *increasing* behavior with an increase in the angular momentum, while for TW the energy $E_{\rm wob}$ *decreases* with increasing angular momentum.

From the nuclei that were mentioned above, most of them are of TW type, with only ^{127}Xe [24], ^{133}La [21], and ^{187}Au [28] having an LW character. The energy that characterizes the type of wobbling in a nuclear system is the energy of the first excited band (the one-phonon $n_w = 1$ wobbling band) relative to the yrast ground band (zero-phonon $n_w = 0$ wobbling band):

$$E_{\rm wob}(I) = E_1(I) - \left(\frac{E_0(I+1) + E_0(I-1)}{2} \right) , \tag{3}$$

with 0 and 1 representing the wobbling phonon number n_w.

The odd nucleons that couple with the rigid triaxial core will influence the appearance of a particular wobbling regime (LW or TW). In all the wobblers, there is a proton from a certain orbital that is coupling with the core, except for the case of ^{105}Pd, where the valence nucleon is a neutron. The nature of the odd quasiparticle (i.e., particle or hole) and its "position" in the deformed j-shell (i.e., bottom or top) will determine whether its angular momentum $\vec{j}$ will align with the *short* (s) or *long* (l) axes of the triaxial rotor, respectively (with the notations short s, long l, and medium m for the axes of a triaxial ellipsoid). The reasoning behind this has to do with the minimization of the overall energy of the system: in the first case, a maximal overlap of its density distribution with the triaxial core will determine a minimal energy, while in the second case, a minimal overlap of the density distribution of the particle with the core will result in a minimal energy. Moreover, if the quasiparticle emerges from the middle of the j-shell, then it tends to align its angular momentum vector $\vec{j}$ with the *medium* (m) axis of the triaxial core. Figure 2 aims at depicting the type of alignment of a quasiparticle with the triaxial core.

As previously mentioned, for a given angular momentum, uniform rotation around the axis with the largest MOI corresponds to minimum energy. For a triaxial rotor emerging from a Liquid Drop, this is equivalent to rotation around the m axis. Therefore, Frauendorf [35] classified the LW as the situation when the odd nucleon will align its angular momentum along the m-axis, while TW being the situation where j is aligned perpendicular to the m-axis (with s- or l-axis alignment depending on the j-shell orbital from which the odd nucleon arises). It is worthwhile to mention the fact that the analysis done in Ref. [35] was performed within a so-called *Frozen Alignment* approximation, where the angular momentum of the odd particle $\vec{j}$ is rigidly aligned with one of the three principal axes of the triaxial ellipsoid (that is s-, l- or m-axis).

For a better understanding of the wobbling regimes in terms of angular momentum alignment, Figure 3 depicts three particular cases, namely a simple wobbler - inset A.0 (the case firstly developed by Bohr and Mottelson [7]), a longitudinal wobbler - inset A.1, and a transverse wobbler - inset A.2.

2.2 Theoretical interpretations of Wobbling Motion

In terms of its theoretical analysis, the wobbling motion has been studied using multiple models and interpretations. The Triaxial Particle Rotor Model (PRM) has been widely used over the recent years [7, 35–38], these

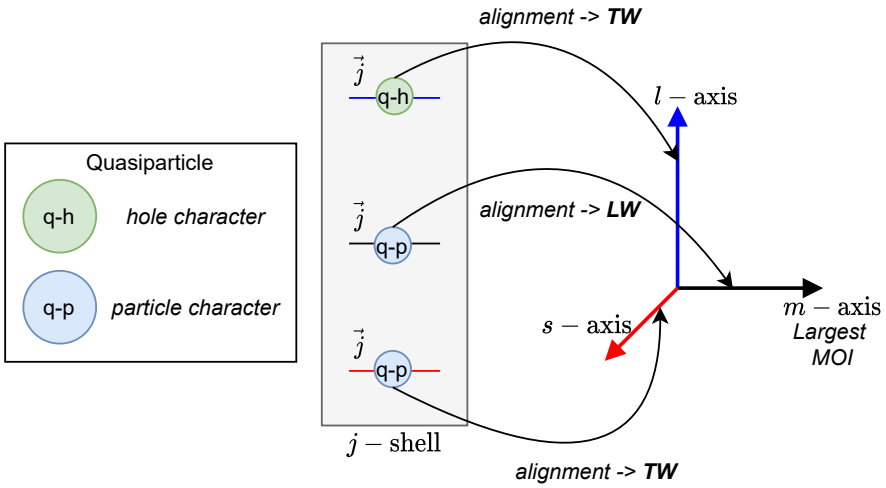

Figure 2: The wobbling regimes, Longitudinal Wobbling (LW) or Transverse Wobbling (TW), based on the type of alignment that an odd quasiparticle makes with the principal axes of a triaxial core. Each case depicts a coupling with an odd quasiparticle which emerges from the bottom/middle/top of a j-shell [35].

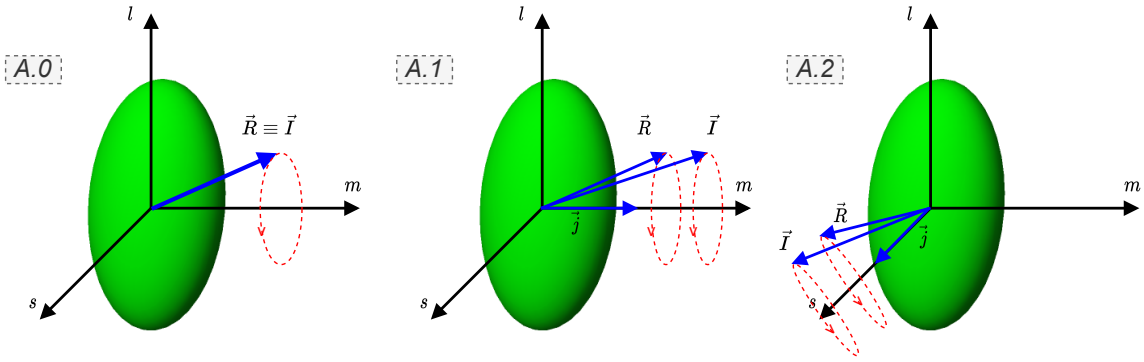

Figure 3: A.0: The geometry for the angular momentum of a simple wobbler. A.1: coupling geometry for a longitudinal wobbler (LW). A.2: coupling geometry for a transverse wobbler (TW). The short-s, long-l, and medium-m axes are defined in the body-fixed frame. The vectors $\vec{R}$, $\vec{j}$, and $\vec{I}$ represent the set of angular momenta of the core, odd particle, and the total nuclear system, respectively.

being quantal models that can be exactly solved in the laboratory frame. TRM was, however, firstly introduced for the motion of a rotating nuclear system by Davydov and Filippov in [39], where they obtained a complete quantal description for the motion of a triaxial nucleus (because the nucleus must have a well-defined potential minimum at a non-zero value for the triaxiality parameter γ). Starting from the framework of Cranking Mean Field Theory (CMFT), there were attempts at extending the cranking model for the study of WM. However, using the mean-field approximations, CMFT only helps at describing the yrast sequence for a given configuration. To improve that, the framework was extended with proper quantum correlations by incorporating the Random Phase Approximation (RPA) theory (see Refs. [40–47] for more details). The method of Collective Hamiltonian [48, 49] was used for the investigation of wobbling spectra in nuclei with the help of deformed potentials which were calculated from the Tilted Axis Cranking (TAC) model. TAC single j-shell model is also used for the description of the chiral vibrations and rotational motion in deformed nuclei [50, 51]. Mean-field approximations were also developed by the so-called *generator coordinate method after angular momentum projection* (GCM+AMP for short), with calculations that emerged from intrinsic cranking states [52]. Some analytical solutions were also developed (based on certain approximations), such as the harmonic approximation (HA) [7,35,48,53], Dyson boson expansion [53,54], and Holstein-Primakoff (HP) formula [37,53–56]. The angular momentum projections were also incorporated into the mean-field framework, with the recent development of a completely microscopic description of the wobbling motion by Shimada et. al. [57]. A Projected Shell Model (PSM) [58] which starts from the shell-model configuration mixing that is based on a Nilsson deformed mean field was also used for the theoretical study concerning WM. There are alternative developments based on the PSM approach, based on Density Functional Theories (DFT) that can be both non-relativistic [59] as well as relativistic [60].

Other tools that proved to be very efficient for the analysis of the wobbling nuclei are the semi-classical approaches, through which one can obtain equations of motion that describe the nuclear system quite well, starting from quantal Hamiltonians and further applying some de-quantization procedures. The semi-classical approach applied to generalized rotor Hamiltonians has the *advantage* of keeping close contact with the classical picture embedded in the dynamic of the systems. Recently, there has been quite an impressive progress towards realistic description of the wobbling motion [15, 35, 53, 61–64].

3 Re-interpretation of the wobbling bands in ^{163}Lu

Considered the *best wobbler* to date, ^{163}Lu has a rich wobbling spectrum [17, 18], with no less than four such wobbling bands: one yrast - TSD_1, (zero-phonon wobbling number $n_w = 0$), and three excited wobbling bands - $TSD_{2,3,4}$ (with their corresponding wobbling phonon numbers $n_w = 1, 2, 3$). The name TSD comes from Triaxial Strongly Deformed bands. The triaxial bands emerge due to the coupling of an odd-$\vec{j}$ nucleon with an even-even triaxial core. Thus, for ^{163}Lu, it is the intruder $\pi(i_{13/2})$ that couples to the triaxial core [17, 19, 36], driving the nuclear system up to large deformation, and stabilizing the deformed structure. Indeed, a triaxial shape with deformation parameters $(\epsilon_2, \gamma) \approx (0.38, +20^\circ)$ is assumed to be in agreement with the observed data, based on calculations using the Ultimate Cranker Code [65] for the potential energy surface (PES).

In terms of the experimental evidence which should be pointing out wobbling nature for the four TSD bands belonging to ^{163}Lu, the large transition quadrupole moment $Q_t \approx 10$ b [66], the predominantly $E2$ character of the transitions linking adjacent bands ($I \to I-1$), a large $E2/M1$ mixing ratio $\delta > 1$ for the transitions linking the yrare ($n_w = 1$) and yrast ($n_w = 0$) bands are all clear fingerprints of wobbling nature. For a set of results concerning these quantities (both theoretical and experimental), see Ref. [53], and the references cited therein. Another quantity that indicates strong deformation with wobbling character is the relative rigid rotor energy, and for this isotope, calculations show that all four bands have similar behavior with respect to this value (see Figures 3 and 4 from Ref. [67]).

Considering the experimental evidence which was indicated above and calculations based on particle rotor models, it can be summarized that the *generally accepted* formalism for the band structure in ^{163}Lu is the following:

- There are three excited wobbling bands (w.b.) TSD_2, TSD_3, and TSD_4 and one ground-state w.b. TSD_1.
- The three excited w.b. have wobbling-phonon numbers $n_{w_2} = 1$, $n_{w_3} = 2$, and $n_{w_4} = 3$, respectively.
- All three bands are built on top of the yrast state (the ground state band) with zero-wobbling-phonon number $n_{w_1} = 0$.
- Stable triaxial super-deformation is achieved due to the alignment of the odd $\pi(i_{13/2})$ nucleon which couples to a triaxially deformed core $\vec{R}$.

- $TSD_{1,2,3}$ have all positive parity $\pi_1 = \pi_2 = \pi_3 = +1$, while the spin states belonging to TSD_4 have negative parity $\pi_4 = -1$. All states within the four bands have a half-integer spin.

In accordance with the band structure which was just formulated, a fully semi-classical approach for the description of the wobbling spectrum of ^{163}Lu was by Raduta et. al. [53]. Therein, with the Time-Dependent Variational Equation (TDVE) applied on the PRM Hamiltonian and a trial wave-function that encapsulates both the states of the deformed nucleus I and the single-particle states j, a set of analytical expressions for the excitation energies of all four bands was obtained. The energies belonging to the excited wobbling phonons were populated by the action of a phonon operator $\Gamma^\dagger$ on the ground state. Indeed, by acting with the phonon operator on the ground state with the spin $I = R + j$ and $R = 0, 2, 4, \ldots$, the states from TSD_2 ($n_w = 1$) can be obtained. By applying twice ($n_w = 2$) the phonon operator, the rotational states from TSD_3 will be created. Lastly, the states from TSD_4 are obtained with the action on the ground state with three ($n_w = 3$) phonon operators: two of positive parity and one of negative parity (due to the overall negative parity $\pi_4 = -1$ of TSD_4). One has to remark the fact that for TSD_4, the model assumes an odd-particle-rotor-coupling with a different intruder: the $\pi(h_{9/2})$ nucleon. This was suggested by the negative parity orbital which might be occupied by this proton, in the spherical shell model. Several calculations in the literature point out that this nucleon might be causing the third excited wobbling band to have negative parity [68]. It is worthwhile mentioning that for the work described in [53], the variational principle was only applied for the states in TSD_1 since the other three wobbling bands are obtained through phononic excitations via the phonon operator $\Gamma^\dagger$.

In what follows, it is useful to introduce some notations that will refer to the formalisms developed in the present paper and the one formulated in [15] for the description of the wobbling motion in ^{163}Lu. As such, the study developed in [15] will be denoted with `W1`, while the current work will be shortly denoted by `W2`. For the sake of a self-consistent presentation, in subsection 3.1 a brief overview of the recently published work `W1` will be made, with further development of `W2` being presented in the subsection 3.2 - representing the *core concept* of the current analysis.

3.1 `W1` - Signature Partner Bands

Working with a semi-classical approach that is based on the triaxial particle rotor model, a full description of the wobbling bands for ^{163}Lu was achieved, but with a slightly modified band structure. Indeed, rather than applying a TDVE just for the yrast TSD_1 band, the states from TSD_2 were also obtained variationally. This was possible due to the different coupling schemes that emerged for TSD_1 and TSD_2, respectively. More precisely, in [15] and [64] there are three different coupling schemes ($\vec{R} + \vec{j}$): states from TSD_1 arise from the odd $\pi(i_{13/2})$ intruder coupling with a core with angular momentum sequence $R_1 = 0, 2, 4, \ldots$; states from TSD_2 arise from the same odd proton but coupling with a different triaxial core with angular momentum sequence $R_2 = 1, 3, 5, \ldots$. The band TSD_3 is obtained as a set of states which are built on top of TSD_2, with the action of an $n_w = 1$ wobbling quanta; this being different than the band structure previously mentioned were the third band was a two-phonon excitation of the yrast TSD_1. Lastly, the fourth band TSD_4 is a ground state band which results from the coupling of the same core as for TSD_2 (that is defined with the angular momentum sequence $R_2 = 1, 3, 5, \ldots$) but with a different odd nucleon: $\pi(h_{9/2})$. Consequently, TSD_2 and TSD_4 are yrast states, alongside TSD_1.

For the first three bands, the MOIs are the same, and they are considered to be free parameters within the numerical calculations. However, this is not true for the fourth band, where a different set of MOIs had to be introduced, since for TSD_4 the core polarization effects are changed by coupling scheme.

Using `W1`, the final results pointed out to the largest MOI corresponding to the 1-axis ($\mathcal{I}_1$ being the largest MOI obtained through the fitting procedure), making the system rotate around the 1-axis (that is the short s-axis). Moreover, the odd proton is aligned to the short axis as well, suggesting that the nucleus has an LW character. By representing the experimental wobbling energies according to Eq. 3, it was obtained that both the theoretical, as well as the experimental values were increasing functions of angular momentum (keep in mind that the first wobbling band $n_w = 1$ within the `W1` model is TSD_3). The agreement between the two sets of data (see Figure 6 from [64]) indicates that the condition for LW/TW character of the wobbling bands stated by Frauendorf et. al. in [35] is not strictly related to the increasing/decreasing wobbling energy E_{wob}. In fact, referring to the case of the wobbling motion for ^{183}Au, Nandi et. al. [27] also point out that the behavior of E_{wob} under spin increase should not be the only indicator of a certain wobbling regime, since for a larger spin interval (if there is experimental data available) there could be regions with both increasing and decreasing trends in wobbling energy. There is an ongoing debate whether the behavior of an LW or TW triaxial nucleus is strictly related to the change in E_{wob} with total a.m. [69–71].

A final aspect that needs to be mentioned regarding `W1` has to do with the interpretation of TSD_1 and TSD_2 as being Signature Partner Bands (SPB). Signature [7] is a quantum property that appears in deformed systems. It is strictly related to the invariance of a system with quadrupole deformation to a rotation by an

angle π around a principal axis. For example, a rotation around the x-axis will be defined as an operator:

$$\hat{R}_x = e^{i\pi \hat{I}_x} \ . \tag{4}$$

As for the framework used in [15, 64], due to the wave-function describing the system being written as a product between the $|I\rangle$ basis state corresponding to the total angular momentum and the single-particle basis state $|j\rangle$, the rotation operator used in `W1` achieves the following form:

$$\hat{R}_x(\pi) = e^{-i\pi \hat{I}_x} \otimes e^{-i\pi \hat{j}_x} \ . \tag{5}$$

If the system has axial symmetry, only the rotation around any of the principal axes that are perpendicular to the symmetry one can define the signature quantum number. Consequently, the signature is a property specific to a deformed system and it translates to a so-called *deformation invariance* with respect to space and time reflection properties [7]. For an even-even nucleus, the signature operator $\hat{R}_x$ has two eigenvalues, -1 and 1. For the even-odd case, the eigenvalues are $-i$ and $+i$, and depending on the total spin, the signatures can have two values, given by the following assignment:

$$\alpha_I = \frac{1}{2}\,(-1)^{I-1/2} \ . \tag{6}$$

Indeed, Eq. 6 describes the signature quantum number for a state of angular momentum I belonging to an odd mass nucleus. Such a rotational band with a sequence of states differing in spin by $\Delta I = 1$ will be divided into two branches, each branch consisting of levels differing in spin by $\Delta I = 2$, being related by the signature number $\alpha_I = \pm 1/2$. In [64] the signature concept is brought to the classical picture associated with a triaxial nucleus employing rotation operators which act on the trial function (this function is a product of two coherent states, one that is associated to the core and one to the valence nucleon). Eqs. 27-29 from [64] will extract two signatures for TSD_1 and TSD_2, namely the *favored* signature $\alpha_{1f} = +1/2$ for the first band, and *un-favored* signature $\alpha_{2u} = -1/2$ for the second band, respectively. A justification for the possibility of TSD_1 and TSD_2 of being SPB was based on the calculation of the triaxial potential (which was systematically performed in [53] and [62]), concluding that the minimum is very deep, preventing in this way the states from TSD_2 to share other minima through tunneling effects. Other experimental and theoretical results [72–75] for deformed nuclei around this mass region suggest that the calculations performed in `W1` regarding the connection between TSD_1 and TSD_2 as belonging to a signature splitting phenomenon are valid and consistent with already existing interpretations.

It is instructive to mention a few key-points which arise based on the above discussion regarding `W1`:

(a) The wobbling band structure in ^{163}Lu was re-interpreted: three bands are now yrast ground states, and only TSD_3 is one-phonon excited wobbling band (built on top of TSD_2)

(b) Both TSD_1 and TSD_2 are obtained variationally, by solving the time dependent variational equation associated to the initial quantal Hamiltonian

(c) There are three different $R + j$ coupling schemes that will produce the entire wobbling spectra of ^{163}Lu (the following naming scheme is exclusive to this work):

  (i) Coupling C_1: The odd proton $j_1 = 13/2$ is coupled to a core sequence with a.m. $R_1 = 0, 2, 4, \ldots$ (even spin states for the triaxial rotor).

  (ii) Coupling C_2: The same odd proton $j_1 = 13/2$ as in C_1 is coupled to a core sequence with a.m. $R_2 = 1, 3, 5, \ldots$ (odd spin states for the triaxial rotor).

  (iii) Coupling C_3: A different odd proton $j_2 = 9/2$ is coupled to the same core as in C_2.

(d) Two different sets of MOIs corresponding to the triaxial nucleus (that is the rotor coupled with the odd proton) are obtained as fitting parameters throughout the numerical calculations: one for the set $TSD_{1,2,3}$ and one for TSD_4.

(e) TSD_1 and TSD_2 are Signature Partner Bands: with TSD_1 (TSD_2) being the favored (un-favored) partner. Their corresponding signature quantum numbers are $\alpha_{1f} = +1/2$ and $\alpha_{2u} = -1/2$.

(f) As a side-by-side comparison with regards to the overall agreement with the experimental data, `W1` yielded better results when compared to the previous work depicted in Ref. [61], although it must be mentioned that both models are based on semi-classical approaches.

A diagram that shows the workflow involved in `W1` can be seen in Figure 15 from the Appendix. Also, a comparison with previous calculations can be seen in Figure 21 from Ref. [64].

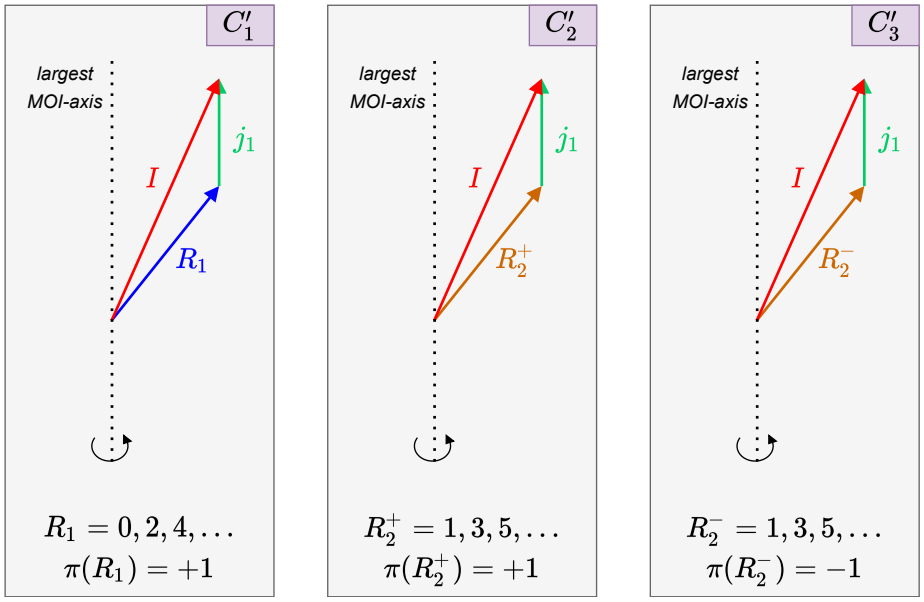

Figure 4: A schematic representation with the three coupling schemes that characterize the `W2` model. The same odd particle ($j_1 = i_{13/2}$ proton) is coupled with two positive cores with even (odd) integer spin sequences for TSD_1 (TSD_2), and one negative core in the case of TSD_4 with odd integer spin sequence. The total spin of the system precesses around the axis with the largest MOI, as it is the case for a triaxial rotor.

3.2 `W2` - Signature Partner Bands + Parity Partner Bands

The main question which can be asked regarding the formalism `W1` that was described in 3.1 is whether it is possible to obtain a *unified* description for all four bands in ^{163}Lu concerning the coupling scheme. In other words, it is worth investigating the possibility of having a unique single-particle state j that is coupled to a core of positive parity for the bands $TSD_{1,2,3}$ and a core of negative parity for TSD_4.

Fortunately, the answer is positive: starting from the semi-classical formalism of `W1`, one can properly adjust the coupling scheme, making sure that the entire numerical recipe used for obtaining the energy spectrum of ^{163}Lu remains consistent with the experimental results.

Regarding the unique single-particle that couples to the triaxial core, it is natural to pick the $i_{13/2}$ proton (that is j_1 from `W1`). The reasoning behind this choice has to do with the microscopic calculations [16, 19, 68] that showed stable triaxial structures in the ^{163}Lu potential energy surface when the triaxial core couples with a highly aligned j-shell particle, indicating the $\pi(i_{13/2})$ proton. Keep in mind that a highly aligned j-nucleon will *prefer* to keep a certain triaxial deformation when coupled to a core [76–78] (in the sense that the triaxiality parameter γ will have a certain value based on the orbital of the odd nucleon), and using microscopic calculations following the Ultimate Cranker code, it has been shown that a value of $\gamma \approx +20^\circ$ is preferred by the odd $\pi(i_{13/2})$ nucleon.

By taking $j = j_1$ as the sole intruder that couples to a positive core and also a negative core, the sequences with even/odd integer spins for the core do not change. In fact, the coupling schemes can be readily obtained:

(a) Coupling C'_1: the odd j_1 proton aligns with the core of even-integer spin sequence $R_1 = 0, 2, 4, \ldots$, with a parity of the R_1 core that is positive $\pi(R_1) = +1$.

(b) Coupling C'_2: the odd j_1 proton aligns with the core of even-integer spin sequence $R_2^+ = 1, 3, 5, \ldots$, with a parity of the R_2^+ core that is positive $\pi(R_2^+) = +1$.

(c) Coupling C'_3: the odd j_1 proton aligns with the core with an odd-integer spin sequence $R_2^- = 1, 3, 5, \ldots$, which has negative parity $\pi(R_2^-) = -1$.

From the three schemes defined above, it is clear that C'_1 corresponds to the yrast TSD_1, C'_2 to the ground state TSD_2, and finally C'_3 to the ground state TSD_4. Obviously, the odd valence nucleon j_1 has a positive parity $\pi_{j_1} = +1$. There has not been attributed a coupling scheme for TSD_3, since this band still remains as the one-wobbling phonon excitation that is built on top of TSD_2 with the action of a phonon operator which will be characterized later on. The three couplings are schematically represented in Figure 4. One should keep in mind the fact that $\vec{j}$ is aligned with the axis with the largest MOI does not necessarily mean the fact that the model works within the Frozen Alignment approximation - it is just an illustration.

The last step in searching for a unified coupling scheme in ^{163}Lu is to establish a possible relationship between the four bands. As per the calculations involved in `W1`, it was proven that signature is a good quantum number

and indeed, a sign that TSD_1 and TSD_2 are signature partners emerged. Their overall similar properties and spin difference enforce this argument. Furthermore, in this new `W2` approach, the difference in parity between the TSD_2 and TSD_4 but the same angular momentum sequence of their corresponding triaxial core R_2^+ and R_2^- strongly suggest that the two bands are *Parity Partner Bands*: two rotational sequences with energy states characterized by opposite parity, increasing energy that follows a trend $\propto I(I+1)$, and a spin difference $\Delta I = 2$ between states belonging to the same band. In the following section, calculations which will show that parity is indeed a good quantum number for the triaxial rotor + odd-particle system will be provided. For what it is worth mentioning now is that the concept of parity partners between TSD_2 and TSD_4 emerge from the idea that a stable strongly deformed structure is achieved from a single quasiparticle that moves in a quadrupole mean-field generated by a triaxial even-even core. However, there is a splitting in two different cases of coupling mechanisms, namely C_2'/C_3' depending on the alignment of the high-j-shell particle with a core of positive/negative parity.

Similar structures with alternating positive-negative parity bands have been also reported in other nuclei such as ^{40}Ca [79], or some heavier isotopes like ^{218}Fr [80]. In fact, a unified description of states with positive and negative parity in odd-mass nuclei was made over the last decade [81, 82], although therein, a quadrupole-octupole term was introduced within the particle-core Hamiltonian to describe this feature. A diagram which shows the workflow involved in `W2` can be seen in the Figure 16 from the Appendix A.

4 Theoretical Formalism

In this section, a description of the framework used for obtaining the wobbling spectrum of ^{163}Lu is made. As stated in the previous section, the system is described with a similar Hamiltonian used in `W1`, namely the Hamiltonian for the triaxial PRM.

$$H = H_{\text{core}} + H_{\text{s.p.}} \ . \tag{7}$$

The Hamiltonian from Eq. 7 describes a system in which an odd j particle interacts with a triaxial even-even core i.e., the odd nucleon is moving in a quadrupole deformed mean-field that is generated by the core. As such, the first term in the Hamiltonian H_{core} describes the motion of a triaxial core, while the second term $H_{\text{s.p.}}$ represents the single-particle potential characterizing the valence proton.

Indeed, the core Hamiltonian is given by:

$$H_{\text{core}} = \sum_{i=1,2,3} \frac{1}{2\mathcal{I}_i}(I_i - j_i)^2 \ , \tag{8}$$

where the core angular momentum is $\vec{R} = \vec{I} - \vec{j}$ and the terms $\mathcal{I}_i$ represent the moments of inertia for a triaxial ellipsoid, along the principal axes. These three moments of inertia will be considered as free parameters in the present calculations, but, compared to the work `W1`, a unique set of MOIs will be attributed to the four bands, since the triaxial core will create an alignment with a unique particle, that is j_1. Because of this, there is no option for their nature (i.e., rigid or hydrodynamic).

The single-particle Hamiltonian from Eq. 7 is derived from the well-known Nilsson potential [83, 84]:

$$h(\beta_2, \gamma) = C\left\{\cos\gamma Y_{20}(\theta,\varphi) + \frac{\sin\gamma}{\sqrt{2}}\left[Y_{22}(\theta,\varphi) + Y_{2-2}(\theta,\varphi)\right]\right\} \ , \tag{9}$$

where the coupling parameter C causes the level splitting in the deformed field and it is proportional to the quadrupole deformation β_2. The potential h from Eq. 9 is written in terms of the quadrupole deformation and triaxiality parameter that play the role of deformation parameters within a triaxial system (β_2, γ). Its expression using the coupling parameter C is widely used when working with a particle-rotor-model [85–87]. In the present this case, the change $h(\beta_2, \gamma) \rightarrow H_{\text{s.p.}}$ is done by applying the Wigner-Eckart theorem for the single-j particle, and the following expression for $H_{\text{s.p.}}$ will be obtained:

$$H_{\text{s.p.}} = \frac{V}{j(j+1)}\left[\cos\gamma(3j_3^2 - \vec{j}^2) - \sqrt{3}\sin\gamma(j_1^2 - j_2^2)\right] + \epsilon_j \ . \tag{10}$$

This term describes the motion of an odd particle with angular momentum j in a mean-field generated by a triaxial core, with a potential strength V characterized by the quadrupole deformation ($V \propto \beta_2$). In fact, the single-particle potential strength V will be considered as the fourth free parameter within the calculations and its behavior will dictate the coupling of the j particle with all four TSD bands. The term ϵ_j from Eq. 10 represents the single-particle energy that corresponds to the odd j proton from the i-orbital. One should not mix up the j_1 proton notation used throughout the paper with the components of the single-particle angular momentum from Eq. 10.

Regarding the triaxial deformation γ which enters in Eq. 10, its value will be considered as another free parameter of the current problem. In other words, having V and γ as free parameters means that the system will be described by its deformation parameters which will be obtained through a fitting procedure, keeping an agreement with the experimental data regarding the excitation energies of the rotational states belonging to $TSD_{1,2,3,4}$.

From Eqs. 8 and 10, the free parameter set can be obtained, hereafter denoted by $\mathcal{P}$. It comprises three moments of inertia, the single-particle potential strength, and the triaxial deformation. As such, $\mathcal{P}$ can be written as:

$$\mathcal{P} = [\mathcal{I}_1, \mathcal{I}_2, \mathcal{I}_3, V, \gamma] \ . \tag{11}$$

Solving the problem of `W2` is equivalent to finding the eigenvalues of H given in Eq. 7. In a similar approach as in `W1`, the eigenvalues of interest are obtained on the base of a semi-classical approach. Thus, the first step is to perform a de-quantization procedure on H through a TDVE [53, 61, 63]:

$$\delta \int_0^t \langle \Psi_{IjM} | \, H - i \frac{\partial}{\partial t'} \, | \Psi_{IjM} \rangle \, dt' = 0 \ . \tag{12}$$

Working within a semi-classical approach allows one to keep close contact with the system's dynamics in terms of equations of motion for the generalized coordinates. The trial function from Eq. 12 is carefully chosen as a product of two basis states comprising the states with total angular momentum I and j, respectively:

$$|\Psi_{IjM}\rangle = \mathbf{N} e^{z\hat{I}_-} e^{s\hat{j}_-} \, |IMI\rangle \, |jj\rangle \ , \tag{13}$$

where the operators $\hat{I}_-$ and $\hat{j}_-$ denote the lowering operators for the intrinsic angular momenta $\vec{I}$ and $\vec{j}$, respectively, and $\mathbf{N}$ plays the role of the normalization constant. One must remark the fact that the states $|IMI\rangle$ and $|jj\rangle$ from Eq. 13 are extremal states for the operators $(\hat{I}^2, \hat{I}_3)$ and $(\hat{j^2}, \hat{j}_3)$, respectively, and they correspond to the maximally allowed states for a given set of angular momenta I and j. As an observation, the trial function is an admixture of components of definite K, which is consistent with the fact that for a triaxial nucleus, K is not a good quantum number.

The variables z and s from Eq. 13 are complex functions of time, and they play the role of classical coordinates in the phase spaces that describe the motion of the core and the odd particle:

$$z = \rho e^{i\varphi} \ , \ s = f e^{i\psi} \ . \tag{14}$$

In order to obtain a set of classical equations in a Hamilton Canonical form, a new pair of variables are introduced:

$$r = \frac{2I}{1+\rho^2} \ , \ t = \frac{2j}{1+f^2} \ , \tag{15}$$

where $r \in [0, 2I]$ and $t \in [0, 2j]$.Thus the equations of motion acquire the form:

$$\begin{aligned} \frac{\partial \mathcal{H}}{\partial r} &= \dot{\varphi} \ ; \ \frac{\partial \mathcal{H}}{\partial \varphi} = -\dot{r} \ , \\ \frac{\partial \mathcal{H}}{\partial t} &= \dot{\psi} \ ; \ \frac{\partial \mathcal{H}}{\partial \psi} = -\dot{t} \ . \end{aligned} \tag{16}$$

The function $\mathcal{H}$ denotes the average of the Hamiltonian operator H (Eq. 7) with the trial function $|\Psi_{IjM}\rangle$ given in Eq. 13, and it plays the role of classical energy:

$$\mathcal{H}(\varphi, r; \psi, t) = \langle \Psi_{IjM} | \, H \, | \Psi_{IjM} \rangle \ , \tag{17}$$

Starting from the equations of motion given in Eq. 16, one can observe that the function $\mathcal{H}$ is a constant of motion, that is $\dot{\mathcal{H}} \equiv 0$. This equation will define a surface, a so-called equi-energy surface $\mathcal{H} = \text{const}$. It is worth mentioning the fact that such equality holds since the entire set of equations of motion emerged from a variational principle. The sign of the Hessian associated to this classical function will indicate its stationary points. Among them, some are minima. The critical points which are of interest for the present study are those obtained when the following ordering for the three moments of inertia holds: $\mathcal{I}_1 > \mathcal{I}_2 > \mathcal{I}_3$. There is no restriction on γ.

With a linearization procedure for the equations of motion around the minimum point of $\mathcal{H}$, a dispersion equation will be obtained:

$$\Omega^4 + B\Omega^2 + C = 0 \ . \tag{18}$$

The above equation describes a harmonic type of motion for the nuclear system, with the solutions to this algebraic equation as the *wobbling frequencies* Ω. The terms B and C are functions of total angular momentum I, single-particle a.m. j, inertial parameters $A_k = 1/(2\mathcal{I}_k)$, $k = 1, 2, 3$, single-particle potential strength V, and triaxiality parameter γ. The B term from Eq. 18 has the expression [64]:

$$-B = [(2I-1)(A_3 - A_1) + 2jA_1]\,[(2I-1)(A_2 - A_1) + 2jA_1] + 8A_2A_3Ij + \mathrm{T}^1_B\mathrm{T}^2_B \ , \tag{19}$$

where the terms T^1_B and T^2_B are defined defined as:

$$\begin{aligned}
\mathrm{T}^1_B &= \left[(2j-1)(A_3 - A_1) + 2IA_1 + V\frac{2j-1}{j(j+1)}\sqrt{3}(\sqrt{3}\cos\gamma + \sin\gamma)\right] \ , \\
\mathrm{T}^2_B &= \left[(2j-1)(A_2 - A_1) + 2IA_1 + V\frac{2j-1}{j(j+1)}2\sqrt{3}\sin\gamma\right] \ .
\end{aligned} \tag{20}$$

Accordingly, the C term from Eq. 18 has the expression [64]:

$$\begin{aligned}
C = &\left\{[(2I-1)(A_3 - A_1) + 2jA_1]\,\mathrm{T}^1_C - 4IjA_3^2\right\} \\
&\times \left\{[(2I-1)(A_2 - A_1) + 2jA_1]\,\mathrm{T}^2_C - 4IjA_2^2\right\} \ ,
\end{aligned} \tag{21}$$

where the terms T^1_C and T^2_C are defined defined as:

$$\begin{aligned}
\mathrm{T}^1_C &= \left[(2j-1)(A_3 - A_1) + 2IA_1 + V\frac{2j-1}{j(j+1)}\sqrt{3}(\sqrt{3}\cos\gamma + \sin\gamma)\right] \ , \\
\mathrm{T}^2_C &= \left[(2j-1)(A_2 - A_1) + 2IA_1 + V\frac{2j-1}{j(j+1)}2\sqrt{3}\sin\gamma\right] \ .
\end{aligned} \tag{22}$$

It can be seen that the terms which enter in B and C, namely $(\mathrm{T}^1_B, \mathrm{T}^2_B)$ from Eq. 20 and $(\mathrm{T}^1_C, \mathrm{T}^2_C)$ from Eq. 22 correspond to the quadrupole deformation that causes the single-particle to move in the mean-field of the triaxial core. The terms also define the triaxiality that the nucleus achieves once the odd proton couples to the triaxial core, driving the system up to a large (and stable) deformation.

Going back to Eq. 18, under the restrictions for the MOIs defined above, the dispersion equation admits two real and positive solutions (hereafter denoted with Ω^I_1 and Ω^I_2, where $\Omega^I_1 < \Omega^I_2$) defined for $j_1 = i_{13/2}$, given by:

$$\Omega^I_{1,2} = \sqrt{\frac{1}{2}\left(-B \mp (B^2 - 4C)^{1/2}\right)} \ . \tag{23}$$

These two solutions are interpreted as *wobbling frequencies* associated with the motion of the core, and the motion of the odd-particle respectively. As such, each wobbling frequency has an associated wobbling-phonon number:

$$\Omega^I_1 \to n_{w_1} \ ; \ \Omega^I_2 \to n_{w_2} \ . \tag{24}$$

Now the analytical expressions for the four TSD bands in ^{163}Lu are readily obtained:

$$\begin{aligned}
E^I_{\mathrm{TSD1}} &= \epsilon_j + \mathcal{H}^{(I,j)}_{\mathrm{min}} + \mathcal{F}^I_{00} \ , \ I = 13/2, 17/2, 21/2 \ldots \\
E^I_{\mathrm{TSD2}} &= \epsilon^1_j + \mathcal{H}^{(I,j)}_{\mathrm{min}} + \mathcal{F}^I_{00} \ , \ I = 27/2, 31/2, 35/2 \ldots \\
E^I_{\mathrm{TSD3}} &= \epsilon_j + \mathcal{H}^{(I-1,j)}_{\mathrm{min}} + \mathcal{F}^{I-1}_{10} \ , \ I = 33/2, 37/2, 41/2 \ldots \\
E^I_{\mathrm{TSD4}} &= \epsilon^2_j + \mathcal{H}^{(I,j)}_{\mathrm{min}} + \mathcal{F}^I_{00} \ , \ I = 47/2, 51/2, 55/2 \ldots \ ,
\end{aligned} \tag{25}$$

where $\mathcal{F}^I_{n_{w_1}n_{w_2}}$ is a function of the wobbling frequencies:

$$\mathcal{F}^I_{n_{w_1}n_{w_2}} = \Omega^I_1\left(n_{w_1} + \frac{1}{2}\right) + \Omega^I_2\left(n_{w_2} + \frac{1}{2}\right) \ , \tag{26}$$

and $\mathcal{H}^{(I,j)}_{\mathrm{min}}$ is the classical energy evaluated in its minimal point. For the present case, its analytical expression is given by the following equation:

$$\mathcal{H}^{(I,j)}_{\mathrm{min}} = (A_2 + A_3)\frac{I+j}{2} + A_1(I-j)^2 - V\frac{2j-1}{j+1}\sin\left(\gamma + \frac{\pi}{6}\right) \ . \tag{27}$$

Band	n_{w_1}	n_{w_2}	π	α	Coupling scheme
TSD_1	0	0	+1	+1/2	C'_1
TSD_2	0	0	+1	-1/2	C'_2
TSD_3	1	0	+1	+1/2	Built on top of TSD_2
TSD_4	0	0	-1	-1/2	C'_3

Table 1: The wobbling phonon numbers, parities, signatures, and coupling schemes assigned to each triaxial band in ^{163}Lu, within the `W2` model. The three coupling schemes were defined in Section 3.2.

A few aspects regarding the energy spectrum defined in Eq. 25 are worth mentioning. To each band, there is a specific energy ϵ_j associated with the single-particle state. In this case, the odd-proton $j_1 = 13/2$ from the i-orbital is the one that couples to the triaxial core. However, for the bands TSD_2 and TSD_4, a different re-normalization of ϵ_j is considered, since TSD_2 is the unfavored signature partner of TSD_1, and TSD_4 is the negative parity partner of TSD_2 within the band structure. These quantities will shift the overall energy states belonging to the two bands, each by a different amount. As a result, both ϵ_j^1 and ϵ_j^2 will be adjusted throughout the numerical calculations such that the energy spectrum is best reproduced. Another aspect concerns the band TSD_3; since this is the only excited wobbling band within the family, its configuration is built on top of TSD_2, with the action of a single phonon ($n_{w_1} = 1$) operator. Consequently, an energy state I belonging to TSD_3 is obtained from a state $I - 1$ from TSD_2. In Table 1, the rest of the wobbling phonon numbers are mentioned, with the parity, signature, and coupling scheme for each band in particular.

4.1 Parity quantum number for the wave-function

In `W1` it was shown that signature emerges from the calculations on the total wave-function as a good quantum number for this triaxial system. This is why in [64] the bands TSD_1 and TSD_2 appeared as Signature Partner Bands (SPB). In `W2`, such property still stands.

Since the backbone of the current work started from the need for a single odd-particle that couples to a triaxial core in ^{163}Lu, one has to look at the band TSD_4 (which was interpreted as having a different nucleon: j_2 with $j = 9/2$ from the h-orbital), and see if its differentiating properties can be linked to *main group* of bands (namely $TSD_{1,2,3}$). Indeed, from the experimental measurements regarding spin and parity assignment [68], it turns out that the parity of the rotational states is negative. Therefore, a forensic analysis on this quantum property should be considered as the necessary ingredient in a unified description of all four bands.

The parity operator is defined as a product of the complex conjugation operation and a rotation of angle π around the 2-axis: $P = e^{-i\pi \hat{I}_2} C$. The total parity operator is the product of an operator corresponding to the core and one corresponding to the single-particle:

$$\mathcal{P}_T = P_{\text{core}} P_{\text{s.p.}} \ . \tag{28}$$

Acting with the total parity operator defined above, on the trial function Ψ associated , the following result is obtained:

$$\mathcal{P}_T \Psi(r, \varphi; t, \psi) = \Psi(r, \varphi + \pi; t, \psi + \pi) \overset{\text{not.}}{=} \bar{\Psi}. \tag{29}$$

The classical energy function $\mathcal{H}$ has an invariance property at changing the angles with π:

$$\mathcal{H}(r, \varphi; t, \psi) = \mathcal{H}(r, \varphi + \pi; t, \psi + \pi) \ . \tag{30}$$

From Eqs. 29 and 30, it can be concluded that the wave-function describing the triaxial system Ψ and its image through $\mathcal{P}_T$, $\bar{\Psi}$, are two linearly dependent functions which differ only by a multiplicative constant p, with $|p| = 1$. Thus, p can either be -1 or +1, such that:

$$\bar{\Psi} = \pm \Psi(r, \varphi; t, \psi) \ . \tag{31}$$

The above result concludes the parity analysis for the wave-function, showing that the triaxial rotor admits eigenfunctions of negative parity. Therefore, a single wave-function characterized by the coupling of a triaxial core to the odd proton $i_{13/2}$ is describing both positive parity states ($\in TSD_{1,2,3}$) as well as negative parity states ($\in TSD_4$). This analysis, together with the fact that TSD_2 and TSD_4 have the same a.m. sequences (although TSD_2 has more states with low spin than TSD_4) suggest the fact that these two bands might be Parity Partners.

4.2 Energy function - geometrical interpretation

The analytical expression for the average of H with the trial function describing the system was previously calculated in `W1`. Indeed, the energy function $\mathcal{H}$ was given in terms of the phase space coordinates $(r, \varphi; t, \psi)$ as follows [64]:

$$\begin{aligned}\mathcal{H} =& \frac{I}{2}(A_1 + A_2) + A_3 I^2 + \frac{2I-1}{2I} r(2I-r)\mathcal{A}_\varphi + \frac{j}{2}(A_1 + A_2) + A_3 j^2 + \frac{2j-1}{2j} t(2j-t)\mathcal{A}_\psi \\ & - 2\sqrt{r(2I-r)t(2j-t)}\mathcal{A}_{\varphi\psi} + A_3\left[r(2j-t) + t(2I-r)\right] - 2A_3 Ij + V\frac{2j-1}{j+1}\mathcal{A}_\gamma \ , \end{aligned} \tag{32}$$

with:

$$\begin{aligned}&\mathcal{A}_\varphi(\varphi) = (A_1\cos^2\varphi + A_2\sin^2\varphi - A_3) \ , \\ &\mathcal{A}_{\varphi\psi}(\varphi,\psi) = (A_1\cos\varphi\cos\psi + A_2\sin\varphi\sin\psi) \ , \\ &\mathcal{A}_\psi(\psi) = (A_1\cos^2\psi + A_2\sin^2\psi - A_3) \ , \\ &\mathcal{A}_\gamma(t,\psi) = \left[\cos\gamma - \frac{t(2j-t)}{2j^2}\sqrt{3}(\sqrt{3}\cos\gamma + \sin\gamma\cos 2\psi)\right] \ . \end{aligned} \tag{33}$$

It is instructive to check the dependence of the energy function on the angular momentum components, e.g., the coordinates $x_k \overset{\text{not.}}{=} I_k \ , \ k = 1,2,3$, where the quantization axis is chosen as the 3-axis. By expressing the angular momentum coordinates $x_{1,2,3}$ in terms of the polar angles (θ, φ) and a radius I , one obtains:

$$x_1 = I\sin\theta\cos\varphi \ , \ x_2 = I\sin\theta\sin\varphi \ , \ x_3 = I\cos\theta \ . \tag{34}$$

Within this spherical coordinates, and evaluating the energy function around its minimum point $p_0 = (0, I; 0, j)$, the following expression for $\mathcal{H}$ results:

$$\mathcal{H}\mid_{p_0} = I\left(I - \frac{1}{2}\right)\sin^2\theta(A_1\cos^2\varphi + A_2\sin^2\varphi - A_3) - 2A_1 Ij\sin\theta + T_{\text{core}} + T_{\text{s.p.}} \ . \tag{35}$$

The last two terms in this equation are independent on the polar angles (θ, φ), and have the form:

$$\begin{aligned}T_{\text{core}} &= \frac{I}{2}(A_1 + A_2) + A_3 I^2 \ , \\ T_{\text{s.p.}} &= \frac{j}{2}(A_2 + A_3) + A_1 j^2 - V\frac{2j-1}{j+1}\sin\left(\gamma + \frac{\pi}{6}\right) \ . \end{aligned} \tag{36}$$

The classical equations of motion admit two constants of motion: the total energy (E) and the total angular momentum (I). Consequently, by finding the intersection line(s) between the surface of the energy ellipsoid E and the surface of the angular momentum, a sphere of radius I, one finds the system trajectory. Such representations will be made in the following section.

The expression of the energy ellipsoid in Cartesian coordinates is:

$$\begin{aligned}E =& \left(1 - \frac{1}{2I}\right)A_1 x_1^2 + \left(1 - \frac{1}{2I}\right)A_2 x_2^2 + \left[\left(1 - \frac{1}{2I}\right)A_3 + A_1\frac{j}{I}\right]x_3^2 - \\ & - I\left(I - \frac{1}{2}\right)A_3 - 2A_1 Ij + T_{\text{rot}} + T_{\text{sp}} \ . \end{aligned} \tag{37}$$

For a total angular momentum $\vec{I}$, the vector generates a sphere of radius $r = I$ described by the equation:

$$I^2 = x_1^2 + x_2^2 + x_3^2 \ . \tag{38}$$

The trajectories obtained through the intersection of Eqs. 37 and 38 will show a classical visualization of the wobbling character for a triaxial nucleus.

5 Numerical results

As a first step, the results concerning the excited spectrum of the four TSD bands will be presented. Regarding the wobbling spectrum of ^{163}Lu, its analytical formulation was given in Eq. 25. As mentioned, those energies

Band	n_s	$\vec{j}$	$\vec{R}$ - Sequence	$\vec{I}$ - Sequence	Coupling scheme
TSD_1	21	j_1	$R_1 = 0, 2, 4, \ldots$	$13/2, 17/2, 21/2, \ldots$	C_1'
TSD_2	17	j_1	$R_2^+ = 1^+, 3^+, 5^+, \ldots$	$27/2, 31/2, 35/2, \ldots$	C_2'
TSD_3	14	j_1	1-phonon excitation	$33/2, 37/2, 41/2, \ldots$	1-phonon excitation
TSD_4	11	j_1	$R_2^- = 1^-, 3^-, 5^-, \ldots$	$47/2, 51/2, 55/2, \ldots$	C_3'

Table 2: The number of energy states n_s within each wobbling band, the a.m. of the proton $\vec{j}$, the core's a.m. $\vec{R}$, the nucleus' a.m. $\vec{I}$, and the corresponding coupling scheme that was established according to the `W2` model. The single-particle is the $j_1 = (i_{13/2})$ proton.

$\mathcal{I}_1$ [$\hbar^2$/MeV]	$\mathcal{I}_2$ [$\hbar^2$/MeV]	$\mathcal{I}_3$ [$\hbar^2$/MeV]	γ [deg.]	V [MeV]
72	15	7	22	2.1

Table 3: The parameter set $\mathcal{P}$ that was determined by a fitting procedure of the excitation energies for ^{163}Lu.

are parametrized in terms of $\mathcal{P}$, which is the set of free parameters to be determined. Indeed, one can find $\mathcal{P}$ by minimizing the χ^2 function:

$$\chi^2 = \frac{1}{N_T} \sum_i \frac{(E_{\rm exp}^{(i)} - E_{\rm th}^{(i)})^2}{E_{\rm exp}^{(i)}} \ , \tag{39}$$

where N_T represents the total number of states. Table 2 contains the number of states within each band, with the spin sequences for the core ($\vec{R}$), the spin sequences for the coupled system (that is the total angular momentum $\vec{I}$), and the coupling schemes specific to `W2` formalism that is used in the current calculations.

The resulting values for $\mathcal{P}$ are given in Table 3. This `W2` method contrasts the approach in `W1`, where a second minimization process was needed separately for TSD_4. The root mean square error provided by the obtained parameter set $\mathcal{P}$ has a value of $E_{\rm rms} \approx 79$ keV. This result is much better than the one obtained with previous formalism `W1` where an $E_{\rm rms} \approx 240$ keV was obtained [64]). As a matter of fact, this is the first semi-classical formalism in the literature that achieves agreement with the experimental data with less than 100 keV for the entire wobbling spectrum of ^{163}Lu. It is worth mentioning that the fitting procedure was done not for the absolute wobbling energies $E^I_{\rm TSDk}$, $k = 1, 2, 3, 4$, but for the *excitation energies* which are relative to the hand-head $I = 13/2^+$ from the first yrast band TSD_1. Comparison between the theoretical values obtained within the current formalism and the experimental data is shown in Figures 5 and 6. For the sake of completeness, the wobbling frequencies which enter in the expression of the $\mathcal{F}^I_{n_{w_1} n_{w_2}}$ given by Eq. 26 are graphically represented as functions of total angular momentum I in Figure 7, for the fixed parameter set. It is remarkable the fact that the wobbling frequency Ω_2^I is much larger than its partner, suggesting the fact the coupling effects caused by the highly aligned proton have a stronger influence in achieving a wobbling character for ^{163}Lu, which is in line with the characteristics of a particle-rotor coupling. Another feature of these wobbling frequencies is their linear behavior with respect to the nuclear spin.

Concerning the single-particle energies from Eq. 25, namely ϵ_j^1 and ϵ_j^2 that emerge from the un-favored signature of TSD_2 and negative parity of TSD_4, respectively, they induce a correction for the mean-field with the quantities $\epsilon_j^1 - \epsilon_j = 0.3$ MeV and $\epsilon_j^2 - \epsilon_j = 0.6$ MeV. Note that since the energy state $I_{13/2} \in TSD_1$ (the band-head of TSD_1) was subtracted from all bands, the single-particle energies for band 2 and 4 are adjusted accordingly.

The quantity $\epsilon_j^1 - e_j$ is added to the second band due to the core, and such a splitting is caused by the fact that two distinct TDVE procedures were performed for the two partner bands $TSD_{1,2}$. The total signature splitting for the band-head and the terminus states of TSD_2 are $E^{27/2}_{TSD2} - E^{25/2}_{TSD2} = 0.492$ MeV and $E^{91/2}_{TSD2} - E^{89/2}_{TSD2} = 0.936$ MeV which agrees with the estimate made by Jensen et. al. in [19]. Although the signature splitting can be determined microscopically by using a deformed single-particle basis amended with a cranking constraint, for the present case it is obtained by applying the TDVE for each spin state and the correction corresponding to the single-particle energies (that is ϵ_j^1).

Another noteworthy aspect of the current formalism is the fact that the difference $\delta_{42} = E^I_{\rm TSD4} - E^I_{\rm TSD2}$ for all the states has an almost constant value $\delta_{42} \approx 0.3$ MeV. This suggests that the states of the same a.m. from TSD_2 and TSD_4 bands might emerge through the parity projection of a sole wave-function that does not have reflection symmetry. In the present case, this is caused by the fact that the wobbling frequency is parity-independent. It is interesting that the action of the parity operator on any rotational state within the angular momentum space will lead to the change of the angular momentum vector from $\vec{I}$ to $-\vec{I}$. Due to this reason, the parity operator commutes with the initial Hamiltonian, and the eigenfunctions of H are characterized by either positive or negative parity (with states of different parities being degenerate). However, one can lift this

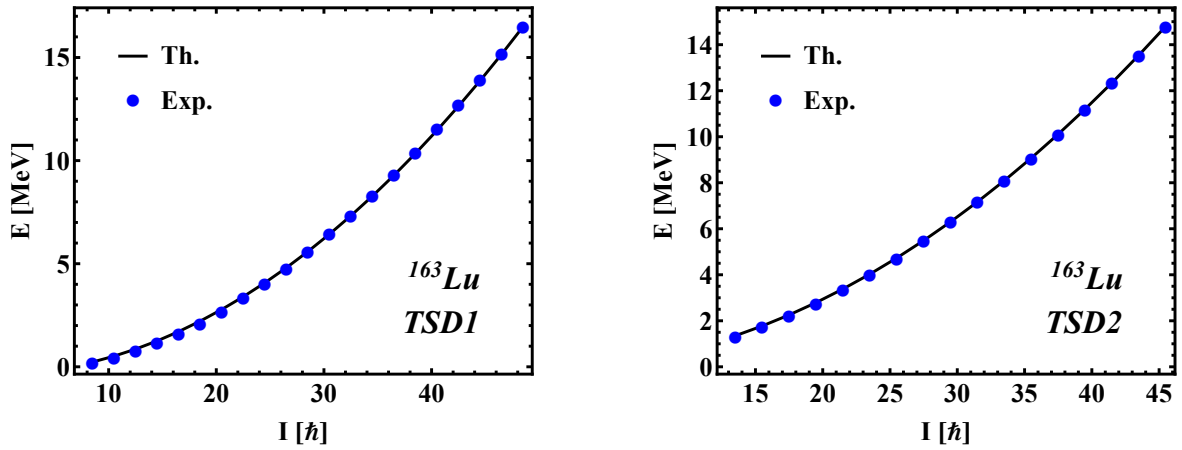

Figure 5: Comparison between theoretical and experimental excitation energies for the first two wobbling bands in ^{163}Lu within the W2 model. The theoretical results are obtained with the parameters listed in Table 3. Experimental data is taken from [88].

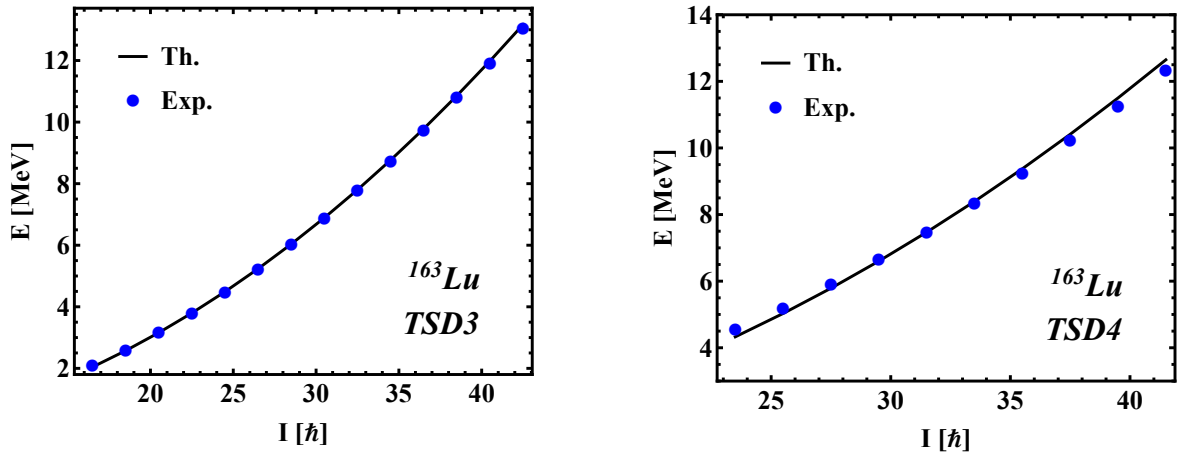

Figure 6: Comparison between theoretical and experimental excitation energies for third and fourth wobbling bands in ^{163}Lu within the W2 model. The theoretical results are obtained with the parameters listed in Table 3. Experimental data is taken from [88].

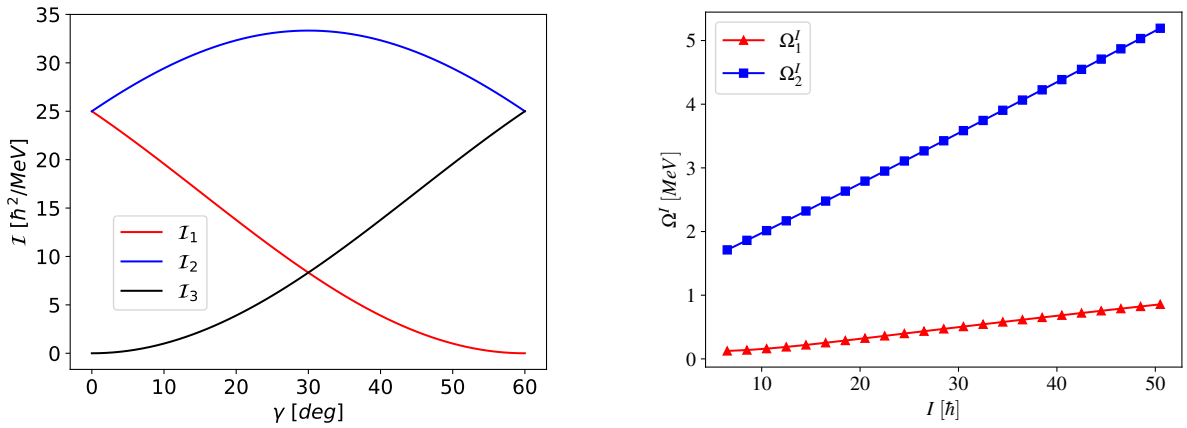

Figure 7: Left-side: The hydrodynamic moments of inertia [37] as function of the triaxiality parameter γ, for the positive interval $\gamma \in [0°, 60°]$, evaluated for a scale factor $\mathcal{I}_0 = 25$ MeV^{-1}. Right-side: The wobbling frequencies defined in Eq. 23 as function of total angular momentum, evaluated with the parameter set $\mathcal{P}$ which was obtained through the fitting procedure.

degeneracy by using an additional linear in the expression H. Since in Eq. 7 such a linear term is missing, an *ad-hoc* correction of the mean-field with the amount 0.6 MeV for the states in TSD_4 is necessary. As a result, the added shift simulates the breaking of parity symmetry. In contrast to this approach, using a microscopic formalism one starts with a single-particle basis generated by a mean-field without space reflection symmetry, followed by the calculation of the many-body wave-functions (being admixtures of both positive and negative parities). Restoration of the parity symmetry is achieved by selecting from all the wave-functions only the components with a definite parity (projecting the good parity), leading to a doublet structure of positive and negative parity states in the spectrum of H. Consequently, the bands TSD_2 and TSD_4 behave as a pair of parity partners, as defined in [89–91].

5.1 Interpretation of the parameter set $\mathcal{P}$

Performing the fitting procedure for the excitation energies of ^{163}Lu will result in the moments of inertia $\mathcal{I}_k$ that are given in Table 3, together with the single-particle potential strength V, and triaxiality parameter γ. Interpretation of their numerical values is mandatory in order to check whether the current formalism is valid or not.

Regarding the moments of inertia, it is clear that the axis of rotation for the energy ellipsoid is the 1-axis, as the largest MOI is $\mathcal{I}_1$, causing a maximal density distribution across this axis [35]. The MOI ordering is $\mathcal{I}_1 > \mathcal{I}_2 > \mathcal{I}_3$, and compared with the results of the previous work `W1`, the current 1-axis MOI is bigger than both $\mathcal{I}_1^{\mathrm{TSD1,2,3}} = 63.2\ \hbar^2/\mathrm{MeV}$ and $\mathcal{I}_1^{\mathrm{TSD4}} = 67\ \hbar^2/\mathrm{MeV}$ (data taken from Table 1 in Ref. [15]). This is expected, since here, the TSD_4 band is obtained by the coupling of a higher aligned j particle, driving the system to an even larger deformation. One must remember that these are the *effective* MOIs of the entire system, that is the triaxial-rotor + odd-particle. No spin dependence has been inferred for the MOIs, so a possible change in the MOIs ordering with the increase in spin I cannot be studied within the current description. Furthermore, this formalism does not contain microscopic terms, so no presumptions on what causes the obtained MOI ordering can be stated. Although, by working with a quadrupole deformed mean-field, the moments of inertia of the triaxial core should be indeed consistent with the hydrodynamic model. For the sake of completeness, Figure 7 shows the evolution of a hydro-dynamical set of MOIs with respect to the triaxiality parameter γ.

Concerning the triaxiality parameterγ, it has a positive value $\gamma = 22°$. This is consistent with the microscopic descriptions based on cranking mechanism for the potential energy surface (PES) of ^{163}Lu (discussion on PES was done in the previous sections). In fact, the agreement is quite good with the predicted deformed minima of $(\beta_2, \gamma) \approx (0.38, 20°)$ [19, 68]. Comparing the current `W2` model with already existing descriptions which take γ to be fixed a-priori throughout the calculations (e.g., [37, 69]), here γ is obtained through the fitting process in a self-consistent manner. Moreover, its value is slightly larger than the one obtained in `W1` formalism ($\gamma = 17°$). This might be due to the larger ratios $\mathcal{I}_1/\mathcal{I}_{2,3}$, which in the present case they appear to be bigger ($\mathcal{I}_1/\mathcal{I}_2 \approx 4.8$ for `W2`, compared to ≈ 3.2 in the previous approach W1).

Finally, the single-particle potential strength, which causes the odd-proton to move in the quadrupole deformed mean-field, has a value of $V = 2.1$ MeV. In `W1`, this parameter was $V^{\mathrm{TSD1,2,3}} = 3.1$ MeV and $V^{\mathrm{TSD4}} = 0.7$ MeV. An explanation for its decrease in the present case might be due to the upward shift in the energy caused by the un-favored partner, or due to the energetic shift of the parity partner, indicating a quenching effect on the quadrupole deformation of the triaxial system. Nevertheless, the obtained value seems

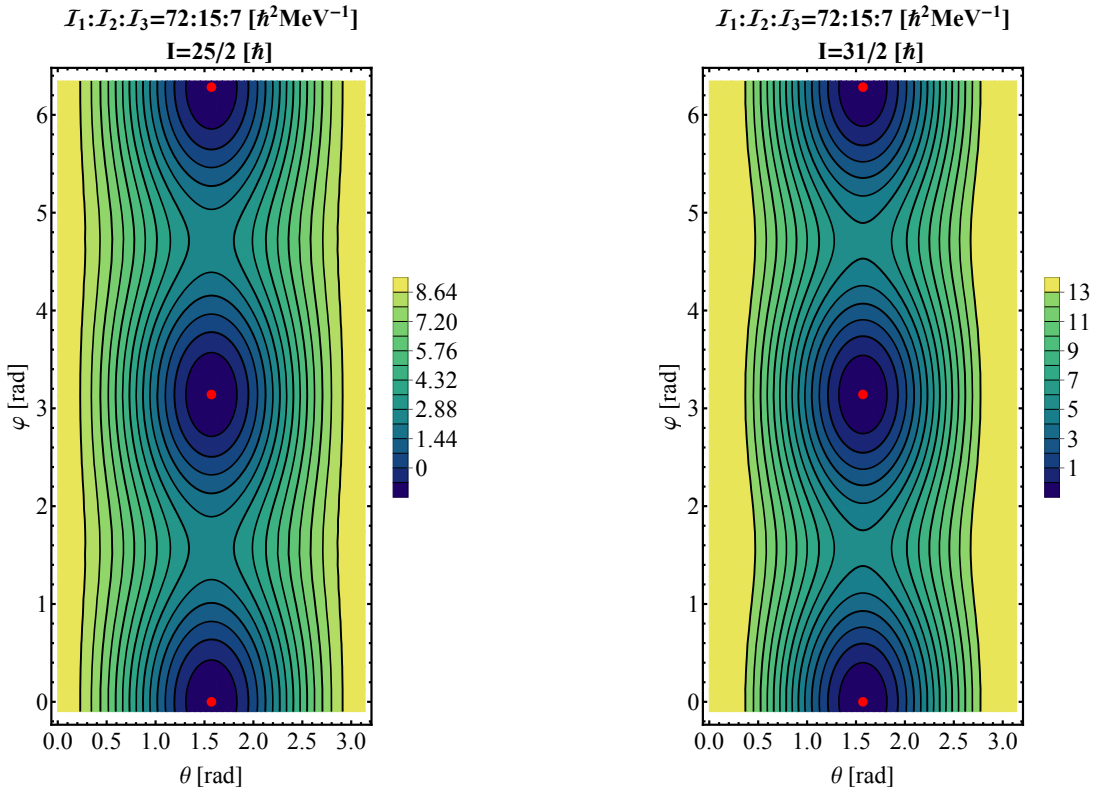

Figure 8: Contour plots with the energy function $\mathcal{H}$ given by Eq. 35 for a state in TSD_1 (left) and a state from TSD_2 (right). Calculations were performed with the numerical parameters obtained from the fitting procedure of the excitation energies. The minimum points for $\mathcal{H}$ are marked by red dots, and they represent the regions in space where the nucleus has a stable wobbling character. The darker *islands* also indicate a stable motion of the triaxial nucleus.

to be consistent with the previous calculations, the current value of V being close to the average value of V's from `W1`. Other interpretations [69] that were developed using a similar single-particle potential term in the Hamiltonian adopted values of around $V = 1.6$ MeV, however, that was for an isotope with smaller quadrupole deformation $\beta_2 = 0.18$. Interesting research using a single-j shell model which was aimed at obtaining a realistic expression for the deformation parameter has been performed in [92]. Therein, results for the potential strength of odd-A nuclei with similar mass, but different quasiparticle configurations were numerically obtained. Adoption of an equivalent description for the odd-j particle within `W2` could be done, and then compare results for a corresponding configuration. This could be the motivating factor for future work. Concluding this subsection, the obtained values of $\mathcal{P}$ seem to not only describe the wobbling spectrum of ^{163}Lu very well (see results in Figures 5 and 6), but they are also consistent with the previous formalism `W1`, or even with other interpretations from the literature.

5.2 Stability of the wobbling region

The expression for the classical energy function, which plays a crucial role in analyzing the nucleus's stability for a given rotational state, was presented in the previous section, through Eq. 35. This will be used within the present numerical calculations to pinpoint the regions in space where the minimal points of $\mathcal{H}$ exist. A special interest is devoted to the low-lying states from each of the four bands. Namely, for each band, a spin-state close to the band-head is chosen, then using the parameter set $\mathcal{P}$, a graphical representation in the (θ, φ)-coordinate space is realized, and in each case, the extremal points with minimum character are identified. These graphical representations are shown in Figures 8 and 9.

The four contour plots shown in Figures 8 and 9 have many similarities, suggesting common collective properties, but also differences which are caused by the fact that the minima have different depths. A common feature consists in that the equi-energy curves surround a sole minimum for low values in energy, but as the energy increases, the trajectories go around all minima, the lack of localization indicating unstable wobbling motion. The unstable regions might also relate to phase transitions, where the nucleus can undergo a major change in its rotational character. This aspect will also be discussed in the next subsection, devoted to the 3-dimensional representation of the energy ellipsoid and the classical trajectories of the triaxial system.

Regarding the minimum points (marked by red dots on the contour plots), their position remains unchanged

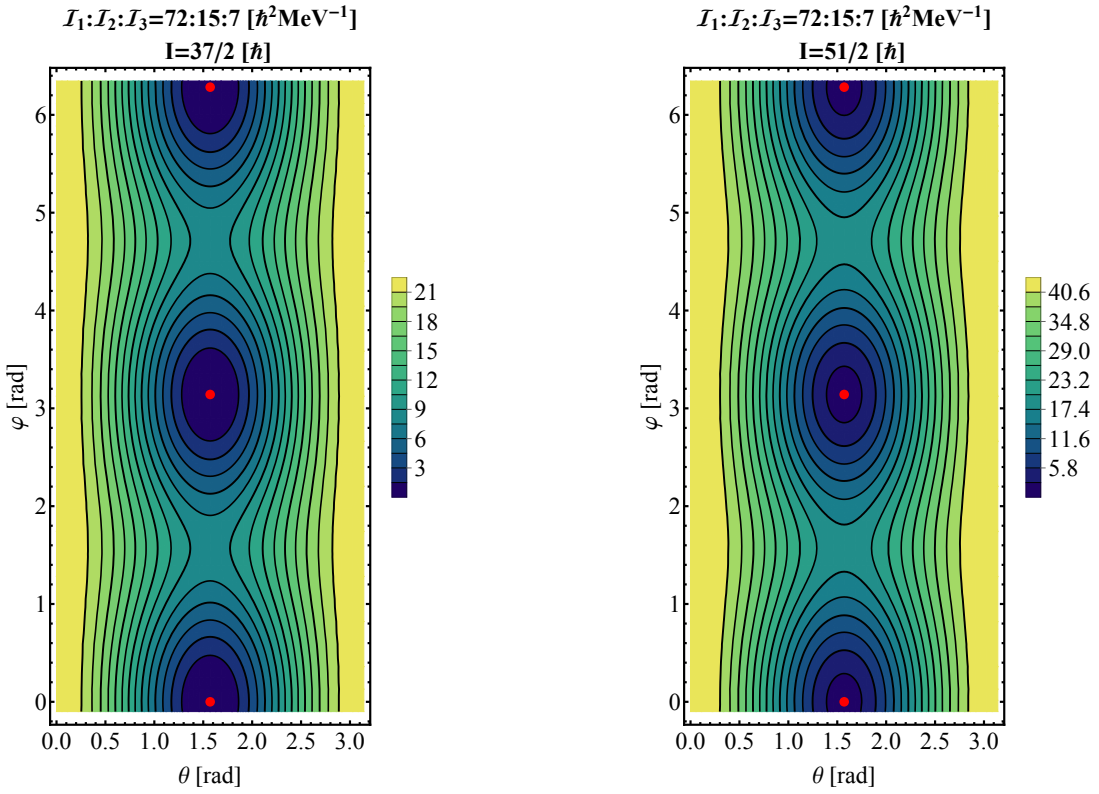

Figure 9: Contour plots with the energy function $\mathcal{H}$ given by Eq. 35 for a state in TSD_3 (left) and a state from TSD_4 (right). Calculations were performed with the numerical parameters obtained from the fitting procedure of the excitation energies. The minimum points for $\mathcal{H}$ are marked by red dots, and they represent the regions in space where the nucleus has a stable wobbling character. The darker *islands* also indicate a stable motion of the triaxial nucleus.

for all four bands and any rotational state I, as long as the MOI order stays the same. Remarkable is the fact that only with the obtained set of parameters (the current MOI ordering) it was possible to define contours with stable motion (marked by the darker regions). Indeed, if the two ratios $\mathcal{I}_1/\mathcal{I}_2$ and $\mathcal{I}_2/\mathcal{I}_3$ would have been smaller, a larger unstable region would prevail (with islands of maximal character), constraining thus the stable wobbling motion. This could indicate the fact that the single-particle term $T_{\text{s.p.}}$ from $\mathcal{H}$ is sensitive to larger triaxiality, and only for certain values will the system achieve a stable motion characterized by large deformation (see Eq. 36).

An additional step consists in the analysis of the energy function, more precisely to see its evolution in one of the minimum points with respect to the angular momentum I. As it was already observed from the contour plots shown in Figures 8-9, the depth of the minima differs from one spin state to another, so it would be useful to have a quantitative view on that change. By fixing $\mathcal{H}$ in one of its critical points (e.g., the minimum $p_{\min}(\theta,\varphi) = (\frac{\pi}{2}, 0)$), the angular momentum I was varied within a large interval, and the evolution of $\mathcal{H}$ was evaluated. Graphical representation is shown in Figure 10.

As it can be seen from Figure 10, the classical energy $\mathcal{H}$ is an increasing function of angular momentum, which is to be expected, since the wobbling energies of the four bands increase with respect to the increase in spin. The negative values of $\mathcal{H}$ for low-lying wobbling states do not indicate that the nucleus has negative energy states since *the rest* of the nucleus' energy is also given by the single-particle energy ϵ_j terms and the phononic $\mathcal{F}^I_{n_{w_1} n_{w_2}}$ terms.

Another useful insight would be the study of the classical energy function $\mathcal{H}$ for the obtained parameter set, as a function of the polar angles (θ, φ). This can be achieved by choosing a minimum point, keeping one of the polar coordinates fixed, and then let the other one vary across its corresponding interval. For ^{163}Lu, such a graphical representation was done for the point $p_{\min} = \left(\frac{\pi}{2}, 0\right)$ (that is the bottom-most red dot from each of the four contour plots depicted in Figures 8-9). Results can be seen in Figure 11.

5.3 Comment on the wobbling nature of ^{163}Lu

It is worthwhile discussing the results obtained regarding the wobbling spectrum of ^{163}Lu. Indeed, by using a fitting procedure that minimized the χ^2 function, it was possible to find a parameter set $\mathcal{P}$ that provides an agreement with the observed experimental data. However, in the current state, there is no clear evidence on

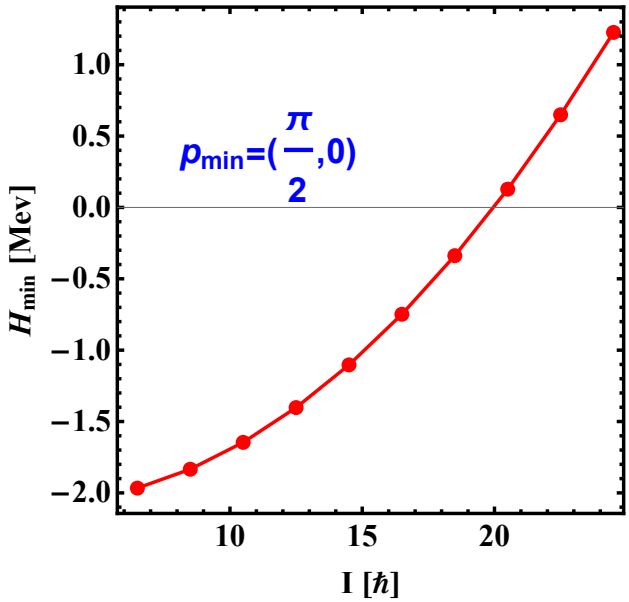

Figure 10: The change in the minimum depth of $\mathcal{H}$, evaluated in the point $(\theta, \varphi) = (\frac{\pi}{2}, 0)$, for the obtained parameter set $\mathcal{P}$.

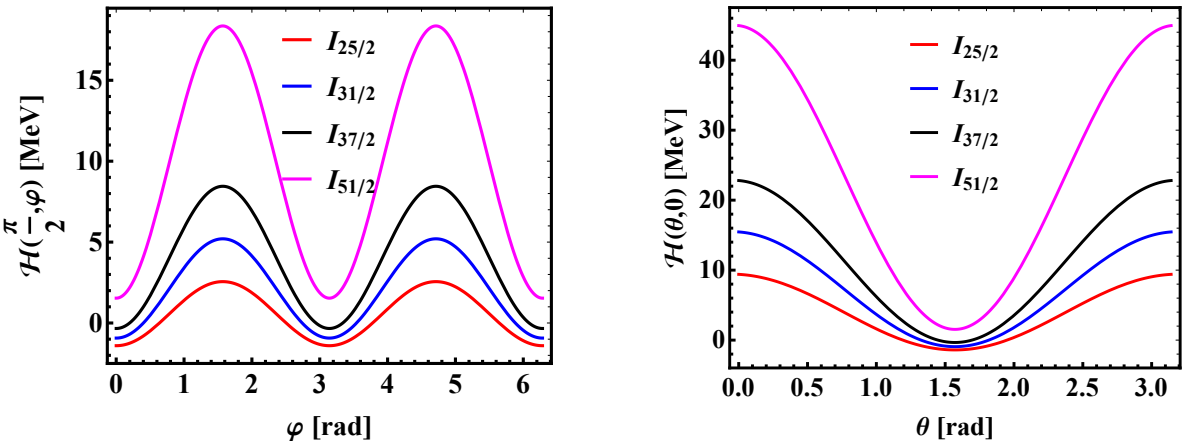

Figure 11: The energy function $\mathcal{H}$, evaluated in one of its minimum points, as a function of the polar coordinates. One coordinate is fixed while the other one is varied within its interval of existence. For $\theta \in [0, \pi]$ and $\varphi \in [0, 2\pi]$. The chosen minimum is $p_{\min} = \left(\frac{\pi}{2}, 0\right)$. Each spin state corresponds to one of the four triaxial bands of ^{163}Lu.

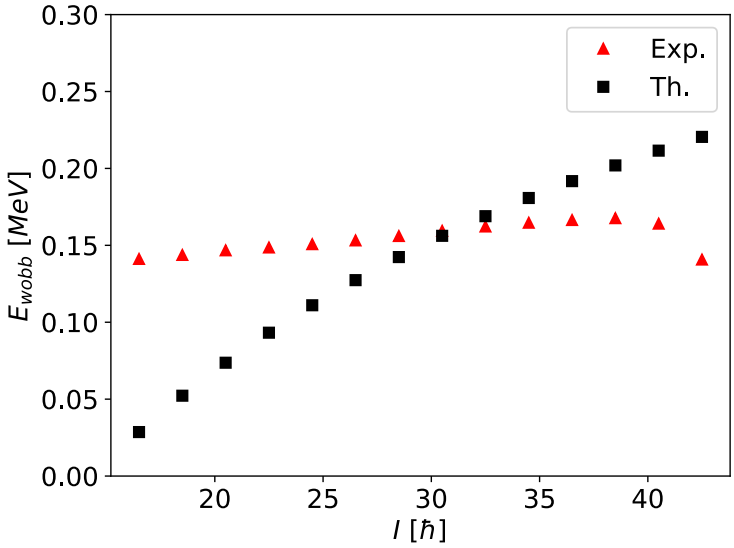

Figure 12: The wobbling energies for ^{163}Lu given as $E_{\text{wob}} = E_1(I) - \frac{1}{2}(E_0(I+1) + E_0(I-1))$. According to the current `W2` formalism, the sets of energies E_1 belong to TSD_3, while E_0 correspond to TSD_2. Experimental data is taken from [88]. Theoretical values were calculated with the parameter set $\mathcal{P}$.

whether the formalism `W2` predicts a TW or an LW behavior for the nucleus. According to [35], the wobbling character is given by the coupling of the odd particle which aligns parallel (LW) or perpendicular (TW) to the axis with the largest MOI. But to see this within the measured data, the interpretation of the wobbling energy as it was defined in Eq. 3 must be performed. As such, according to the definition, one has to subtract an energy state within the first excited wobbling band (the one-wobbling-phonon band) from the average of its adjacent energies that belong to the yrast partner. In the present calculations, the first excited state is TSD_3, with its yrast partner being the band TSD_2. Following this procedure, both the experimental wobbling energies, as well as the theoretical ones were calculated according to the Eq. 3. The obtained results are plotted in Figure 12.

From the behavior of E_{wob} from Figure 12, it can be seen that the theoretical wobbling spectrum is an increasing function of angular momentum I, suggesting that ^{163}Lu would have an LW character. This contrasts the current interpretation on which the wobbling energies are decreasing functions with respect to increasing angular momentum. However, within those formalisms [35, 70], the wobbling energies are obtained from TSD_2 and TSD_1, since the one-wobbling-phonon band is TSD_2, in contradistinction to the present `W2` model, where the first excited wobbling band is TSD_3.

Analyzing the experimental data points from Figure 12, a slight increase with spin can also be observed, suggesting as well that the coupling scheme in ^{163}Lu achieves an LW character. Indeed, from the lower limit of around $11/2\ \hbar$ and up to a spin of about $39/2\ \hbar$, the energy is increasing, then it starts to decrease once $I \geq 39/2\ \hbar$. The increasing behavior of the theoretical data also appears to be quenched in the high-spin limit, indicating that indeed, once the nucleus reaches high rotational states, a change in the wobbling regime might emerge, and the nucleus can transition from a wobbling regime (LW) to another (TW).

Referring back to the the case of ^{183}Au [27], the two observed wobbling bands are based on different alignments: the $\pi(i_{13/2})$ nucleon (for the so-called *positive parity band*) and the $\pi(h_{9/2})$ nucleon (for the *negative-parity* band) coupled to a triaxial rotor, respectively. The remarking aspect of this research is that within a PRM model amended with the HFA (harmonic frozen alignment) approximation, it is implied that the configurations of both bands have a transverse (TW) character. However, the wobbling energies E_{wob} in these bands have different behavior with respect to the increase of angular momentum. Namely, E_{wob} increases (decreases) with spin for the positive (negative) parity configurations (see Figures 3 and 5 from [27]). This indicates that an increasing/decreasing behavior for E_{wob} is not enough evidence for asserting a wobbling character on a triaxial nucleus (at least, not without some strong constraints on the coupling scheme between the core and the odd particle).

Concluding this comment on the wobbling nature for ^{163}Lu, if the behavior of the wobbling energies with spin is the sole player in determining the wobbling character of a nucleus, then one could argue that indeed, based on the current results, ^{163}Lu behaves as a longitudinal wobbler. On the other hand, considering the newly obtained results discussed in the previous paragraphs, the evidence is not enough for making a clear assumption on which type of wobbling motion occurs.

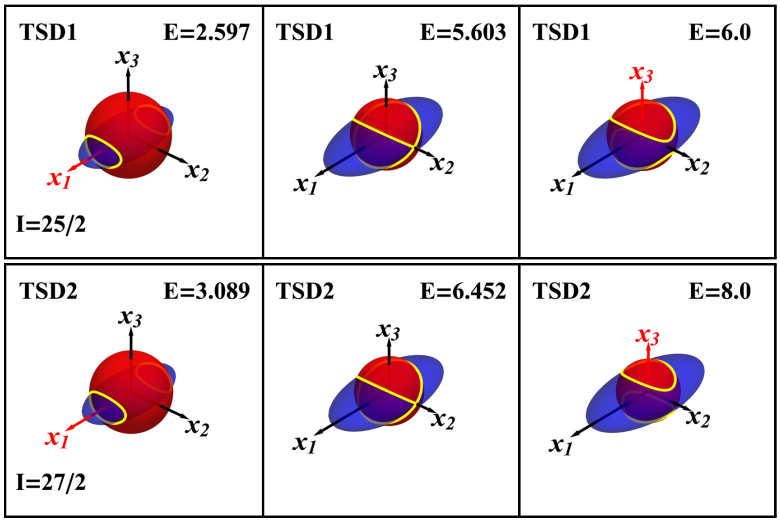

Figure 13: The nuclear trajectories of the system, evaluated for two spin states belonging to TSD_1 and TSD_2. Intersection lines marked by yellow color represents the actual orbits. Axis colored in red represents the direction along which the system rotates (it precesses). The left-most inset corresponds to the real excitation energy for that particular spin state I.

5.4 Classical trajectories - 3-dimensional representation

The final step of the present work is to obtain an insight into the classical features of the ^{163} triaxial nucleus in terms of its motion within the angular momentum space. As already mentioned, the trajectories are given by the intersection curves of the energy ellipsoid E given in Eq. 37 with the angular momentum sphere I^2 given in Eq. 38. In the 3-dimensional space generated by the three components of the angular momentum vector $\vec{I}$, these intersection curves characterize the motion of the system, as each curve will be oriented along with one of the three axes x_k , $k = 1, 2, 3$, suggesting a rotational motion (the precession of the total a.m.) around a particular direction preferred by the system.

The dependence of the classical trajectories on the angular momenta as well as on energies is thus analyzed in `W2`. Indeed, when the model Hamiltonian is diagonalized for a given I, a set of $2I + 1$ energies are obtained. Therefore, it is justified to study the evolution of trajectories when the energy of the nucleus is increasing. The curves are represented as the manifold given by the intersection of the two constants of motion, that is E and I^2. An example of such trajectories are depicted in Figures 13-14.

Each row from the Figures 13-14 represents a rotational state within a band. A low-lying spin state was chosen from each band in particular as an example. The left inset within each row represents the real excitation energy for the state I at which the energy ellipsoid is evaluated. It can be seen that two distinct (but symmetric) trajectories are observed along the 1-axis, for all four states. This suggests that the states of the triaxial nucleus are obtained from the rotation of the angular momentum along x_1. Indeed, for low energies, the rotation is more pronounced along the x_1- and $-x_1$-axes. As the energy of the nucleus increases, the two trajectories approach each other, which results in a tilted rotation axis corresponding to both curves. The tilted axis implies that the rotation axis is being misaligned, the rotational axis moving away from its *equilibrium point*, marking the tilted-axis-rotation. Note that this picture is fully consistent with the one described by Lawrie et al. [93]. Further increase in energy will result in the two trajectories intersect with each other. That particular point where the intersection between the two orbits occurs is marked in the middle inset from each figure. Consequently, the intersection of these two orbits marks an unstable motion within the system. Finally, when the energy increases even more, beyond this *critical point*, one arrives again in a two-trajectories regime but with a different rotation axis, lying closer to the x_3 axis. This case is shown in the right inset within each figure, where the axis x_3 is marked by red color, signaling the change in the rotational mode of the nucleus. However, it is worth noting that such energies are way too large for such a phase transition to occur naturally in ^{163}Lu. For example, in the case of $I_{25/2} \in TSD_1$, the energy at which ^{163}Lu undergoes a phase transition with regards to the rotational mode is close to 5.6 MeV (middle inset for TSD_1 from Figure 8), but the real excitation energy which corresponds to this state is half that (left inset for TSD_1 from Figure 13). Nevertheless, it is a remarkable fact that with the current model, a phase transition between rotational modes in a triaxial nucleus can be identified. A proper microscopic formalism based on this current approach might also provide a more detailed picture with regards to the allowed trajectories for the system.

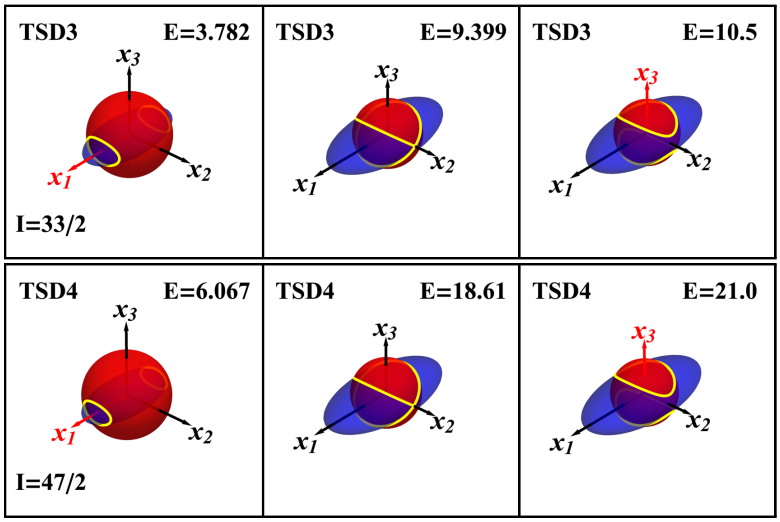

Figure 14: The nuclear trajectories of the system, evaluated for two spin states belonging to TSD_3 and TSD_4. Intersection lines marked by yellow color represents the actual orbits. Axis colored in red represents the direction along which the system rotates (it precesses). The left-most inset corresponds to the real excitation energy for that particular spin state I.

6 Conclusions & Outlook

The purpose of the present work was two-fold. On one hand, a detailed overview regarding the current experimental observations for wobbling motion in both even- and odd-mass nuclei across several mass regions was made in the introductory part (covered in Section 2.1). This was accompanied by a brief mention of the theoretical methods that are used for the microscopic/macroscopic description of the wobbling phenomenon (see Section 2.2). Also in the first part of the paper, a schematic analysis on the characteristics of the wobbling motion was made, which concerned the particle-core configurations in a longitudinal/transverse wobbler. Therein, it was shown that depending on the alignment of the odd quasiparticle with the triaxial core, a certain wobbling regime will prevail, thus concluding the introduction.

On the other hand, the second objective of the current paper was to extend a previous model that describes the ^{163}Lu using a re-interpretation of its four wobbling bands $TSD_{1,2,3,4}$. The previous model (denoted here by `W1`) introduced the concept of signature partners between the bands TSD_1 and TSD_2. One showed that the nucleus can be described as a particle that is moving in a quadrupole deformed mean field generated by the core. In `W1`, there was an $i_{13/2}$ proton involved in the particle-rotor-coupling for the description of the first three triaxial bands, and another proton with negative parity, i.e., the $\pi(h_{9/2})$ intruder for band TSD_4. Based on `W1`, a new approach was developed here as an extension, denoted throughout the paper by `W2`. The new formalism starts with the same Hamiltonian, however, in the present case a single trial function is constructed to admit eigenstates with both positive and negative parity. Indeed, despite the fact that TSD_4 is of an opposite parity than the first three, all bands are described by the coupling of a unique single-particle ($i_{13/2}$ with positive parity $\pi_j = +1$) to the core states of positive parity for $TSD_{1,2,3}$ and core states of negative parity for TSD_4. The coupling schemes for the wobbling bands within `W2` were denoted throughout the paper by C_1', C_2', C_3'. From the quantal Hamiltonian specific to a Particle Rotor Model (given by Eq. 7), by applying a Time-Dependent Variational Principle (TDVE) as in Eq. 12 with the trial function carefully chosen so that it allows a mixture of both positive and negative parity states, a set of analytical expressions for the excitation energies of each band were obtained (defined in Eq. 25). The excitation energies comprise a term that represents the classical energy function, obtained as the average of the Hamiltonian with the trial wave function (Eq. 27). A second term has a phonon character (Eq. 26), being composed of two wobbling frequencies that were obtained from the solutions to a dispersion-like equation as defined in Eq. 18.

From the theoretical formalism of the excitation energies of ^{163}Lu, a set of free parameters emerged, containing the three moments of inertia, the single-particle potential strength V, and the triaxiality parameter γ. They were obtained through a fitting procedure which was done for all four bands, unlike the previous `W1` approach. The resulted parameter set provides an impressive agreement between the existing theoretical and experimental data concerning the wobbling spectrum of this isotope, with an r.m.s. of about 79 keV. An interpretation of the numerical values for the obtained parameters was done in Section 5.1, and indeed, the obtained values are consistent with other formalisms from the literature. Furthermore, the study of the classical energy function was done in a polar coordinate system, obtaining the contour plots for spin states belonging to each triaxial band (Section 5.2). The critical points from those contour maps indicate stability in terms of wobbling behavior

(with closed orbits signaling stable trajectories). Unstable regions also emerge at high rotational energies. An additional comment on the wobbling nature of ^{163}Lu was made (see Section 5.3), and an analysis of the wobbling energy behavior with spin showed that the increasing trend might indicate a longitudinal character. Lastly, by intersecting the angular momentum sphere with the energy ellipsoid, the classical trajectories can be obtained. The results of this 3-dimensional representation are discussed throughout Section 5.4. From the graphical illustrations, three situations might occur for any given spin state of ^{163}Lu. i) At low energies, the rotation axis is either the 1-axis or the -1-axis, resulting in two trajectories along this axis. ii) At a particular energy - *critical energy* - the two orbits get close to each other until they intersect, marking the point of unstable motion for the nucleus. iii) If the energy increases even more, then the triaxial nucleus performs a tilted-axis-rotation, where the rotational axis slowly moves away from x_1, approaching x_3 and thus becoming misaligned. The change from one step to the other marks a phase transition. When the nucleus undergoes a transformation with regards to its rotational behavior it is actually changing its wobbling regime. Remarkable the fact that the current semi-classical approach is able to predict the change in the wobbling regime, this being of large interest in the nuclear community since evidence of such behavior was missing.

Concluding the present work, this newly developed formalism proves to be a successful tool for accurately describing the wobbling spectrum of ^{163}Lu and also for providing an insight into the rotational motion of the nuclear system with respect to its total spin.

Acknowledgments

This work was supported by UEFISCU, through the project **PCE-16/2021**.

A Appendix - Workflow Diagrams

The two models described in Section 2, namely the formalism `W1` (see Section 3.1) and `W2` (see Section 3.2) are schematically represented, based on the discussions made for each of the two approaches. The `W1` mode corresponds to the work given in Refs. [15,64], and the `W2` corresponds to the formalism developed in the present paper. For the formalism `W1`, the diagram is shown in Figure 15, while for the newly developed approach `W2`, the diagram is shown in Figure 16.

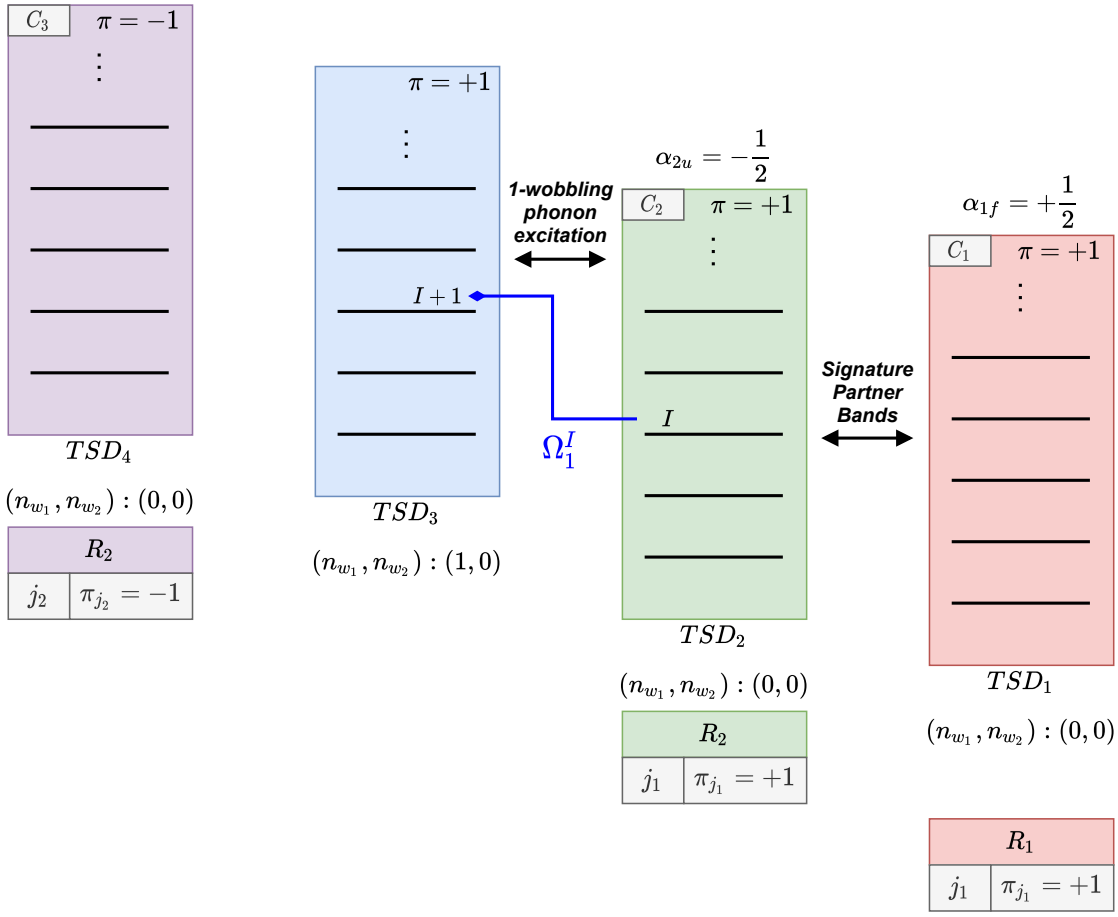

Figure 15: Schematic representation of the band structure adopted for ^{163}Lu in the `W1` model. For each band, the wobbling phonon numbers are shown. The main features and linking properties between bands are represented with arrows. The bottom part shows the coupling scheme (the core and the valence nucleon) for each wobbling band as described in the text, namely C_1, C_2, C_3 (see Section 3.1). The blue arrow marks the activation of TSD_3 states via the phonon operator.

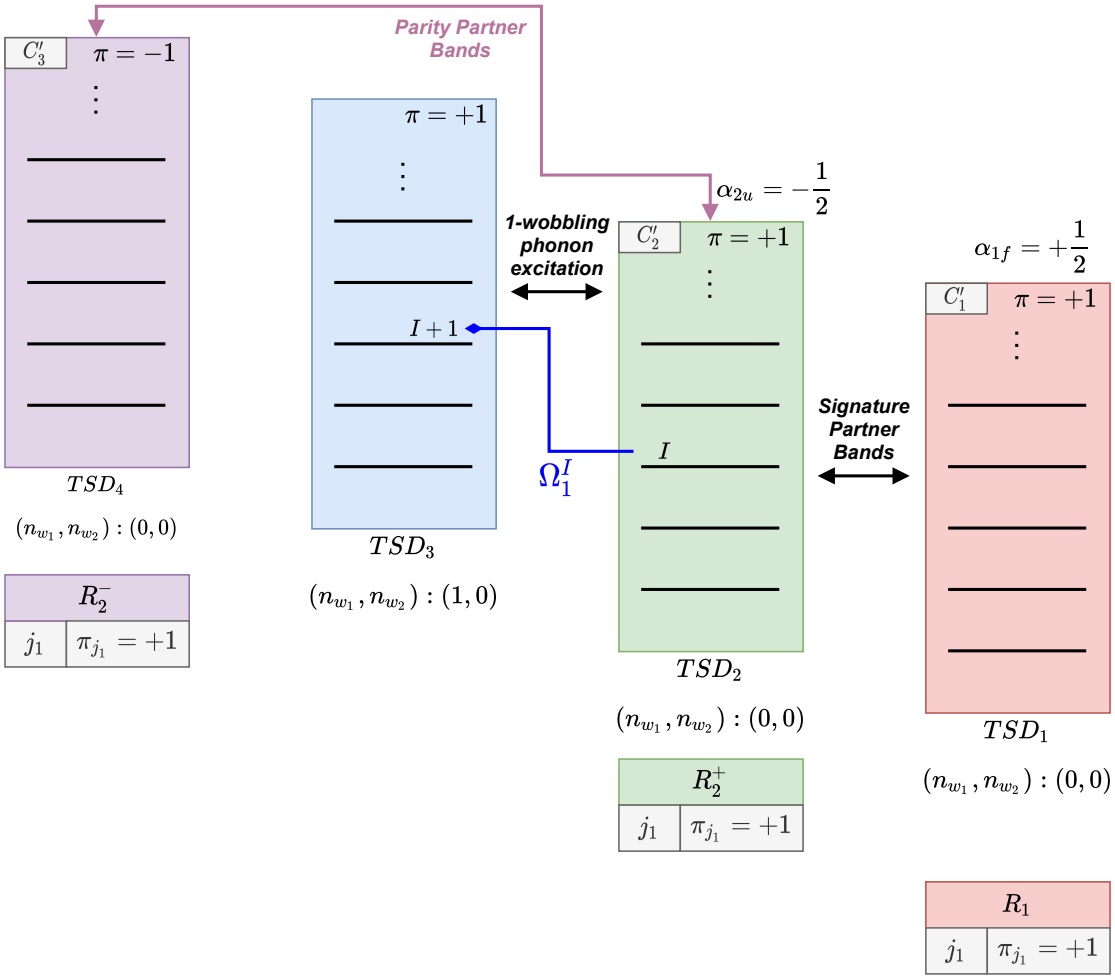

Figure 16: Schematic representation of the band structure adopted for ^{163}Lu in the `W2` model. For each band, the wobbling phonon numbers are shown. The main features and linking properties between bands are represented with arrows. The bottom part shows the coupling scheme (the core and the valence nucleon) for each wobbling band as described in the text, namely C'_1, C'_2, C'_3. The blue arrow marks the activation of TSD_3 states via the phonon operator.

References

[1] Peter Möller, Ragnar Bengtsson, B Gillis Carlsson, Peter Olivius, and Takatoshi Ichikawa. *Physical review letters*, 97(16):162502, 2006.

[2] Peter Möller, Arnold J Sierk, Takatoshi Ichikawa, Akira Iwamoto, Ragnar Bengtsson, Henrik Uhrenholt, and Sven Åberg. *Physical Review C*, 79(6):064304, 2009.

[3] I Hamamoto and H Sagawa. *Physics Letters B*, 201(4):415–419, 1988.

[4] R Bengtsson, H Frisk, FR May, and JA Pinston. *Nuclear Physics A*, 415(2):189–214, 1984.

[5] J Stachel, N Kaffrell, E Grosse, H Emling, H Folger, R Kulessa, and D Schwalm. *Nuclear Physics A*, 383(3):429–467, 1982.

[6] Stefan Frauendorf and Jie Meng. *Nuclear Physics A*, 617(2):131–147, 1997.

[7] Aage Niels Bohr and Ben R Mottelson. *Nuclear Structure (In 2 Volumes)*.

[8] BW Xiong and YY Wang. *Atomic Data and Nuclear Data Tables*, 125:193–225, 2019.

[9] VI Dimitrov, S Frauendorf, and F Dönau. *Physical review letters*, 84(25):5732, 2000.

[10] T Koike, K Starosta, CJ Chiara, DB Fossan, and DR LaFosse. *Physical Review C*, 67(4):044319, 2003.

[11] J Meng, J Peng, SQ Zhang, and S-G Zhou. *Physical Review C*, 73(3):037303, 2006.

[12] AA Raduta, Al H Raduta, and CM Petrache. *Journal of Physics G: Nuclear and Particle Physics*, 43(9):095107, 2016.

[13] CM Petrache, BF Lv, A Astier, E Dupont, YK Wang, SQ Zhang, PW Zhao, ZX Ren, J Meng, PT Greenlees, et al. *Physical Review C*, 97(4):041304, 2018.

[14] BF Lv, CM Petrache, QB Chen, J Meng, A Astier, E Dupont, P Greenlees, H Badran, T Calverley, DM Cox, et al. *Physical Review C*, 100(2):024314, 2019.

[15] AA Raduta, R Poenaru, and CM Raduta. *Journal of Physics G: Nuclear and Particle Physics*, 47(2):025101, 2020.

[16] Gudrun B Hagemann and Ikuko Hamamoto. *Nuclear Physics News*, 13(3):20–24, 2003.

[17] SW Ødegård, GB Hagemann, DR Jensen, M Bergström, B Herskind, G Sletten, S Törmänen, JN Wilson, PO Tjøm, I Hamamoto, et al. *Physical review letters*, 86(26):5866, 2001.

[18] DR Jensen, GB Hagemann, I Hamamoto, SW Ødegård, B Herskind, G Sletten, JN Wilson, K Spohr, H Hübel, P Bringel, et al. *Physical review letters*, 89(14):142503, 2002.

[19] D Ringkøbing Jensen, GB Hagemann, I Hamamoto, SW Ødegård, M Bergström, B Herskind, G Sletten, S Törmänen, JN Wilson, PO Tjøm, et al. *Nuclear Physics A*, 703(1-2):3–44, 2002.

[20] H Schnack-Petersen, Ragnar Bengtsson, RA Bark, P Bosetti, A Brockstedt, H Carlsson, LP Ekström, GB Hagemann, B Herskind, F Ingebretsen, et al. *Nuclear Physics A*, 594(2):175–202, 1995.

[21] S Biswas, R Palit, S Frauendorf, U Garg, W Li, GH Bhat, JA Sheikh, J Sethi, S Saha, Purnima Singh, et al. *The European Physical Journal A*, 55(9):1–7, 2019.

[22] James Till Matta. Transverse wobbling in 135 pr. In *Exotic Nuclear Excitations: The Transverse Wobbling Mode in 135 Pr*, pages 77–93. Springer, 2017.

[23] N Sensharma, U Garg, S Zhu, AD Ayangeakaa, S Frauendorf, W Li, GH Bhat, JA Sheikh, MP Carpenter, QB Chen, et al. *Physics Letters B*, 792:170–174, 2019.

[24] S Chakraborty, HP Sharma, SS Tiwary, C Majumder, AK Gupta, P Banerjee, S Ganguly, S Rai, S Kumar, A Kumar, et al. *Physics Letters B*, 811:135854, 2020.

[25] C M Petrache. *LNL Annual Report*, 2018.

[26] J Timár, QB Chen, B Kruzsicz, D Sohler, I Kuti, SQ Zhang, J Meng, P Joshi, R Wadsworth, K Starosta, et al. *Physical review letters*, 122(6):062501, 2019.

[27] S Nandi, G Mukherjee, QB Chen, S Frauendorf, R Banik, Soumik Bhattacharya, Shabir Dar, S Bhattacharyya, C Bhattacharya, S Chatterjee, et al. *Physical Review Letters*, 125(13):132501, 2020.

[28] N Sensharma, U Garg, QB Chen, S Frauendorf, DP Burdette, JL Cozzi, KB Howard, S Zhu, MP Carpenter, P Copp, et al. *Physical review letters*, 124(5):052501, 2020.

[29] S Guo, XH Zhou, CM Petrache, EA Lawrie, S Mthembu, YD Fang, HY Wu, HL Wang, HY Meng, GS Li, et al. *arXiv preprint arXiv:2011.14354*, 2020.

[30] JH Hamilton, SJ Zhu, YX Luo, AV Ramayya, S Frauendorf, JO Rasmussen, JK Hwang, SH Liu, GM Ter-Akopian, AV Daniel, et al. *Nuclear Physics A*, 834(1-4):28c–31c, 2010.

[31] YX Luo, JH Hamilton, AV Ramaya, JK Hwang, SH Liu, JO Rasmussen, S Frauendorf, GM Ter-Akopian, AV Daniel, Yu Ts Oganessian, et al. Triaxial and triaxial softness in neutron rich ru and pd nuclei. In *Exotic Nuclei: EXON-2012*, pages 215–224. World Scientific, 2013.

[32] CM Petrache, PM Walker, S Guo, QB Chen, S Frauendorf, YX Liu, RA Wyss, D Mengoni, YH Qiang, A Astier, et al. *Physics Letters B*, 795:241–247, 2019.

[33] YK Wang, FQ Chen, and PW Zhao. *Physics Letters B*, 802:135246, 2020.

[34] QB Chen, S Frauendorf, and CM Petrache. *Physical Review C*, 100(6):061301, 2019.

[35] S Frauendorf and F Dönau. *Physical Review C*, 89(1):014322, 2014.

[36] Ikuko Hamamoto. *Physical Review C*, 65(4):044305, 2002.

[37] Kosai Tanabe and Kazuko Sugawara-Tanabe. *Physical Review C*, 73(3):034305, 2006.

[38] Shi Wen-Xian and Chen Qi-Bo. *Chinese Physics C*, 39(5):054105, 2015.

[39] AS Davydov and GF Filippov. *Nuclear Physics*, 8:237–249, 1958.

[40] Yoshifumi R Shimizu and Masayuki Matsuzaki. *Nuclear Physics A*, 588(3):559–596, 1995.

[41] Masayuki Matsuzaki, Yoshifumi R Shimizu, and Kenichi Matsuyanagi. *Physical Review C*, 65(4):041303, 2002.

[42] Masayuki Matsuzaki, Yoshifumi R Shimizu, and Kenichi Matsuyanagi. *The European Physical Journal A-Hadrons and Nuclei*, 20(1):189–190, 2003.

[43] Masayuki Matsuzaki and Shin-Ichi Ohtsubo. *Physical Review C*, 69(6):064317, 2004.

[44] Masayuki Matsuzaki, Yoshifumi R Shimizu, and Kenichi Matsuyanagi. *Physical Review C*, 69(3):034325, 2004.

[45] Yoshifumi R Shimizu, Masayuki Matsuzaki, and Kenichi Matsuyanagi. *Physical Review C*, 72(1):014306, 2005.

[46] Yoshifumi R Shimizu, Takuya Shoji, and Masayuki Matsuzaki. *Physical Review C*, 77(2):024319, 2008.

[47] Takuya Shoji and Yoshifumi R Shimizu. *Progress of theoretical physics*, 121(2):319–355, 2009.

[48] QB Chen, SQ Zhang, PW Zhao, and J Meng. *Physical Review C*, 90(4):044306, 2014.

[49] QB Chen, SQ Zhang, J Meng, et al. *Physical Review C*, 94(5):054308, 2016.

[50] S Mukhopadhyay, D Almehed, U Garg, S Frauendorf, T Li, PV Madhusudhana Rao, X Wang, SS Ghugre, MP Carpenter, S Gros, et al. *Physical review letters*, 99(17):172501, 2007.

[51] Bin Qi, SQ Zhang, J Meng, SY Wang, and S Frauendorf. *Physics Letters B*, 675(2):175–180, 2009.

[52] Makito Oi, Ahmad Ansari, Takatoshi Horibata, and Naoki Onishi. *Physics Letters B*, 480(1-2):53–60, 2000.

[53] AA Raduta, R Poenaru, and L Gr Ixaru. *Physical Review C*, 96(5):054320, 2017.

[54] AA Raduta, CM Raduta, and R Poenaru. *Journal of Physics G: Nuclear and Particle Physics*, 48(1):015106, 2020.

[55] K Tanabe and K Sugawara-Tanabe. *Physics Letters B*, 34(7):575–578, 1971.

[56] Kosai Tanabe and Kazuko Sugawara-Tanabe. *Physical Review C*, 77(6):064318, 2008.

[57] Mitsuhiro Shimada, Yudai Fujioka, Shingo Tagami, and Yoshifumi R Shimizu. *Physical Review C*, 97(2):024318, 2018.

[58] Kenji Hara and Yang Sun. *International Journal of Modern Physics E*, 4(04):637–785, 1995.

[59] PW Zhao, P Ring, and J Meng. *Physical Review C*, 94(4):041301, 2016.

[60] M Konieczka, Markus Kortelainen, and W Satuła. *Physical Review C*, 97(3):034310, 2018.

[61] AA Raduta, R Budaca, and CM Raduta. *Physical Review C*, 76(6):064309, 2007.

[62] AA Raduta, R Poenaru, and Al H Raduta. *Journal of Physics G: Nuclear and Particle Physics*, 45(10):105104, 2018.

[63] R Budaca. *Physical Review C*, 97(2):024302, 2018.

[64] AA Raduta, R Poenaru, and CM Raduta. *Physical Review C*, 101(1):014302, 2020.

[65] Tord Bengtsson. *Nuclear Physics A*, 512(1):124–148, 1990.

[66] A Görgen, RM Clark, M Cromaz, P Fallon, GB Hagemann, H Hübel, IY Lee, AO Macchiavelli, G Sletten, D Ward, et al. *Physical Review C*, 69(3):031301, 2004.

[67] GB Hagemann. *Acta Physica Polonica B*, 36(4):1043, 2005.

[68] DR Jensen, GB Hagemann, I Hamamoto, B Herskind, G Sletten, JN Wilson, SW Ødegård, K Spohr, H Hübel, P Bringel, et al. *The European Physical Journal A-Hadrons and Nuclei*, 19(2):173–185, 2004.

[69] Kosai Tanabe and Kazuko Sugawara-Tanabe. *Physical Review C*, 95(6):064315, 2017.

[70] S Frauendorf. *Physical Review C*, 97(6):069801, 2018.

[71] Kosai Tanabe and Kazuko Sugawara-Tanabe. *Physical Review C*, 97(6):069802, 2018.

[72] Yang Sun, Shuxian Wen, et al. *Physical Review C*, 50(5):2351, 1994.

[73] AM Khalaf, Hayam Yassin, and Eman R Abo Elyazeed. *Journal: Journal Of Advances In Physics*, 11(1), 2015.

[74] VS Uma and Alpana Goel. *The European Physical Journal Plus*, 130(6):1–6, 2015.

[75] HM Mittal and Anshul Dadwal. In *Proceedings of the DAE-BRNS Symp. on Nucl. Phys*, volume 61, page 134, 2016.

[76] Ikuko Hamamoto and Ben Mottelson. *Physics Letters B*, 127(5):281–285, 1983.

[77] Ikuko Hamamoto. *Physics Letters B*, 193(4):399–404, 1987.

[78] Ikuko Hamamoto. *Physica Scripta*, 91(2):023004, 2016.

[79] S Torilov, S Thummerer, W Von Oertzen, Tz Kokalova, G De Angelis, HG Bohlen, A Tumino, M Axiotis, E Farnea, N Marginean, et al. *The European Physical Journal A-Hadrons and Nuclei*, 19(3):307–317, 2004.

[80] ME Debray, MA Cardona, D Hojman, AJ Kreiner, M Davidson, J Davidson, H Somacal, G Levinton, DR Napoli, S Lenzi, et al. *Physical Review C*, 62(2):024304, 2000.

[81] AA Radutaa and CM Radutab. *arXiv preprint arXiv:0903.0076*, 2009.

[82] AA Raduta and CM Raduta. *Annals of the University of Craiova, Physics*, 21(1):28–53, 2011.

[83] J Meyer-ter Vehn. *Nuclear Physics A*, 249(1):111–140, 1975.

[84] SY Wang, SQ Zhang, B Qi, J Peng, JM Yao, J Meng, et al. *Physical Review C*, 77(3):034314, 2008.

[85] J Peng, J Meng, and SQ Zhang. *Physical Review C*, 68(4):044324, 2003.

[86] T Koike, K Starosta, and I Hamamoto. *Physical review letters*, 93(17):172502, 2004.

[87] SY Wang, SQ Zhang, B Qi, and J Meng. *Physical Review C*, 75(2):024309, 2007.

[88] CW Reich and Balraj Singh. *Nuclear Data Sheets*, 111(5):1211–1469, 2010.

[89] RR Chasman. *Physics Letters B*, 96(1-2):7–10, 1980.

[90] AA Raduta, CM Raduta, and Amand Faessler. *Physics Letters B*, 635(2-3):80–84, 2006.

[91] AA Raduta, Al H Raduta, and CM Raduta. *Physical Review C*, 74(4):044312, 2006.

[92] Wang Shou-Yu, Qi Bin, and Zhang Shuang-Quan. *Chinese Physics Letters*, 26(5):052102, 2009.

[93] EA Lawrie, O Shirinda, and CM Petrache. *Physical Review C*, 101(3):034306, 2020.

EXTENSIVE STUDY OF THE POSITIVE AND NEGATIVE PARITY WOBBLING STATES FOR AN ODD-MASS TRIAXIAL NUCLEUS II: CLASSICAL TRAJECTORIES

R. POENARU[1,2,a], A. A. RADUTA[2,3,b]

[1]Doctoral School of Physics, University of Bucharest, Bucharest, Romania
E-mail[a]: robert.poenaru@drd.unibuc.ro
[2]Department of Theoretical Physics - *Horia Hulubei* National Institute for Physics and Nuclear Engineering, Măgurele-Bucharest, Romania
E-mail[b]: raduta@nipne.ro (corresponding author)
[3]Academy of Romanian Scientists, Bucharest, Romania

Received: *April 24, 2021* (RJP v2.0 r2018a)

Abstract. The wobbling properties of ^{163}Lu are described within a semi-classical view by using a new interpretation of the band structure of this isotope. Namely, the bands TSD_2 and TSD_4 are considered as *Parity Partner Bands*: two $\Delta I = 2$ rotational bands with identical spins but opposite parity that emerge from a sole wave-function which is an admixture of both positive and negative parity states. The classical energy function $\mathcal{H}$ of the system is obtained from the dequantization procedure of the Particle Rotor Hamiltonian, and it is expressed in terms of generalized coordinates and momenta. By analyzing its behavior near the critical points, regions where wobbling motion has a stable (unstable) character arise, this being represented by the closed (opened) trajectories surrounding these points in the contour plots. Furthermore, the two constants of motion for the deformed nucleus, i.e., the energy E and total angular momentum I are graphically represented as 3-dimensional surfaces in the space generated by the components I_1, I_2, I_3 of the angular momentum. From their intersection, the classical orbits can be obtained, and their geometric interpretation gives an insight into the rotational character of ^{163}Lu. Indeed, obtaining a classical view for the motion of quantum object is a remarking feature of the present work.

Key words: Triaxial Nuclei, Wobbling Motion, Angular Momentum, Energy Ellipsoid.

1. INTRODUCTION

Collective phenomena in deformed nuclei such as the *wobbling motion* have been drawing a lot of attention lately, mainly due to their elusive character, but also due to the real experimental and theoretical challenges it implies. Considered as a clear fingerprint of nuclear triaxiality, wobbling motion (w.m.) has been predicted theoretically by Bohr and Mottelson more than 40 years ago [1], when they were discussing the excited spectra of even-even nuclei using a triaxial rigid rotor with three different moments of inertia (MOI).

W.m. can be viewed as the quantum analogue for the motion of the asymmet-

ric top, whose rotation around the axis with the largest moment of inertia (MOI) is energetically the most favored. A uniform rotation about this axis will have the lowest energy for a given angular momentum (spin). As the energy increases, this axis will start to precess, due to the anisotropy of the three moments of inertia, with a harmonic type of oscillation about the space-fixed angular momentum vector, giving rise to a family of wobbling bands, each characterized by a wobbling phonon number n_w. The resulting quantal spectrum will be a sequence of $\Delta I = 2\hbar$ rotational bands, with an alternating signature number ($\alpha = \pm\frac{1}{2}$ in odd-A nuclei and $\alpha = 0, 1$ in even-A nuclei) for each wobbling excitation.

Although Bohr and Mottelson made predictions for these excitations in even-even nuclei, the first experimental evidence of this nuclear behavior has been identified in an odd-mass nucleus: the $A = 163$ isotope of Lu, where a single one-phonon wobbling band was measured initially [2], followed by two additional wobbling bands discovered one year later [3, 4]. Other experimental evidence came quickly after that and now the following nuclei are considered as wobblers: ^{105}Pd [5], ^{127}Xe [6], ^{133}La [7], ^{135}Pr [8, 9], ^{161,163,165,167}Lu [3, 4, 10–12], ^{167}Ta [13], ^{183,187}Au [14, 15]. Regarding the wobbling motion for the even-even nuclei the ^{112}Ru ($Z = 44$) nucleus has three wobbling bands [16], two of them being the excited one- and two-wobbling phonon bands. Another nucleus is ^{114}Pd [17], with two excited bands of wobbling character, similar to ^{112}Ru. The even-even nucleus ^{130}Ba ($Z = 56$) [18–20] was also confirmed very recently to exhibit wobbling behavior.

Compared to the wobbling mode described in [1], which has a purely collective form, in the case of odd-A nuclei, it turns out that the wobbling mode appears due to the coupling of a valence nucleon (the so-called $\pi(i_{13/2})$ intruder) to a triaxial core, driving the nucleus up to large deformation ($\epsilon \approx 0.4$) [21] and giving rise to excited states of the deformed nuclear system, each belonging to a particular wobbling band.

Frauendorf et al. [22] showed that in the case of odd-A nuclei, depending on the coupling between the triaxial core (with a.m. $\vec{R}$) and the single-particle ("valence" nucleon with a.m. $\vec{j}$), there can be two wobbling regimes: transverse (TW) and longitudinal (LW). The triaxial core is viewed as a Liquid Drop, such that that the main rotation is along the intermediate m-axis (since this one has the largest MOI). When the odd particle aligns its angular momentum along the m-axis, then the system is said to achieve a *longitudinal wobbling* character (LW). If the odd-particle aligns its a.m. with an axis that is perpendicular to the m-axis (i.e., either the long l- or short s-axis of the triaxial rotor), then the system achieves a so-called *transverse wobbling* character. For a better understanding of the wobbling regimes in terms of angular momentum alignment, Fig. 1 depicts three particular cases, namely a simple wobbler - inset A.0 (the case firstly developed by Bohr and Mottelson [1]), a longitudinal wobbler - inset A.1, and a transverse wobbler - inset A.2.

The current work represents the second piece of a two-part series of papers that

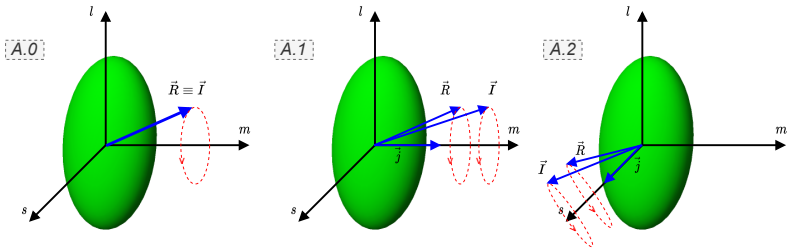

Fig. 1 – A.0: The geometry for the angular momentum of a simple wobbler. A.1: coupling geometry for a longitudinal wobbler (LW). A.2: coupling geometry for a transverse wobbler (TW). The short-s, long-l, and medium-m axes are defined in the body-fixed frame. The vectors $\vec{R}$, $\vec{j}$, and $\vec{I}$ represent the set of angular momenta of the core, odd particle, and the total nuclear system, respectively.

focuses on the description of the wobbling properties in odd-mass nuclei. Starting from an existing formalism concerning the interpretation of the wobbling structure of ^{163}Lu [23, 24], that initial framework (which will be further denoted by `W1`) is extended with a proper description of the states with positive and negative parity, by adopting the concept of *Parity Partner Bands*. In the newly developed approach (denoted hereafter by `W2`), a single particle (the odd $i_{j=13/2}$ proton) couples to the triaxial core, generating a sequence of four triaxial strongly deformed bands (called TSD_1, TSD_2, TSD_3 and TSD_4), with a total of 63 rotational states in all the bands. Previously in `W1`, two different particle-core couplings were considered: one that consisted in the $i_{j=13/2}$ proton+core for the bands $TSD_{1,2,3}$ and one $h_{j=9/2}$ proton+core for TSD_4 band, which resulted in two separate fitting procedures required to obtain the energy spectrum of this isotope. Within `W2`, as per the first part of this series of papers (denoted throughout the paper with **I** [25]), a single fitting procedure was required to find the excitation energies of ^{163}Lu, since only one proton was considered to align its angular momentum with that of the triaxial core. A successful description of the wobbling spectrum of ^{163}Lu was made in **I**, together with calculation of other relevant quantities (e.g. rotational frequencies) that put `W2` to the test in terms of correctness. The obtained agreement with the experimental data was impressive.

In this second part (hereafter denoted by **II**), attention is given to the properties of the classical energy function of ^{163}Lu, and the geometrical interpretation of the total angular momentum. The classical expression of the energy function, which can be obtained via the Time-Dependent Variational Principle (TDVE) applied in **I** allows the study of the wobbling stability, and also provides an insight into the classical features of nucleonic motion within the angular momentum space. Its expression signifies the initial quantal Hamiltonian of the deformed system but is brought to a dequantized form with the help of a set of coordinates that describe the dynamics. By expressing the angular momentum squared $\vec{I}^2$ of the triaxial nucleus and the energy function E as surfaces in a three-dimensional space, it is possible to obtain the

trajectories of the rotating system by intersecting the two shapes. This aspect will be analyzed in detail later on.

The structure of this work is as follows. In Section 2 a brief overview of the key characteristics for the W2 approach that emerged from **I** is made. In Section 3, the prerequisites for obtaining a classical expression of the energy function are formulated. Section 4 is devoted to the numerical results concerning the wobbling stability of ^{163}Lu. Wobbling stability is studied in terms of contour plots of the aforementioned energy function. The nuclear trajectories (i.e., the intersection curves of the energy surface with angular momentum surface) of the system are graphically represented for given values of angular momentum and energy. Several regimes of rotational motion emerge from this analysis. Discussion of the results is also made in Section 4. The conclusions of this current work are given in Section 5.

2. NEW FORMALISM FOR THE DESCRIPTION OF WOBBLING STATES

The W2 formalism which emerged in **I** [25] consists in a re-interpretation of the four wobbling bands from ^{163}Lu. Namely, the bands TSD_2 and TSD_4 are *parity partner bands*: $\Delta I = 2$ sequences with identical spins but opposite parity ($\pi_2 = +1$ and $\pi_4 = -1$). Arguments for this came from the analysis of the wave function of the system. The function is an admixture of states with both positive and negative parity since the initial Hamiltonian is symmetric to rotations by a specific amount (D_2 implies invariance to rotations by π). A complete description of the properties of the wave function and the Hamiltonian concerning the parity property is made in **I**. In terms of wobbling excitations, both TSD_2 and TSD_4 are considered to be ground-state bands (zero-wobbling-phonon), obtained by coupling the $j_1 = 13/2$ proton (with parity $\pi_{j_1} = +1$) to a triaxial core of odd spins $R_2^+ = 1^+, 3^+, 5^+, \ldots$ for TSD_2 and $R_2^- = 1^-, 3^-, 5^-, \ldots$ for TSD_4. The band TSD_1 is also regarded as as a ground state band, but here the proton couples to a core of even spin states $R_1 = 0^+, 2^+, 4^+, \ldots$, and TSD_3 is indeed an excited wobbling band (one-wobbling-phonon) that is built on top of TSD_2 via the action of a phonon operator. The coupling schemes for W2 are described in **I** (denoted by C_1', C_2', and C_3'). For a clearer picture, Appendix A contains a diagram with all three mechanisms (see Fig. 11).

It is worth noting that this interpretation of the wobbling structure of ^{163}Lu contrasts the previously known band configuration [22, 26, 27] where the bands TSD_2 and TSD_3 were regarded as one- and two-wobbling phonon excitations built on the yrast TSD_1 band. However, it was recently shown [23, 24, 28] that TSD_1 and TSD_2 behave as signature partner bands, both being ground states with the favored (unfavored) $\alpha_f = +\frac{1}{2}$ ($\alpha_u = -\frac{1}{2}$) band as TSD_1 (TSD_2). This aspect, together with the fact that TSD_2 and TSD_4 are parity partners comprise the main ideas behind

the W2 formalism adopted in **I** and **II**. The workflow involved in W2 is drawn in Fig. 10, and for the sake of completeness, the initial W1 approach is also sketched in Fig. 9 from Appendix A.

3. THEORETICAL FORMALISM

Concerning the odd nucleus ^{163}Lu, system can be treated within the Particle Rotor Model (PRM) [22, 29, 30]. This approach is an extension of the Triaxial Rotor Model (TRM) that was firstly developed by Bohr and Mottelson [1], and then treated in a fully quantal approach by Davydov and Filippov [31]. Thus, the deformed system is described with a similar Hamiltonian used in W1, namely the Hamiltonian for the triaxial PRM:

$$H = H_{\text{core}} + H_{\text{s.p.}} = \\ = \sum_{i=1,2,3} \frac{1}{2\mathcal{I}_i}(I_i - j_i)^2 + \frac{V}{j(j+1)}\left[\cos\gamma(3j_3^2 - \vec{j}^2) - \sqrt{3}\sin\gamma(j_1^2 - j_2^2)\right] + \epsilon_j \ . \tag{1}$$

The Hamiltonian from Eq. 1 describes a system in which an odd particle with a.m. $\vec{j}$ interacts with a triaxial even-even core of a.m. $\vec{R}$, that is the odd nucleon is moving in a quadrupole deformed mean-field which is generated by the core. As such, the first term in the Hamiltonian H_{core} describes the motion of a triaxial core, while the second term $H_{\text{s.p.}}$ represents the single-particle potential characterizing the valence proton (the well-known deformed Nilsson potential [32, 33]). ϵ_j represents the single-particle energy of the nucleon itself, a value that depends on the orbital where it belongs to. In Eq. 1 the core angular momentum is $\vec{R} = \vec{I} - \vec{j}$ and the terms $\mathcal{I}_i$ represent the moments of inertia for a triaxial ellipsoid, along the principal axes. γ is the triaxiality parameter [1] which can be considered as a measure of asymmetry between the three moments of inertia. The strength parameter V from the expression of the deformed potential is related to the quadrupole deformation parameter β_2 [1].

Solving the problem of W2 is equivalent to finding the eigenvalues of H given in Eq. 1. In a similar approach as in W1, the eigenvalues of interest are obtained on the base of a semi-classical approach. This is preferred since it working within a semi-classical approach allows one to keep close contact with the system's dynamics in terms of equations of motion for the generalized coordinates. However, exact calculations of the initial quantal Hamiltonian were performed for W1 and the agreement with the experimental data was checked (see Refs. [24, 28]). Thus, the first step is to perform a de-quantization procedure of H through the TDVE [34–36]:

$$\delta \int_0^t \langle \Psi_{IjM} | H - i\frac{\partial}{\partial t'} | \Psi_{IjM} \rangle \, dt' = 0 \ . \tag{2}$$

The trial function from Eq. 2 is carefully chosen as a product of two basis states comprising the states with total angular momentum I and j, respectively:

$$|\Psi_{IjM}\rangle = \mathbf{N} e^{z\hat{I}_-} e^{s\hat{j}_-} |IMI\rangle |jj\rangle \ , \tag{3}$$

where the operators $\hat{I}_-$ and $\hat{j}_-$ denote the lowering operators for the intrinsic angular momenta $\vec{I}$ and $\vec{j}$, respectively, and $\mathbf{N}$ plays the role of the normalization constant. One must remark the fact that the states $|IMI\rangle$ and $|jj\rangle$ from Eq. 3 are extremal states for the operators $(\hat{I}^2, \hat{I}_3)$ and $(\hat{j^2}, \hat{j}_3)$, respectively, and they correspond to the maximally allowed states for a given set of angular momenta I and j. As an observation, the trial function is an admixture of components of definite K, which is consistent with the fact that for a triaxial nucleus, K is not a good quantum number.

The variables z and s from Eq. 3 are complex functions of time, and they play the role of classical coordinates in the phase space that describe the motion of the core and the odd particle, respectively:

$$z = \rho e^{i\varphi} \ , \ s = f e^{i\psi} \ . \tag{4}$$

In order to obtain a set of classical equations in a Hamilton Canonical form, a new pair of variables are introduced:

$$r = \frac{2I}{1+\rho^2} \ , \ t = \frac{2j}{1+f^2} \ , \tag{5}$$

where $r \in [0, 2I]$ and $t \in [0, 2j]$. Thus the equations of motion acquire the form:

$$\begin{aligned} \frac{\partial \mathcal{H}}{\partial r} = \dot{\varphi} \ ; \ \frac{\partial \mathcal{H}}{\partial \varphi} = -\dot{r} \ , \\ \frac{\partial \mathcal{H}}{\partial t} = \dot{\psi} \ ; \ \frac{\partial \mathcal{H}}{\partial \psi} = -\dot{t} \ . \end{aligned} \tag{6}$$

The explicit form of the above equations of motion are given in Appendix A of [37]. The function $\mathcal{H}$ denotes the average of the Hamiltonian operator H (Eq. 1) with the trial function $|\Psi_{IjM}\rangle$ given in Eq. 3, and it plays the role of classical energy function:

$$\mathcal{H}(\varphi, r; \psi, t) = \langle \Psi_{IjM} | H | \Psi_{IjM} \rangle \ , \tag{7}$$

$\mathcal{H}$ is a constant of motion, meaning that $\dot{\mathcal{H}} \equiv 0$. This equation will define a surface, a so-called *equi-energy surface* $\mathcal{H} = \text{const}$. It is worth mentioning the fact that such equality holds because the entire set of equations of motion emerged from a variational principle. The sign of the Hessian associated with this classical function will indicate its stationary points. Among them some are minima, and the critical points which are of interest for the present study are minimal, and obtained when the following ordering for the three moments of inertia holds: $\mathcal{I}_1 > \mathcal{I}_2 > \mathcal{I}_3$. There are no restrictions for the triaxiality parameter γ and the single-particle potential strength

V (which can implicitly be considered as a measure of the quadrupole deformation parameter β_2). As such, the set of coordinates $(\varphi, r; \psi, t)$ will provide a minimum value for $\mathcal{H}$ only for certain values that will be discussed in the following part. Regarding the physical meaning of $(\varphi, r; \psi, t)$, one can see that the angles φ and ψ play the role of generalized coordinates, while r and t represent the conjugate momenta.

3.1. ENERGY FUNCTION - GEOMETRICAL INTERPRETATION

The analytical expression for the average of H with the trial function describing the system was previously calculated in `W1`. Indeed, the energy function $\mathcal{H}$ was given in terms of the phase space coordinates $(r, \varphi; t, \psi)$ as follows [23]:

$$\begin{aligned}\mathcal{H} =& \frac{I}{2}(A_1+A_2) + A_3 I^2 + \frac{2I-1}{2I} r(2I-r)\mathcal{A}_\varphi + \frac{j}{2}(A_1+A_2) + A_3 j^2 + \\ &+ \frac{2j-1}{2j} t(2j-t)\mathcal{A}_\psi - 2\sqrt{r(2I-r)t(2j-t)}\mathcal{A}_{\varphi\psi} + \\ &+ A_3\left[r(2j-t) + t(2I-r)\right] - 2A_3 Ij + V\frac{2j-1}{j+1}\mathcal{A}_\gamma \end{aligned} \tag{8}$$

with:

$$\begin{aligned}&\mathcal{A}_\varphi(\varphi) = (A_1\cos^2\varphi + A_2\sin^2\varphi - A_3)\ , \\ &\mathcal{A}_{\varphi\psi}(\varphi,\psi) = (A_1\cos\varphi\cos\psi + A_2\sin\varphi\sin\psi)\ , \\ &\mathcal{A}_\psi(\psi) = (A_1\cos^2\psi + A_2\sin^2\psi - A_3)\ , \\ &\mathcal{A}_\gamma(t,\psi) = \left[\cos\gamma - \frac{t(2j-t)}{2j^2}\sqrt{3}(\sqrt{3}\cos\gamma + \sin\gamma\cos 2\psi)\right]\ . \end{aligned} \tag{9}$$

For the condition $A_1 > A_2 > A_3$, the expression from Eq. 8 is minimal in the point $p_0|_{\min} = (0, I; 0, j)$, since p_0 is a critical point of $\mathcal{H}$. The same critical point was used within **I** in order to obtain the expression of $\mathcal{H}^{(I,j)}_{\min}$ which entered in the expressions of the excitation energies for ^{163}Lu (See Eqs. 7-9 from **I**). Therein, it was possible to parametrize the total energy of the system in terms of the three MOIs, the triaxiality parameter γ, and the single-particle potential strength V, having them as free parameters (denoted as $\mathcal{P}$ in **I**). Performing a least square fitting procedure for the entire energy spectrum of ^{163}Lu, a set $\mathcal{P}$ was obtained which provided the best overall agreement with experimental data concerning these excitation energies. In fact, looking back at Eqs. 8 and 9 written above, the same parameters are also present here. Since the inertial parameters A_k are $A_k = \frac{1}{2\mathcal{I}_k}$, $k = 1, 2, 3$, it follows that:

$$\mathcal{H} = \texttt{fct}(\mathcal{I}_1, \mathcal{I}_3, \mathcal{I}_3, \gamma, V)\ . \tag{10}$$

This will help in the numerical application of the current research since one can just adopt the numerical values for $\mathcal{P} \equiv [\mathcal{I}_{1,2,3}, \gamma, V]$ obtained via the fitting pro-

cedure that was applied for the excitation energies in **I**. Indeed, the classical energy function $\mathcal{H}$ plays a crucial role in both determining the *wobbling energies* of the isotope, but also (as it will be shown) determining the *geometry* of the deformed system.

Furthermore, it is instructive to check the dependence of the energy function on the angular momentum components, e.g., the coordinates $x_k \overset{\text{not.}}{=} I_k\ ,\ k=1,2,3$, where the quantization axis is chosen as the 3-axis. By expressing the angular momentum coordinates $x_{1,2,3}$ in terms of the polar angles (θ,φ) and a radius I, one obtains:

$$x_1 = I\sin\theta\cos\varphi\ ,\ x_2 = I\sin\theta\sin\varphi\ ,\ x_3 = I\cos\theta\ . \tag{11}$$

Using this coordinate system and evaluating the energy function around its minimum point $p_0=(0,I;0,j)$, the following expression for $\mathcal{H}$ will be obtained:

$$\mathcal{H}\mid_{p_0} = I\left(I-\frac{1}{2}\right)\sin^2\theta\cdot\mathcal{A}_\varphi(\varphi) - 2A_1Ij\sin\theta + T_{\text{core}} + T_{\text{s.p.}}\ . \tag{12}$$

The last two terms in this equation are independent on the polar angles (θ,φ) and they have the following form:

$$T_{\text{core}} = \frac{I}{2}(A_1+A_2) + A_3I^2\ , \tag{13}$$

$$T_{\text{s.p.}} = \frac{j}{2}(A_2+A_3) + A_1j^2 - V\frac{2j-1}{j+1}\sin\left(\gamma+\frac{\pi}{6}\right)\ . \tag{14}$$

A quantitative analysis on these two terms is useful in order to see how a different A_k ordering would affect T_{core}, and also how is the single-particle a.m. influencing $T_{\text{s.p.}}$. Results are graphically represented in Fig. 2.

The classical equations of motion admit two constants of motion: the total energy (E) and the total angular momentum (I). Consequently, by finding the intersection line(s) between the energy surface E and the surface of the angular momentum, the system's trajectory at that particular energy and spin is obtained. Such representations will be made in the following section.

By changing the form of Eq. 12 from polar coordinates into Cartesian coordinates, the energy surface E will become:

$$E = \left(1-\frac{1}{2I}\right)A_1x_1^2 + \left(1-\frac{1}{2I}\right)A_2x_2^2 + \left[\left(1-\frac{1}{2I}\right)A_3 + A_1\frac{j}{I}\right]x_3^2 - \\ - I\left(I-\frac{1}{2}\right)A_3 - 2A_1Ij + T_{\text{rot}} + T_{\text{sp}}\ . \tag{15}$$

Indeed, one can notice that the three coordinates x_k appear as a squared sum. If some notations are made for the terms appearing next to the coordinates and the

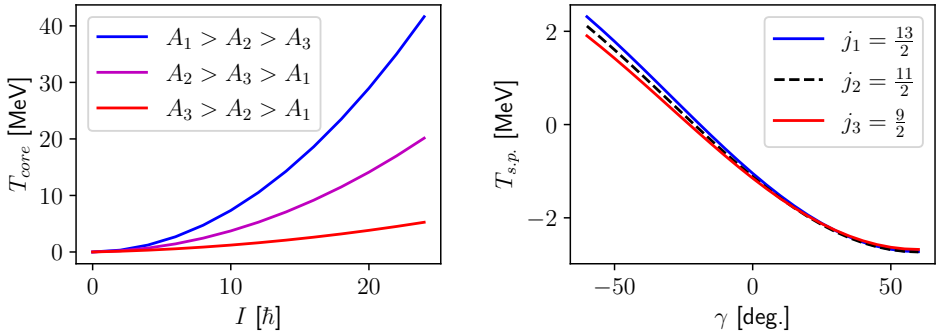

Fig. 2 – **Left:** The free term from Eq. 13 which corresponds to the core, for different orderings of the MOIs. For the ordering $A_1 > A_2 > A_3$, the parameters from Table 1 were taken. **Right:** The free term from Eq. 14 which corresponds to the single-particle. The evaluation of $T_{\text{s.p.}}$ was made for the parameters listed in Table 1. For illustrative purpose only, three different a.m. values j were chosen for the single-particle. Note that j_1 corresponds to the actual odd proton that couples to the triaxial core of ^{163}Lu, in the `W2` formalism.

coordinate-free terms, one arrives at the following expression for the energy surface:

$$E = \mathcal{S}_1 x_1^2 + \mathcal{S}_2 x_2^2 + \mathcal{S}_3 x_3^2 + \mathcal{S}_0^{\text{rot+sp}} \ . \tag{16}$$

From Eq. 16, it is now clear that the energy surface will be an ellipsoid with the *semi-axes* of lengths $\sqrt{(E - \mathcal{S}_0^{rot+sp})/\mathcal{S}_{1,2,3}}$. It is remarkable the fact that the quality of the fitting results from **I** is reflected in the present work through the classical geometric interpretation of the triaxial particle-core ellipsoid, via the parameters $\mathcal{P}$.

Furthermore, for a total angular momentum $\vec{I}$, the vector generates a sphere of radius $r = I$ described by the equation:

$$I^2 = x_1^2 + x_2^2 + x_3^2 \ . \tag{17}$$

The trajectories obtained through the intersection of Eqs. 16(i.e. an ellipsoid) and 17 (i.e., a sphere of radius $r = I$) will give a classical visualization of the wobbling character for a triaxial nucleus, and the possible trajectories of the system concerning its motion inside the angular momentum space.

4. NUMERICAL RESULTS

As already mentioned in the previous section, for the numerical part of this research, the parameters obtained from the fitting procedure made in **I** will also be adopted here for consistency of the `W2` approach, their values being listed in Table 1. It is worth noting that for the case of `W1`, the geometrical interpretation of the classical energy function would have required two such sets of parameters, and therefore, two sets of calculations (one for the bands $TSD_{1,2,3}$ and one for TSD_4). This is

Table 1

The parameter set $\mathcal{P}$ that was determined by a fitting procedure of the excitation energies for ^{163}Lu, provided via calculations from **I**.

$\mathcal{I}_1$ $[\hbar^2/\text{MeV}]$	$\mathcal{I}_2$ $[\hbar^2/\text{MeV}]$	$\mathcal{I}_3$ $[\hbar^2/\text{MeV}]$	γ [deg.]	V [MeV]
72	15	7	22	2.1

another remarking feature that emerges from the fact that TSD_2 and TSD_4 are parity partners, and the bands have the same $\vec{j}$ odd-proton in the coupling with the triaxial core.

Here, by using the parameters from Table 1, numerical calculations of $\mathcal{H}$ expressed in the polar coordinates via Eq. 12 are performed, with graphical visualization of its behavior. Furthermore, the surfaces E and I^2 described in Eqs. 15-17 will be represented for different values of the energy and the total spin.

4.1. STABILITY OF THE WOBBLING REGION

The expression for the classical energy function, which plays a crucial role in analyzing the nucleus's stability for a given rotational state, was presented in the previous section, through Eq. 12. This will be used within the numerical calculations to pinpoint the regions in space where the minimal points of $\mathcal{H}$ do exist. A special interest is devoted to the low-lying states from each of the four bands. Namely, for each band, a spin-state close to the band-head is chosen, then using the parameter set $\mathcal{P}$, a graphical representation in the (θ, φ)-coordinate space is realized, and in each case, the extremal points with minimum character are identified. These graphical representations are shown in Figs. 3 and 4. For the sake of completeness, the critical points of $\mathcal{H}$ which are minimal are listed separately in Table 2.

Table 2

The minimum points of $\mathcal{H}$, numerically evaluated for the parameter set $\mathcal{P}$. The points are represented as the *red dots* on the contour plots from Figs. 3-4.

Minimal point	θ [rad]	φ [rad]	A_k ordering
p_0	$\pi/2$	0	$A_3 > A_2 > A_1$
p_1	$\pi/2$	π	$A_3 > A_2 > A_1$
p_2	$\pi/2$	2π	$A_3 > A_2 > A_1$

The four contour plots shown in Figs. 3 and 4 have many similarities, suggesting common collective properties, but also differences which are caused by the fact that the minima have different depths. A common feature consists in that the equi-energy curves surround a sole minimum for low values in energy, but as the energy

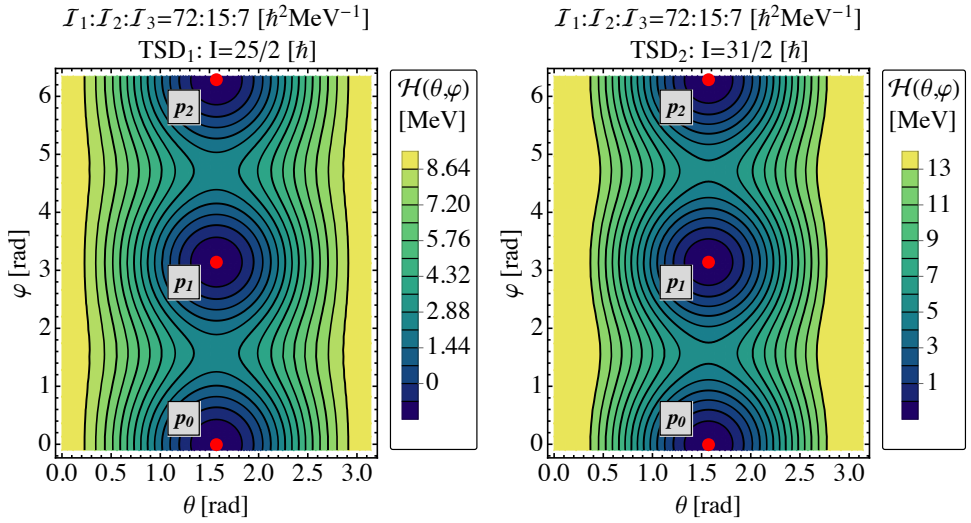

Fig. 3 – The classical energy function $\mathcal{H}$ given by Eq. 12 for a state in TSD_1 (left) and a state from TSD_2 (right). Calculations were performed with the numerical parameters given in Table 1. The minimum points for $\mathcal{H}$ are marked by red dots (see also Table 2), and they represent the regions in space where the nucleus has the most stable wobbling character (i.e., the precessional motion of the total a.m. is relatively small). The closed contours represent trajectories surrounding the minimum points, where wobbling motion can occur, while the contours surrounding all three minima represent the unstable motion of the nucleus, where the wobbling regime is forbidden.

increases, the trajectories go around all minima, the lack of localization indicating unstable wobbling motion. The unstable regions might also relate to phase transitions, where the nucleus can undergo a major change in its rotational character. This aspect will also be discussed in the next subsection, devoted to the 3-dimensional representation of the energy ellipsoid and the classical trajectories of the triaxial system.

Regarding the minimum points of $\mathcal{H}$ from Table 2, their position remains unchanged for all four bands and any rotational state I, as long as the ratio of the inertial parameters A_k (or implicitly the MOIs) stays the same. Remarkable is the fact that only with the adopted set of parameters $\mathcal{P}$ (i.e., the MOI order $\mathcal{I}_1 > \mathcal{I}_2 > \mathcal{I}_3$) it was possible to define regions with stable motion (marked by the dark-colored regions from Figs. 3 and 4). Indeed, if the two ratios $\mathcal{I}_1/\mathcal{I}_2$ and $\mathcal{I}_2/\mathcal{I}_3$ would have been smaller, a larger unstable region would prevail (with regions of maximal character), constraining thus the stable wobbling motion. This could indicate the fact that the single-particle term $T_{\text{s.p.}}$ from the expression of $\mathcal{H}$ is sensitive to larger triaxiality, and only for certain values will the system achieve a stable motion characterized by large deformation (see Eq. 14). In fact, Fig. 2 shows the change in magnitude of $T_{\text{s.p.}}$ concerning the triaxiality parameter γ.

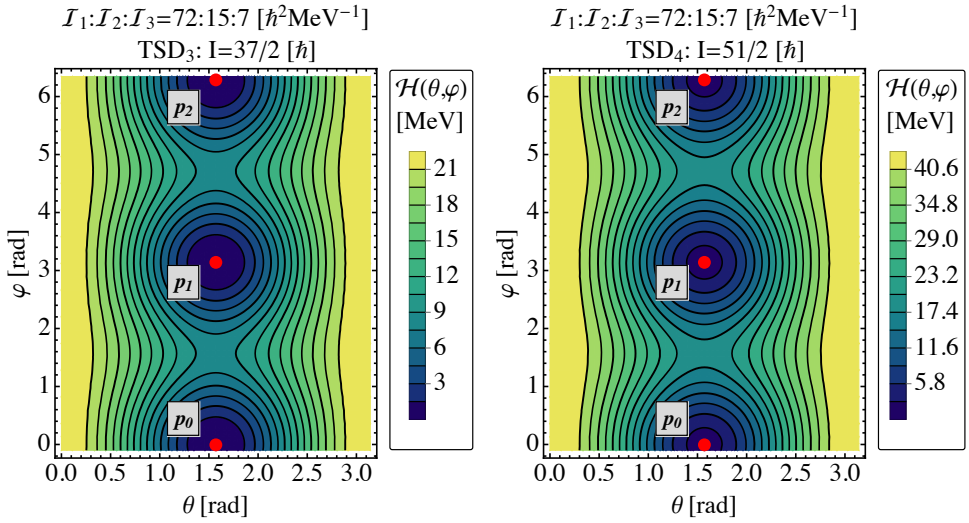

Fig. 4 – The classical energy function $\mathcal{H}$ given by Eq. 12 for a state in TSD_3 (left) and a state from TSD_4 (right). Calculations were performed with the numerical parameters given in Table 1. The minimum points for $\mathcal{H}$ are marked by red dots (see also Table 2), and they represent the regions in space where the nucleus has the most stable wobbling character (i.e., the precessional motion of the total a.m. is relatively small). The closed contours represent trajectories surrounding the minimum points, where wobbling motion can occur, while the contours surrounding all three minima represent the unstable motion of the nucleus, where the wobbling regime is forbidden.

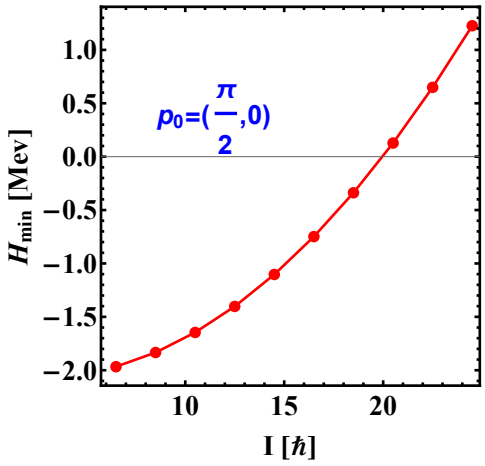

Fig. 5 – The change in the minimum depth of $\mathcal{H}$, evaluated in the one of its critical points $p_0(\theta,\varphi) = (\frac{\pi}{2},0)$, using the parameters given in Table 1.

An additional step consists in the analysis of the energy function, more precisely to see its evolution in one of the minimum points with respect to the angular momentum I. As it was already observed from the contour plots shown in Figs. 3-4, the depth of the minima differs from one spin state to another, so it would be useful to have a quantitative view on that change. By fixing $\mathcal{H}$ in one of its critical points (e.g., the minimum point $p_0 = (\frac{\pi}{2},0)$), the angular momentum I was varied within a large interval, and the evolution of $\mathcal{H}$ was evaluated. Graphical representation is shown in Fig. 5.

As it can be seen from Fig. 5, the classical energy $\mathcal{H}$ is an increasing function of angular momentum, which is to be expected, since the wobbling energies of the four bands increase with respect to the increase in spin. The negative values of $\mathcal{H}$ for low-lying states do not indicate that the nucleus has negative energy since the rest of the nucleus' energy is also given by the single-particle energy ϵ_j that appears in the initial Hamiltonian and the phononic terms (see Eq. 8 from **I** for the physical meaning of the phononic terms $\mathcal{F}$).

Another useful insight would be the study of the classical energy function $\mathcal{H}$ as separate functions of the polar coordinates θ and φ, respectively. This can be achieved by choosing a minimum point, keeping one of the polar coordinates fixed, and then let the other one vary across its corresponding interval. For ^{163}Lu, such a graphical representation was done for the point $p_0 = \left(\frac{\pi}{2},0\right)$ (that is the bottom-most red dot from each of the four contour plots depicted in Figs. 3-4). Results can be seen in Fig. 6.

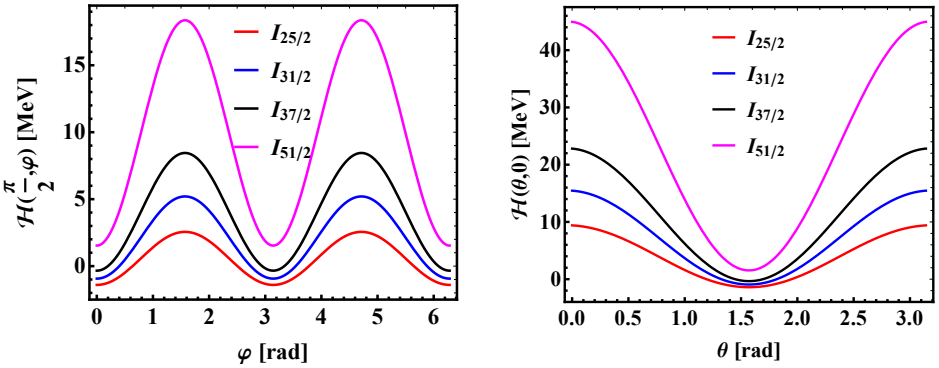

Fig. 6 – The energy function $\mathcal{H}$, evaluated in one of its minimum points, with respect to only one of the polar coordinates. One coordinate is fixed while the other one is varied within its interval of existence ($\theta \in [0,\pi]$ and $\varphi \in [0,2\pi]$). The chosen minimum is $p_0 = \left(\frac{\pi}{2},0\right)$. Each spin state corresponds to one of the four triaxial bands of ^{163}Lu (with $I_{25/2} \in TSD_1$, $I_{31/2} \in TSD_2$, $I_{37/2} \in TSD_3$, and $I_{51/2} \in TSD_4$).

4.2. CLASSICAL TRAJECTORIES - 3D REPRESENTATION

The final step of the present work is to obtain an insight into the classical features of ^{163}Lu concerning the total angular momentum and its rotational motion. As already mentioned, the trajectories are given by the intersection curves of the energy ellipsoid E given in Eq. 15 with the angular momentum sphere I given in Eq. 17. In the 3-dimensional space generated by the three components of the angular momentum vector $\vec{I}$, these intersection curves characterize the motion of the system, as each curve will be oriented along with one of the three axes x_k , $k = 1,2,3$, suggesting a rotational motion (the precession of the total a.m.) around a particular direction preferred by the system.

The meaning of a trajectory can be described from a geometrical standpoint as the *collection* of points in space along which the total angular momentum $\vec{I}$ orbits, making a precessional motion (Fig. 1 shows the orbiting character of $\vec{I}$). As discussed in the introductory part of this paper, the precession is caused by the asymmetry in the three MOIs of the triaxial nucleus this causing the nucleus to wobble with a harmonic-like frequency (the wobbling frequencies for ^{163}Lu were analyzed in **I**).

The dependence of the classical trajectories on the angular momenta as well as on energies must be analyzed in `W2`. Indeed, when the model Hamiltonian is diagonalized for a given I, a set of $2I+1$ energies are obtained. Therefore, it is justified to study the evolution of trajectories when the energy of the nucleus is increasing. The curves are represented as the manifold given by the intersection of the two constants of motion E and I. Examples of such trajectories are depicted in Figs. 7-8.

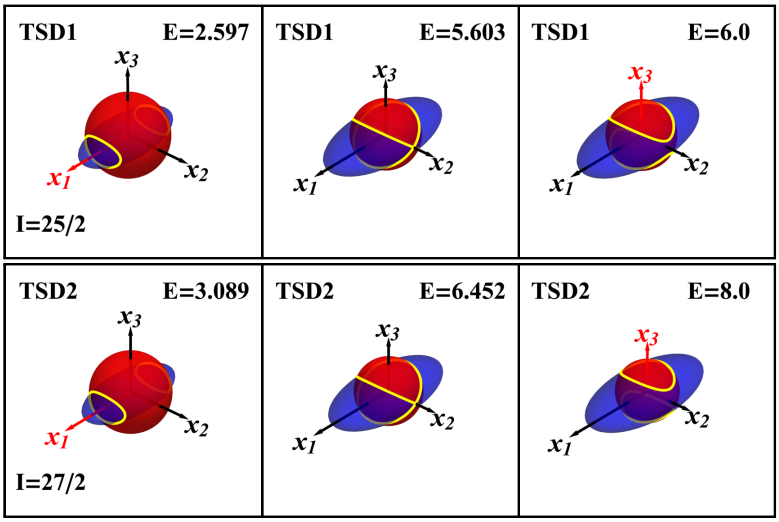

Fig. 7 – The nuclear trajectories of the system, evaluated for two spin states belonging to TSD_1 and TSD_2. Intersection lines marked by yellow color represents the actual orbits. Axis colored in red represents the direction along which the system rotates (it precesses). The left-most inset corresponds to the real excitation energy for that particular spin state I.

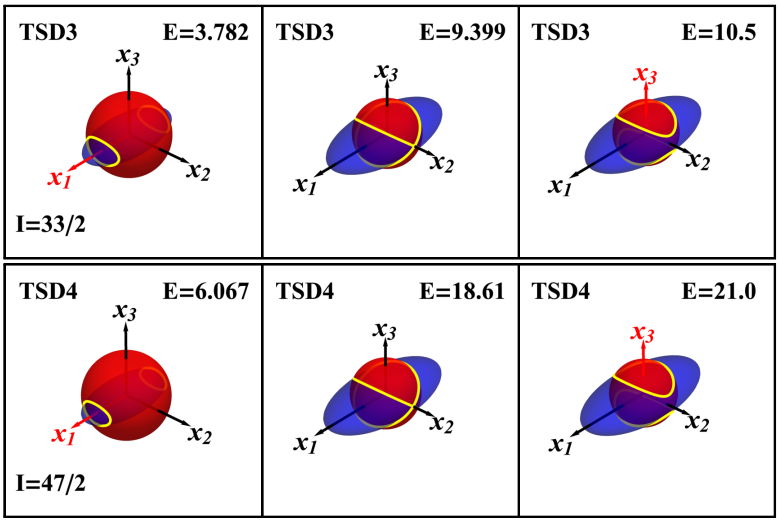

Fig. 8 – The nuclear trajectories of the system, evaluated for two spin states belonging to TSD_3 and TSD_4. Intersection lines marked by yellow color represents the actual orbits. Axis colored in red represents the direction along which the system rotates (it precesses). The left-most inset corresponds to the real excitation energy for that particular spin state I.

Each row from the Figs. 7-8 represents a rotational state within a band. A low-lying spin state was chosen from each band in particular as an example. The left inset of each row represents the real excitation energy for the state I at which the energy ellipsoid is evaluated. It can be seen that two distinct (but symmetric) trajectories are observed along the x_1-axis, for all four states. This suggests that the states of the triaxial nucleus are obtained from the rotation of the angular momentum along x_1. Indeed, for low energies, the rotation is more pronounced along the x_1- and $-x_1$-axes. As the energy of the nucleus increases, the two trajectories approach each other, which results in a tilted rotation axis corresponding to both curves. The tilted axis implies that the rotation axis is being misaligned, the rotational axis moving away from its *equilibrium point*, marking the tilted-axis rotation. Note that this picture is fully consistent with the one described by Lawrie et al. [38]. Further increase in energy will result in the two trajectories intersect with each other. The point where the intersection between the two orbits occurs is marked in the middle inset from each figure. Consequently, the intersection of these two orbits marks an unstable motion within the system. Finally, when the energy increases even more, beyond this *critical point*, one arrives again in a two-trajectories regime but with a different rotation axis, lying closer to the x_3 axis. This case is shown in the right inset within each figure, where the axis x_3 is marked by red color, signaling the change in the rotational mode of the nucleus. However, it is worth noting that such energies are way too large for such a phase transition to occur naturally in ^{163}Lu. For example, in the case of $I_{25/2} \in TSD_1$, the energy at which ^{163}Lu undergoes a phase transition with regards to the rotational mode is close to 5.6 MeV (middle inset for TSD_1 from Fig. 7), but the real excitation energy which corresponds to this state is half that value (left inset for TSD_1 from Fig. 7). Nevertheless, it is a remarkable fact that with the current model, a phase transition between rotational modes in a triaxial nucleus can be identified. A proper microscopic formalism based on this approach might also provide a more detailed picture with regards to the allowed trajectories for the system.

It is worth mentioning that in **I**, the analysis of the wobbling energy of ^{163}Lu as defined in [22] pointed out that there might be a *critical spin* value $I_{\rm cr}$ where the energy changes its behavior: going from an increasing function of I to a decreasing function of I (for reference, see Fig. 4 from **I**). Therein, based on the obtained values of the moments of inertia, it was concluded that this critical spin value marks the point where the system undergoes a change in its wobbling regime from Longitudinal Wobbling to Transverse Wobbling. Here, the critical energy obtained from Figs. 7 and 8 might also indicate a change in the wobbling regime from LW to TW (since the MOIs used for calculations are the same). However, one must obtain the classical trajectories for each spin-state of the wobbling bands in ^{163}Lu, then find the critical energy at which unstable wobbling occurs, and finally, conclude the actual changes.

Such a tedious process might be considered as a motivation for future work.

5. CONCLUSIONS & OUTLOOK

This work represents the second part from a series of two papers, with the first part denoted throughout the text with **I**. Starting with **I**, a new formalism called `W2` was developed for the description of the wobbling bands of ^{163}Lu by making a renormalization of the band structure via the concept of Signature Partners and Parity Partners [25]. Through a Time-Dependent Variational Equation, it was possible to dequantize the Particle-Rotor Hamiltonian associated to ^{163}Lu and describe its wobbling spectrum for the positive and negative parity states belonging to four triaxial strongly-deformed bands. The overall agreement with the experimental data was very good for a semi-classical approach (with an RMS of about ≈ 0.079 MeV). The energy spectrum was described in terms of five free parameters (three moments of inertia, the triaxiality parameter γ, and the single-particle potential strength V) which were determined through a fitting procedure.

With the TDVE from **I** as a backbone, in this second part, the *classical energy function* (given by Eq. 12) was obtained in the semi-classical way. Its expression was evaluated and graphically represented through contour plots, and regions in space where the wobbling motion is stable/unstable have been identified. For the numerical calculations presented here, the parameters obtained in **I** were used, making the calculations consistent with the previous work. The behavior of the energy function $\mathcal{H}$ with respect to the angular components was the first objective of the paper.

The second objective was to obtain a geometrical view on the classical trajectories of the deformed nucleus, namely the orbits of the angular momentum $\vec{I}$ during its precessional motion that is typical to a wobbler. This was done by analyzing the two constants of motion for the system, i.e., the total energy E and the total a.m. I. Equations that define surfaces for each of the quantities were obtained, and by intersecting the two shapes the classical trajectories emerged. Graphical representation for each band of the isotope was made, with interesting results which were pointed out in subsection 4.2. A remarking feature of this kind of representation is the possibility of identifying regions where the nucleus might undergo a shape transition, or a phase transition concerning its wobbling regime (e.g., TW or LW). Indeed, energies, where the wobbling motion becomes unstable and then changes from LW to TW, have been discovered for each band in particular (although, only for a single value of angular momentum).

Concluding the present work, this newly developed formalism proves to be a successful tool for accurately describing the wobbling properties of ^{163}Lu and also for providing an insight into the rotational motion of the nuclear system with respect

to its total spin.

Acknowledgments. This work was supported by UEFISCU, through the project **PNIII-PCE-2020/0149**.

A. APPENDIX - WORKFLOW DIAGRAMS

The two models described throughout the paper, namely the formalisms `W1` and `W2` are schematically represented. The `W1` model corresponds to the work given in Refs. [23, 24], and the `W2` corresponds to the formalism developed in this two-part series of papers. For `W1`, the diagram is shown in Fig. 9, while for the newly developed approach `W2`, the diagram is shown in Fig. 10. The coupling scheme for `W2` is also represented in Fig. 11.

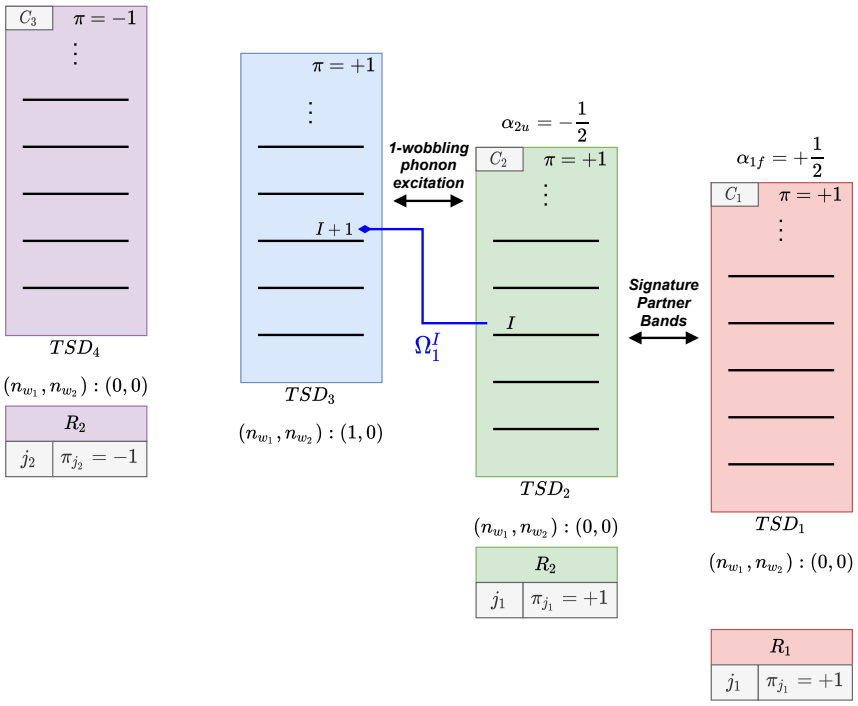

Fig. 9 – Schematic representation of the band structure adopted for ^{163}Lu in the `W1` model [23, 24]. For each band, the wobbling phonon numbers are shown. The main features and linking properties between bands are represented with arrows. The bottom part shows the coupling scheme (the core and the valence nucleon) for each wobbling band. The blue arrow marks the activation of TSD_3 states via the phonon operator.

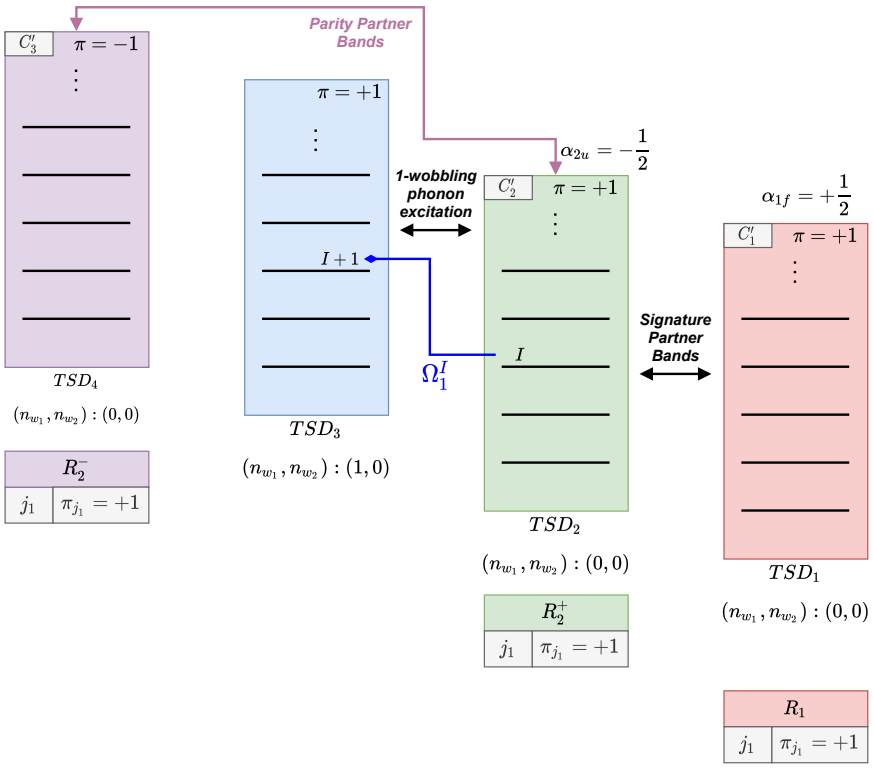

Fig. 10 – Schematic representation of the band structure adopted for ^{163}Lu in the W2 model [25]. For each band, the wobbling phonon numbers are shown. The main features and linking properties between bands are represented with arrows. The bottom part shows the coupling scheme (the core and the valence nucleon) for each wobbling band. The blue arrow marks the activation of TSD_3 states via the phonon operator.

REFERENCES

1. Aage Niels Bohr and Ben R Mottelson. *Nuclear Structure (In 2 Volumes)*. World Scientific Publishing Company, 1998.
2. SW Ødegård, GB Hagemann, DR Jensen, M Bergström, B Herskind, G Sletten, S Törmänen, JN Wilson, PO Tjøm, I Hamamoto, et al. *Physical review letters*, 86(26):5866, 2001.
3. DR Jensen, GB Hagemann, I Hamamoto, SW Ødegård, B Herskind, G Sletten, JN Wilson, K Spohr, H Hübel, P Bringel, et al. *Physical review letters*, 89(14):142503, 2002.
4. D Ringkøbing Jensen, GB Hagemann, I Hamamoto, SW Ødegård, M Bergström, B Herskind, G Sletten, S Törmänen, JN Wilson, PO Tjøm, et al. *Nuclear Physics A*, 703(1-2):3–44, 2002.
5. J Timár, QB Chen, B Kruzsicz, D Sohler, I Kuti, SQ Zhang, J Meng, P Joshi, R Wadsworth, K Starosta, et al. *Physical review letters*, 122(6):062501, 2019.
6. S Chakraborty, HP Sharma, SS Tiwary, C Majumder, AK Gupta, P Banerjee, S Ganguly, S Rai, S Kumar, A Kumar, et al. *Physics Letters B*, 811:135854, 2020.

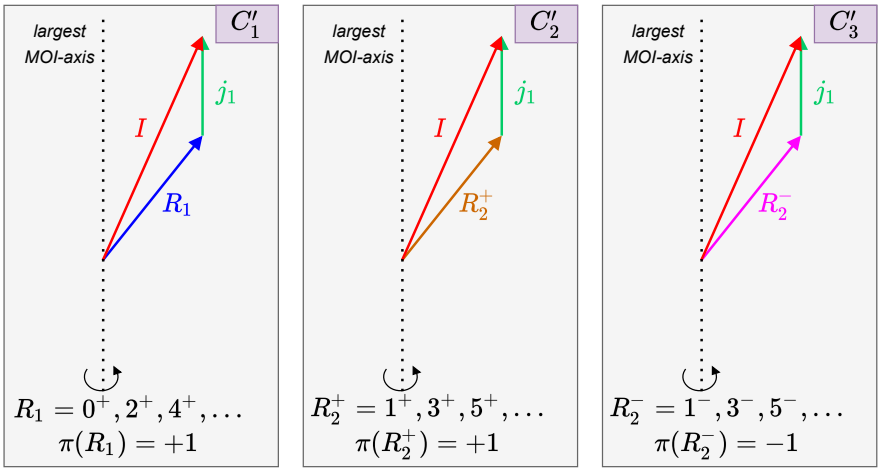

Fig. 11 – A schematic representation with the three coupling schemes that characterize the W2 model [25]. The same odd particle ($j_1 = i_{13/2}$ proton) is coupled with two positive cores with even (odd) integer spin sequences for TSD_1 (TSD_2), and one negative core in the case of TSD_4 with odd integer spin sequence. The total spin of the system precesses around the axis with the largest MOI, as it is the case for a triaxial rotor. The naming $C'_{1,2,3}$ of the three cases depicted here is defined and explained in **I**.

7. S Biswas, R Palit, S Frauendorf, U Garg, W Li, GH Bhat, JA Sheikh, J Sethi, S Saha, Purnima Singh, et al. *The European Physical Journal A*, 55(9):1–7, 2019.
8. James Till Matta. In *Exotic Nuclear Excitations: The Transverse Wobbling Mode in 135 Pr*, pages 77–93. Springer, 2017.
9. N Sensharma, U Garg, S Zhu, AD Ayangeakaa, S Frauendorf, W Li, GH Bhat, JA Sheikh, MP Carpenter, QB Chen, et al. *Physics Letters B*, 792:170–174, 2019.
10. P Bringel, GB Hagemann, H Hübel, A Al-Khatib, P Bednarczyk, A Bürger, D Curien, G Gangopadhyay, B Herskind, DR Jensen, et al. *The European Physical Journal A-Hadrons and Nuclei*, 24(2):167–172, 2005.
11. G Schönwaßer, H Hübel, GB Hagemann, P Bednarczyk, G Benzoni, A Bracco, P Bringel, R Chapman, D Curien, J Domscheit, et al. *Physics Letters B*, 552(1-2):9–16, 2003.
12. H Amro, WC Ma, GB Hagemann, RM Diamond, J Domscheit, P Fallon, A Görgen, B Herskind, H Hübel, DR Jensen, et al. *Physics Letters B*, 553(3-4):197–203, 2003.
13. DJ Hartley, RVF Janssens, LL Riedinger, MA Riley, A Aguilar, MP Carpenter, CJ Chiara, P Chowdhury, IG Darby, U Garg, et al. *Physical Review C*, 80(4):041304, 2009.
14. S Nandi, G Mukherjee, QB Chen, S Frauendorf, R Banik, Soumik Bhattacharya, Shabir Dar, S Bhattacharyya, C Bhattacharya, S Chatterjee, et al. *Physical Review Letters*, 125(13):132501, 2020.
15. N Sensharma, U Garg, QB Chen, S Frauendorf, DP Burdette, JL Cozzi, KB Howard, S Zhu, MP Carpenter, P Copp, et al. *Physical review letters*, 124(5):052501, 2020.
16. JH Hamilton, SJ Zhu, YX Luo, AV Ramayya, S Frauendorf, JO Rasmussen, JK Hwang, SH Liu, GM Ter-Akopian, AV Daniel, et al. *Nuclear Physics A*, 834(1-4):28c–31c, 2010.

17. YX Luo, JH Hamilton, AV Ramaya, JK Hwang, SH Liu, JO Rasmussen, S Frauendorf, GM Ter-Akopian, AV Daniel, Yu Ts Oganessian, et al. In *Exotic Nuclei: EXON-2012*, pages 215–224. World Scientific, 2013.
18. CM Petrache, PM Walker, S Guo, QB Chen, S Frauendorf, YX Liu, RA Wyss, D Mengoni, YH Qiang, A Astier, et al. *Physics Letters B*, 795:241–247, 2019.
19. YK Wang, FQ Chen, and PW Zhao. *Physics Letters B*, 802:135246, 2020.
20. QB Chen, S Frauendorf, and CM Petrache. *Physical Review C*, 100(6):061301, 2019.
21. H Schnack-Petersen, Ragnar Bengtsson, RA Bark, P Bosetti, A Brockstedt, H Carlsson, LP Ekström, GB Hagemann, B Herskind, F Ingebretsen, et al. *Nuclear Physics A*, 594(2):175–202, 1995.
22. S Frauendorf and F Dönau. *Physical Review C*, 89(1):014322, 2014.
23. AA Raduta, R Poenaru, and CM Raduta. *Physical Review C*, 101(1):014302, 2020.
24. AA Raduta, R Poenaru, and CM Raduta. *Journal of Physics G: Nuclear and Particle Physics*, 47(2):025101, 2020.
25. R.Poenaru and A.A. Raduta. *Submitted to Romanian Journal of Physics*, 2021.
26. DR Jensen, GB Hagemann, I Hamamoto, B Herskind, G Sletten, JN Wilson, SW Ødegård, K Spohr, H Hübel, P Bringel, et al. *The European Physical Journal A-Hadrons and Nuclei*, 19(2):173–185, 2004.
27. Kosai Tanabe and Kazuko Sugawara-Tanabe. *Physical Review C*, 73(3):034305, 2006.
28. AA Raduta, CM Raduta, and R Poenaru. *Journal of Physics G: Nuclear and Particle Physics*, 48(1):015106, 2020.
29. Ikuko Hamamoto. *Physical Review C*, 65(4):044305, 2002.
30. Gudrun B Hagemann and Ikuko Hamamoto. *Nuclear Physics News*, 13(3):20–24, 2003.
31. AS Davydov and GF Filippov. *Nuclear Physics*, 8:237–249, 1958.
32. J Meyer-ter Vehn. *Nuclear Physics A*, 249(1):111–140, 1975.
33. SY Wang, SQ Zhang, B Qi, J Peng, JM Yao, J Meng, et al. *Physical Review C*, 77(3):034314, 2008.
34. AA Raduta, R Budaca, and CM Raduta. *Physical Review C*, 76(6):064309, 2007.
35. R Budaca. *Physical Review C*, 97(2):024302, 2018.
36. AA Raduta, R Poenaru, and L Gr Ixaru. *Physical Review C*, 96(5):054320, 2017.
37. AA Raduta, R Poenaru, and Al H Raduta. *Journal of Physics G: Nuclear and Particle Physics*, 45(10):105104, 2018.
38. EA Lawrie, O Shirinda, and CM Petrache. *Physical Review C*, 101(3):034306, 2020.

Simultaneous description of wobbling and chiral properties in even-odd triaxial nuclei

C. M. Raduta [a)], A. A. Raduta[a),b)], R. Poenaru [a),c)] and Al.H. Raduta [a)]
[a)] *Department of Theoretical Physics, National Institute of Physics and Nuclear Engineering, Bucharest, POBox MG6, Romania*
[b)] *Academy of Romanian Scientists, 54 Splaiul Independentei, Bucharest 050094, Romania and*
[c)] *Doctoral School of Physics, Bucharest University,*
Soseaua Panduri, nr. 90, Sector 5, 050663, Bucharest, Romania

A particle-triaxial rigid core Hamiltonian is semi-classically treated. The coupling term corresponds to a particle rigidly coupled to the triaxial core, along a direction that does not belong to any principal plane of the inertia ellipsoid.The equations of motion for the angular momentum components provide a sixth-order algebraic equation for one component and subsequently equations for the other two. Linearizing the equations of motion, a dispersion equation for the wobbling frequency is obtained. The equations of motion are also considered in the reduced space of generalized phase space coordinates. Choosing successively the three axes as quantization axis will lead to analytical solutions for the wobbling frequency, respectively. The same analysis is performed for the chirally transformed Hamiltonian. With an illustrative example one identified wobbling states whose frequencies are mirror image to one another. Changing the total angular momentum I, a pair of twin bands emerged. Note that the present formalism conciliates between the two signatures of triaxial nuclei, i.e., they could coexist for a single nucleus.

I. INTRODUCTION

Most of the nuclei from the nuclear chart are axially symmetric and for this reason, the triaxial nuclei were not studied much. The first paper devoted to this issue is that of Davydov and Filippov [1]. In refs.[1–8] the specific features of triaxial nuclei were studied. Therein two distinct properties are considered as signatures of triaxial nuclei, namely the wobbling motion and chiral doublets [9–14]. While these features were extensively studied over the recent years [15–26],only a separate treatment was considered. A possible justification of this is that up to date the two signatures were experimentally identified in different nuclei. However, it is interesting to investigate whether the two properties may be seen in a single nucleus. For this, we have to conciliate two distinct aspects, namely that in the case of chiral states the rotation axis stays outside any principal plane, while in the case of wobbling motion this property is lacking.

The mentioned signatures of triaxial nuclei are here studied, at a time for even-odd isotopes. A particle-triaxial rotor Hamiltonian is firstly dequantized and then the classical equations of motion for the angular momentum components are explicitly written and an algebraic equation for the stationary angular momentum components are obtained, in Section 2. In Section 3, an equation for the wobbling frequency is derived. The equations of motion in the reduced space of he angular momenta space are considered in Section 4. An illustrative example is treated in Section 5, while the final conclusions are presented in Section 6.

II. CLASSICAL DESCRIPTION OF THE PARTICLE TRIAXIAL CORE COUPLING

We thus study an odd-mass system consisting of an even-even core described by a triaxial rotor Hamiltonian H_{rot} and a single j-shell proton moving in a quadrapole deformed mean-field:

$$H_{sp} = \epsilon_j + \frac{V}{j(j+1)}\left[\cos\gamma(3j_3^2 - \mathbf{j}^2) - \sqrt{3}\sin\gamma(j_1^2 - j_2^2)\right]. \tag{2.1}$$

Here ϵ_j is the single particle energy and γ, the deviation from the axial symmetric picture. In terms of the total angular momentum $\mathbf{I}(= \mathbf{R} + \mathbf{j})$ and the angular momentum carried by the odd particle, $\mathbf{j}$, the rotor Hamiltonian is written as:

$$H_{rot} = \sum_{k=1,2,3} A_k (I_k - j_k)^2. \tag{2.2}$$

where A_k are half of the reciprocal moments of inertia associated to the principal axes of the inertia ellipsoid, i.e. $A_k = 1/(2\mathcal{I}_k)$, which are considered as free parameters.

The expressions for the single particle coupling potential, H_{sp}, and the triaxial rotor term, H_{rot}, have been previously used by many authors, the first being Davydov [27]. In the context of rigid coupling of the single particle to the core, the term H_{sp} does not contribute to the equations of motion for the angular momentum components I_k, k=1,2,3.

We consider that the maximal moment of inertia (MoI) is $\mathcal{J}_1$. For a rigid coupling of the odd proton to the triaxial core, we suppose that $\mathbf{j}$ stays out of any principal plane: $\mathbf{j} = (j\cos\theta_0, j\sin\theta_0\cos\varphi_0, j\sin\theta_0\sin\varphi_0)$.

We recall that within the liquid drop model (LDM) the odd nucleon may be coupled either to the deformation or to the core angular momentum. Correspondingly, the single particle angular momentum is oriented either to the symmetry axis or to the core's angular momentum [28]. These scenarios are reached for weak and strong coupling regimes, respectively. For an intermediate coupling one may meet the situation when $\mathbf{j}$ lays outside the principal planes. Within a microscopic picture, the orientation of the single particle angular momentum depends on the location of the Fermi level. Thus, when the Fermi level of valence nucleon is located in the lower/upper part of a high-j subshell, its angular momentum is oriented along the short/long axis of the triaxial core, and in the middle part with its angular momentum easily aligned with the intermediate axis with the maximum MoI. When the Fermi level is different from these special cases, the angular momentum of the odd proton might be oriented along a line which is different from the three mentioned axes. In these phenomenological and microscopic contests, it seems reasonable to fix the single particle angular momentum outside any principal plane of the triaxial core.

Note that the linear term in $\hat{I}$ from (2.2) looks like the cranking term in the microscopic cranking formalism. According to the pioneering paper of Bengston [29] the equations for a general orientation of the cranking term admit a real solution.

In this context we ask ourselves, whether the phenomenological Hamiltonian (2.2) admits a harmonic solution within a classical treatment. To this aim we dequantize the model Hamiltonian by replacing the operators $\hat{I}_k$, k=1,2,3 with the classical components of the angular momentum hereafter denoted by x_k,k=1,2,3, respectively, and the commutators with the Poisson brackets:

$$\begin{aligned} &\hat{I}_k \to x_k, \\ &[,] \to i\{,\}. \end{aligned} \tag{2.3}$$

with 'i' denoting the imaginary unity. The Poisson brackets are defined as follows. Let f and g two functions defined on the phase space spanned b the coordinates and conjugate momenta (q_k, p_k) . Then the associated Poisson Bracket is defined as:

$$\{f,g\} = \sum_k (\frac{\partial f}{\partial q_k}\frac{\partial g}{\partial p_k} - \frac{\partial f}{\partial p_k}\frac{\partial g}{\partial q_k}). \tag{2.4}$$

According to these rules, the classical energy can be written as:

$$\begin{aligned} \mathcal{H}_{rot} &= AH' + A_1 I^2 + \sum_{k=1,2,3} A_k j_k^2, \text{ with} \\ H' &= x_2^2 + u x_3^2 + 2v_1 x_1 + 2v_2 x_2 + 2v_3 x_3, \\ u &= \frac{A_3 - A_1}{A_2 - A_1},\ v_k = -\frac{j_k A_k}{A_2 - A_1}, k = 1,2,3., A = A_2 - A_1. \end{aligned} \tag{2.5}$$

Also, the angular momentum components obey:

$$\{x_i, x_j\} = -\epsilon_{i,j,k} x_k. \tag{2.6}$$

where $\epsilon_{i,j,k}$ denotes the three dimensional unity tensor. Given an operator O defined on the phase space and considered in the interaction representation, this obeys the Heisenberg equation:

$$[O,H] = i\frac{\partial O}{\partial t}. \tag{2.7}$$

According to the dequantization rules the classical counterpart of the above equation is:

$$\{o,H\} = i\frac{\partial o}{\partial t}. \tag{2.8}$$

with o denoting the classical image of O.

Since $\mathcal{H}_{rot}$ and H' differ from each other by one multiplicative and one additive constant, the motion described by $\mathcal{H}rot$ is readily known once that corresponding to H' is given. Due to this feature, it is convenient to deal first with H'. Thus, the equations of motion for the components x_k are:

$$
\begin{aligned}
\{x_1, H'\} &= \overset{\bullet}{x}_1 = -2\left[x_2x_3(1-u) + v_2x_3 - v_3x_2\right], \\
\{x_2, H'\} &= \overset{\bullet}{x}_2 = -2\left[ux_1x_3 - v_1x_3 + v_3x_1\right], \\
\{x_3, H'\} &= \overset{\bullet}{x}_3 = -2\left[-x_1x_2 + v_1x_2 - v_2x_1\right], \\
\{\varphi_1, H'\} &= \overset{\bullet}{\varphi}_1 = -2\frac{A_1}{A}(x_1 - j_1), \\
\{\varphi_2, H'\} &= \overset{\bullet}{\varphi}_2 = -2\frac{A_2}{A}(x_2 - j_2), \\
\{\varphi_3, H'\} &= \overset{\bullet}{\varphi}_3 = -2\frac{A_3}{A}(x_3 - j_3).
\end{aligned} \tag{2.9}
$$

where the symbol "$\bullet$" signifies the first derivative with respect to time, while φ_k (k=1,2,3) are the conjugate coordinates of x_k (k=1,2,3), respectively. Note that Eqs.(2.9) are directly obtainable from the Hamilton equations associated to the conjugate coordinates x_k and φ_k. The stationary points of the classical trajectories $(x_1(t), x_2(t), x_3(t))|_t$ are obtained by cancelling the first derivatives with respect to time of x_k, which results in obtaining simple relations between the components x_k:

$$
\begin{aligned}
&\frac{v_1}{x_1} - \frac{v_2}{x_2} = 1, \\
&\frac{v_1}{x_1} - \frac{v_3}{x_3} = u, \\
&\frac{v_2}{x_2} - \frac{v_3}{x_3} = u - 1.
\end{aligned} \tag{2.10}
$$

From these relations we can express x_2 and x_3 in terms of x_1 and then insert the result in the angular momentum conservation equation:

$$
x_1^2 + x_2^2 + x_3^2 = I^2. \tag{2.11}
$$

It results an algebraic equation for the component x_1:

$$
F(x_1) \equiv \sum_{k=0}^{6} B_k x_1^k = 0, \tag{2.12}
$$

with the coefficients B_k given by:

$$
\begin{aligned}
B_0 &= -I^2 v_1^4, \\
B_1 &= 2v_1^3(1+u)I^2, \\
B_2 &= v_1^2\left(v_1^2 + v_2^2 + v_3^2\right) - v_1^2\left(1 + 4u + u^2\right)I^2, \\
B_3 &= -2\left(v_1^3(1+u) + v_1(v_2^2u + v_3^2)\right) + 2v_1u(1+u)I^2, \\
B_4 &= v_1^2\left(1 + 4u + u^2\right) + v_2^2u^2 + v_3^2 - u^2I^2, \\
B_5 &= -2v_1u(1+u), \\
B_6 &= u^2.
\end{aligned} \tag{2.13}
$$

We note that, since $B_0 \neq 0$, the equation (2.12) does not admit vanishing solutions, which as a matter of fact is a specific feature for the chiral motion. The solution lead to the stationary points $(\overset{\circ}{x}_1, \overset{\circ}{x}_2, \overset{\circ}{x}_3)$ for the surface of constant energy:

$$
H' = E. \tag{2.14}
$$

Among the stationary points some are minima. Let us denote by $\overset{\circ}{x}_1$ a solution of (2.12) which corresponds to the deepest minimum of H'. Then from (2.10) one gets:

$$
\begin{aligned}
\overset{\circ}{x}_2 &= \frac{v_2\,\overset{\circ}{x}_1}{v_1 - \overset{\circ}{x}_1}, \\
\overset{\circ}{x}_3 &= \frac{v_3\,\overset{\circ}{x}_1}{v_1 - u\,\overset{\circ}{x}_1}.
\end{aligned} \tag{2.15}
$$

and thus the minimum point denoted by $\overset{\circ}{P} = (\overset{\circ}{x}_1, \overset{\circ}{x}_2, \overset{\circ}{x}_3)$, is fully determined.

III. SMALL OSCILLATIONS AROUND THE DEEPEST MINIMUM

The equations of motion for the components x_k are non-linear. However, these can be linearized by replacing one factor of the quadratic terms with the coordinates of the deepest minimum point. In this way one obtains the following system of linear equations:

$$\begin{aligned}
\{x_1, H'\} = \dot{x}_1 &= -\left(2v_2 + \mathring{x}_2\,(1-u)\right) x_3 - \left(\mathring{x}_3\,(1-u) - 2v_3\right) x_2, \\
\{x_2, H'\} = \dot{x}_2 &= -\left(u\,\mathring{x}_3 + 2v_3\right) x_1 - \left(u\,\mathring{x}_1 - 2v_1\right) x_3, \\
\{x_3, H'\} = \dot{x}_3 &= \left(\mathring{x}\,2 + 2v_2\right) x_1 - \left(-\,\mathring{x}_1 + 2v_1\right) x_2.
\end{aligned} \tag{3.1}$$

A solution of the linear system of equations may be found by searching for the linear combination:

$$C^* = X_1 x_1 + X_2 x_2 + X_3 x_3, \tag{3.2}$$

such that the following equation is fulfilled:

$$\{C^*, H'\} = \omega C^* \tag{3.3}$$

This restriction leads to a homogeneous system of linear equations for the coefficients X_1, X_2, X_3. The compatibility condition yields an equation for the frequency ω:

$$\omega^3 + 3S\omega - 2T = 0. \tag{3.4}$$

with the coefficients given by:

$$\begin{aligned}
3S &= -\left(2v_1 - u\,\mathring{x}_1\right)\left(\mathring{x}_1 - 2v_1\right) + \left(u\,\mathring{x}_3 + 2v_3\right)\left(2v_3 - (1-u)\,\mathring{x}_3\right) + \left(\mathring{x}_2 + 2v_2\right)\left(2v_2 + (1-u)\,\mathring{x}_2\right), \\
2T &= \left(2v_3 + u\,\mathring{x}_3\right)\left(2v_2 + (1-u)\,\mathring{x}_2\right)\left(\mathring{x}_1 - 2v_1\right) - \left(\mathring{x}_2 + 2v_2\right)\left((1-u)\,\mathring{x}_3 - 2v_3\right)\left(2v_1 - u\,\mathring{x}_1\right).
\end{aligned} \tag{3.5}$$

The solutions of Eq.(3.4) are analytically given in Appendix A.

IV. THE TREATMENT WITHIN THE REDUCED SPACE

Note that the system under consideration exhibits two constants of motion, namely the energy and the angular momentum squared. Furthermore, there is only one independent angular momentum component; adding to this the corresponding conjugate momentum one arrives at a two dimensional phase space, which is conventionally called the *the reduced space*. To define this space, it is convenient to use the polar coordinates. We treat separately three cases:

A. Axis 1 is the quantization axis

In this case the coordinates x_k are:

$$x_1 = I\cos\theta_1,\ x_2 = I\sin\theta_1\cos\varphi_1,\ x_3 = I\sin\theta_1\sin\varphi_1. \tag{4.1}$$

The coordinates x_2 and x_3 can be expressed in terms of x_1 and φ_1 by replacing first $I\sin\theta_1$ by $\sqrt{I^2 - x_1^2}$ and then expanding the square root factor in second order, which results:

$$x_2 = \left(I - \frac{1}{2I}x_1^2\right)\cos\varphi_1,\ x_3 = \left(I - \frac{1}{2I}x_1^2\right)\sin\varphi_1. \tag{4.2}$$

Inserting these in H' one obtains:

$$\begin{aligned}
H' &= x_1^2\left(-\cos^2\varphi_1 - u\sin^2\varphi_1 - \frac{1}{I}(v_2\cos\varphi_1 + v_3\sin\varphi_1)\right) \\
&+ I^2\cos^2\varphi_1 + uI^2\sin^2\varphi_1 + 2v_2\cos\varphi_1 + 2v_3\sin\varphi_1 + 2v_1x_1.
\end{aligned} \tag{4.3}$$

Note that since the factor $A_2 - A_1$ accompanying H' in Eq.(2.5) is positive, the two Hamiltonians, H' and H_{rot}, exhibit the same minima. Let $(\overset{\circ}{x}_1, \overset{\circ}{\varphi}_1)$ be the coordinates of the deepest minimum point for H'.This minimum point will be determined in next section. Expanding now H' around the deepest minimum point one obtains:

$$\begin{aligned} H' &= \left(-\cos^2\overset{\circ}{\varphi}_1 - u\sin^2\overset{\circ}{\varphi}_1 + \frac{v_2}{I}\cos\overset{\circ}{\varphi}_1 - \frac{v_3}{I}\sin\overset{\circ}{\varphi}_1\right)(x_1 - \overset{\circ}{x}_1)^2 \\ &+ \left[\overset{\circ}{x}_1^2\left(\cos 2\overset{\circ}{\varphi}_1 - u\cos 2\overset{\circ}{\varphi}_1 + \frac{v_2}{2I}\cos\overset{\circ}{\varphi}_1 + \frac{v_3}{2I}\sin\overset{\circ}{\varphi}_1\right)\right. \\ &- \left.(1-u)I^2\cos 2\overset{\circ}{\varphi}_1 - v_2 I\cos\overset{\circ}{\varphi}_1 - v_3 I\sin\overset{\circ}{\varphi}_1\right](\varphi_1 - \overset{\circ}{\varphi}_1)^2. \end{aligned} \tag{4.4}$$

It is worth noting that the above Taylor expansion is lacking the first order as well as the mixed second order derivatives. The reason is that the first order derivatives are vanishing in a minimum point. As for the other mising term this is omitted since violates the time reversal symmetry, being linear in momenta

For positive coefficients of the deviations squared, the above equation describes a harmonic oscillator of frequency:

$$\begin{aligned} \omega^{(1)} &= 2\left[\left(\cos^2\overset{\circ}{\varphi}_1 + u\sin^2\overset{\circ}{\varphi}_1 + \frac{1}{I}(v_2\cos\overset{\circ}{\varphi}_1 + v_3\sin\overset{\circ}{\varphi}_1)\right)\right. \\ &\times \left.\left((I^2 - \overset{\circ}{x}_1^2)(1-u)\cos 2\overset{\circ}{\varphi}_1 + \frac{1}{I}(I^2 - \frac{\overset{\circ}{x}_1^2}{2})(v_2\cos\overset{\circ}{\varphi}_1 + v_3\sin\overset{\circ}{\varphi}_1\right)\right]^{1/2}. \end{aligned} \tag{4.5}$$

B. Axis 2 is the quantization axis

In this case we choose the coordinates as:

$$x_2 = I\cos\theta_2,\ x_3 = I\sin\theta_2\cos\varphi_2,\ x_1 = I\sin\theta_2\sin\varphi_2. \tag{4.6}$$

Following the procedure from the previous subsection, the energy function H' is expressed in terms of the conjugate coordinate (x_2, φ_2):

$$\begin{aligned} H' &= x_2^2 + 2v_2x_2 - ux_2^2\cos^2\varphi_2 - \frac{1}{I}x_2^2(v_1\sin\varphi_2 + v_3 I\cos\varphi_2) \\ &+ uI^2\cos^2\varphi_2 + 2v_1\sin\varphi_2 + 2v_3 I\cos\varphi_2. \end{aligned} \tag{4.7}$$

The deepest minimum is reached in $(\overset{\circ}{x}_2, \overset{\circ}{\varphi}_2)$, to be determined in next section.

Expanding H' around this minimum one gets:

$$\begin{aligned} H' &= \left[1 - u\cos^2\overset{\circ}{\varphi}_2 - \frac{1}{I}\left(v_1\sin\overset{\circ}{\varphi}_2 + v_3\cos\overset{\circ}{\varphi}_2\right)\right](x_2 - \overset{\circ}{x}_2)^2 \\ &+ \left[(\overset{\circ}{x}_2^2 - I^2)u\cos 2\overset{\circ}{\varphi}_2 + (\frac{\overset{\circ}{x}_2^2}{2I} - I)\left(v_1\sin\overset{\circ}{\varphi}_2 + v_3\cos\overset{\circ}{\varphi}_2\right)\right](\varphi_2 - \overset{\circ}{\varphi}_2)^2. \end{aligned} \tag{4.8}$$

If the coefficients of the variation of $(x_2 - \overset{\circ}{x}_2)^2$ and $(\varphi_2 - \overset{\circ}{\varphi}_2)^2$, respectively, are positive,the Hamiltonian H' describes a linear oscillator of frequency:

$$\begin{aligned} \omega^{(2)} &= 2\left[\left(1 - u\cos^2\overset{\circ}{\varphi}_2 - \frac{1}{I}\left(v_1\sin\overset{\circ}{\varphi}_2 + v_3\cos\overset{\circ}{\varphi}_2\right)\right)\right. \\ &\times \left.\left((\overset{\circ}{x}_2^2 - I^2)u\cos 2\overset{\circ}{\varphi}_2 + (\frac{\overset{\circ}{x}_2^2}{2I} - I)\left(v_1\sin\overset{\circ}{\varphi}_2 + v_3\cos\overset{\circ}{\varphi}_2\right)\right)\right]^{/2}. \end{aligned} \tag{4.9}$$

C. Axis 3 is the quantization axis

To this case the following polar coordinates correspond:

$$x_3 = I\cos\theta_3,\ x_1 = I\sin\theta_3\cos\varphi_3,\ x_1 = I\sin\theta_3\sin\varphi_3. \tag{4.10}$$

Inserting these coordinates in the expression of H', it results:

$$\begin{aligned} H' &= \left(I^2 - x_3^2\right)\sin^2\varphi_3 + ux_3^2 + v_3x_3 \\ &+ 2I(v_1\cos\varphi_3 + v_2\sin\varphi_3) - \frac{x_3^2}{I}(v_1\cos\varphi_3 + v_2\sin\varphi_3). \end{aligned} \tag{4.11}$$

The minimum of H' is given by $(\overset{\circ}{x}_3, \overset{\circ}{\varphi}_3)$, which is introduced in next section.

The quadratic expansion of H' around the deepest minimum point $(\overset{\circ}{x}_3, \overset{\circ}{\varphi}_3)$ is:

$$\begin{aligned} H' &= \left(-\sin^2\overset{\circ}{\varphi}_3 + u - \frac{1}{I}(v_1\cos\overset{\circ}{\varphi}_3 + v_2\sin\overset{\circ}{\varphi}_3)\right)(x_3 - \overset{\circ}{x}_3)^2 \\ &+ \left((I^2 - \overset{\circ}{x}_3^2\cos 2\overset{\circ}{\varphi}_3 + (\frac{\overset{\circ}{x}_3^2}{2I} - I)(v_1\cos\overset{\circ}{\varphi}_3 + v_2\sin\overset{\circ}{\varphi}_3)\right)(\varphi_3 - \overset{\circ}{\varphi}_3)^2 \end{aligned} \tag{4.12}$$

Under circumstances that the second derivatives of H' with respect to x_3 and φ_3, respectively, are positive, H' describes a linear oscillator having the frequency:

$$\begin{aligned} \omega^{(3)} &= 2\left[\left(-\sin^2\overset{\circ}{\varphi}_3 + u - \frac{1}{I}(v_1\cos\overset{\circ}{\varphi}_3 + v_2\sin\overset{\circ}{\varphi}_3)\right)\right. \\ &\times \left.\left((I^2 - \overset{\circ}{x}_3^2)\cos 2\overset{\circ}{\varphi}_3 + (\frac{\overset{\circ}{x}_3^2}{2I} - I)(v_1\cos\overset{\circ}{\varphi}_3 + v_2\sin\overset{\circ}{\varphi}_3)\right)\right]^{1/2}. \end{aligned} \tag{4.13}$$

If the frequencies (4.5), (4.9), (4.13) are all real, then these describe the wobbling frequencies for the motion along the axes 1,2,3, respectively. It is interesting to see what is the relations between the frequencies given in subsections A, B and C and the solutions of the cubic equation (3.4) from the previous section. This issue will be pointed out in next section.

In the space of angular momentum, a chiral transformation is equivalent to the space inversion operation, i.e. $C = \mathbf{I} \to -\mathbf{I}$. Due to the linear terms in angular momentum components, the Hamiltonian H' is not invariant to chiral transformations. On the other hand, if there exists an operator O which anti-commutes with a given Hamiltonian H,

$$\{H, O\} = 0, \tag{4.14}$$

then, if Ψ is an eigenfunction of H corresponding to the eigenvalue λ, it results that $O\Psi$ is also an eigenfunction of H with the eigenvalue $-\lambda$. Therefore, the eigenvalues λ and -λ are mirror images of one another. In our case H' is a sum of two terms, one invariant, H_1, and another non-invariant, H_2, to chiral transformations C. The non-invariant term H_2 and the transformation C satisfy Eq.(4.14). Due to this feature the eigenvalues of H' are mirror images of those for $CH'C^{-1}$.The two sets of energies define the so called chiral bands. We note that $CH'C^{-1}$ is obtained from H' by changing $v_k \to -v_k$, which results that the wobbling frequencies, $\omega_{ch}^{(k)}$, built up with $CH'C^{-1}$ are obtained

from those obtained with H' with the transformation $v_k \to -v_k$.Thus, we have:

$$\begin{aligned}
\omega_{ch}^{(1)} &= 2\left[\left(\cos^2\mathring{\varphi}_1 + u\sin^2\mathring{\varphi}_1 - \frac{1}{I}(v_2\cos\mathring{\varphi}_1 + v_3\sin\mathring{\varphi}_1)\right)\right. \\
&\quad \left.\times\left((I^2 - \mathring{x}_1^2)(1-u)\cos 2\mathring{\varphi}_1 - \frac{1}{I}(I^2 - \frac{\mathring{x}_1^2}{2})(v_2\cos\mathring{\varphi}_1 + v_3\sin\mathring{\varphi}_1\right)\right]^{1/2}, \\
\omega_{ch}^{(2)} &= 2\left[\left(1 - u\cos^2\mathring{\varphi}_2 + \frac{1}{I}\left(v_1\sin\mathring{\varphi}_2 + v_3\cos\mathring{\varphi}_2\right)\right)\right. \\
&\quad \left.\times\left((\mathring{x}_2^2 - I^2)u\cos 2\mathring{\varphi}_2 - (\frac{\mathring{x}_2^2}{2I} - I)\left(v_1\sin\mathring{\varphi}_2 + v_3\cos\mathring{\varphi}_2\right)\right)\right]^{/2}, \\
\omega_{ch}^{(3)} &= 2\left[\left(-\sin^2\mathring{\varphi}_3 + u + \frac{1}{I}(v_1\cos\mathring{\varphi}_3 + v_2\sin\mathring{\varphi}_3)\right)\right. \\
&\quad \left.\times\left((I^2 - \mathring{x}_3^2\cos 2\mathring{\varphi}_3 - (\frac{\mathring{x}_3^2}{2I} - I)(v_1\cos\mathring{\varphi}_3 + v_2\sin\mathring{\varphi}_3)\right)\right]^{1/2}. \qquad (4.15)
\end{aligned}$$

The spectrum of H_{rot} is:

$$\begin{aligned}
E_{I,n}^{(1)} &= (A_2 - A_1)\left(H_{min}'^{(1)} + \omega^{(1)}(n + \frac{1}{2})\right) + \sum_{k=1,2,3} A_k j_k^2, \\
E_{I,n}^{(2)} &= (A_2 - A_1)\left(H_{min}'^{(2)} + \omega^{(2)}(n + \frac{1}{2})\right) + \sum_{k=1,2,3} A_k j_k^2, \\
E_{I,n}^{(3)} &= (A_2 - A_1)\left(H_{min}'^{(3)} + \omega^{(3)}(n + \frac{1}{2})\right) + \sum_{k=1,2,3} A_k j_k^2, n = 0,1,2,.... \qquad (4.16)
\end{aligned}$$

The mirror images of these energies through the Chiral transformation are:

$$\begin{aligned}
E_{ch,I,n}^{(1)} &= (A_2 - A_1)\left(H_{ch,min}'^{(1)} + \omega_{ch}^{(1)}(n + \frac{1}{2})\right) + \sum_{k=1,2,3} A_k j_k^2, \\
E_{ch,I,n}^{(2)} &= (A_2 - A_1)\left(H_{ch,min}'^{(2)} + \omega_{ch}^{(2)}(n + \frac{1}{2})\right) + \sum_{k=1,2,3} A_k j_k^2, \\
E_{ch,I,n}^{(3)} &= (A_2 - A_1)\left(H_{ch,min}'^{(3)} + \omega_{ch}^{(3)}(n + \frac{1}{2})\right) + \sum_{k=1,2,3} A_k j_k^2, n = 0,1,2,.... \qquad (4.17)
\end{aligned}$$

The notations $H_{min}'^{(k)}$ and $H_{ch,min}'^{(k)}$ are used for minimal energy when the axis "k" is the quantization axis. According to Eq.(4.5), (4.9), (4.13), and (4.15), the energies are angular momentum dependent. For a given n and I=α+2n with α being the signature, the set of energies $E_{I,n}^{(k)}$ defines a wobbling band, while $E_{ch,I,n}^{(k)}$ the chiral partner band. In this way we found out a set of states which are simultaneously of wobbling and chiral character. The wobbling motion is conciliated with the ingredient that the rotation axis is outside the principal planes.

Before closing this section few details about the chiral transformations are necessary. The chiral transformation is bringing a right handed frame to a left handed frame. For example, if (x_1, x_2, x_3) is right handed, then $(-x_1, -x_2, -x_3)$ is left handed. The components of the angular momentum $\mathbf{j}$ in the two frames are (j_1, j_2, j_3) and $(-j_1, -j_2, -j_3)$, respectively. The correspondence between $\mathbf{j}$ and $-\mathbf{j}$ is a chiral transformation (C) in the space of angular momenta. This definition allows us to study the Hamiltonians whose eigenvalues are sensitive to the change of the rotation sense for the system under consideration. Here, this type of chiral transformation is studied. We note that the transformation $C_3 = (j_1, j_2, j_3) \to (j_1, j_2, -j_3)$ is also chiral. So are $C_1 = (j_1, j_2, j_3) \to (-j_1, j_2, j_3)$ and $C_2 = (j_1, j_2, j_3) \to (j_1, -j_2, j_3)$. Moreover, the wobbling frequency for the chiral image of H_{rot} through the transformations C_k is obtained from Eqs.(4.5), (4.9) and (4.13) by changing v_k to $-v_k$, respectively. Obviously,the transformations C_k, k=1,2,3 are related to the chiral transformation C by:

$$C = C_1 C_2 C_3. \qquad (4.18)$$

V. AN ILLUSTRATIVE EXAMPLE

Here we consider an odd particle from the single particle orbit $j = i_{13/2}\hbar$ moving around a triaxial rigid rotor core with the moments of inertia (MoI):

$$(\mathcal{J}_1, \mathcal{J}_2, \mathcal{J}_3) = (60, 20, 30)\hbar^2 MeV^{-1}. \tag{5.1}$$

The composite system moves in a state of angular momentum $I = 35/2\hbar$. The odd particle is rigidly coupled to the core such that its angular momentum orientation is outside the principal planes of the triaxial ellipsoid. Thus, the polar coordinates of the vector $\mathbf{j}$ are: $\mathbf{j} = (j, \theta_0, \varphi_0) = (13/2, \pi/4, \pi/4)$. The stationary points for the equations of motion for the classical angular momentum components x_k, k=1,2,3, obey a set of equations which leads to an algebraic sixth-order equation for x_1 ,i.e $F(x_1, I) = 0$. The function $F(x_1, I)$ is pictorially given in Fig.1. This function

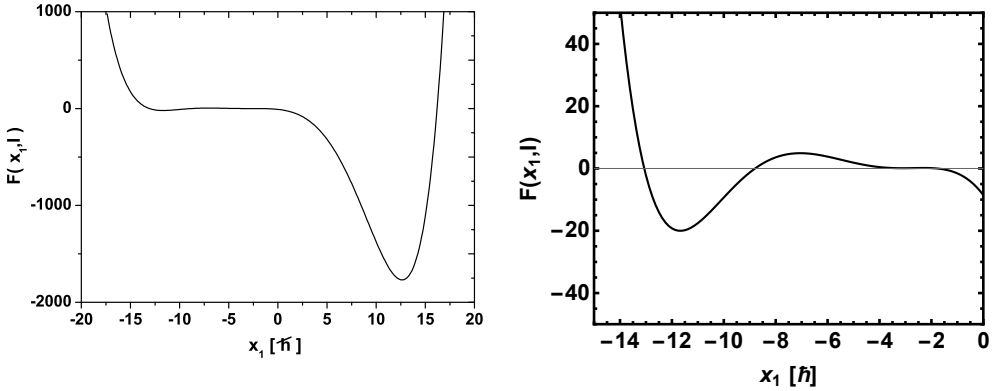

FIG. 1: The function $F(x_1, I)$ given by Eq.(2.9), is represented (left panel) as function of x_1 for the angular momentum $I = 35/2\hbar$. The same function is plotted within a shorter interval (right panel) such that the first three solutions are visible.

admits four real solutions for x_1:$-13.062; -8.811; -1.81; 16.185[\hbar]$. Making use of relations expressing x_2 and x_3 in terms of x_1 one arrives at the final result:

$$(\mathring{x}_1, \mathring{x}_2, \mathring{x}_3) = \begin{pmatrix} -13.062 & 5.916 & 10.029 \\ -8.811 & 6.595 & 13.588 \\ -1.810 & 16.886 & -4.223 \\ 16.185 & 4.269 & 5.062 \end{pmatrix} \hbar. \tag{5.2}$$

To the four stationary vectors the following classical energies correspond:

$$H_{rot} = \begin{pmatrix} axis-1 & axis-2 & axis-3 \\ 3.542 & 3.027 & 2.887 \\ 3.559 & 3.093 & 2.839 \\ 5.921 & 4.920 & 5.793 \\ 1.200 & 1.452 & 1.424 \end{pmatrix} \text{MeV}. \tag{5.3}$$

For example, for the stationary angular momenta components from the row 1 of Eq. (5.2), the energies of the row 1 from Eq.(5.3) correspond, for the situations when the quantization axes are the axis-1,axis-2 and axis-3, respectively.

The frequencies characterizing the linearized equations of motion satisfy a third order algebraic equation. The minimum value for the energy H_{rot} when $\mathbf{I} \parallel \mathbf{j}$, i.e. when the two angular momenta are aligned, is 1.765 MeV. With this data there exists a real solution for the wobbling frequency:

$$\omega = 0.362\text{MeV}. \tag{5.4}$$

The chiral partner state has the frequency equal to 3.651 MeV.

Furthermore, we studied the equations of motion for H' in the reduced space of generalized phase space coordinates.

The coordinates and spins of all minima are collected in Table I; these minima are taken from the contour plots shown in Figs.2, 3 and 4, respectively. Details about the behavior of H_{rot} around its minima can be seen in Fig. 5,

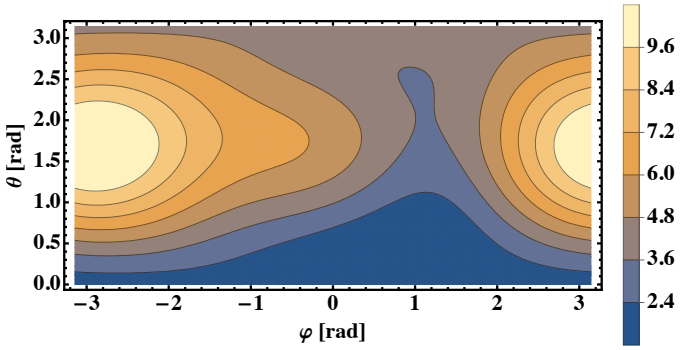

FIG. 2: (Color online) The energy function is H_{rot} given by Eq. (2.2) as a function of the polar coordinates. Contour plot when the axis-1 is the quantization axis.

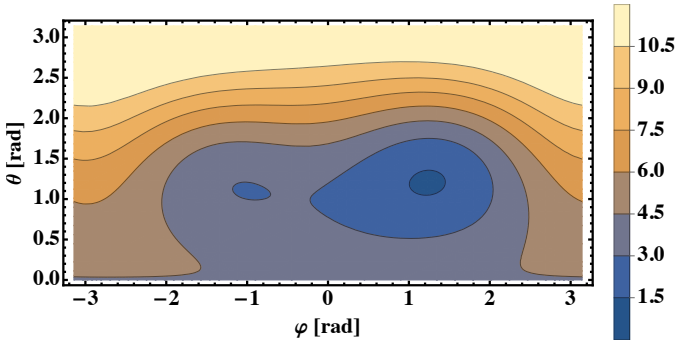

FIG. 3: (Color online) The energy function is H_{rot} given by Eq. (2.2) as a function of the polar coordinates. Contour plot with the axis-2 as the quantization axis.

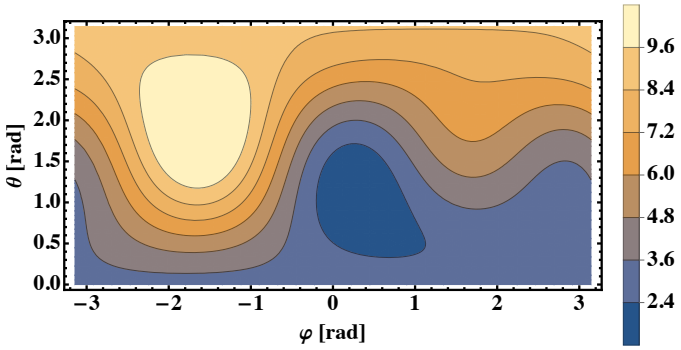

FIG. 4: (Color online) The energy function is H_{rot} given by Eq. (2.2) as a function of the polar coordinates. Contour plot with the axis-3 as the quantization axis.

where the energy function is represented separately as a function of φ and θ, respectively, when the other variable is fixed in its minimum value.

It is worth mentioning that the stationary components of angular momentum given in the first row of Table I describing the minimum of Fig. 1, coincide with those from the last row of Eq.(5.2), which are obtained by solving the equations (2.9) and (2.7), and this happens despite the fact the two sets correspond to different spaces,one generated

quantization axis	θ_{min}[rad]	φ_{min}[rad]	$I_1[\hbar]$	$I_2[\hbar]$	$I_3[\hbar]$	$H_{rot,min}$[MeV]
axis-1	0.388	0.8703	16.198	4.269	5.063	1.203
axis-2	1.206	1.236	15.443	6.238	5.370	1.381
axis-2	1.104	-0.983	- 13.003	7.879	8.666	2.960
axis-3	1.124	0.283	15.152	4.403	7.569	1.361

TABLE I: Coordinates of the minima points for H_{rot} and the corresponding values of the spin components.

by the angular momentum components and one is a two dimensional phase space.

A major conclusion of this analysis is that irrespective of the chosen quantization axis, the deepest minimum of H_{rot} is met for an angular momentum lying outside any principal plane of the inertia ellipsoid which is a prerequisite of a chiral motion.

The wobbling frequencies are determined by Eqs.(4.5), (4.9) and (4.13).Our calculations indicate that for the situation when the axis-1 is the quantization axis the system exhibits a minimum around which the system oscillates with a frequency equal to 0.245 MeV, while for axis-2 and axis-3 the system oscillates around the true minima with the frequency of 0.205 MeV and 0.065 MeV, respectively.

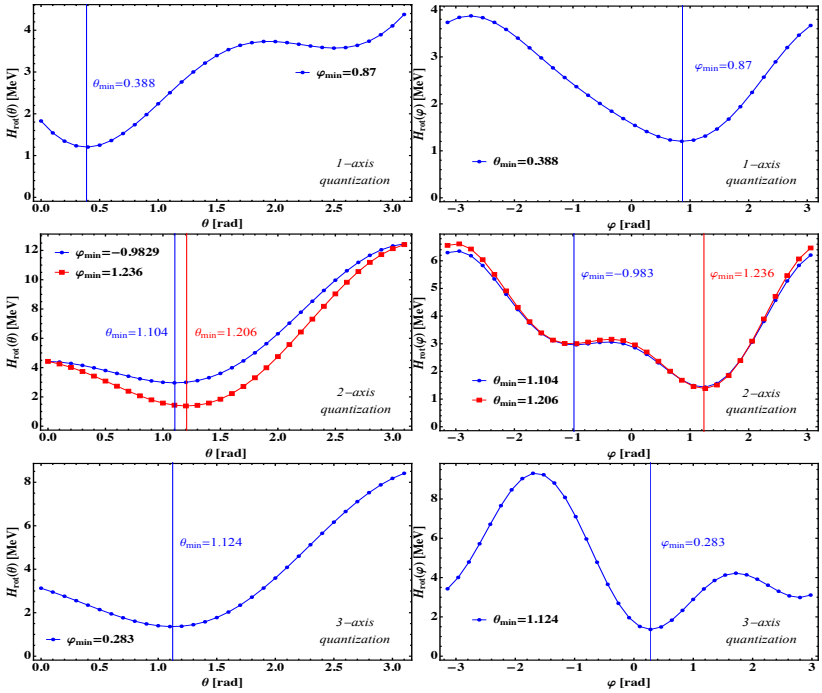

FIG. 5: (Color online).The classical energy function H_{rot} as function of the angle φ when θ is fixed at its minimum value as well as of function of θ for φ taken in its minimal value. These plots are made for three distinct situations, namely when the quantization axis is axix-1 (first row), axis-2 (second row) and axis-3 (third row), respectively.

The transformed Hamiltonian H^{ch}_{rot} has the contour plots graphically represented in Figs. 6, 7 and 8 for the quantization axes 1, 2 and 3 respectively, with the minima coordinates collected in Table II. Fixing one coordinate in its minimal value, H^{ch}_{rot} becomes a function of a single variable which exhibits several stationary points. These are plotted in Fig. 9. From there one can see that there are situations when beside the main minimum the system exhibits several local minima.

The wobbling frequencies corresponding to the deepest minima when the quantization axis is the axis 1, 2 and 3 respectively, have the values:0.245, 0.209, 0.210 MeV, respectively. One notes that when axis-1 is the quantization axis, the Hamiltonians H_{rot} and H^{ch}_{rot} have the same wobbling frequencies, while for axis-2 as quantization axis the wobbling frequencies are very close to each other. Moreover the two Hamiltonians have the same/almost the same values in the respective minima. This is a reflection of the fact that for the two cases the chiral invariant part of H_{rot} prevails over the non-invariant part. Consequently, for the cases when the quantization axis is the axis-1 or 2, one can build up two wobbling bands with a similar structure which results in having a twin pair of bands.

quantization axis	θ_{min}	φ_{min}	$I_1[\hbar]$	$I_2[\hbar]$	$I_3[\hbar]$	$H^{ch}_{rot,min}[MeV]$
axis-1	2.753	- 2.27	- 16.198	- 4.269	- 5.063	1.202
axis-1	2.894	3.141	- 16.965	- 4.293	≈0.0	1.478
axis-2	1.935	- 1.905	- 15.443	- 6.238	- 5.370	1.381
axis-2	2.148	3.141	≈ 0	- 9.553	- 14.662	2.873
axis-3	2.018	- 2.859	- 15.152	- 4.403	- 7.568	1.361
axis-3	2.021	3.142	- 15.754	≈ 0	- 7.620	1.719

TABLE II: Coordinates of the minima points for the chirally transformed Hamiltonian, H^{ch}_{rot}, and the corresponding values of the spin components

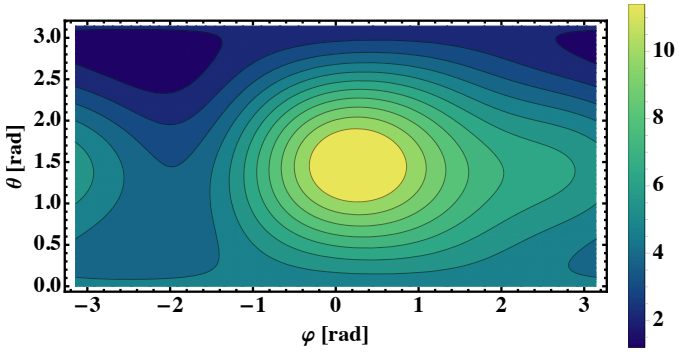

FIG. 6: (Color online) Contour plot when the axis-1 is the quantization axis. The energy function is H^{ch}_{rot}, the chiral image of the classical energy given by Eq. (2.2).

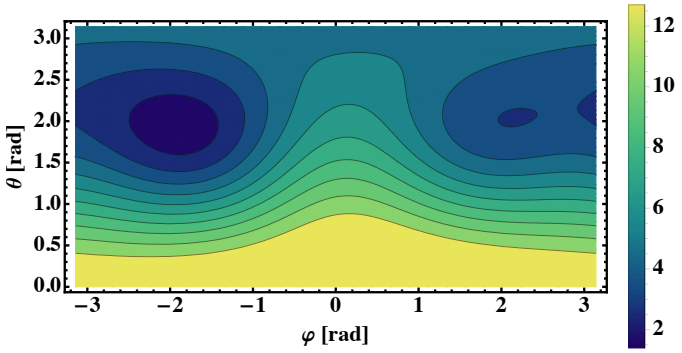

FIG. 7: (Color online) Contour plot when the axis-2 is the quantization axis. The energy function is H^{ch}_{rot}, the chiral image of of the classical energy given by Eq. (2.2).

Note that contrary to the previous publications, where the odd nucleon was rigidly fixed either to an axis [26] or to a principal plane [25] of the inertia ellipsoid, here the rigid coupling is achieved to a direction which does not belong to a principal plane. In this way one conciliates between the two signatures of triaxial nuclei, these being simultaneously considered.

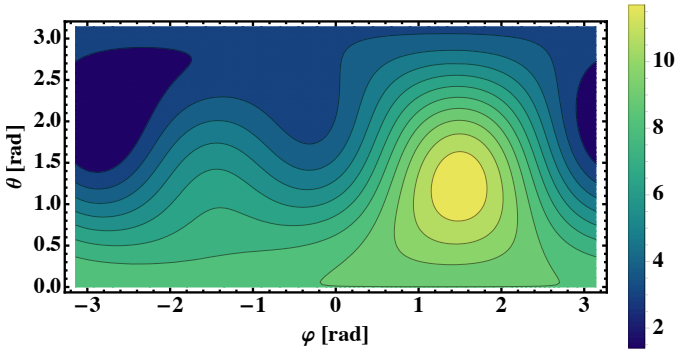

FIG. 8: (Color online) Contour plot when the axis-3 is the quantization axis. The energy function is H^{ch}_{rot}, the chiral image of of the classical energy given by Eq. (2.2).

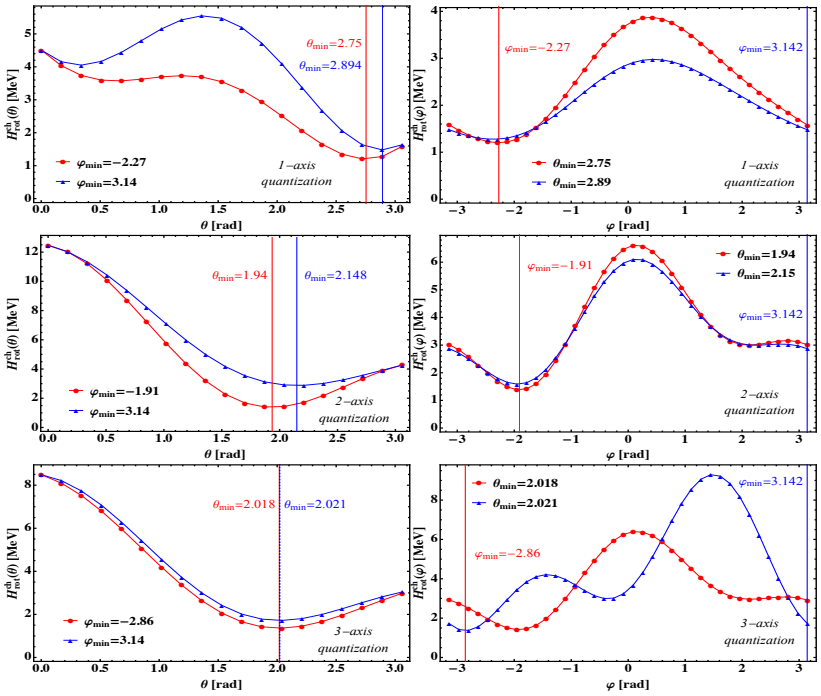

FIG. 9: (Color online).The classical energy function H^{ch}_{rot} as function of the angle φ when θ is fixed at its minimum value as well as of function of theta for φ taken in its minimal value. These plots are made for three distinct situations, namely when the quantization axis is axix-1 (first row), axis-2 (second row) and axis-3 (third row), respectively.

VI. CONCLUSIONS

In the previous section we developed a classical interpretation of the wobbling motion of an even-odd system described by a particle-triaxial rigid core coupling. The odd particle is rigidly coupled to the deformation and the total angular momentum such that its angular momentum lays outside any principal plane of the inertia ellipsoid. Equations of motion for the angular momentum components are studied both in the space of angular momenta and in the reduced space of the generalized phase space coordinates. By a quadratic expansion of the classical energy function around a stationary point one finds the analytical expression of the wobbling frequency. The same procedure was applied also for the chirally transformed Hamiltonian. Formalism was applied to an illustrative example. One found out that there exist minimum points for the energy function where the model Hamiltonian and its chiral image admit real wobbling frequencies.Extending the calculations to a set of total angular momenta one certainly obtains a pair of chiral twin doublet band with similar properties. Concluding, this work provides an inedited picture of triaxial nuclei,

by being able to potentially unify two signatures in a consistent manner. Moreover the semi-classical treatment of the problem is indeed a remarking for the proposed model. To our knowledge, there are no other approaches within the literature that aim at describing both phenomena simultaneously. Nevertheless, new experimental data is necessary for testing grounds.

Acknowledgment. This work was supported by the Romanian Ministry of Research and Innovation through the project PN19060101/2019

VII. APPENDIX A

The solutions for Eq.(3.4) are given by the Cardano formulas:

$$\begin{aligned}\omega_1 &= s_1+s_2,\\ \omega_2 &= -\frac{1}{2}(s_1+s_2)+\frac{i\sqrt{3}}{2}(s_1-s_2),\\ \omega_3 &= -\frac{1}{2}(s_1+s_2)-\frac{i\sqrt{3}}{2}(s_1-s_2).\end{aligned} \tag{A.1}$$

where the following notations have been used:

$$\begin{aligned}s_1 &= \left(T+(T^2+S^3)^{1/2}\right)^{1/3},\\ s_2 &= \left(T-(T^2+S^3)^{1/2}\right)^{1/3}.\end{aligned} \tag{A.2}$$

If $T^2+S^3>0$,at least one solution is real. If $T^2+S^3<0$ all solutions are imaginary, while if $T^2+S^3=0$ solutions are real and at least two are equal.

[1] A.S. Davydov and G.F. Filippov, Nucl. Phys. **8** (1958) 788.
[2] J. Meyer-ter-Vehn, F. S. Stephens and R.M. Diamond, Phys. Rev. Lett. **32** (1974)1383; J. Meyer-ter-Vehn, Nucl. Phys. **A249** (1975) 111, 141.
[3] L. Wilets and M. Jean, Phys. Rev. **102**, (1956)788.
[4] E. R. Marshalek, Nucl. Phys. **A 331** (1979) 429.
[5] St. Frauendorf, Rev. Mod. Phys., vol. **73**, (2001)463.
[6] D. Bonatsos *et al.* Phys. Lett. **B 584** (2004) 40.
[7] D. Bonatsos, D. Lenis, D. Petrellis and P. A. Terziev, Phys. Lett. **B 588**,(2004)172.
[8] D. Bonatsos, D. Lenis, D. Petrellis, P. A. Terziev and I. Yigitoglu, Phys. Lett. **B 621** (2005) 102.
[9] A. Bohr and B. Mottelson, *Nuclear Structure* (Benjamin, Reading, MA, 1975), Vol. II, Ch. 4.
[10] A. A. Raduta, Progress in Particle and Nuclear Physics 90 (2016) 241.
[11] C. M. Petrache *et al.,* Nucl. Phys. **A597** (1996) 106.
[12] C. M. Petrache, *et al.*, Phys. Rev. Lett. **96** (2006) 112502.
[13] S. Frauendorf and J. Meng, Nucl. Phys. **A 617** (1997) 131.
[14] S. Frauendorf and F. Donau, Phys. Rev. C**89**(2014) 014322.
[15] I. Hamamoto, Phys. Rev. **C 65** (2002) 044305.
[16] I. Hamamoto and G. B. Hagemann, Phys. Rev. **C 67** (2003) 014319.
[17] K. Tanabe and K. Sugawara Tanabe, Phys. Rev. C **95** (2017) 064315.
[18] S. Frauendorf, Phys. Rev. **C97**(2018) 069801.
[19] K. Tanabe and K. Sugawara Tanabe, Phys. Rev. C **97**,(2018) 069802 .
[20] A. A. Raduta, R. Budaca and C. M. Raduta, Phys. Rev. **C 76**, (2007) 064309.
[21] A. A. Raduta, R. Poenaru and L. Gr. Ixaru, Phys. Rev. C **96**,(2017) 054320.
[22] A. A. Raduta, R. Poenaru and Al. H. Raduta, J. Phys. G: Nucl. Part. Phys. **45**,(2018) 105104 .
[23] A. A. Raduta, R Poenaru and C M Raduta, J. Phys. G: Nucl. Part. Phys. **47**,(2020) 025101 .
[24] A. A. Raduta, R Poenaru and C M Raduta, Phys. Rev. C **101**,(2020)014302 .
[25] A.A.Raduta, C.M. Raduta, and R. Poenaru,J. Phys. G: Nucl. Part. Phys. **48**, (2020) 015106.
[26] R. Budaca, Phys. Rev. C **97** (2018) 024302.
[27] A.C. Davydov, *Teoria atomnova yadra*, Moscva, 1958 (in russian), chapters 19,20.
[28] P. Ring and P. Schuck,*The Nuclear Many Body Problem* Springer-Verlag, Berlin, Heidelberg 2000, p.110
[29] H. Frisk and R. Bengston, Phys. Lett. **196 B** (1987) 14.

Double-β transition $0^+ \rightarrow 2^+$ within a fully renormalized proton-neutron quasiparticle random-phase approximation with the gauge symmetry restored

A. A. Raduta,[1,2] C. M. Raduta,[1] and R. Poenaru[1,3]

[1]*Department of Theoretical Physics, Institute of Physics and Nuclear Engineering, P.O. Box MG6, Bucharest 077125, Romania*
[2]*Academy of Romanian Scientists, 54 Splaiul Independentei, Bucharest 050094, Romania*
[3]*Doctoral School of Physics, University of Bucharest, Bucharest 050663, Romania*

(Received 28 May 2022; accepted 14 September 2022; published 4 October 2022)

The $2\nu\beta\beta$ decay from the ground to the first excited 2^+ state is considered for eight nuclei where experimental data are available. The transition amplitude is calculated with a projected spherical single-particle basis, a fully renormalized proton-neutron quasiparticle random-phase approximation (pnQRPA) for the Gamow-Teller (GT) dipole transition operator and a renormalized QRPA for charge conserving quadrupole operators. Also for the transition operator the first-order boson expansion expression is employed. Using the phase space integral corresponding to the transition $0^+ \rightarrow 2^+$ and the GT transition amplitude, the process half-life is readily obtained. The single-$\beta^{\mp}$ transition strengths are studied as function of the energies of the fully renormalized pnQRPA with the gauge symmetry restored. The single-β transition operators are used to calculate the $\log_{10} ft$ values for the electron capture of the intermediate odd-odd nucleus to the mother nucleus as well as for the β^- transition to the daughter nucleus. For the final state in the daughter nucleus the $B(E2)$ values for the transition $2^+ \rightarrow 0^+$ and the half-life of the electromagnetic decaying state are calculated. The Ikeda sum rule for the mother nucleus is satisfied. The mentioned results are compared with the corresponding available data and a reasonable agreement is shown. The gauge projection quenches the half-life in the case of ^{150}Nd, ^{116}Cd, and ^{100}Mo and enhances it for the remaining considered nuclei. Keeping the same parameters for the model Hamiltonian the ground to ground double-β transition is also treated and a good agreement with the existing data is obtained.

DOI: 10.1103/PhysRevC.106.044301

I. INTRODUCTION

One of the hot subjects of nuclear physics concerns double-β decay. The process may take place through two modes, neutrinoless double β ($0\nu\beta\beta$) and double β with two neutrinos in the final state ($2\nu\beta\beta$). The first mode is most interesting since its existence decides whether a neutrino is a Dirac or a Majorana particle. However, there is no direct reliable test for the matrix elements which are used for the $0\nu\beta\beta$ process.

The $2\nu\beta\beta$ decay is interesting on its own but is also very attractive since it provides a test for some matrix elements which are used for the process of $0\nu\beta\beta$. The history of the subject was outlined in several review papers [1–11]. The formalism which yields closest results to the experimental data is the proton-neutron quasiparticle random-phase approximation (pnQRPA) involving particle-hole (ph) and particle-particle (pp) as independent interactions. This is caused by the fact that the second leg of the decay matrix element is very sensitive to changing the relative strength of the pp interaction. Since the pp interaction is attractive, increasing its strength results in the transition amplitude decreasing and consequently one reaches a critical value where the first root of the pnQRPA becomes imaginary. In the decreasing interval one also meets the value which corresponds to the experimental data. Unfortunately this value lies close to the critical value where the ground state is unstable. To stabilize the ground state we have to go beyond the pnQRPA approach, which was achieved either by the boson expansion method [12,13] applied to the Gamow-Teller (GT) transition operator or by renormalizing the pnQRPA equation [14]. Later on, the renormalization procedure was improved by adding the scattering terms [15]. The drawback of the higher pnQRPA formalisms is that the Ikeda sum rule is violated. Restoring the sum rule is a challenge for any description of the process. It is worth mentioning that at the pnQRPA level the transition from the ground to the excited 2^+ state is forbidden. However, going beyond the pnQRPA, such a process is allowed. Moreover, there are experimental data concerning the low bounds of the half-life of the transition. A large volume of work has been devoted to the description of the relevant properties for the double-β transition $0^+ \rightarrow 2^+$ [11,16–31].

It is commonly accepted that double-β decay takes place via two successive virtual β^- decays. It is a natural question whether by replacing the β^- with β^+ the resulting process exists or not. A possible answer was attempted in Ref. [32]. This subject was *in extenso* treated in a review paper [33] about neutrinoless double electron capture. It was shown that the process exhibits a resonance when the initial and final states are degenerate.

In the present paper we study the double-β decay on the first excited 2^+ state within a formalism of fully renormalized pnQRPA with the gauge symmetry restored (GRFRpnQRPA).

It is well established that any symmetry is associated with the conservation of a certain physical quantity. In the present context the gauge symmetry determines the conservation of the total number of nucleons. The mentioned symmetry reflects the system invariance to rotations around the z axis in the space of quasispin [34]. This is different from the gauge symmetry for electromagnetic interaction where the charge is conserved whenever a U(1) transformation (a phase factor) is performed. Note that although both the third isospin component, T_3, and the nuclear charge, Q, are not preserved in the double-β process, the total number of nucleons, $N+Z=2(-T_3+Q/e)$, is conserved.

One important ingredient of our approach is the use of the projected spherical single-particle basis whose main properties are briefly described in Sec. II. The many-body Hamiltonian which describes the ground to 2^+ transitions is introduced in Sec. III. In Sec. IV one describes the fully renormalized pnQRPA, while the gauge symmetry is projected out in Sec. V. The amplitude of the GT transition is considered in Sec. VI and the numerical calculations are presented in Sec. VII. The summary and final conclusions are given in Sec. VIII.

II. PROJECTED SINGLE-PARTICLE BASIS

The angular momentum projected single-particle basis, defined in Ref. [35], seems to be suitable for the description of the single-particle motion in a deformed mean field generated by the particle-core interaction. Such a projected spherical single-particle basis has been used to study the collective $M1$ states in deformed nuclei [35–37] as well as the rate of the double-β process [38–41].

Other groups also used various deformed single-particle bases corresponding to specific deformed mean field potentials, like the SU(3), Nilsson, Skyrme interaction, or Woods-Saxon potential, to evaluate the double-β decay rate [42–51].

To fix the necessary notations and moreover for the sake of a self-contained presentation, we describe briefly the main ideas underlying the construction of the projected single-particle basis.

The single-particle mean field is determined by a particle-core Hamiltonian:

$$\tilde{H}=H_{sm}+H_{\rm core}-M\omega_0^2r^2\sum_{\lambda=0,2}\sum_{-\lambda\leqslant\mu\leqslant\lambda}\alpha^*_{\lambda\mu}Y_{\lambda\mu}, \tag{2.1}$$

where H_{sm} denotes the spherical shell model Hamiltonian, while $H_{\rm core}$ is a harmonic quadrupole boson (b^+_μ) Hamiltonian associated to a phenomenological core. The interaction of the two subsystems is accounted for by the third term of the above equation, written in terms of the shape coordinates $\alpha_{00},\alpha_{2\mu}$. The quadrupole coordinates are related to the quadrupole boson operators by the canonical transformation:

$$\alpha_{2\mu}=\frac{1}{k\sqrt{2}}(b^\dagger_{2\mu}+(-)^\mu b_{2,-\mu}), \tag{2.2}$$

where k is an arbitrary C number. The monopole shape coordinate is to be determined from the volume conservation condition.

Averaging $\tilde{H}$ on a given eigenstate of H_{sm}, denoted as usual by $|nljm\rangle$, one obtains a deformed quadrupole boson Hamiltonian which admits the axially symmetric coherent state

$$\Psi_g=\exp[d(b^+_{20}-b_{20})]|0\rangle_b \tag{2.3}$$

as eigenstate. $|0\rangle_b$ stands for the vacuum state of the boson operators while d is a real parameter which simulates the nuclear deformation. However, averaging $\tilde{H}$ on Ψ_g, one obtains a single-particle mean field operator for the single-particle motion, similar to the Nilsson Hamiltonian. Concluding, by averaging the particle-core Hamiltonian with a factor state the rotational symmetry is broken and the mean field mentioned above may generate, by diagonalization, a deformed basis for treating the many-body interacting systems. However, this standard procedure is tedious since the final many-body states should be projected over the angular momentum.

Our procedure defines first a spherical basis for the particle-core system, by projecting out the angular momentum from the deformed state:

$$\Psi^{pc}_{nlj}=|nljm\rangle\Psi_g. \tag{2.4}$$

The projected states are obtained, in the usual manner, by acting on these deformed states with the projection operator

$$P^I_{MK}=\frac{2I+1}{8\pi^2}\int D^{I}_{MK}{}^*(\Omega)\hat{R}(\Omega)d\Omega. \tag{2.5}$$

We consider the subset of projected states

$$\Phi^{IM}_{nlj}(d)=\mathcal{N}^I_{nlj}P^I_{MI}[|nljI\rangle\Psi_g]\equiv\mathcal{N}^I_{nlj}\Psi^{IM}_{nlj}(d), \tag{2.6}$$

which are orthonormalized and form a basis for the particle-core system. This basis exhibits useful properties which have been presented in some of our previous publications.

To the projected spherical states, one associates the "deformed" single-particle energies defined as the average values of the particle-core Hamiltonian $H'=\tilde{H}-H_{\rm core}$:

$$\epsilon^I_{nlj}=\langle\Phi^{IM}_{nlj}(d)|H'|\Phi^{IM}_{nlj}(d)\rangle. \tag{2.7}$$

Since the core contribution to this average value does not depend on the quantum numbers of the single-particle energy levels, it produces a constant shift for all energies. For this reason such a term is omitted in Eq. (2.7). The deformation dependence of the new single-particle energies is similar to that shown by the Nilsson model [52]. Therefore, the average values ϵ^I_{nlj} may be viewed as approximate single-particle energies in deformed Nilsson orbits [52]. We may account for the deviations from the exact eigenvalues by considering, at a later stage when a specific treatment of the many-body system is performed, the exact matrix elements of the two-body interaction. The dependence of single-particle energies on deformation parameter d is shown in Fig. 1 for protons and neutrons, respectively, in the major shell with $N=5$ and $N=6$.

Although the energy levels are similar to those of the Nilsson model, the quantum numbers in the two schemes are different. Indeed, here we generate from each j a multiplet of $(2j+1)$ states distinguished by the quantum number I, which plays the role of the Nilsson quantum number Ω and runs from $1/2$ to j. Moreover, the energies corresponding to the quantum

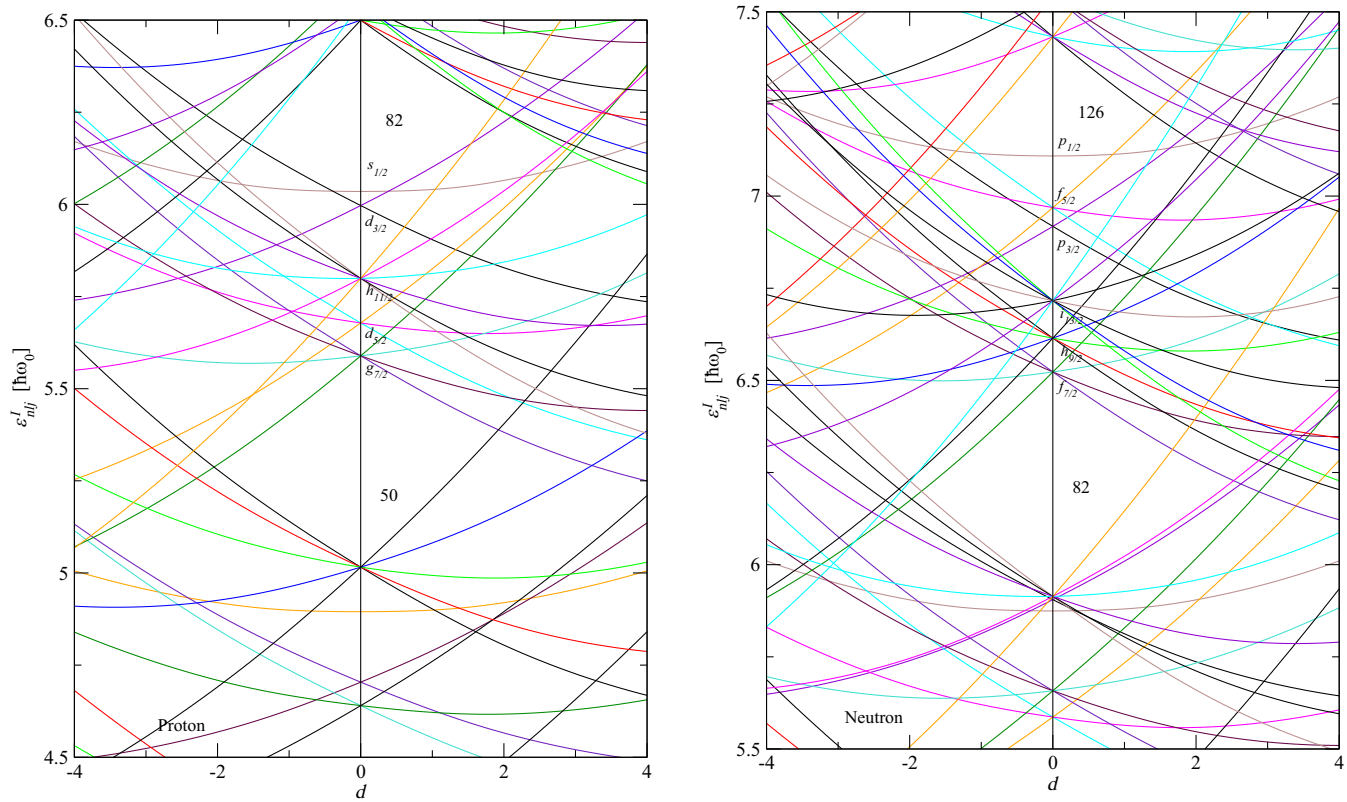

FIG. 1. Proton and neutron single-particle energies in the region of $N = 5$ and $N = 6$ shells, respectively, given by Eq. (2.7) where the shell model parameters $\kappa = 0.0637$ and $\mu = 0.60$ for protons and $\mu = 0.42$ for neutrons were used. The canonical transformation constant is fixed to $k = 10$.

numbers K and $-K$ are equal to each other. However, for a given I there are $2I + 1$ degenerate substates, while the Nilsson states are only double degenerate. As explained in Ref. [15], the redundancy problem can be solved by changing the normalization of the model functions:

$$\left\langle \Phi^{IM}_{\alpha} \middle| \Phi^{IM}_{\alpha} \right\rangle = 1 \Longrightarrow \sum_{M} \left\langle \Phi^{IM}_{\alpha} \middle| \Phi^{IM}_{\alpha} \right\rangle = 2. \tag{2.8}$$

Due to this weighting factor the particle density function is providing the consistency result that the number of particles which can be distributed on the $(2I + 1)$ substates is at most 2, which agrees with the Nilsson model. Here α stands for the set of shell model quantum numbers nlj. Due to this normalization, the states Φ^{IM}_{α} used to calculate the matrix elements of a given operator should be multiplied with the weighting factor $\sqrt{2/(2I + 1)}$.

The projected states might be thought of as eigenstates of an effective rotational invariant fermionic one-body Hamiltonian H_{eff}, with the corresponding energies given by Eq. (2.7):

$$H_{\text{eff}} \Phi^{IM}_{\alpha} = \epsilon^I_{\alpha}(d) \Phi^{IM}_{\alpha}. \tag{2.9}$$

As shown in Ref. [35] in the vibrational limit, $d \to 0$, the projected spherical basis goes to the spherical shell model basis and ϵ^I_{nlj} to the eigenvalues of H_{sm}.

A fundamental result obtained in Ref. [53] for the product of two single-particle states, which comprises a product of two core components, deserves to be mentioned. Therein, we have proved that the matrix elements of a two-body interaction corresponding to the present scheme are very close to the matrix elements corresponding to spherical states projected from a deformed product state with one factor being a product of two spherical single-particle states, and a second factor consisting of a unique collective core wave function. The small discrepancies of the two types of matrix elements could be washed out by using slightly different strengths for the two-body interaction in the two methods. Due to this property the basis (2.6) might be used for studying any two-body interaction.

As for the matrix elements of a one-body operator T^k_{μ}, the result is

$$\begin{aligned} \left\langle \Phi^{I}_{nlj} \middle|\middle| T^k \middle|\middle| \Phi^{I'}_{n'l'j'} \right\rangle &= f^{n'l'j'I'}_{nljI}(d) \langle nlj||T^k||n'l'j' \rangle, \quad \text{with} \\ f^{n'l'j'I'}_{nljI}(d) &= \mathcal{N}^{I}_{nlj}(d) \mathcal{N}^{I'}_{n'l'j'}(d) \hat{j}\hat{I}' \\ &\quad \times \sum_{J} C^{j\,J\,I}_{I\,0\,I} C^{j'\,J\,I'}_{I'\,0\,I'} W(jkJI'; j'I) \left(N^g_J\right)^{-2}. \end{aligned} \tag{2.10}$$

This expression is used to calculate the reduced matrix elements of the Gamow-Teller interaction as well as of the quadrupole interaction. $\mathcal{N}^{I}_{nlj}(d)$ denotes the norm of the projected spherical single-particle state, while N^g_J is the norm of the core projected state. Also, the Rose convention is used for the reduced matrix elements [54].

III. THE MODEL HAMILTONIAN

We suppose that the states describing the nuclei involved in a $2\nu\beta\beta$ process are described by a many-body Hamiltonian which may be written in the projected spherical basis as

$$\begin{aligned} H = & \sum_{\tau,\alpha,I,M} \frac{2}{2I+1}(\epsilon_{\tau\alpha I} - \lambda_{\tau\alpha}) c^{\dagger}_{\tau\alpha IM} c_{\tau\alpha IM} \\ & - \sum_{\tau,\alpha,I,I'} \frac{G_{\tau}}{4} P^{\dagger}_{\tau\alpha I} P_{\tau\alpha I'} \\ & + 2\chi \sum_{pn;p'n';\mu} \beta^{-}_{\mu}(pn)\beta^{+}_{-\mu}(p'n')(-)^{\mu} - 2\chi_1 \\ & \times \sum_{pn;p'n';\mu} P^{-}_{\mu}(pn) P^{+}_{-\mu}(p'n')(-)^{\mu} \\ & - \sum_{\mu,\tau} X_{\tau,\tau'} Q^{\tau}_{\mu} Q^{\tau'}_{-\mu'}(-)^{\mu}, \end{aligned} \tag{3.1}$$

where $c^{\dagger}_{\tau\alpha IM}$ ($c_{\tau\alpha IM}$) denotes the creation (annihilation) operator of one nucleon of the type $\tau(=p,n)$ in the state Φ^{IM}_{α}, with α being an abbreviation for the set of quantum numbers nlj. The Hamiltonian H contains the mean field term, the pairing interaction for alike nucleons and the Gamow-Teller dipole-dipole interaction in the ph and pp channels, characterized by the strengths χ and χ_1, respectively, and the quadrupole-quadrupole interaction.

To simplify the notations, hereafter the set of quantum numbers $\alpha(=nlj)$ will be omitted. All the two-body interactions are separable with the factors defined by the following expressions:

$$\begin{aligned} P^{\dagger}_{\tau I} &= \sum_{M} \frac{2}{2I+1} c^{\dagger}_{\tau IM} c^{\dagger}_{\tau\widetilde{IM}}, \\ \beta^{-}_{\mu}(pn) &= \sum_{M,M'} \frac{\sqrt{2}}{\hat{I}} \langle pIM|\sigma_{\mu}|nI'M'\rangle \frac{\sqrt{2}}{\hat{I}'} c^{\dagger}_{pIM} c_{nI'M'}, \\ P^{-}_{1\mu}(pn) &= \sum_{M,M'} \frac{\sqrt{2}}{\hat{I}} \langle pIM|\sigma_{\mu}|nI'M'\rangle \frac{\sqrt{2}}{\hat{I}'} c^{\dagger}_{pIM} c^{\dagger}_{\widetilde{nI'M'}}, \\ Q^{\tau}_{\mu} &= \sum_{M,M'} \frac{\sqrt{2}}{\hat{I}} \langle \tau IM|\sqrt{\frac{16\pi}{5}} r^2 Y_{2_{\mu}}|\tau I'M'\rangle \frac{\sqrt{2}}{\hat{I}'}. \end{aligned} \tag{3.2}$$

The remaining operators from Eq. (3.1) can be obtained from the above-defined operators, by Hermitian conjugation.

Passing to the quasiparticle representation through the Bogoliubov-Valatin transformation,

$$\begin{aligned} a^{\dagger}_{\tau IM} &= U_{\tau I} c^{\dagger}_{\tau IM} - s_{IM} V_{\tau I} c_{\tau I-M}, \quad s_{IM} = (-)^{I-M}, \\ \tau &= p,n, \quad U^2_{\tau I} + V^2_{\tau I} = 1, \end{aligned} \tag{3.3}$$

the first two terms of H are replaced by the independent quasiparticle term, $\sum E_{\tau I} a^{\dagger}_{\tau IM} a_{\tau IM}$, while the ph and pp interactions are expressed in terms of the dipole two quasiparticle (qp) and the qp density operators:

$$\begin{aligned} A^{\dagger}_{1\mu}(pn) &= \sum C^{I_p\, I_n\, 1}_{m_p\, m_n\, \mu} a^{\dagger}_{pI_pm_p} a^{\dagger}_{nI_nm_n}, \\ A_{1\mu}(pn) &= (A^{\dagger}_{1\mu}(pn))^{\dagger}, \\ B^{\dagger}_{1\mu}(pn) &= \sum C^{I_p\, I_n\, 1}_{m_p\, -m_n\, \mu} a^{\dagger}_{pj_pm_p} a_{nI_nm_n}(-)^{I_n-m_n}, \\ B_{1\mu}(pn) &= (B^{\dagger}_{1\mu}(pn))^{\dagger}, \\ A^{\dagger}_{2\mu}(\tau\tau') &= \sum C^{I_{\tau}\, I_{\tau'}\, 2}_{m_{\tau}\, m_{\tau'}\, \mu} a^{\dagger}_{\tau I_{\tau}m_{\tau'}} a^{\dagger}_{\tau' I_{\tau'}m_{\tau'}}, \\ A_{2\mu}(\tau\tau') &= (A^{\dagger}_{2\mu}(\tau\tau'))^{\dagger}, \\ B^{\dagger}_{2\mu}(\tau\tau') &= \sum C^{I_{\tau}\, I_{\tau'}\, 2}_{m_{\tau}\, -m_{\tau'}\, \mu} a^{\dagger}_{\tau j_{\tau}m_{\tau}} a_{\tau' I_{\tau'}m_{\tau'}}(-)^{I_{\tau'}-m_{\tau'}}, \\ B_{2\mu}(\tau\tau') &= (B^{\dagger}_{2\mu}(\tau\tau'))^{\dagger}. \end{aligned} \tag{3.4}$$

IV. THE FULLY RENORMALIZED pnQRPA

A. The case of the proton-neutron interaction

In Ref. [15], we showed that all these operators can be renormalized as suggested by the commutation equations:

$$\begin{aligned} &[A_{1\mu}(k), A^{\dagger}_{1\mu'}(k')] \approx \delta_{k,k'}\delta_{\mu,\mu'}\left[1 - \frac{\hat{N}_n}{\hat{I}^2_n} - \frac{\hat{N}_p}{\hat{I}^2_p}\right], \\ &[B^{\dagger}_{1\mu}(k), A^{\dagger}_{1\mu'}(k')] \approx [B^{\dagger}_{1\mu}(k), A_{1\mu'}(k')] \approx 0, \\ &[B_{1\mu}(k), B^{\dagger}_{1\mu'}(k')] \approx \delta_{k,k'}\delta_{\mu,\mu'}\left[\frac{\hat{N}_n}{\hat{I}^2_n} - \frac{\hat{N}_p}{\hat{I}^2_p}\right], \ k = (I_p, I_n). \end{aligned} \tag{4.1}$$

Indeed, denoting by $C^{(1)}_{I_p,I_n}$ and $C^{(2)}_{I_p,I_n}$ the averages of the right-hand sides of Eqs. (4.1) with the renormalized random-phase approximation (RPA) vacuum state, the renormalized operators defined as

$$\bar{A}_{1\mu}(k) = \frac{1}{\sqrt{C^{(1)}_k}} A_{1\mu}, \quad \bar{B}_{1\mu}(k) = \frac{1}{\sqrt{|C^{(2)}_k|}} B_{1\mu}, \tag{4.2}$$

obey bosonlike commutation relations:

$$\begin{aligned} &[\bar{A}_{1\mu}(k), \bar{A}^{\dagger}_{1\mu'}(k')] = \delta_{k,k'}\delta_{\mu,\mu'}, \\ &[\bar{B}_{1\mu}(k), \bar{B}^{\dagger}_{1\mu'}(k')] = \delta_{k,k'}\delta_{\mu,\mu'} f_k, \quad f_k = \mathrm{sign}\big(C^{(2)}_k\big). \end{aligned} \tag{4.3}$$

Further, these operators are used to define the phonon operator:

$$\begin{aligned} C^{\dagger}_{1\mu} = \sum_{k} & [X_1(k)\bar{A}^{\dagger}_{1\mu}(k) + Z_1(k)\bar{D}^{\dagger}_{1\mu}(k) - Y_1(k) \\ & \times \bar{A}_{1-\mu}(k)(-)^{1-\mu} - W_1(k)\bar{D}_{1-\mu}(k)(-)^{1-\mu}], \end{aligned} \tag{4.4}$$

where $\bar{D}^{\dagger}_{1\mu}(k)$ is equal to $\bar{B}^{\dagger}_{1\mu'}(k')$ or $\bar{B}_{1\mu}(k)$ depending on whether f_k is $+$ or $-$. The phonon amplitudes are determined by the equations

$$[H, C^{\dagger}_{1\mu}] = \omega C^{\dagger}_{1\mu}, \quad [C_{1\mu}, C^{\dagger}_{1\mu'}] = \delta_{\mu\mu'}. \tag{4.5}$$

Interesting properties for these equations and their solutions are discussed in our previous publications [15]. The renormalized pnQRPA (pnRQRPA) vacuum describes the ground

state of the parent nucleus, while the excited one phonon states describe the dipole states of the intermedite odd-odd nucleus.

B. The case of the quadrupole-quadrupole (QQ) interaction

For the charge preserving operators we can apply similar considerations. Indeed, the commutators of the quadrupole two-quasiparticle and quadrupole quasiparticle density operators may be approximated as

$$\begin{aligned}
&[A_{2\mu}(\tau,a,b),A^\dagger_{2\mu'}(\tau',a',b')]\\
&\quad\approx \delta_{\tau,\tau'}\delta_{a,a'}\delta b,b'\delta_{\mu,\mu'}\left[1-\frac{\hat N_a}{\hat I_a^2}-\frac{\hat N_b}{\hat I_b^2}\right],\\
&[B^\dagger_{2\mu}(\tau,a,b),A^\dagger_{2\mu'}(\tau',a',b')]\\
&\quad\approx [B^\dagger_{1\mu}(\tau,a,b),A_{2\mu'}(\tau',a',b')]\\
&\quad\approx [B_{2\mu}(\tau,a,b),B^\dagger_{2\mu'}(\tau',a',b')]\approx 0. \qquad (4.6)
\end{aligned}$$

Note that in contradistinction to the case of the *pn* interaction the quadrupole scattering operators are not normalizable to unity. As for the two quasiparticle operators, denoting by F_2 the average of the approximated commutators with the quadrupole boson vacuum,

$$F_2 = {}_2\langle 0|\left[1-\frac{\hat N_a}{\hat I_a^2}-\frac{\hat N_b}{\hat I_b^2}\right]|0\rangle_2, \qquad (4.7)$$

one obtains the normalized to unity boson operator:

$$\bar A_{2\mu}(\tau,a,b)=\frac{1}{\sqrt{F_2}}A_{2\mu}(\tau,a,b). \qquad (4.8)$$

Indeed it is conspicuous that

$$[\bar A_{2\mu}(\tau,a,b),\bar A^\dagger_{2\mu}(\tau',a',b')]=\delta_{\tau,\tau'}\delta_{a,a'}\delta_{b,b'}. \qquad (4.9)$$

Therefore, we can define the quadrupole phonon operator:

$$\begin{aligned}
C^\dagger_{2\mu}=\sum[&X_2(\tau,a,b)\bar A^\dagger_{2\mu}(\tau,a,b)\\
&-Y_2(\tau,a,b)\bar A_{2,-\mu}(\tau,a,b)(-)^\mu], \qquad (4.10)
\end{aligned}$$

such that the following two equations are fulfilled:

$$[H,C^\dagger_{2\mu}]=\omega_2 C^\dagger_{2\mu},\quad [C_{2\mu},C^\dagger_{2\mu'}]=\delta_{\mu\mu'}. \qquad (4.11)$$

The vacuum state $|0\rangle_2$ describes the ground state of the daughter nucleus, while the quadrupole phonon operator excites the daughter nucleus to a 2^+ state.

V. GAUGE PROJECTION OF THE FULLY RENORMALIZED pnQRPA EQUATIONS

The beautiful feature of the quasiparticle random-phase approximation (QRPA) formalism is that the so-called Ikeda sum rule (ISR) is exactly satisfied. The sum rule is considered a measure of how realistic is the approach which is used. Therefore, going beyond the QRPA we have to take care of the sum rule in order to get a consistent description. Unfortunately, the higher QRPA approaches violate the Ikeda sum rule. Indeed the sum rule is satisfied neither by the boson expansion procedure nor by the renormalization approach. However, in order to describe the double-β decay ground state to the first quadrupole phonon state we have to go beyond the QRPA level. It seems that renormalizing the QRPA equations underestimates the ISR, while the boson expansion overestimates it. This feature suggested use of the boson expansion on top of the renormalized pnQRPA state, i.e., that the Gamow-Teller transition operators be expanded in terms of the renormalized phonon operators. In this way the calculated ISR was brought close to the $N-Z$ value. We recall the fact that the pnQRPA which includes also the quasiparticle scattering terms is called the fully renormalized pnQRPA (FRpnQRPA) equation. The renormalized ground state, i.e., the vacuum state for the phonon operator defined by the FRpnQRPA approach, is a superposition of components describing the neighboring nuclei $(N-1,Z+1)$, $(N+1,Z-1)$, $(N+1,Z+1)$, $(N-1,Z-1)$. The first two components conserve the total number of nucleons $(N+Z)$ but violate the third component of isospin, T_3. By contrast, the last two components violate the total number of nucleons but preserve T_3. Actually, the last two components contribute to the violation of the ISR. One can construct linear combinations of the basic operators $A^\dagger, A, B^\dagger, B$ which excite the nucleus (N,Z) to the nuclei $(N-1,Z+1)$, $(N+1,Z-1)$, $(N+1,Z+1)$, $(N-1,Z-1)$, respectively. These operators are

$$\begin{aligned}
\mathcal{A}^\dagger_{1\mu}(pn)&=U_pV_nA^\dagger_{1\mu}(pn)+U_nV_pA_{1,-\mu}(pn)(-)^{1-\mu}\\
&\quad+U_pU_nB^\dagger_{1\mu}(pn)-V_pV_nB_{1,-\mu}(pn)(-)^{1-\mu}\\
&=-[c^\dagger_p c_{\tilde n}]_{1\mu},\\
\mathcal{A}_{1\mu}(pn)&=U_pV_nA_{1\mu}(pn)+U_nV_pA^\dagger_{1,-\mu}(pn)(-)^{1-\mu}\\
&\quad+U_pU_nB_{1\mu}(pn)-V_pV_nB^\dagger_{1,-\mu}(pn)(-)^{1-\mu}\\
&=-[c^\dagger_p c_{\tilde n}]^\dagger_{1\mu},\\
\mathbf{A}^\dagger_{1\mu}(pn)&=U_pU_nA^\dagger_{1\mu}(pn)-V_pV_nA_{1,-\mu}(pn)(-)^{1-\mu}\\
&\quad-U_pV_nB^\dagger_{1\mu}(pn)-V_pU_nB_{1,-\mu}(pn)(-)^{1-\mu}\\
&=[c^\dagger_p c^\dagger_n]_{1\mu},\\
\mathbf{A}_{1\mu}(pn)&=U_pU_nA_{1\mu}(pn)-V_pV_nA^\dagger_{1,-\mu}(pn)(-)^{1-\mu}\\
&\quad-U_pV_nB_{1\mu}(pn)-V_pU_nB^\dagger_{1,-\mu}(pn)(-)^{1-\mu}\\
&=[c^\dagger_p c^\dagger_n]^\dagger_{1\mu}.
\end{aligned}$$

Thus, the operators from the first two rows excite the nucleus (N,Z) to the nuclei $(N-1,Z+1)$ and $(N+1,Z-1)$, respectively, while the operators $\mathbf{A}^\dagger_{1\mu}(pn)$ and $\mathbf{A}_{1\mu}(pn)$ bring (N,Z) to $(N+1,Z+1)$ and $(N-1,Z-1)$, respectively. In the quasiparticle Hamiltonian we keep only the terms which preserve the total number of nucleons. Similarly, the quadrupole two-quasiparticle operators which conserve the total number of nucleons are

$$\begin{aligned}
\mathcal{A}^\dagger_{2\mu}(\tau,a,b)&=U_aU_bB^\dagger_{2\mu}(\tau,a,b)+U_aV_bA^\dagger_{2\mu}(\tau,a,b)\\
&\quad+V_aU_b(-)^\mu A_{2,-\mu}(\tau,a,b)\\
&\quad-V_aV_b(-)^\mu B_{2,-\mu}(\tau,a,b)\\
&=[c^\dagger_a c_{\tilde b}]_{2\mu}. \qquad (5.1)
\end{aligned}$$

Note that the particle-particle interaction violates the gauge and therefore is neglected. However, one knows that an attractive interaction is necessary in order to bring the transition amplitude close to the experimental value. For that reason we introduced an attractive two-body interaction which preserves the total number of nucleons:

$$\Delta H = -X_{dp}\sum_{\substack{pn;p'\\ n';\mu}}(\beta^-_\mu(pn)\beta^-_{-\mu}(p'n') + \beta^+_{-\mu}(p'n')\beta^+_\mu(pn))(-1)^{1-\mu}. \tag{5.2}$$

The picture for the quadrupole interaction is opposite. Indeed, the interaction is attractive and the minimal two quasiparticle energies in the gauge invariance picture become close to zero and therefore a repulsive interaction is needed. The simplest form for such an interaction is a diagonal one. With these details the final Hamiltonian to be used looks like

$$\begin{aligned} H = &\sum_{\tau jm} E_{\tau j} a^\dagger_{\tau jm} a_{\tau jm} \\ &+ 2\chi \sum_{pn,p'n';\mu} \sigma_{pn;p'n'} \mathcal{A}^\dagger_{1\mu}(pn)\mathcal{A}_{1\mu}(p'n') \\ &- X_{dp}\sum_{\substack{pn;p'\\ n';\mu}} \sigma_{pn;p'n'}(\mathcal{A}^\dagger_{1\mu}(pn)\mathcal{A}^\dagger_{1,-\mu}(p'n') \\ &+ \mathcal{A}_{1,-\mu}(p'n')\mathcal{A}_{1\mu}(pn))(-)^{1-\mu} \\ &- \sum X_{\tau,\tau'} q^{\tau,\tau'}(ik;i'k')\mathcal{A}^\dagger_{2\mu}(\tau;I_iI_k)\mathcal{A}_{2\mu}(\tau';I_{i'}I_{k'}) \\ &+ X_2 \sum \mathcal{A}^\dagger_{2\mu}(\tau;I_iI_k)\mathcal{A}_{2\mu}(\tau;I_iI_k), \end{aligned} \tag{5.3}$$

where the following abbreviations have been used:

$$\begin{aligned} \sigma_{pn;p'n'} &= \frac{2}{\sqrt{3}\hat{I}_n}\langle I_p||\sigma||I_n\rangle \frac{2}{\sqrt{3}\hat{I}_{n'}}\langle I_{p'}||\sigma||I_{n'}\rangle, \\ q^{\tau\tau'}(ab;a'b') &= \frac{2}{\sqrt{5}\hat{I}_b}\langle \tau a||r^2Y_2||\tau b\rangle \frac{2}{\sqrt{5}\hat{I}_{b'}}\langle \tau' a'||r^2Y_2||\tau' b'\rangle. \end{aligned} \tag{5.4}$$

The dipole and quadrupole operators commute with each other and therefore the pnQRPA equations will be decoupled. Since the above-defined Hamiltonian preserves the gauge, the resulting harmonic approximated equation will be conventionally called the GRFRpnQRPA equation. For this reason they will be separately treated. Adding the first-order corrections to the quasiboson approximation, we have

$$\begin{aligned} &[\mathcal{A}_{1\mu}(pn), \mathcal{A}^\dagger_{1\mu'}(p'n')] \\ &\approx \delta_{\mu,\mu'}\delta_{j_p,j_{p'}}\delta_{j_n,j_{n'}}\Big[U_p^2 - U_n^2 + \frac{U_n^2 - V_n^2}{\hat{I}_n^2}\hat{N}_n \\ &\quad - \frac{U_p^2 - V_p^2}{\hat{I}_p^2}\hat{N}_p\Big]. \end{aligned} \tag{5.5}$$

The average of the rhs of this equation with the GRFRpnQRPA vacuum state is denoted by:

$$\begin{aligned} D_1(pn) = U_p^2 - U_n^2 &+ \frac{1}{2I_n+1}s\big(U_n^2 - V_n^2\big)\langle\hat{N}_n\rangle \\ &- \frac{1}{2I_p+1}\big(U_p^2 - V_p^2\big)\langle\hat{N}_p\rangle. \end{aligned} \tag{5.6}$$

The equations of motion show that the two qp energies are renormalized too:

$$E^{\rm ren}(pn) = E_p\big(U_p^2 - V_p^2\big) + E_n\big(V_n^2 - U_n^2\big). \tag{5.7}$$

The space of pn dipole states, $\mathcal{S}$, is written as a sum of three subspaces defined as:

$$\begin{aligned} &\mathcal{S}_+ = \{(p,n)|D_1(pn) > 0, \quad E^{\rm ren}(pn) > 0,\}, \\ &\mathcal{S}_- = \{(p,n)|D_1(pn) < 0, \quad E^{\rm ren}(pn) < 0,\}, \\ &\mathcal{S}_{sp} = \mathcal{S} - (\mathcal{S}_+ + \mathcal{S}_-), \quad \mathcal{N}_\pm = \dim(\mathcal{S}_\pm), \quad \mathcal{N}_{sp} = \dim(\mathcal{S}_{sp}), \\ &\mathcal{N} = \mathcal{N}_+ + \mathcal{N}_- + \mathcal{N}_{sp}. \end{aligned} \tag{5.8}$$

The third line of the above equations specify the dimensions of these subspaces. In $\mathcal{S}_+$ one defines the renormalized operators:

$$\begin{aligned} \bar{\mathcal{A}}^\dagger_{1\mu}(pn) &= \frac{1}{\sqrt{D_1(pn)}}\mathcal{A}^\dagger_{1\mu}(pn), \\ \bar{\mathcal{A}}_{1\mu}(pn) &= \frac{1}{\sqrt{D_1(pn)}}\mathcal{A}_{1\mu}(pn), \end{aligned} \tag{5.9}$$

while in $\mathcal{S}_-$ the renormalized operators are

$$\begin{aligned} \bar{\mathcal{F}}^\dagger_{1\mu}(pn) &= \frac{1}{\sqrt{|D_1(pn)|}}\mathcal{A}_{1\mu}(pn), \\ \bar{\mathcal{F}}_{1\mu}(pn) &= \frac{1}{\sqrt{|D_1(pn)|}}\mathcal{A}^\dagger_{1\mu}(pn). \end{aligned} \tag{5.10}$$

Indeed, the operator pairs $\mathcal{A}_{1\mu}, \mathcal{A}^\dagger_{1\mu}$ and $\mathcal{F}_{1\mu}, \mathcal{F}^\dagger_{1\mu}$ satisfy commutation relations of boson type. An RPA treatment within $\mathcal{S}_{sp}$ would yield either vanishing or negative energies. The corresponding states are therefore spurious. FRpnQRPA with the gauge symmetry projected defines the phonon operator as

$$\begin{aligned} \Gamma^\dagger_{1\mu} = \sum_k [&X(k)\bar{\mathcal{A}}^\dagger_{1\mu}(k) + Z(k)\bar{\mathcal{F}}^\dagger_{1\mu}(k) - Y(k)\bar{\mathcal{A}}_{1-\mu}(k)(-)^{1-\mu} \\ &- W(k)\bar{\mathcal{F}}_{1-\mu}(k)(-)^{1-\mu}], \end{aligned} \tag{5.11}$$

with the amplitudes determined by the equations

$$[H, \Gamma^\dagger_{1\mu}] = \omega\Gamma^\dagger_{1\mu}, \quad [\Gamma_{1\mu}, \Gamma^\dagger_{1\mu'}] = \delta_{\mu,\mu'}. \tag{5.12}$$

The first equation may be written as

$$\begin{pmatrix} \mathcal{A} & \mathcal{B} \\ -\mathcal{B} & -\mathcal{A} \end{pmatrix}\begin{pmatrix} X(pn) \\ Z(pn) \\ Y(pn) \\ W(pn) \end{pmatrix} = \omega_1 \begin{pmatrix} X(pn) \\ Z(pn) \\ Y(pn) \\ W(pn) \end{pmatrix}, \tag{5.13}$$

where the matrices $\mathcal{A}$ and $\mathcal{B}$ have the dimension $(\mathcal{N}_+ + \mathcal{N}_-) \times (\mathcal{N}_+ + \mathcal{N}_-)$ and the analytical expressions

$$(\mathcal{A}) = \begin{pmatrix} \left(E^{\rm ren}(pn)\delta_{pn;p_1n_1} + 2\chi\sigma^{(1)T}_{p_1n_1;pn}\right)_{\substack{(p,n)\in\mathcal{S}_+\\(p_1,n_1)\in\mathcal{S}_+}} & -2X_{dp}\left(\sigma^{(1)T}_{p_1n_1;pn}\right)_{\substack{(p,n)\in\mathcal{S}_+\\(p_1,n_1)\in\mathcal{S}_-}} \\ -2X_{dp}\left(\sigma^{(1)T}_{p_1n_1;pn}\right)_{\substack{(p,n)\in\mathcal{S}_-\\(p_1,n_1)\in\mathcal{S}_+}} & \left(|E^{\rm ren}(pn)|\delta_{pn;p_1n_1} + 2\chi\sigma^{(1)T}_{p_1n_1;pn}\right)_{\substack{(p,n)\in\mathcal{S}_-\\(p_1,n_1)\in\mathcal{S}_-}} \end{pmatrix},$$

$$(\mathcal{B}) = \begin{pmatrix} -2X_{dp}\left(\sigma^{(1)T}_{p_1n_1;pn}\right)_{\substack{(p,n)\in\mathcal{S}_+\\(p_1,n_1)\in\mathcal{S}_+}} & 2X_{dp}\left(\sigma^{(1)T}_{p_1n_1;pn}\right)_{\substack{(p,n)\in\mathcal{S}_+\\(p_1,n_1)\in\mathcal{S}_-}} \\ 2X_{dp}\left(\sigma^{(1)T}_{p_1n_1;pn}\right)_{\substack{(p,n)\in\mathcal{S}_+\\(p_1,n_1)\in\mathcal{S}_+}} & -2X_{dp}\left(\sigma^{(1)T}_{p_1n_1;pn}\right)_{\substack{(p,n)\in\mathcal{S}_+\\(p_1,n_1)\in\mathcal{S}_+}} \end{pmatrix}, \tag{5.14}$$

where the matrix $\sigma^{(1)}_{pn;p'n'}$ has the expression

$$\sigma^{(1)}_{pn;p'n'} = |D_1(pn)|^{1/2}\sigma_{pn;p'n'}|D_1(p'n')|^{1/2}, \tag{5.15}$$

while the index T suggests that the accompanying matrix is to be transposed.

To solve the equation we need the renormalization factors D_1 which in turn depend on the averages $\langle\hat{N}_p\rangle$ and $\langle\hat{N}_n\rangle$. Using the boson expansion principle the quasiparticle number operators are expressed as a linear combination of $\mathcal{A}^\dagger\mathcal{A}$ and $\mathcal{F}^\dagger\mathcal{F}$ determined such that their commutators with $\mathcal{A}^\dagger$, $\mathcal{A}$ and $\mathcal{F}^\dagger$, $\mathcal{F}$ are preserved. The results are

$$\langle\hat{N}_p\rangle = V_p^2(2I_p+1) + 3\left(U_p^2 - V_p^2\right)\left(\sum_{\substack{n',k\\(p,n')\in\mathcal{S}_+}}(Y_k(p,n'))^2 - \sum_{\substack{n',k\\(p,n')\in\mathcal{S}_-}}(W_k(p,n'))^2\right),$$

$$\langle\hat{N}_n\rangle = V_n^2(2I_n+1) + 3\left(U_n^2 - V_n^2\right)\left(\sum_{\substack{p',k\\(p',n)\in\mathcal{S}_+}}(Y_k(p',n))^2 - \sum_{\substack{p',k\\(p',n)\in\mathcal{S}_-}}(W_k(p',n))^2\right). \tag{5.16}$$

Equations (5.13) and (5.16) and the norm restriction,

$$\sum_{\substack{n',k\\(p,n')\in\mathcal{S}_+}}(X(pn)^2 - Y(pn)^2) + \sum_{\substack{n',k\\(p,n')\in\mathcal{S}_-}}(Z(pn)^2 - W(pn)^2) = 1, \tag{5.17}$$

are to be simultaneously considered and solved iteratively. It is worth mentioning that using the quasiparticle representation for the basic operators $\mathcal{A}^\dagger_{1\mu}$, $\mathcal{F}^\dagger_{1\mu}$, $\mathcal{A}_{1,-\mu}(-1)^{1-\mu}$, and $\mathcal{F}_{1,-\mu}(-)^{1-\mu}$, one obtains for $\Gamma^\dagger_{1\mu}$ an expression which involves the scattering *pn* operators. Thus, the present approach is, indeed, the GRFRpnQRPA.

The case of quadrupole interaction is much simpler since there is no term involved in the model Hamiltonian which might generate back-going phonon amplitude. We denote

$$\begin{aligned} Q^{(\tau,\tau')}(mn;ik) &= D_2^{1/2}(\tau;mn)q^{(\tau,\tau')}(mn;ik)D_2^{1/2}(\tau';ik),\\ E^{\rm ren}(\tau;ab) &= E_{\tau a}\left(U_{\tau a}^2 - V_{\tau a}^2\right) + E_{\tau b}(U_{\tau b}^2 - V_{\tau b}^2)\\ &= \epsilon_{\tau a} - \epsilon_{\tau b},\\ D_2(\tau;ab) &= U_{\tau a}^2 - U_{\tau b}^2. \end{aligned} \tag{5.18}$$

The quadrupole phonon operator is defined as

$$\Gamma^\dagger_{a,2\mu} = \sum_{tau;ik} X_a(\tau,ik)\bar{\mathcal{A}}^\dagger_{2\mu}(\tau;ik), \tag{5.19}$$

with the renormalized boson operator

$$\bar{\mathcal{A}}^\dagger_{2\mu}(\tau;ik) = \frac{1}{\sqrt{D_2(\tau,ab)}}\mathcal{A}^\dagger_{2\mu}(\tau,ab). \tag{5.20}$$

The phonon amplitudes satisfy the equation

$$\begin{aligned} \mathbf{A}_{\tau ik;\tau' mn}X_a(\tau,ik) &= \omega_2 X_a(\tau',mn), \quad \text{with}\\ \mathbf{A}_{\tau ik;\tau' mn} &= (E^{\rm ren}(\tau,ik) + X_2)\delta_{\tau,\tau'}\delta_{ik,mn}\\ &\quad - X_{\tau\tau'}Q^{(\tau'\tau)}(mn;ik) \end{aligned} \tag{5.21}$$

and the normalization condition

$$\sum_{\tau,mn} X_a(\tau,mn)^2 = 1. \tag{5.22}$$

VI. THE GAMOW-TELLER TRANSITION AMPLITUDE

The GRFRpnQRPA states defined in the previous section are used to describe the amplitude of the double-β transition $0^+ \to 2^+$:

$$M^{(02)}_{GT} = \sqrt{3}\sum_{k,m}\frac{{}_i\langle 0||\beta_i^+||k,m\rangle_{ii}\langle k,m|k'm'\rangle_{ff}\langle k'm'||\beta_f^+||2_1^+\rangle_f}{(E_{km} + \Delta E + E_{1^+})^3}. \tag{6.1}$$

In the above equation, the denominator consists of three terms: (a) ΔE, the energy carried by leptons in the intermediate state approximated by the sum of the rest energy of the emitted electron and the half of the Q value of the $\beta\beta$ decay process

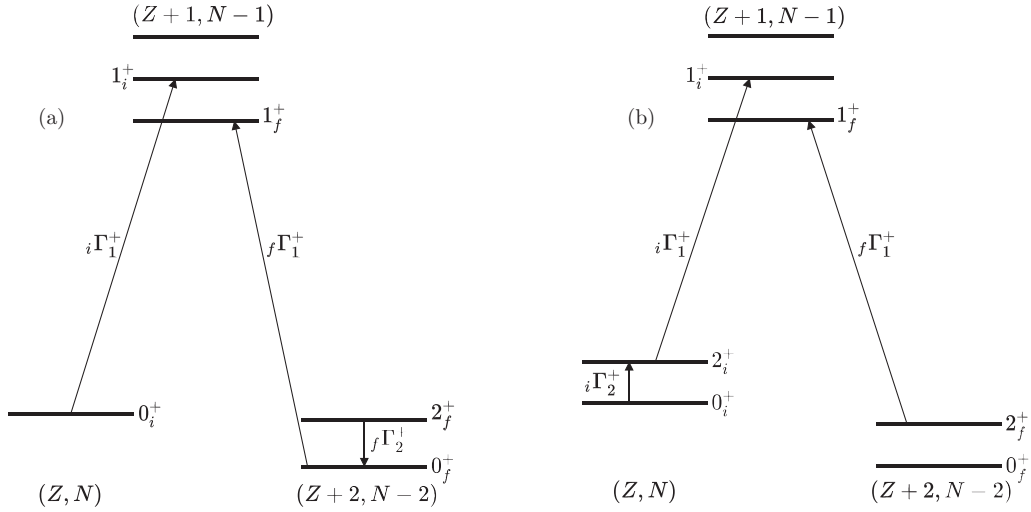

FIG. 2. Illustration of the GT transition $0^+ \to 2^+$ via (a) one- and (b) two-phonon state.

from the ground state of the mother nucleus to the first excited 2^+ state of the daughter nucleus,

$$\Delta E = m_e c^2 + \tfrac{1}{2} Q_{\beta\beta}^{(0\to 2)}; \tag{6.2}$$

(b) the average value of the mth GRFRpnQRPA energy for the k-boson state normalized to the particular value corresponding to $m = 1$; and (c) the experimental energy for the lowest 1^+ state. The indices carried by the β^+ operators indicate that they act in the space spanned by the GRFRpnQRPA states associated to the initial (i) or final (f) nucleus. The overlap matrix elements (m.e.) of the k phonon states in the initial and final nuclei, respectively, are calculated within GRFRpnQRPA. In Eq. (6.1), the Rose convention for the reduced m.e. is used [54]. The ground state of the mother nucleus, $|0\rangle_i$, and the first excited 2^+ state of the daughter nucleus may be excited to the kth phonon state built up with the mth root of the GRFRpnQRPA equations by means of the β^- and β^+ transition operators, respectively. The connection between the states excited from the mother nucleus and those excited from the daughter nucleus is achieved by the overlap matrix ${}_i\langle k, m|k'm'\rangle_f$. In Eq. (6.1), the index k takes the values 1 and 2 while m runs over the complete set of the GRFRpnQRPA equations for the dipole phonons and $m = 1$ for the quadrupole phonon. The mechanisms which contribute to the double-β process are illustrated in Fig. 2. Note that Fig. 2(a) suggests that the first leg of the transition is determined by the one dipole phonon operator, while the second transition is caused by the dipole-quadrupole double phonon operator. The scenario of Fig. 2(b) is different; namely, the first β^- transition has a double phonon character, while the second one is a single dipole phonon transition.

Once the transition amplitude is calculated, the half-life of the process is readily obtained:

$$T_{1/2}^{2\nu}(0_i^+ \to 2_f^+)^{-1} = G_{02}\left|M_{GT}^{(02)}\right|^2, \tag{6.3}$$

where G_{02} is an integral on the phase space, independent of the nuclear structure.

VII. NUMERICAL RESULTS

The formalism presented in the previous sections was applied to eight double-β emitters with the one quadrupole phonon state 2^+ as the final state. The spherical shell model single-particle basis is defined using the parameters given in Ref. [52]:

$$\hbar\omega_0 = 41A^{-1/3},\ C = -2\hbar\omega_0\kappa,\ D = -\hbar\Omega_0\mu. \tag{7.1}$$

The parameters $(\kappa;\mu)$ for the proton system are $(0.08;0)$ for ^{76}Ge, ^{76}Se, ^{82}Se, ^{82}Kr, and ^{116}Cd, and $(0.0637;0.6)$ for ^{116}Sn, ^{128}Te, ^{128}Xe, ^{130}Te, ^{130}Xe, ^{150}Nd, and ^{130}Xe, while for the neutron systems of the two groups of nuclei mentioned above, the values are (0.08; 0) and (0.0637; 0.42), respectively. The proton and neutron pairing strengths are listed in Table I and illustrated in Fig. 3.

The pairing calculation corresponds to Z protons and N neutrons, respectively, while the quasiparticle correlations are accounted for by means of the states from outside the core mentioned in Table I. For the strengths from Fig. 3 we solved the pairing equations and obtained the gaps plotted in Fig. 4 as a function of A and compared them with the experimental data approximated by $12/\sqrt{A}$ and $13/\sqrt{A}$, respectively [55]. The calculated gaps are spread around the mentioned experimental data. What is generating the discrepancies? The sum rule is sensitive to changing the dimension of the single-particle basis as well as to the pairing strength. Therefore, we slightly modified the pairing strengths towards improving the agreement with the sum rule.

The projected spherical single-particle basis depends on two parameters, namely, the deformation d and the parameter k relating the quadrupole boson operator and the quadrupole collective coordinate. These parameters were taken as in Ref. [56]. Their connection with the deformation β was *in extenso* studied in Refs. [39,56]. From Table I we see that we meet the situation when the mother and daughter nuclei have similar deformation ((^{82}Se; ^{82}Kr), (^{128}Te; ^{128}Xe), (^{150}Nd; ^{150}Sm)) and the case where the initial and final nuclei are

TABLE I. The parameters of the projected spherical single-particle basis (the deformation d and the k defining the canonical transformation relating the quadrupole bosons and collective coordinates), the strengths of the pairing interactions, G_p and G_n, the strengths of the Gamow-Teller interactions, $\chi(1)$, $\chi(2)$, and χ_{dp}, and the strengths of the QQ interaction are listed. We also give the dimension of the inert core, the number of states for protons and neutrons, respectively, (p, n), the number of iterations needed to find the solution of the pnQRPA equations, and the Ikeda sum rule. All the mentioned parameters correspond to the parent and daughter nuclei listed in the first column.

	d	k	G_p (keV)	G_n (keV)	$\chi(i)$ (MeV)	X_{dp} (MeV)	b^4X_{pp} (keV)	X_2 (MeV)	Core (Z, N)	No. states (p, n)	No. iterations	ISR/3
^{76}Ge	1.6	10	360	380	0.25	0.20	31.5	3.260	(20,20)	(18,18)	4	12.09
^{76}Se	1.9	10	240	325	0.25	0.20	19.7	4.017	(20,20)	(18,18)	4	
^{82}Se	0.2	9	340	360	0.01	0.05	19.1	2.031	(26,26)	(20,20)	5	14.05
^{82}Kr	0.2	9	340	360	0.01	0.05	19.7	2.173	(26,26)	(20,20)	5	
^{96}Zr	1.5	10	180	433	0.22	0.11	25.8	3.635	(20,20)	(20,20)	6	16.1
^{96}Mo	1.2	12	220	338	0.22	0.11	25.8	2.636	(20,20)	(20,20)	6	
^{100}Mo	−1.4	10	380	360	0.06	1.65	31.5	1.857	(28,28)	(19,19)	4	16.03
^{100}Ru	−0.6	3.6	385	365	0.06	1.65	28.0	1.872	(28,28)	(19,19)	4	
^{116}Cd	−1.8	3.0	200	245	0.98	1.60	30.0	2.187	(26,26)	(27,27)	4	19.96
^{116}Sn	−1.2	3.0	135	275	0.98	1.60	7.00	1.148	(26,26)	(27,27)	4	
^{128}Te	1.7	7.17	270	220	0.80	1.56	12.0	1.852	(38,38)	(30,30)	5	24.09
^{128}Xe	1.7	8.0	270	220	0.80	1.56	12.0	1.240	(38,38)	(30,30)	5	
^{130}Te	1.0	8.0	270	240	0.30	0.33	12.1	1.753	(40,40)	(29,29)	6	26.00
^{130}Xe	1.4	8.0	260	220	0.30	0.33	17.3	2.130	(40,40)	(29,29)	6	
^{150}Nd	1.952	3.0	240	260	0.64	1.45	27.3	2.187	(50,50)	(25,25)	5	29.77
^{150}Sm	1.952	2.0	220	240	0.64	1.45	27.3	2.148	(50,50)	(25,25)	5	

characterized by different deformations. Our calculations show that deformation enhances the half-life of the process. The same effect of deformation on the GT matrix elements was pointed out also by Zamick and Auerbach [42]. In the quoted reference the mentioned authors calculated the GT transition matrix elements for the neutrino capture $\nu_\mu +$

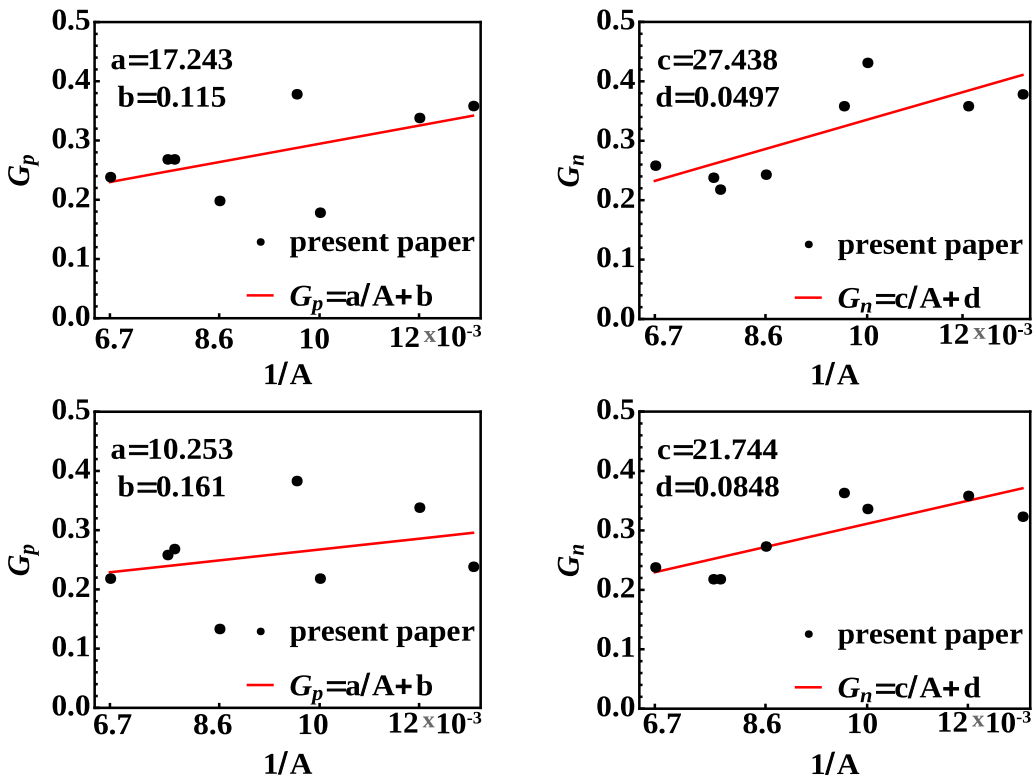

FIG. 3. The proton and neutron pairing strengths for mother (first row) and daughter nuclei (second row), respectively. The results were interpolated by a linear function of $1/A$.

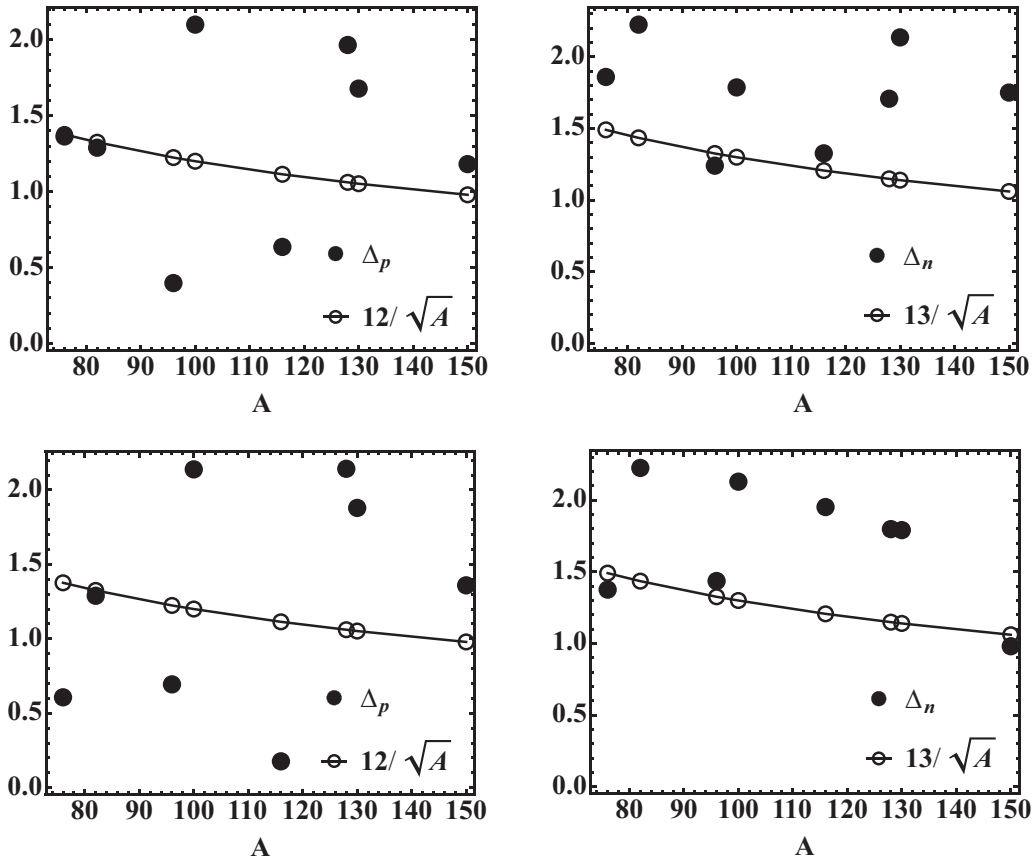

FIG. 4. Calculated proton (Δ_p) and neutron (Δ_n) gap parameters for mother (first row) and daughter (second row) nuclei, compared with experimental data, approximated by $12/\sqrt{A}$ and $13/\sqrt{A}$, respectively.

$^{12}\mathrm{C} \to {}^{12}\mathrm{N} + \mu^-$ using different structures for the ground state: (a) a spherical ground state, (b) asymptotic limits of the wave functions, and (c) deformed states with the deformation $\delta = -0.3$. The results for the transition rate were 5.333, 0, and 0.987, respectively. The ratio between the transition rates obtained with spherical and deformed bases explains the factor of 5 overestimate in the calculations of Ref. [57].

The strength of the repulsive *pn* interaction was fixed such that the position of the giant Gamow-Teller resonance was reproduced, while the attractive interaction strength is chosen so that the result for the $\log_{10} ft$ value associated with the single-β^- decay of the intermediate odd-odd nucleus to the ground state of the daughter nucleus was close to the corresponding experimental data. If the experimental data are missing the restriction refers to the exiting data in the neighboring region.

The QQ interactions are fixed so that the properties of the first excited 2^+ state are properly described. In Table I we also give the value of the Ikeda sum rule. The number of proton and neutron single-particle states used in our calculations is also mentioned in Table I.

To calculate the half-lives for ground to 2^+ and ground to ground transitions, one needs the phase space factors G_{02} and G_{00}, respectively. These were determined following the procedure described in Ref. [4]. Having the parameters involved in the model Hamiltonian fixed, the amplitude of the transition $0^+ \to 2^+$ is obtained from Eq. (6.1). Results are listed in Table II together with the half-life of the process. These are compared with the predictions of different approaches. For the transitions of the parent nuclei ^{76}Ge, ^{76}Ge, ^{82}Se, ^{96}Zr, ^{128}Te, and ^{139}Te, projecting the gauge symmetry enhances the half-lives, while for ^{100}Mo, ^{116}Cd, and ^{150}Nd the effect is opposite. As we showed before, breaking the spherical symmetry makes the process less probable. Also, in Ref. [51] the SU(4) symmetry, broken by the mean field approximation, was restored by the Pyatov method [65] and thus the effect of restoring the symmetry on the transition rates of four double-β processes was investigated. For these transitions a quenching of the matrix elements was pointed out. From the three examples discussed above we cannot draw a definite conclusion about quenching or enhancing the transition rates when a symmetry is restored. Note that the results for the half-lives are in the range of the measured data.

Unfortunately, only the low limits of the half-lives are experimentally known. Therefore, in order to point out the virtues of the proposed model, the extension to the ground to ground transition for the same parameters as those used for the ground to 2^+ transition is necessary. Thus the amplitude describing the transition $0^+ \to 0^+$ is given

TABLE II. The double-β transition amplitudes the half lives obtained with our formalism are compared with the corresponding experimental data as well as with those provided by other formalism. On the first column, the double-β emitters are listed. For ^{150}Nd the first data corresponds to the nuclear deformation $\beta = 0.28$, while the second one to $\beta = 0.19$. The last three columns concern the data for the ground to ground double-β transition.

Parent	$M_{GT}^{0^+\to 2^+}$	$T_{1/2}^{2\nu}(0_i^+ \to 2_f^+)$ (yr)				$M_{GT}^{0^+\to 0^+}$	$T_{1/2}^{2\nu}(0_i^+ \to 0_f^+)$ (yr)	
nucleus	[MeV^{-3}]	Present	Expt.	Ref. [58]	Ref. [59]	(MeV^{-1})	Present	Expt.
^{76}Ge	0.131×10^{-4}	1.166×10^{34}	$>1.1 \times 10^{21}$ [4] $>1.6 \times 10^{23}$ [17]	5.75×10^{28}	1.0×10^{26}	2.647×10^{-2}	1.16×10^{22}	$(1.5 \pm 0.1) \times 10^{21}$ [9]
^{82}Se	0.677×10^{-5}	2.478×10^{30}	$>1.4 \times 10^{21}$ [4] $>1.0 \times 10^{22}$ [18]	1.70×10^{27}	3.3×10^{26} [60]	2.611×10^{-2}	3.84×10^{20}	$(1.1^{+0.8}_{-0.3}) \times 10^{20}$ [61]
^{96}Zr	0.145×10^{-5}	7.500×10^{30}	$>7.9 \times 10^{19}$ [9]	2.27×10^{25}	4.8×10^{21}	0.816×10^{-2}	3.19×10^{21}	$(2.3 \pm 0.2) \times 10^{19}$ [9]
^{100}Mo	0.426×10^{-2}	1.223×10^{24}	$>2.5 \times 10^{21}$ [20]	1.21×10^{25}	3.9×10^{24}	2.447×10^{-2}	7.22×10^{20}	$(0.115^{+0.03}_{-0.02}) \times 10^{20}$ [61]
^{116}Cd	0.724×10^{-2}	1.671×10^{26}	$>2.3 \times 10^{21}$ [21]	3.4×10^{26}	1.1×10^{24}	0.233	3.33×10^{21}	3.75×10^{19} [62]
^{128}Te	0.606×10^{-3}	6.684×10^{34}	$>4.7 \times 10^{21}$ [4]	4.7×10^{33}	1.6×10^{30}	0.416	0.26×10^{23}	$(1.9 \pm 0.4) \times 10^{24}$ [9]
^{130}Te	0.693×10^{-6}	5.562×10^{32}	$>4.5 \times 10^{21}$ [4] $>2.8 \times 10^{21}$ [22]	6.94×10^{26}	2.7×10^{23}	0.81×10^{-2}	12.00×10^{21}	$(2.7 \pm 0.1) \times 10^{21}$ [63]
^{150}Nd	0.317×10^{-2}	0.461×10^{21}	$>8.0 \times 10^{18}$ [4] $>2.2 \times 10^{20}$ [31]	1.50×10^{23}	7.2×10^{24} [64] 1.2×10^{25} [64]	0.744	0.789×10^{17}	$(8.2 \pm 0.9) \times 10^{19}$ [9]

by

$$M_{GT}^{(00)} = \sqrt{3} \sum_{k,k'} \frac{{}_i\langle 0||\beta_i^+||k\rangle_{ii}\langle k|k'\rangle_{ff}\langle k'||\beta_i^+||0\rangle_f}{E_k + \Delta E_1 + E_{1^+}}, \quad (7.2)$$

where the energy shift from the denominator is the sum between the electron rest mass and half of the ground to ground Q value:

$$\Delta E_1 = m_e c^2 + \tfrac{1}{2} Q_{\beta\beta}^{(0\to 0)}. \quad (7.3)$$

E_{1^+} denotes the experimental energy of the first state 1^+ in the intermediate odd-odd nucleus, while $|k\rangle_l$ is the kth dipole phonon state obtained by exciting the initial (final) nucleus, for $l = i$ ($l = f$). This transition amplitude determines the half-life of the process by means of

$$T_{1/2}^{2\nu}(0_i^+ \to 0_f^+)^{-1} = G_{00} \left| M_{GT}^{(00)} \right|^2, \quad (7.4)$$

where G_{00} is the phase space integral specific to the ground to ground transition. The matrix elements involved in Eq. (7.2) have the following expressions:

$$\begin{aligned}
\langle 0||\beta_i^+||k\rangle &= \sqrt{3} \sum_{ab} P_1(ab) \sqrt{|D_1(ab)|} X_{1k}(a,b), \\
\langle k'||\beta_i^+||0\rangle &= \sum_{a'b'} P_1(a'b') \sqrt{|D_1(a'b')|} Y_{1k}(a'b'), \\
\langle k|k'\rangle &= \sum_{a'b'} (X_{1k}(a'b') X_{1k'}(a'b') - Y_{1k}(a'b') Y_{1k'}(a'b')).
\end{aligned} \quad (7.5)$$

Results for the transition amplitude and the transition half-life are collected in Table II. By inspection, we notice that the transition amplitude for the transition $0^+ \to 2^+$ is one to three orders of magnitude smaller than that corresponding to the ground to ground decay. The calculations for the half-lives are in a reasonable agreement with the corresponding experimental data.

We recall that the double-β process is supposed to take place via two consecutive virtual β^- transitions. In other words, the dipole states of the intermediate odd-odd nucleus are fed through either the virtual β^- decay of the parent nucleus or by the β^+ transition of the daughter nucleus. Note that the same matrix elements are involved in the real transitions from the intermediate odd-odd nucleus to the mother nucleus by a β^+/Electron Capture (EC) process or to the daughter via a (p, n) reaction. The two transitions are characterized by the $\log_{10} ft$ value with ft given by the expression

$$\begin{aligned}
ft_{\mp} &= \frac{6160}{\left[{}_l\langle 1_1||\beta^{\pm}||k\rangle_l g_A\right]^2}, \quad l = m, d, \\
k &= 0\delta_{l,m} + (2or0)\delta_{l,d},
\end{aligned} \quad (7.6)$$

where $|1_1 M\rangle$ denotes the first dipole phonon state in the intermediate odd-odd nucleus, while $|k\rangle_l$ denotes the GRFRpnQRPA ground state if $l = m$ and the state 2^+ if $l = d$. The lower index takes the values m and d depending on whether the end state of the transition is characterizing the mother or the daughter nucleus. f is an integral on the phase space which does not depend on the nuclear structure. This was calculated using the analytical expression from Ref. [4]. We chose $g_A = 1.0$ in order to take account of the distance states responsible for the "missing strength" in the giant GT resonance [4]. Results are compared with the corresponding experimental data in Table III. One notes a reasonable agreement with the existent experimental data. The big discrepancies between the $\log_{10} ft$ value corresponding to the transitions $0^+ \to 2^+$ and $0^+ \to 0^+$, respectively, reflect the fact that the transition to the excited state is much less likely than that of ground to ground.

A few comments about the connection between the $\log_{10} ft$ values and ISR are necessary. For small values of the attrac-

TABLE III. The $\log_{10} ft$ values characterizing the β^- transition of the intermediate odd-odd nucleus staying in the state 1^+ to the daughter nucleus in the state 2^+ and the transition β^+/EC from the intermediate odd-odd nucleus in the state 1^+ to the ground state of the mother nucleus, respectively.

Parent nucleus	$\log_{10} ft$	Odd-odd nucleus	$\log_{10} ft$		Daughter nucleus
^{76}Ge	$0^+ \xleftarrow{\beta^+/EC} 1^+$	^{76}As	$1^+ \xrightarrow{\beta^-} 2^+$	$1^+ \xrightarrow{\beta^-} 0^+$	^{76}Se
Theor.	5.59		13.47	7.81	
^{82}Se	$0^+ \xleftarrow{\beta^+/EC} 1^+$	^{82}Br	$1^+ \xrightarrow{\beta^-} 2^+$	$1^+ \xrightarrow{\beta^-} 0^+$	^{82}Kr
Theor.	8.38		12.66	8.6	
^{96}Zr	$0^+ \xleftarrow{\beta^+/EC} 1^+$	^{96}Nb	$1^+ \xrightarrow{\beta^-} 2^+$	$1^+ \xrightarrow{\beta^-} 0^+$	^{96}Mo
Theor.	8.86		14.34	8.2	
^{100}Mo	$0^+ \xleftarrow{\beta^+/EC} 1^+$	^{100}Tc	$1^+ \xrightarrow{\beta^-} 2^+$	$1^+ \xrightarrow{\beta^-} 0^+$	^{100}Ru
Theor.	3.18		9.46	5.16	
Expt.	4.3 [67]		6.4 [67], 6.63 [68]	4.59 [68]	
^{116}Cd	$0^+ \xleftarrow{\beta^+/EC} 1^+$	^{116}In	$1^+ \xrightarrow{\beta^-} 2^+$	$1^+ \xrightarrow{\beta^-} 0^+$	^{116}Sn
Theor.	3.20		10.92	3.44	
Expt.	4.47 [69]		5.85 [69]		
^{128}Te	$0^+ \xleftarrow{\beta^+/EC} 1^+$	^{128}I	$1^+ \xrightarrow{\beta^-} 2^+$	$1^+ \xrightarrow{\beta^-} 0^+$	^{128}Xe
Theor.	4.09		9.71	3.05	
Expt.	6.01 [70] 5.049 [72]		6.498 [70]	6.061 [71]	
^{130}Te	$0^+ \xleftarrow{\beta^+/EC} 1^+$	^{130}I	$1^+ \xrightarrow{\beta^-} 2^+$	$1^+ \xrightarrow{\beta^-} 0^+$	^{76}Xe
Theor.	6.49		13.18	9.39	
^{150}Nd	$0^+ \xleftarrow{\beta^+/EC} 1^+$	^{150}Pm	$1^+ \xrightarrow{\beta^-} 2^+$	$1^+ \xrightarrow{\beta^-} 0^+$	^{150}Sm
Theor.	2.84		8.99	3.71	
Expt.			8.62 [73]		

tive interaction strength X_{dp}, the ISR exceeds the value of $N-Z$. However, the β^- matrix element associated to the transition $1^+ \to 0^+$ from the intermediate odd-odd nucleus to the ground state of the daughter nucleus is mainly determined by the repulsive interaction and consequently is large, which means a small value for the corresponding $\log_{10} ft$. Increasing the strength of X_{dp}, the mentioned matrix element is decreasing and therefore the $\log_{10} ft$ value is increasing. Approaching the critical value where the energy of the first excited dipole state is vanishing, the amplitude of the back-going graph, $Y_k(ab)$, is increasing and so is the strength of the β^+ transition, which determines a decrease of the ISR. The adopted procedure of fixing the value of X_{dp} consists of fitting the value of $\log_{10} ft$, characterizing the transition from the dipole state 1^+ of the intermediate odd-odd nucleus to the ground state of the daughter nucleus. In some cases the obtained value yields for ISR a value which is different from $N-Z$. In such a case the parameter X_{dp} is modified so that the ISR is brought close to $N-Z$.

Using expression (B2), the single-β transition strengths associated with the decays of the mother nucleus were calculated and the results are represented in Figs. 5 and 6 as functions of the GRFRpnQRPA energies. There we give also the strength of the β^+ transition of the daughter nucleus from the first excited 2^+ state. For ^{76}Ge, ^{128}Te, and ^{150}Nd the β^- strength is accumulated in a narrow peak, while for the remaining emitters the giant resonance exhibits a broad width and a complex structure. For a given nucleus the difference between areas under the curves of figures from the first and second columns, respectively, defines the Ikeda sum rule. We note that the shape of the β^+ strength of the daughter nucleus has a similar shape as that of the β^- strength for the mother decay. Apart from their magnitudes, the maximal strength is reached for the GT resonance energy.

For ^{76}Ge, ^{82}Se, ^{128}Te, and ^{130}Te, the results of our calculations are compared with the corresponding experimental data. One can remark on the quality of the agreement with the experimental data for ^{130}Te. For the other three nuclei the two sets of data agree with each other in the low part of the spectra, while the GT resonance locations are different by 1–2 MeV.

For some of the double-β emitters there are available data concerning the total $B(GT)_-$ strength. Since a limited interval of energies of the odd-odd nucleus is considered, the data are to be compared with 0.6 of the theoretical results. Another feature refers to the fact that the total strength $B(GT)_-$ accounts also for the background contribution. Despite this, the strength for ^{128}Te and ^{130}Te, for example, represents only 72% and 71% of the $N-Z$ value [66]. If the background contribution to the total strength is eliminated, the total measured strength amounts to about 56% and 59%, respectively, of the

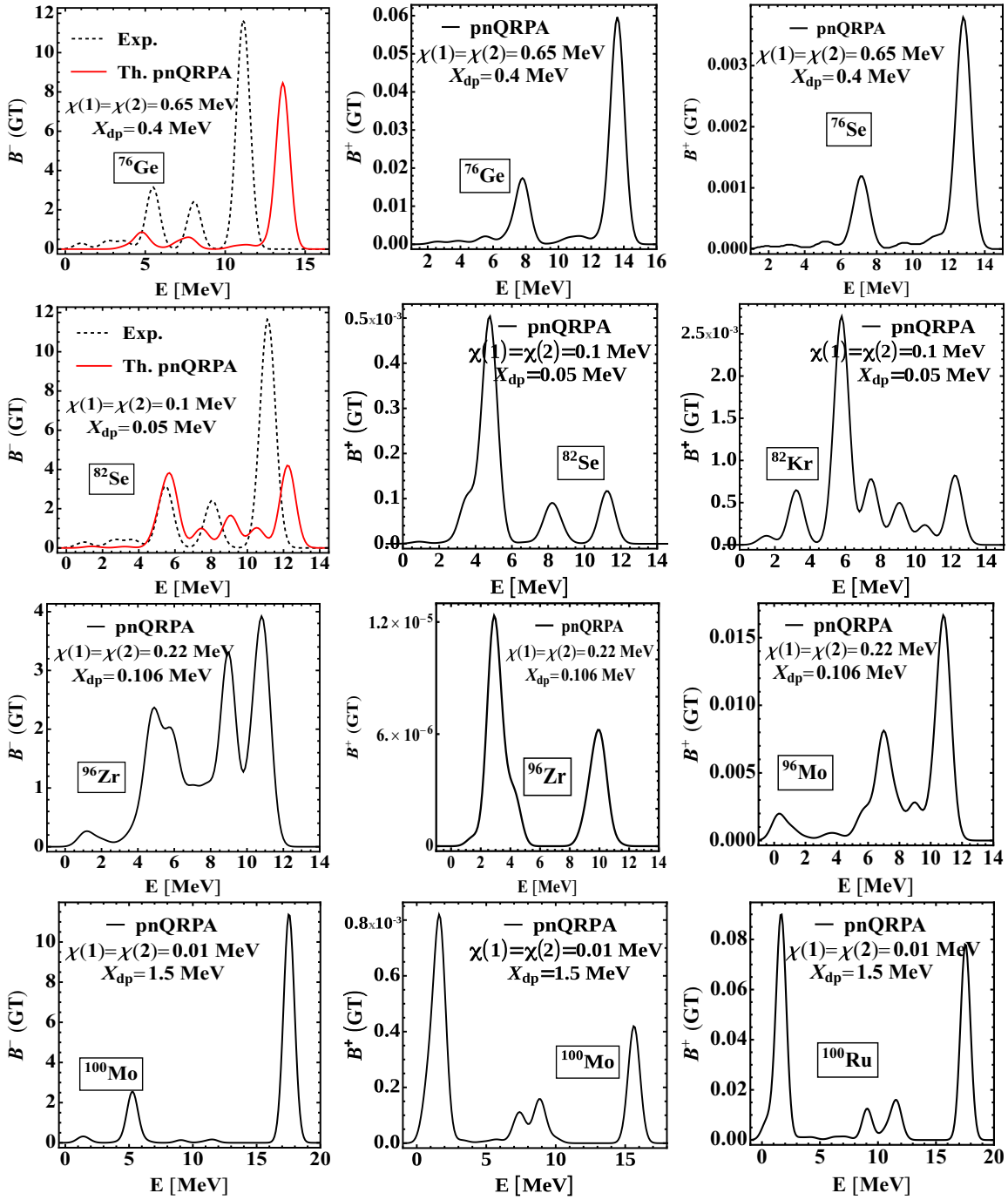

FIG. 5. The strengths for the β^- and β^+ transitions of the double-β emitters are shown in the figures from the first and second columns. Also, the β^+ strengths for the transitions $2^+ \rightarrow 1^+$ in the daughter nuclei are given in the panels of the third column. The strengths were folded with Gaussian functions having a width of 1 MeV. The calculated strength distributions for ^{76}Ge and ^{82}Se are compared with the corresponding experimental data from Ref. [66].

$N - Z$ value. The results of such a comparison are given in Table IV.

The final state in the daughter nucleus is the first excited 2^+ state, which decays to the ground state by the γ emission. The half-life of this process is of the order of picoseconds. Therefore, detecting the two electrons emerging from the double-β process in coincidence with the quadrupole γ quanta resulting from the transition of 2^+ to the ground state would be an experimental way of identifying the double-β process to the state 2^+. Using the results of Appendix C, we calculated the $B(E2)$ value of the transition $2^+ \rightarrow 0^+$ and the corresponding half-life. Results were compared with the existent experi-

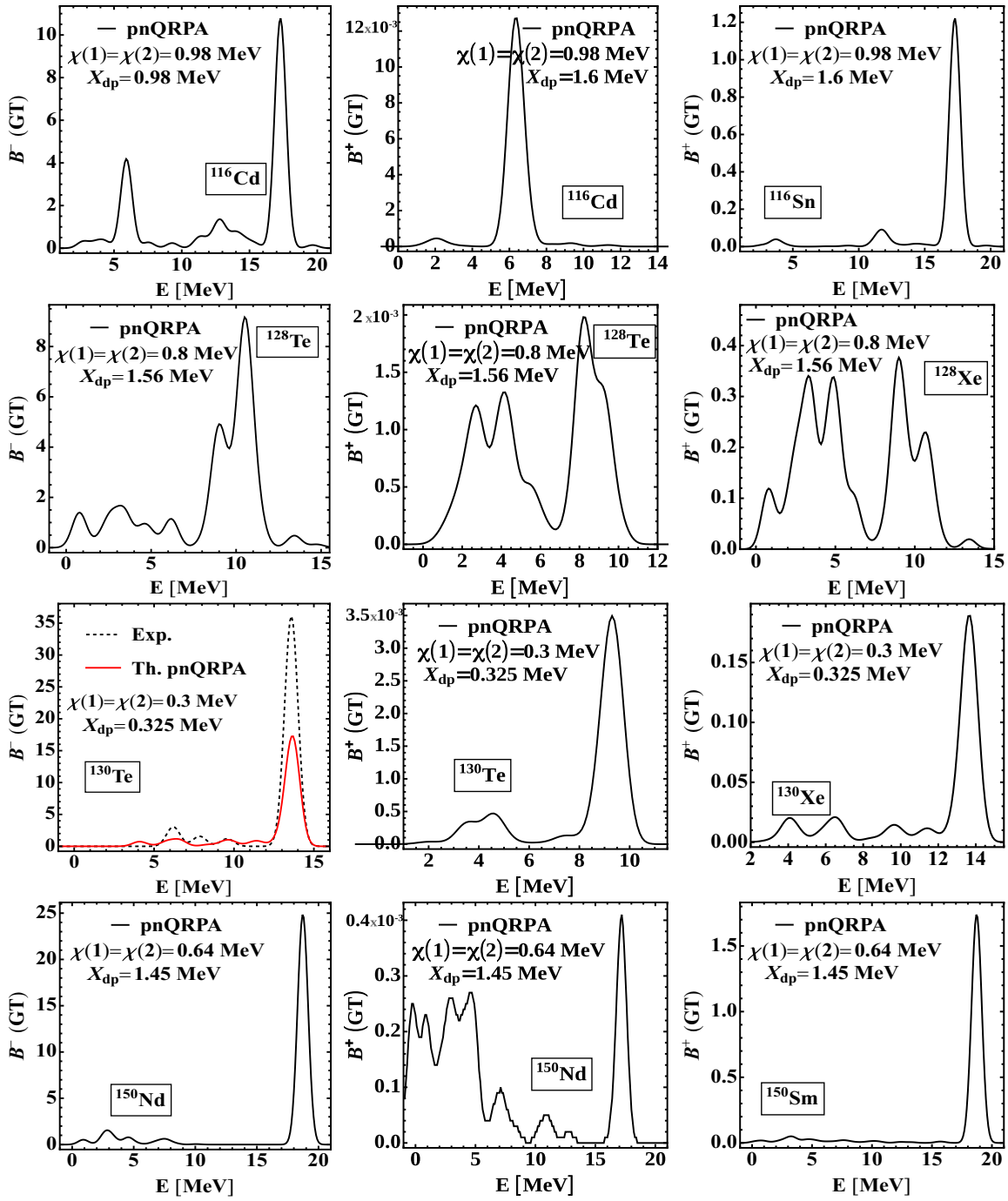

FIG. 6. The same as in Fig. 5 but for other mothers (^{116}Cd, ^{128}Te, ^{130}Te, ^{150}Nd) and daughters (^{116}Sn, ^{128}Xe, ^{130}Xe, ^{150}Sm), respectively. The calculated strength distributions for ^{128}Te and ^{130}Te are compared with the corresponding experimental data from Ref. [66].

mental data, in Table V. The obtained $B(E2)$ value is used to calculate the nuclear deformation. This is compared with the d/k value and the corresponding experimental nuclear deformation. One notes a reasonable agreement between the three sets of data.

VIII. SUMMARY AND CONCLUSIONS

In the previous sections we developed a formalism with gauge invariance restored for the double-β transition $0^+ \rightarrow 2^+$ with two neutrinos in the final state. The aim of this investigation was to bring the Ikeda sum rule close to the $N - Z$ value. Indeed, to describe the transition from the ground to the first excited 2^+ state, one has to go beyond the pnQRPA approach. This is achieved by combining two higher QRPA approaches, namely, the fully renormalized QRPA and the boson expansion approximation. Each of these violates the sum rule. It seems that the renormalization of the QRPA equations underestimates the sum rule, while the boson expansion overestimates it. The idea underlying the present paper is that

TABLE IV. Total strengths for the Gamow-Teller β^- (first column) and β^+ (third column) transitions, quenched by a factor of 0.6, compared with the corresponding available experimental data. Also, the results for the total strength of the β^+ transition from the state 2^+ of the daughter nucleus are given.

Nucleus	$0.6\sum B(GT)_-$	$\sum[B(GT)_-]_{\text{expt}}$	Nucleus	$0.6\sum B(GT)_+$	$\sum[B(GT)_+]_{\text{expt}}$	$0.6\sum[B(GT)_+]_{2_1^+\to 1_k^+}$
^{76}Ge	21.706	23.3 [66]	^{76}Se	0.0935	1.45 ± 0.07 [74]	0.598×10^{-2}
^{82}Se	25.307	24.6 [66]	^{82}Kr	0.0112		0.324×10^{-6}
^{100}Mo	29.263	26.69 [75]	^{100}Ru	0.4110		0.153×10^{-5}
^{116}Cd	38.675	32.70 [75]	^{116}Sn	2.756		0.6×10^{-7}
^{128}Te	47.113	40.08 [66]	^{128}Xe	3.751		0.111×10^{-4}
^{130}Te	47.372	45.90 [66]	^{130}Xe	0.574		0.111×10^{-6}

breaking the gauge symmetry is responsible for the deviation of the sum rule from the $N-Z$ value. In a previous paper we restored the gauge symmetry for the process of ground to ground double-β decay with two neutrinos in the final state. Here the formalism is extended to the transition from ground to the first excited 2^+ state. In an earlier publication we treated the double-β transition $0^+ \to 2^+$ without projecting the gauge symmetry [58]. Results for the transition $0^+ \to 2^+$ were compared with those of the ground to ground transition as well as with those obtained without the gauge symmetry restored. One can remark on the good agreement between calculated half-lives for ground to ground transition and the corresponding experimental data.

The hypothesis that the gauge symmetry should be conserved is supported, first of all, by the fact that the single β minus transition,

$$n \to p + e + \tilde{\nu}, \tag{8.1}$$

takes place with conserving the gauge.

Several features are addressed in the proposed formalism:

(i) The charge conserved QRPA equations were renormalized. Projecting out the gauge symmetry, the equations attain the Tamm-Dancoff form. Considering the quasiparticle representation for the quadrupole operator $(c_\tau^+ c_\tau)_{2\mu}$ results in the specific shape of the quadrupole operators being of renormalized form.

(ii) Using the second order for the perturbation approximation we calculated the amplitude for the transition $0^+ \to 2^+$ and then the half-life of the process. For five transitions, projecting the gauge will enhance the half-life, while for the other three the effect is opposite. Comments on the effect of other symmetries like rotations and SU(4) symmetry are included.

(iii) Although the transition $0^+ \to 2^+$ takes place via two successive single-β virtual transitions, involved matrix elements are the same as for the real transitions β^+/EC and β^- of the intermediate odd-odd nuclei to the mother and daughter nuclei, respectively. For these transitions we calculated the corresponding $\log_{10} ft$ values and compared them with the existent experimental data.

(iv) The single-$\beta^\mp$ transition strengths are presented as a function of the GRFRpnQRPA energies and compared with the existing experimental data.

(v) The final state, i.e., 2^+, is a short lived state decaying by γ emission. For this state we calculated the $B(E2)$ value and the corresponding half-life, $t_{1/2}$. We suggest that by measuring the γ quanta yielded by the decay of 2^+, in coincidence with identifying the two electrons accompanying the double-β transition, we could experimentally point out the $\beta\beta$ transition $0^+ \to 2^+$. Having the $B(E2)$ value calculated, the theoretical nuclear deformation is readily obtained. This is compared with the experimental nuclear deformation as well as with the deformation parameter d.

In conclusion, the present formalism accounts quantitatively for some properties of the double-β transition $0^+ \to 2^+$ and at a time preserves the Ikeda sum rule which is specific to the pnQRPA.

ACKNOWLEDGMENT

This work was supported by UEFISCU through the Project No. PCE-16/2021.

APPENDIX A

Here we give the analytical expressions for the boson expansion associated with the dipole operators defining the single-β^+ transition operator:

$$\begin{aligned}\beta_\mu^+(p,n) &= \sum_M \frac{\sqrt{2}}{\hat{I}} \langle pIM|\sigma_\mu|nI'M'\rangle \frac{\sqrt{2}}{\hat{I}'} c_{nIM}^+ c_{pI'M'} \\ &\equiv P_k(pn)(c_n^+ c_p)_{1\mu}, \\ P_k(ab) &= \frac{2}{\hat{I}_a}{}_k\langle a||\sigma||b\rangle_k \frac{2}{\hat{I}_b}, \quad k = i, f. \end{aligned} \tag{A1}$$

Here the indices i and f are for the initial and final nucleus, respectively. In terms of the renormalized pnQRPA phonon operators the dipole operators $(c_n^+ c_p)_{1\mu}$ can be expressed as

$$\begin{aligned}(c_n^+ c_p)_{1\mu} = &\sum_k (X_1(k;p,n)\Gamma_{1\mu}^+(k) + Y_1(k;p,n)\Gamma_{1\mu}(k)) \\ &+ \sum_{i,k} S_{i,k}^1(pn)(\Gamma_1^+(i)\Gamma_2(k))_{1\mu} \\ &+ \sum_{i,k} S_{i,k}^2(pn)(\Gamma_1(i)\Gamma_2(k))_{1\mu}, \end{aligned} \tag{A2}$$

where X and Y denote the forward and backward amplitudes, respectively. The coefficients $S^{(1)}$ and $S^{(1)}$ are calculated as follows:

$$S^{(1)}_{i,k}(pn) = [\Gamma_{1\mu_1}(i), [(c^+_n c_p)_{1\mu}, \Gamma^+_{2\mu_2}(k)]]C^{1\ 2\ 1}_{\mu_1\ \mu_2\ \mu},$$
$$S^{(2)}_{i,k}(pn) = [\Gamma^+_{1\mu_1}(i), [(c^+_n c_p)_{1\mu}, \Gamma^+_{2\mu_2}(k)]]C^{1\ 2\ 1}_{\mu_1\ \mu_2\ \mu}. \quad \text{(A3)}$$

The standard notation for the Clebsch-Gordan coefficient has been used. In this way the following expressions for the expansion coefficients are obtained:

$$S^{(1)}_{i,k}(pn) = \sqrt{15}\Bigg[Y_1(i;pn')X_2(k;n'n)\sqrt{\frac{D_1(pn')}{D_2(n'n)}}W(1I_p2I_n;I_{n'}1) + Y_1(i;p'n)X_2(k;pp')\sqrt{\frac{D_1(p'n)}{D_2(pp')}}W(1I_n2I_p;I_{p'}1)\Bigg],$$

$$S^{(2)}_{i,k}(pn) = -\sqrt{15}\Bigg[X_1(i;pn')X_2(k;n'n)\sqrt{\frac{D_1(pn')}{D_2(n'n)}}W(1I_p2I_n;I_{n'}1) + X_1(i;p'n)X_2(k;pp')\sqrt{\frac{D_1(p'n)}{D_2(pp')}}W(1I_n2I_p;I_{p'}1)\Bigg]. \quad \text{(A4)}$$

In this expression, $W(abcd;ef)$ denotes the Racah coefficients.

The expansion coefficients $S^{(1)}$ and $S^{(2)}$ are used for calculating the matrix elements characterizing the two legs of the double β. Thus, the product of the single-β transition amplitudes are given analytically by

$$_i\langle 0||\beta^+||1_k\rangle_{ii}\langle 1_k|1_j\rangle_{ff}\langle 1_j||\beta^+||2^+_1\rangle_f = \sum_{ab;a'b'}\sqrt{3}\sqrt{|D_1(ab)|}X_{1k}(ab)(X_{1k}(a'b')X_{1j}(a'b') - Y_{1k}Y_{1j}(a'b'))S^{(1)}_{j1}(a'b')P_1(ab)P_2(a'b'). \quad \text{(A5)}$$

This matrix element corresponds to the graph from Fig. 2(a). The graph in Fig. 2(b) is calculated using the following equation:

$$_i\langle 0||\beta^+||1_j2_k\rangle_{ii}\langle 1_j2_k|1_j2_1\rangle_{ff}\langle 1_j2_1||\beta^+||2^+_1\rangle_f = \sum_{ab;a'b'}\sqrt{3}S^{(2)}_{jk}(ab)P_1(ab) \times (X_{1j}(ab)X_{1j'}(ab) - Y_{1j}(ab)Y_{1j'}(ab))X_{2k}(a'b')X_{21}(a'b') \times \sqrt{|D_1(a'b')|}Y_{1j'}(a'b')P_2(a'b'). \quad \text{(A6)}$$

APPENDIX B

The Gamow-Teller interaction generates dipole states whose strengths are governed by the so-called Ikeda sum rule (ISR).This is the nuclear structure counterpart of the famous sum rule from atomic physics, pointed out by Reiche and Kuhn [76–78]. The ISR asserts that for the double-β emitter the difference between the β^- and β^+ strengths equals three times the neutron excess, i.e., $3(N-Z)$. This equality is exactly satisfied within the pnQRPA framework. However, in order to conciliate the agreement with the experimental data and the ground state stability, one has to go beyond the pnQRPA level. This is achieved either by boson expansion of the GT transition operator or by renormalizing the pnQRPA equations by taking care of a piece of the anharmonic interaction. It seems that the two procedures affect the ISM in a different manner. Indeed, while the renormalization formalism underestimates, the boson expansion overestimates the ISR. This fact suggested to one of the authors (A.A.R. in collaboration) to elaborate the boson expansion on the top of a renormalized pnQRPA [53]. Indeed, the GT operator was expressed in terms of the renormalized pnQRPA phonon operators. Thus, the agreement with the ISR was much improved. Although the present formalism restores the gauge symmetry, it remains a higher RPA approach and thereby the ISR is violated. To see what causes such a deviation, a few details about ISR derivation are necessary. Indeed, let us calculate the commutator of the single-β transition operators, written in the second quantization corresponding to the above-defined single-particle basis:

$$\begin{aligned}[\beta^+_\mu, \beta^-_{-\mu}(-)^\mu] &= \Bigg[\frac{\sqrt{2}}{\hat{I}_n}\langle n|\sigma_\mu|p\rangle\frac{\sqrt{2}}{\hat{I}_p}c^+_{I_nM_n}c_{I_pM_p}, \frac{\sqrt{2}}{\hat{I}_{p'}}\langle p'|\sigma_{-\mu}(-)^\mu|n'\rangle \times \frac{\sqrt{2}}{\hat{I}_{n'}}c^+_{I_{p'}M_{p'}}c_{I_{n'}M_{n'}}\Bigg] \\ &= \langle n|\sigma_\mu|p\rangle\langle p|\sigma_{-\mu}|n'\rangle(-)^\mu c^+_{I_nM_n}c_{I_n'M_n'}\frac{2}{2I_n+1} - \langle p'|\sigma_\mu|n\rangle\langle n|\sigma_{-\mu}|p\rangle(-)^\mu c^+_{I_{p'}M_{p'}}c_{I_pM_p}\frac{2}{2I_p+1} \\ &= 3(\hat{\mathcal{N}}_n - \hat{\mathcal{N}}_p), \end{aligned} \quad \text{(B1)}$$

where $\hat{\mathcal{N}}_n$ and $\hat{\mathcal{N}}_p$ denote the neutron and proton number operator, respectively. Averaging this equation with the pnQRPA vacuum state and then inserting between the single-β operators the unity operator defined with the phonon dipole state, we obtain

$$\begin{aligned}\sum_k\langle 0|\beta^+_\mu|1_kM_k\rangle\langle 1_kM_k|\beta^-_{-\mu}(-)^\mu|0\rangle &- \sum_k\langle 0|\beta^-_{-\mu}(-)^\mu|1_kM_k\rangle\langle 1_kM_k|\beta^+_\mu|0\rangle \\ &= 3(\langle 0|\hat{\mathcal{N}}_n|0\rangle - \langle 0|\hat{\mathcal{N}}_p|0\rangle). \end{aligned} \quad \text{(B2)}$$

Defining the single-*beta* transition strength functions as

$$\beta^{(-)} = \sum_k\langle 0||\beta^+||1_k\rangle^2, \quad \beta^{(+)} = \sum_k\langle 0||\beta^-||1_k\rangle^2, \quad \text{(B3)}$$

and approximating further the pnQRPA vacuum with the BCS vacuum, one obtains

$$\beta^{(-)} - \beta^{(+)} = 3(N-Z). \quad \text{(B4)}$$

TABLE V. Results of our calculations for the $B(E2)$ values and the half-lives of the final state 2^+, in the daughter nucleus, compared with the corresponding experimental data. Energies of the state 2^+ are also listed. The scaling factor Q_0, involved in Eq. (C1) is adimensional.

Daughter		$B(E2; 2^+ \to 0^+)$ (W.u.)		$t_{1/2}$ (ps)		
Nucleus	E_{2^+} (MeV)	Expt.	Theor.	Expt.	Theor.	Q_0
^{76}Se	0.559	44.0	43.60	12.30	12.41	2.82
^{82}Kr	0.776	21.3	12.28	4.45	7.71	1.00
^{96}Mo	0.778	20.7	19.89	3.67	3.81	1.73
^{100}Ru	0.539	0.094	38.45	12.56	11.67	2.82
^{116}Sn	1.293	12.4	11.47	0.374	13.6	1.00
^{128}Xe	0.443	48.0	34.56	18.00	25.04	2.82
^{130}Xe	0.536	38.5	41.04	8.60	7.95	2.82
^{150}Sm	0.331	57.1	30.48	48.40	98.95	2.82

The above-mentioned approximation is not valid within the present formalism. Indeed, writing the particle number operators in terms of the quasiparticle operators, one finds

$$\begin{aligned}
&(\langle 0|\hat{\mathcal{N}}_n|0\rangle - \langle 0|\hat{\mathcal{N}}_p|0\rangle) \\
&\quad = N - Z + \sum_n \frac{2}{2I_n+1}\left(U_n^2 - V_n^2\right)\sum_{M_n}\langle 0|a^+_{nM_n}a_{nM_n}|0\rangle \\
&\qquad - \sum_n \frac{2}{2I_n+1}U_nV_n \\
&\qquad \times \sum_{M_n}\langle 0|a^+_{nM_n}a^+_{n,-M_n}(-)^{M_n} + a_{n,-M_n}a_{n,M_n}(-)^{M_n}|0\rangle \\
&\qquad - \sum_p \frac{2}{2I_p+1}\left(U_p^2 - V_p^2\right)\sum_{M_p}\langle 0|a^+_{pM_p}a_{pM_p}|0\rangle \\
&\qquad + \sum_p \frac{2}{2I_p+1}U_pV_p \\
&\qquad \times \sum_{M_p}\langle 0|a^+_{pM_p}a^+_{p,-M_p}(-)^{M_p} + a_{p,-M_p}a_{p,M_p}(-)^{M_p}|0\rangle.
\end{aligned} \tag{B5}$$

Recalling that a specific feature of our formalism is that the renormalized pnQRPA vacuum state comprises quasiparticles, it becomes conspicuous that the averages involved in the above equation are nonvanishing. However, we found a dimension of the single-particle basis and a set of parameters defining the mean field and the pairing properties which provides a vanishing value for the sum of the mentioned terms in the above equation. Thus, although the present formalism is based on a renormalized pnQRPA and a boson expansion, the ISR is to high accuracy satisfied.

Since satisfying the ISR is an appraisal for the approximation quality of the proposed formalism, one may assert that the present approach is a reliable one.

APPENDIX C

The electric quadrupole transition operator is

$$Q_{2\mu} = Q^{(0)}e_{\text{eff}}\sqrt{\frac{16\pi}{5}}r^2Y_{2\mu}. \tag{C1}$$

The scaling factor $Q^{(0)}$ was introduced to account for the contribution of the core nucleons. The reduced matrix element of $Q_{2\mu}$ corresponding to the projected spherical basis is

$$\left\langle \Phi^I_{nlj}\middle|\middle|Q_2\middle|\middle|\Phi^{I'}_{n'l'j'}\right\rangle = f^{j'I'}_{jI;2}(d)\langle nlj||Q_2||n'l'j'\rangle, \tag{C2}$$

with the factor $f^{j'I'}_{jI;2}(d)$ defined as in Ref. [35] and given by Eq. (2.10). Using the second quantization representation, we have

$$\begin{aligned}
q_\mu &= C^{I_k 2 I_i}_{m_k \mu m_i} Q^{(0)} e_{\text{eff}} \langle I_i||\sqrt{\frac{16\pi}{5}}r^2Y_2||I_k\rangle c^+_i c_k \\
&\equiv q^{(2)}_{ik}(c^+_{I_i}c_{I_k})_{2\mu} \\
&= q^{(2)}_{ik}\sqrt{D_2(\tau, ik)}\bar{\mathcal{A}}^+_{2\mu}(\tau, i, k).
\end{aligned} \tag{C3}$$

From here, by simple manipulations one obtains

$$\begin{aligned}
\langle 2^+||q^{(2)}||0^+\rangle = Q^{(0)}q^{(2)}_{ik}[&e_{\text{eff}}(p)\sqrt{D_{2p}(1, ik)}X_{2p}(1, ik) \\
&+ e_{\text{eff}}(n)\sqrt{D_{2n}(1, ik)}X_{2n}(1, ik)].
\end{aligned} \tag{C4}$$

Furthermore the $B(E2)$ value is obtained from

$$B(E2; 2^+ \to 0^+) = [\langle 2^+||q^{(2)}||0^+\rangle]^2. \tag{C5}$$

TABLE VI. Results for calculated and experimental nuclear deformations compared with the deformation parameter involved in the projected spherical single-particle basis.

Daughter	β_{expt}	β	d/k
^{76}Se	0.263	0.262	0.190
^{82}Kr	0.168	0.128	0.022
^{96}Mo	0.135	0.132	0.100
^{100}Ru	0.009	0.173	0.167
^{116}Sn	0.082	0.079	0.400
^{128}Xe	0.145	0.123	0.213
^{130}Xe	0.129	0.134	0.175
^{150}Sm	0.131	0.096	0.697

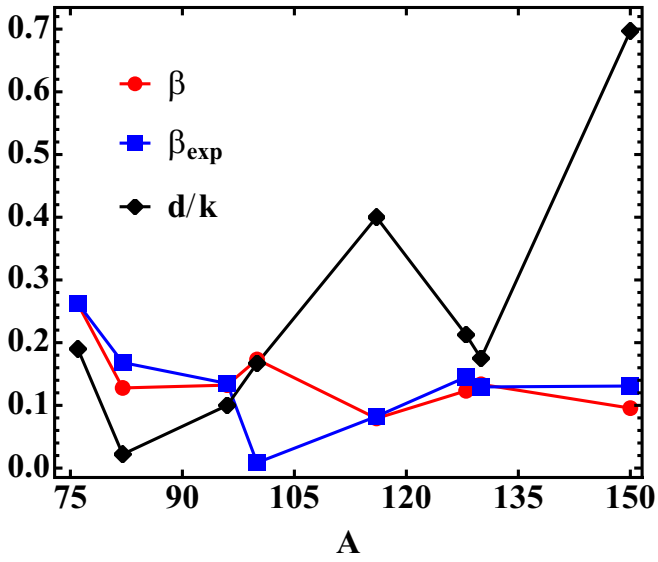

FIG. 7. Calculated and experimental nuclear deformations given by Eq. (C7) are compared with the parameter d defining the projected single-particle basis.

Using this expression the half-life of the collective state 2^+ is

$$t_{1/2} = \frac{15}{5.498} \times 10^{-21} \ln 2 \left[\frac{E_{2^+}[\text{MeV}]}{197.33}\right]^{-5} \times [B(E2; 2^+ \to 0^+)[e^2\,\text{fm}^4]]^{-1}[\text{s}]. \quad \text{(C6)}$$

Results for the $B(E2)$ values and half-lives are collected in Table V.

Having the $B(E2)$ values calculated, the nuclear deformation is readily obtained from the equation

$$\sqrt{5B(E2; 2^+ \to 0^+)} = \frac{3}{4\pi} eZR^2\beta, \quad \text{(C7)}$$

where R denotes the nuclear radius: $R = r_0 A^1/3$, $r_0 = 1.2$ fm. Similarly, by inserting in the rhs of the above equation the experimental $B(E2)$ value, one obtains the experimental nuclear deformation. The results are collected in Table VI. Note that ß agrees reasonable well with experiment. Except for the spherical nuclei ^{116}Sn and ^{150}Sm, their values are close to the parameter d/k, which defines the projected spherical single-particle basis [79]. This is shown in Fig. 7.

[1] H. Primakof and S. Rosen, Rep. Prog. Phys. **22**, 121 (1959).
[2] W. C. Haxton and G. J. Stephenson, Jr., Prog. Part. Nucl. Phys. **12**, 409 (1984).
[3] J. D. Vergados, Phys. Rep. **361**, 1 (2001).
[4] J. Suhonen and O. Civitarese, Phys. Rep. **300**, 123 (1998).
[5] T. Tomoda, Rep. Prog. Phys. **54**, 53 (1991).
[6] A. Faessler, Prog. Part. Nucl. Phys. **21**, 183 (1988).
[7] A. A. Raduta, Prog. Part. Nucl. Phys. **48**, 233 (2002).
[8] F. T. Avignone III, S. Elliot, and J. Engel, Rev. Mod. Phys. **80**, 481 (2008).
[9] A. S. Barabash, Phys. Rev. C **81**, 035501 (2010).
[10] B. Pritychenko, Nucl. Data Sheets **120**, 102 (2014).
[11] Y. K. Singh, R. Chandra, P. K. Raina, and P. K. Rath, Eur. Phys. J. **53**, 244 (2017).
[12] A. A. Raduta, A. Faessler, and S. Stoica, Nucl. Phys. A **534**, 149 (1991).
[13] A. A. Raduta, A. Faessler, S. Stoica, and W. Kaminsky, Phys. Lett. B **254**, 7 (1991).
[14] J. Toivanen and J. Suhonen, Phys. Rev. Lett. **75**, 410 (1995).
[15] A. A. Raduta, C. M. Raduta, W. Kaminski, and A. Faessler, Nucl. Phys. A **634**, 497 (1998).
[16] M. J. Hornish, L. De Braeckeleer, A. S. Barabash, and V. I. Umatov, Phys. Rev. C **74**, 044314 (2006).
[17] M. Agostini *et al.* (GERDA Collaboration), J. Phys. G: Nucl. Part. Phys. **42**, 115201 (2015).
[18] J. W. Beeman *et al.*, Eur. Phys. J. C **75**, 591 (2015).
[19] A. S. Barabash *et al.*, J. Phys. G: Nucl. Part. Phys. **22**, 487 (1996).
[20] R. Arnold *et al.*, Nucl. Phys. A **925**, 25 (2014).
[21] A. Piepke *et al.*, Nucl. Phys. A **577**, 493 (1994).
[22] E. Bellotti *et al.*, Europhys. Lett. **3**, 889 (1987).
[23] P. Belli *et al.*, Universe **6**, 239 (2020).
[24] K. Asakura *et al.*, Nucl. Phys. A **946**, 171 (2016).
[25] R. Saakyan, Annu. Rev. Nucl. Part. Sci. **63**, 503 (2013).
[26] K. Nakamura *et al.*, J. Phys. G: Nucl. Part. Phys. **37**, 075021 (2010).
[27] A. S. Barabash, in *Workshop on Calculation of Double-Beta-Decay Matrix Elements (MEDEX'17)*, edited by O. Civitarese, I. Stekl, and J. Suhonen, AIP Conf. Proc. No. 1894 (AIP, New York, 2017), p. 020002.
[28] I. J. Arnquist *et al.*, Phys. Rev. C **103**, 015501 (2021).
[29] S. Unlu, Chin. Phys. Lett. **31**, 042101 (2014).
[30] A. Armatol *et al.* (NEMO-3 Collaboration), Nucl. Phys. A **996**, 121701 (2020).
[31] A. S. Barabash, P. Hubert, A. Nachab, and V. I. Umatov, Phys. Rev. C **79**, 045501 (2009).
[32] R. YkeJiao and R. Zhong-Zhou, Sci. China Phys. Mech. Astron. **58**, 012002 (2015).
[33] K. Blaum, S. Eliseev, F. A. Danevich, V. I. Tretyak, S. Kovalenko, M. I. Krivoruchenko, Y. N. Novikov, and J. Suhonen, Rev. Mod. Phys. **92**, 045007 (2020).
[34] P. Ring and P. Schuck, *The Nuclear Many-Body Problem*, (Springer, Berlin, 2000), p. 447.
[35] A. A. Raduta, D. S. Delion, and N. Lo Iudice, Nucl. Phys. A **564**, 185 (2000).
[36] A. A. Raduta, N. Lo Iudice, and I. I. Ursu, Nucl. Phys. A **584**, 84 (1995).
[37] A. A. Raduta, A. Escuderos, and E. Moya de Guerra, Phys. Rev. C **65**, 024312 (2002).
[38] A. A. Raduta, A. Escuderos, A. Faessler, E. Moya de Guerra, and P. Sarriguren, Phys. Rev. C **69**, 064321 (2004).
[39] A. A. Raduta, C. M. Raduta, and A. Escuderos, Phys. Rev. C **71**, 024307 (2005).
[40] A. A. Raduta, A. Faessler, and D. S. Delion, Phys. Lett. B **312**, 13 (1993).
[41] A. A. Raduta, D. S. Delion, and A. Faessler, Nucl. Phys. A **617**, 176 (1997).
[42] L. Zamick and N. Auerbach, Phys. Rev. C **26**, 2185 (1982).

[43] R. Álvarez-Rodríguez, P. Sarriguren, E. Moya de Guerra, L. Pacearescu, A. Faessler, and F. Simkovic, Phys. Rev. C **70**, 064309 (2004).

[44] F. Šimkovic, L. Pacearescu, and A. Faessler, Nucl. Phys. A **733**, 321 (2004).

[45] O. Moreno, R. Alvarez-Rodriguez, P. Sarriguren, E. M. de Guerra, F. Simkovic, and A. Faessler, J. Phys. G: Nucl. Part. Phys. **36**, 015106 (2009).

[46] M. S. Yousef, V. Rodin, A. Faessler, and F. Simkovic, Phys. Rev. C **79**, 014314 (2009).

[47] D.-L. Fang, A. Faessler, V. Rodin, and F. Simkovic, Phys. Rev. C **83**, 034320 (2011).

[48] M. T. Mustonen and J. Engel, Phys. Rev. C **87**, 064302 (2013).

[49] D. Navas-Nicolas and P. Sarriguren, Phys. Rev. C **91**, 024317 (2015).

[50] P. Sarriguren, O. Moreno, and E. Moya de Guerra, Adv. High Energy Phys. **2016**, 6391052 (2016).

[51] S. Unlu and N. Cakmak, Acta Phys. Pol. B **53**, 3-A3 (2022).

[52] S. G. Nilsson, Mat. Fys. Medd. K. Dan. Vidensk. Selsk. **29**, 16 (1955).

[53] A. A. Raduta, F. Simkovich, and A. Faessler, J. Phys. G: Nucl. Part. Phys. **26**, 793 (2000).

[54] M. E. Rose, *Elementary Theory of Angular Momentum* (Wiley, New York, 1957).

[55] P. Ring and P. Schuck, *The Nuclear Many-Body Problem* (Springer, Berlin, 2000), p. 236.

[56] C. M. Raduta, A. A. Raduta, and I. I. Ursu, Phys. Rev. C **84**, 064322 (2011).

[57] E. Kolbe, K. Langanke, F. K. Thielemann, and P. Vogel, Phys. Rev. C **52**, 3437 (1995).

[58] C. M. Raduta and A. A. Raduta, Phys. Rev. C **76**, 044306 (2007).

[59] J. Toivanen and J. Suhonen, Phys. Rev. C **55**, 2314 (1997).

[60] M. Aunola and J. Suhonen, Nucl. Phys. A **602**, 133 (1996).

[61] H. Ejiri *et al.*, Phys. Lett. B **258**, 17 (1991).

[62] H. V. Klapdor and K. Grotz, Phys. Lett. B **142**, 323 (1984).

[63] S. W. Hennecke, O. K. Emanuel, and D. D. Sabu, Phys. Rev. **11**, 1378 (1975).

[64] J. G. Hirsch, O. Castanos, P. O. Hess, and O. Civitarese, Phys. Rev. C **51**, 2252 (1995).

[65] N. I. Pyatov and D. I. Salamov, Nucleonica **22**, 127 (1977).

[66] R. Madey, B. S. Flanders, B. D. Anderson, A. R. Baldwin, J. W. Watson, S. M. Austin, C. C. Foster, H. V. Klapdor, and K. Grotz, Phys. Rev. C **40**, 540 (1989).

[67] B. Sinh and J. Chen, Nuclear Data Sheets **172**, 1 (2021).

[68] V. Guadilla, A. Algora, J. L. Tain, J. Agramunt, D. Jordan, A. Montaner-Piza, S. E. A. Orrigo, B. Rubio, E. Valencia, J. Suhonen, O. Civitarese, J. Aysto, J. A. Briz, A. Cucoanes, T. Eronen, M. Estienne, M. Fallot, L. M. Fraile, E. Ganioglu, W. Gelletly, D. Gorelov, J. Hakala, A. Jokinen, A. Kankainen, V. Kolhinen, J. Koponen, M. Lebois, T. Martinez, M. Monserrate, I. Moore, E. Nacher, H. Penttila, I. Pohjalainen, A. Porta, J. Reinikainen, M. Reponen, S. Rinta-Antila, K. Rytkonen, T. Shiba, V. Sonnenschein, A. A. Sonzogni, V. Vedia, A. Voss, J. N. Wilson, and A. A. Zakari-Issoufou, Phys. Rev. C **96**, 014319 (2017).

[69] J. Blachot, Nuclear Data Sheets **111**, 717 (2010).

[70] Z. Elekes and J. Timar, Nuclear Data Sheets **129**, 191 (2015).

[71] M. Kanbe and K. Kitao, Nucl. Data Sheets **94**, 227 (2001).

[72] C. M. Lederer and V. S. Shirley, *Table of Isotopes*, 7th ed. (Wiley, New York, 1978), p. 631.

[73] S. K. Basu and A. A. Sonzogni, Nuclear Data Sheets **114**, 435 (2013).

[74] R. Helmer *et al.*, Phys. Rev. C **55**, 2802 (1997).

[75] H. Akimune *et al.*, Phys. Lett. B **394**, 23 (1997).

[76] W. Thomas, Naturwissenschaften **13**, 627 (1925).

[77] F. Reiche and W. Thomas, Z. Phys. **34**, 510 (1925).

[78] W. Kuhn, Z. Phys. **33**, 408 (1925).

[79] N. Lo Iudice, A. A. Raduta, and D. S. Delion, Phys. Rev. C **50**, 127 (1994).

Microscopic description of the Pygmy and Giant Dipole Resonances in even-even nuclei. Application to the isotopes ^{150,152,154,156,158,160}Gd.

A. A. Raduta[a),b)], C. M. Raduta [a)] and R. Poenaru [a)]
[a)] *Department of Theoretical Physics, Institute of Physics and Nuclear Engineering, Bucharest, POBox MG6, Romania and*
[b)] *Academy of Romanian Scientists, 54 Splaiul Independentei, Bucharest 050094, Romania*

A many body Hamiltonian consisting of a spherical shell model mean field term, a pairing interaction for alike nucleons and a dipole-dipole interaction, with the dipole operator involving a cubic term in the radial coordinate, is studied within a quasiparticle random phase approximation (QRPA) and applied numerically to six even-even isotopes of Gd.The resulting wave functions are further used to calculate the B(E1) values as well as the energy weighted sum rule (EWSR). One distinguishes two regions corresponding to the Pygmy Dipole Resonance (PDR),[0,10] MeV, and to the Giant Dipole Resonance (GDR), [10,20] MeV, respectively. The dipole strength distribution with energy is plotted for the PDR region. The dominant transitions have an isovector character for three isotopes and isoscalar for another three. The PDR states carry only 1.15-3.1% of the total EWSR. The dependence of the dipole strength on nuclear deformation is evidenced. For the whole interval of [0,20] MeV the dipole strength was first folded by Lorentzians of 1 MeV width and then plotted as function of the QRPA energies. The peaks belonging to each of the two ranges are analyzed in detail and their nature, isovector/isoscalar, was pointed out. The r-cubic term and the nuclear deformation have opposite effects on the dipole strength. The famous Thomas Reiche Kuhn sum rule formula is generalized to the case of the Schiff dipole momentum. The new EWSR is very well satisfied. The photoabsorbtion cross section is calculated and compared with experimental data in a figure showing its dependence on energy. The total cross section is also calculated. The main features of PDR and GDR are realistically described.

I. INTRODUCTION

Since the pioneering paper of Goldhaber and Teller [1] describing the giant dipole resonance (GDR) as a linear out of phase oscillation of neutrons and protons respectively, showed up [2], many papers have been devoted to the study of the relative motion of protons and neutrons [3–5]. One of the hot subject of the last decades is that of Pygmy dipole resonance (PDR), which appears at an energy lower than the GDR peak, around the neutron emission energy threshold. It is commonly accepted that such a resonance is determined by the neutron excess oscillation against the protons from an isospin saturated core [6, 7].

The presence of the PDR in nuclei with neutrons excess could be related with the symmetry energy parameters. Several attempts have been made to use the PDR data to constrain the symmetry energy and extract a relation with the neutron skin thickness in neutron rich nuclei. The neutron skin thickness is defined as the difference between the root mean square of neutron and proton radii: $r_{skin} = r^n_{rms} - r^p_{rms}$. There exists a strong correlation between neutron skin thickness and the dipole polarizability defined as:

$$\alpha_D = \frac{8\pi e^2}{9} m_{-1}(E1), \tag{2.1}$$

where $m_{-1}(E1)$ denotes the sum of the inverse energy weighted dipole strengths. The product $\alpha_D \mathcal{J}$, with $\mathcal{J}$ standing for the symmetry energy at saturation density, is related with the neutron skin thickness r_{skin} and with the slope of the symmetry energy at the saturation density, L [8]. Therefore, a precise measurement of α_D would allow to determine a relation between the symmetry energy $\mathcal{J}$ and the slope L, which, of course, improves our knowledge about the symmetry energy.

Pygmy resonance in neutron rich nuclei is an important topic of study at the new generation of radioactive ion beam facilities [9, 12]. Furthermore, important nuclear-structure effects have to be taken into account in order to interpret results obtained in the next generation of neutrinoless double-beta decay ($0\nu\beta\beta$) experiments. Knowledge of the nuclear matrix elements, governed by the PDR, for example, will be indispensable for reliably deducing the effective Majorana mass.

The knowledge of the electromagnetic transition strength is very important for the calculation of the neutron capture rates in the r-process (rapid neutron capture process), a phenomenon which competes with the β decay and is responsible for producing about half of the heavy elements. The Pygmy resonance taking place near the neutron threshold has also important astrophysical implications. Indeed, the reaction rates of (γ,n) and (n,γ) reactions in explosive nucleosynthesis of certain neutron deficient nuclei may be significantly enhanced by the PDR [9].

Experimentally, the PDR are studied by: a) isovector probes like i) Relativistic Coulomb excitation; ii) Nuclear Resonance Fluorescence technique, (γ, γ'); iii) Coulomb excitations by (p,p') scattering [10]; b) isoscalar probes like:

(α,α')[11]; (^{17}O,^{17}O'); (^{68}Ni,^{68}Ni' γ). The PDR states split into two parts, one belonging to an energy range between 4 and 6 MeV, which is excited in $(\alpha,\alpha'\gamma)$ as well as (γ,γ') experiments, and one part at higher energy, excited only in (γ,γ'). This phenomenon is known under the name of isospin splitting or of isospin mixing.

Many theoretical approaches have been used to reveal various properties of the PDR. To save the space here we mention only few of them. Thus, the isoscalar dipole strength distribution was studied within a self-consistent RPA approach in Ref. [15] . Also, in Ref. [16] starting with the Skyrme mean field calculation, some properties of the electric dipole strength in Ca isotopes are studied by taking into account the coupling of one and two phonon terms in the wave functions of the excited states. Such a coupling was also used in Ref.[17] to describe the fine structure of the giant resonance. The effect of center of mass motion on the structure of the Pygmy dipole resonance was removed in Ref.[18] for some even-even isotopes of Gd. Calculation performed within Hartree Fock Bogoliubov (HFB) plus quasiparticle random phase approximation (QRPA), with Skyrme interaction for Nd and Sm isotopes, the summed dipole strength dependence on nuclear deformation has been studied [19]. In Ref.[20] it was shown that the isoscalar dipole strength distribution contributes to the Schiff moment. The PDR in ^{154}Sm was also studied in Ref.[21]. The spectral statistics and the fine structure of the Pygmy dipole resonance in the isotones with N=82 has been studied in Ref.[22]. The relativistic random phase approximations (RRPA) was used for describing some features of the PDR[23, 24]. Solving the self-consistent Landau-Vlasov equation, the dependence of the PDR properties on the symmetry energy has been explored. Also, the existence of a isoscalar dipole mode below the GDR has been pointed out [25, 26].

In the present paper we propose a formalism for describing the properties of the PDR states. The main ingredients of our approach consist of using a projected spherical single particle basis as well as of a Schiff dipole momentum in the dipole-dipole interaction. The paper is organized as follows: In section 2 we introduce the single particle basis states, which is used for treating a many body Hamiltonian, presented in Section 3, through a QRPA method. The electric dipole transition probability is considered in Section 4. Section 5 is devoted to the description of the energy weighted sum rule (EWSR), while Section 6 presents the results of a numerical application to the isotopes ^{150,152,154,156,158,160}Gd. Section 7 summarizes the main conclusions.

II. PROJECTED SPHERICAL SINGLE PARTICLE BASIS

In this paper a projected single particle basis will be used to describe the dipole excitations. This was previously defined in Ref. [24] and used for studying the magnetic states of scissors type [24-26] as well as to evaluate the transition rate of a double beta decay process [27-29, 35]. A few words about the underlying ingredients of the mentioned basis are necessary. Thus, it is obtained by projecting out the good angular momentum components from a deformed particle-core wave function:

$$\Psi^{pc}_{nlj} = |nljm\rangle\Psi_g(d), \tag{2.1}$$

where $\Psi_g(d)$ is a quadrupole deformed coherent state, which describes phenomenologically a core, while $|nljm\rangle$ is a spherical shell model function, with the standard notation for the defining quantum numbers. Acting on this state with the projection operator P^J_{MK}, one obtains a set of wave functions of good angular momentum. From this set we subtract a subset which exhibits very useful properties:

$$\Phi^{IM}_{nlj}(d) = \mathcal{N}^I_{nlj}P^I_{MI}[|nljI\rangle\Psi_g] \equiv \mathcal{N}^I_{nlj}\Psi^{IM}_{nlj}(d). \tag{2.2}$$

Indeed, this subset is orthonormal and constitutes a basis for the particle-core system. Moreover, this can be used as a single particle basis for treating a many body Hamiltonian involving both a one and a two body interaction. Details about this feature may be found in Refs. [33, 34]. To each of the involved state one associates a single particle energy, defined by averaging a Hamiltonian involving a spherical mean field term and a particle-core interaction of monopole-monopole plus quadrupole-quadrupole type, with the angular momentum projected state:

$$\epsilon^I_{nlj} \;=\; \langle\Phi^{IM}_{nlj}(d)|H'|\Phi^{IM}_{nlj}(d)\rangle. \tag{2.3}$$

One obtains an expression depending on the parameter d which simulates the nuclear deformation. It is remarkable the fact that the new single particle energies depend on the deformation parameter d in a similar way as the Nilsson model energies depend on the nuclear deformation. Note that the angular momentum I plays the role of the Nilsson quantum number Ω. The difference is that, while the Ω states are double degenerate, the I states have $(2I+1)$ degenerate sub-states. This inconsistency can be removed by changing the normalization of the wave functions in the following manner:

$$\langle\Phi^{IM}_{\alpha}|\Phi^{IM}_{\alpha}\rangle = 1 \Longrightarrow \sum_M\langle\Phi^{IM}_{\alpha}|\Phi^{IM}_{\alpha}\rangle = 2. \tag{2.4}$$

As seen in (2.2), the deformation of the projected state is generated by a deformed core. This is also reflected in the structure of the matrix elements. Indeed, in calculating the matrix element of a particle-like operator, one first integrates over the core collective, and then on the particle coordinates. As a result one gets a factorized form, one factor being the matrix element of the chosen operator between spherical shell model states, and one carrying the dependence on the deformation parameter d. In fact, this is a specific feature of the proposed projected spherical single particle basis.

Concluding, the projected single particle basis is defined by Eq. (2.2) and corresponds to the energies given by (2.3). In order to have a full picture of the above defined basis and, moreover, to get a flavor of its usefulness in studying the spherical, transitional and well deformed nuclei in an unified fashion, we advise the reader to consult Ref. [33].

III. THE MODEL HAMILTONIAN

Within the second quantization adapted to the projected spherical single particle basis, the many-body Hamiltonian suitable for describing the states participating to the dipole excitation looks like:

$$H = \sum_{\tau,\alpha,I,M} \frac{2}{2I+1}(\epsilon_{\tau\alpha I} - \lambda_{\tau\alpha}) c^{\dagger}_{\tau\alpha IM} c_{\tau\alpha IM} \tag{3.1}$$
$$- \sum_{\tau,\alpha,I,I'} \frac{G_\tau}{4} P^{\dagger}_{\tau\alpha I} P_{\tau\alpha I'} - \sum_{\tau ab;\tau' cd;\mu} X_{\tau,\tau'} D_{1\mu}(\tau; ab) D_{1,-\mu}(\tau'; cd)(-)^{\mu},$$

where the notations $c^{\dagger}_{\tau\alpha,IM}$ ($c_{\tau\alpha,IM}$) stand for the creation (annihilation) operator for one particle of the type τ(=p,n) in the state Φ^{IM}_{α}, with α being an abbreviation for the spherical shell model quantum numbers nlj. The terms involved in the model Hamiltonian are associated to the mean field, to the pairing interaction and to the Schiff dipole-dipole interaction, respectively.

In order to save the space, in what follows the set of quantum numbers α is omitted. The two body interactions are separable with the factors defined by the following expressions:

$$P^{\dagger}_{\tau I} = \sum_{M} \frac{2}{2I+1} c^{\dagger}_{\tau IM} \widetilde{c^{\dagger}_{\tau IM}}, \tag{3.2}$$

$$D_{1\mu}(\tau; II') = \tag{3.3}$$
$$\sum_{M,M'} \frac{\sqrt{2}}{\hat{I}} \langle \tau; IM | (r - \frac{3}{5}\frac{r^3}{b^2}) Y_{1\mu} | \tau; I'M' \rangle \frac{\sqrt{2}}{\hat{I}'} c^{\dagger}_{\tau;IM} c^{\dagger}_{\tau;I'M'} \equiv d_1(\tau; II') \left(c^{\dagger}_{\tau;I} c_{\tau;I'} \right)_{1\mu},$$

where:

$$d_1(\tau; II') = \frac{2}{\hat{1}\hat{I}'} \mathcal{N}^{I}_{nlj}(d) \mathcal{N}^{I'}_{n'l'j'}(d) \tag{3.4}$$
$$\times \sum_{J} C^{j\ J\ I}_{I\ 0\ I} C^{j\ J\ I'}_{I'\ 0\ I'} W(j1JI'; j'I) \left(N^{(g)}_{J}(d) \right)^{-2} \langle nlj || \left(r - \frac{3}{5}\frac{r^3}{b^2} \right) Y_{1\mu} || n'l'j' \rangle.$$

The dipole operator involves the oscillator length denoted by $b = \sqrt{\frac{\hbar}{M\omega}}$. Also, the norm of the core projected states are denoted by $N^{(g)}_{J}(d)$. Note that the matrix element of the Schiff dipole operator is a product of two factors, one carrying the deformation dependence and one being a matrix element corresponding to the standard spherical shell model states.

We may ask ourselves why do we use the Schiff dipole operator instead of the standard form, linear in r, showing up naturally as the first order expansion of the Coulomb interaction between the charge of the target nucleus and the electric field generated by the projectile. To answer this question we first notice that the corrective term and the standard dipole term have opposite phases, and by this it induces a screening effect on the transition matrix elements. On the other hand this term is the one which generates $\Delta N = 3$ transitions which, as we shall see later, are relevant for the considered resonances. It is conspicuous that the Hamiltonian (3.2) does not commute with the center of mass linear momentum and, consequently, this magnitude is not conserved. However, the contribution to the H energies, of the spurious components of the wave function, due to the center of mass linear momentum non-conservation, is small, of the order of $1/A$, with A denoting the atomic mass number [42, 43]. This small contribution is still diminished by

the presence of the cubic term in the expression of the Schiff dipole operator. Two of the present team (AAR and AlHR) used a Schiff-type dipole transition operator for the description of the photoabsorbtion cross-section spectra in the medium atomic clusters of Na [44]. Therein, a good agreement with the experimental data was pointed out.

The first two terms of the model Hamiltonian are treated through the BCS formalism, defined by the Bogoliubov-Valatin transformation:

$$\begin{aligned} & a^{\dagger}_{\tau IM} = U_{\tau I} c^{\dagger}_{\tau IM} - s_{IM} V_{\tau I} c_{\tau I-M}, \;\; s_{IM} = (-)^{I-M}, \\ & U^2_{\tau I} + V^2_{\tau I} = 1, \;\; \tau = p, n, \end{aligned} \tag{3.5}$$

which results in replacing them by the diagonal form $\sum E_{\tau} a^{\dagger}_{\tau IM} a_{\tau IM}$, where E_{τ} denotes the quasiparticle energy. In its turn, the dipole-dipole interaction is expressed in terms of the dipole two qp and the qp density operators:

$$\begin{aligned} A^{\dagger}_{1\mu}(\tau; II') &= \sum C^{I\; I'\; 1}_{m\; m'\; \mu} a^{\dagger}_{\tau;Im} a^{\dagger}_{\tau;I'm'}, \\ A_{1\mu}(\tau; II') &= \left(A^{\dagger}_{1\mu}(\tau; II') \right)^{\dagger}, \\ B^{\dagger}_{1\mu}(\tau; II') &= \sum C^{I\; I'\; 1}_{m\; -m\; \mu} a^{\dagger}_{\tau;Im} a_{\tau;I'm'} (-)^{I'-m'}, \\ B_{1\mu}(\tau; II') &= \left(B^{\dagger}_{1\mu}(II') \right)^{\dagger}. \end{aligned} \tag{3.6}$$

Thus, the Schiff dipole operator acquires the form:

$$\begin{aligned} D_{1\mu}(\tau; II') = & \sum_{E_{\tau I} < E_{\tau I'}} d_1(\tau; II') \Big[\xi^{(-)}(\tau, II') \left(A^{\dagger}_{1\mu}(\tau; II') - (-)^{1-\mu} A_{1,-\mu}(\tau; II') \right) \\ + \;\; & \eta^{(-)}(\tau, II') \left(B^{\dagger}_{1\mu}(\tau; II') - (-)^{1-\mu} B_{1,-\mu}(\tau; II') \right) \Big], \\ & \xi^{(-)}(\tau, II') = U_{\tau I} V_{\tau I'} - U_{\tau I'} V_{\tau I}, \;\; \eta^{(-)}(\tau, II') = U_{\tau I} U_{\tau I'} - V_{\tau I} V_{\tau I'}. \end{aligned}$$

With a quasi-boson approximation for the above defined dipole operators, the quasiparticle random phase approximation (QRPA) is introduced by looking for the phonon operator:

$$\Gamma^{\dagger}_{1\mu} = \sum_{\tau; II'} \left[X(\tau; II') A^{\dagger}_{1\mu}(\tau; II') + Y(\tau; II') (-)^{1-\mu} A_{1,-\mu}(\tau; II') \right], \tag{3.7}$$

which satisfies the restrictions:

$$\left[H, \Gamma^{\dagger}_{1\mu} \right] = \omega \Gamma^{\dagger}_{1\mu}, \;\; \left[\Gamma_{1\mu}, \Gamma^{\dagger}_{1\mu'} \right] = \delta_{\mu,\mu'}. \tag{3.8}$$

The first relation (3.8) leads to the QRPA equation:

$$\begin{pmatrix} \mathcal{A} & \mathcal{B} \\ -\mathcal{B} & -\mathcal{A} \end{pmatrix} \begin{pmatrix} X(\tau; II') \\ Y(\tau; II')) \end{pmatrix} = \omega \begin{pmatrix} X(\tau; II') \\ Y(\tau; II') \end{pmatrix}. \tag{3.9}$$

To simplify the notations, we abbreviate the set of quantum numbers τI by a and the two quasiparticle energies $E_a + E_b$ by E_{ab}. Thus, the QRPA matrices acquire a compact form:

$$\begin{aligned} \mathcal{A}_{ab;a'b'} &= E_{ab} \delta_{aa'} \delta_{bb'} - \frac{X_{\tau,\tau'}}{2} d_1(ab) \xi^{(-)}(ab) d_1(a'b') \xi^{(-)}(a'b'), \\ \mathcal{B}_{ab;a'b'} &= \frac{X_{\tau,\tau'}}{2} d_1(ab) \xi^{(-)}(ab) d_1(a'b') \xi^{(-)}(a'b'). \end{aligned}$$

The equation (3.9) determines the amplitudes X and Y up to a multiplicative factor which that has to be determined by the second equation (3.8), which can be written as:

$$\sum_{\substack{a,b \\ E_a < E_b}} \left(X(ab)^2 - Y(ab)^2 \right) = 1. \tag{3.10}$$

Since the dipole-dipole interaction is separable, the compatibility condition for the homogeneous linear equations provides an equation for ω. Also, the QRPA amplitudes can be analytically expressed.

IV. ELECTRIC DIPOLE TRANSITIONS

The dipole transition operator is:

$$E_{1\mu} = \sqrt{\frac{4\pi}{3}} e \left(r - \frac{3}{5} \frac{r^3}{b^2} \right) Y_{1\mu}. \tag{4.1}$$

In the quasiparticle representation, for a system of Z protons and N neutrons, this operator acquires the form:

$$\begin{aligned} E_{1\mu} &= \sqrt{\frac{4\pi}{3}} \left[e^{(p)}_{eff} \sum_{E_a<E_b} d_1(p;ab)\xi^{(-)}(p,ab) \left(A^{\dagger}_{1\mu}(p,ab) - (-)^{1-\mu} A_{1,-\mu}(p,ab) \right) \right. \\ &+ \left. e^{(n)}_{eff} \sum_{E_a<E_b} d_1(n;ab)\xi^{(-)}(n,ab) \left(A^{\dagger}_{1\mu}(n,ab) - (-)^{1-\mu} A_{1,-\mu}(n,ab) \right) \right], \end{aligned} \tag{4.2}$$

where $e^{(p)}_{eff}$ and $e^{(n)}_{eff}$ denote the effective charge for protons and neutrons, respectively. The reduced dipole transition probability from the QRPA ground state $|0\rangle$ to the dipole state $|1_k,\mu\rangle$ corresponding to the k-th root of the QRPA equations, has the expression:

$$\begin{aligned} &B(E1;0^+ \to 1^-_k) = \left(\langle 0||E_1||1_k\rangle \right)^2 = 4\pi \\ &\times \left[\sum_{E_a<E_b} d_1(p;ab)\xi^{(-)}(p,ab) \left(X_k(p,ab) + Y_k(p,ab) \right) \sum_{E_a<E_b} d_1(n;ab)\xi^{(-)}(n,ab) \left(X_k(n,ab) + Y_k(n,ab) \right) \right]^2 . \end{aligned} \tag{4.3}$$

The effective charges which take care of the center of mass momentum conservation as well as of the polarization effect induced by the charged particles motion are:

$$e^{(p)}_{eff} = \frac{N}{A}, \;\; e^{(n)}_{eff} = -\frac{Z}{A}. \tag{4.4}$$

V. THE ENERGY WEIGHTED SUM RULE (EWSR)

Here we evaluate the sum of the weighted reduced dipole transition probabilities:

$$\begin{aligned} S_l &= \sum_k \omega_k B(E1;0^+ \to 1^-_k) = 3 \sum_{k,\mu} \omega_k |\langle 1_k\mu | E_{1\mu} | 0\rangle|^2 \\ &= 3 \sum_{n,\mu} \omega_k \langle 0 | E_{1,-\mu} (-)^{\mu} | 1_n\mu\rangle \langle 1_n\mu | E_{1\mu} | 0\rangle \\ &= \frac{3}{2} \sum_{\mu} \langle 0 | \left[E_{1\mu}, [H, E_{1,-\mu}(-)^{\mu}] \right] | 0\rangle. \end{aligned} \tag{5.1}$$

Here, ω_k (k$\neq 0$) denotes the k-th QRPA energy, which corresponds to the eigenstate $|1_k\mu\rangle$. H is the model Hamiltonian defined by Eq. (3.2). Note that to the commutators involved in Eq.(5.1) only one term of H does contribute, namely the kinetic energy $\sum_{i=1}^{A} \frac{p_i^2}{2M}$, with M denoting the nucleon mass. Let us denote the last term of Eq.(5.1) by S_r. By direct and cumbersome manipulations one arrives at the following expression:

$$\begin{aligned} &S_r = \frac{27\hbar^2}{2M} \\ &\times \left\{ (e^p_{eff})^2 \left[Z - 2 \sum_{i=1}^{Z} \langle 0 | \frac{r_i^2}{b^2} | 0\rangle + \frac{33}{25} \sum_{i=1}^{Z} \langle 0 | \frac{r_i^4}{b^4} | 0\rangle \right] \right. \\ &\times \left. (e^n_{eff})^2 \left[N - 2 \sum_{i=1}^{N} \langle 0 | \frac{r_i^2}{b^2} | 0\rangle + \frac{33}{25} \sum_{i=1}^{N} \langle 0 | \frac{r_i^4}{b^4} | 0\rangle \right] \right\}. \end{aligned} \tag{5.2}$$

Note that if instead of the Schiff dipole momentum the standard one was used, then in the last expression of S_r only the first term would survive, which results in getting the famous sum rule of Thomas-Reiche-Kuhn (TRK)[46–48]:

$$S_{TRK} = \frac{27\hbar^2}{2M}\frac{ZN}{A}. \tag{5.3}$$

This sum rule is model independent and is obtained by an exact evaluation of the double commutators from Eq. (5.1). When $S_l = S_{TRK}$, one says that the EWSR is satisfied. The accuracy of the sum rule obedience is actually a measure of the adopted approximation consistency. In this paper we shall analyze the contribution of the major humps in the E1 strength distribution to the EWSR.

The last two terms from Eq.(5.3) are due to the cubic term in the radial coordinate. These can be calculated either based on microscopic ground or phenomenologically. Here we adopt the first option and we start by noticing that:

$$\begin{aligned}
\langle o|r_\tau^2|0\rangle &= \sum_{k,mu}\langle o|(r_\tau)_{1,-\mu}(-1)^\mu|1_k,\mu\rangle\langle_k,\mu|(r_\tau)_{1\mu}|0\rangle, \\
\langle o|r_\tau^4|0\rangle &= \left(\sum_{k,mu}\langle o|(r_\tau)_{1,-\mu}(-1)^\mu|1_k,\mu\rangle\langle_k,\mu|(r_\tau)_{1\mu}|0\rangle\right)^2, \quad \tau = p,n.
\end{aligned} \tag{5.4}$$

Inserting the matrix elements for the proton and neutron dipole operators, the expression of S_r becomes:

$$\begin{aligned}
S_{cor} &= \frac{27\hbar^2}{2M}\left\{\frac{ZN}{A} - \frac{8\pi}{3b^2}\frac{N^2}{A^2}\sum_k\left[\sum_{E_a<E_b} d(p;ab)\xi^{(-)}(p,ab)\left(X_k(p,ab)+Y_k(p,ab)\right)\right]^2\right. \\
&- \frac{8\pi}{3b^2}\frac{Z^2}{A^2}\sum_k\left[\sum_{E_a<E_b} d(n;ab)\xi^{(-)}(n,ab)\left(X_k(n,ab)+Y_k(n,ab)\right)\right]^2 \\
&+ \frac{16\pi^2}{9b^4}\frac{N^2}{A^2}\frac{33}{25}\sum_k\left[\sum_{E_a<E_b} d(p;ab)\xi^{(-)}(p,ab)\left(X_k(p,ab)+Y_k(p,ab)\right)\right]^4 \\
&+ \left.\frac{16\pi^2}{9b^4}\frac{Z^2}{A^2}\frac{33}{25}\sum_k\left[\sum_{E_a<E_b} d(n;ab)\xi^{(-)}(n,ab)\left(X_k(n,ab)+Y_k(n,ab)\right)\right]^4\right\},
\end{aligned} \tag{5.5}$$

where the factor $d(\tau, ab)$ is obtained from Eq.(3.5) restricting in the last factor, the Schiff momentum to the linear term in the radial coordinate. Note that the above expression is fully consistent with the dipole strength. Indeed in both cases the transition operator is the same, i.e., the Schiff momentum.

VI. NUMERICAL RESULTS

The formalism presented in the previous sections was applied to six even-even isotopes of Gd, ^{150,152,154,156,158,160}Gd. The spherical shell model single particle basis is defined by using the parameters given in Ref.[35]:

$$\hbar\omega_0 = 41A^{-1/3},\ C = -2\hbar\omega_0\kappa,\ D = -\hbar\Omega_0\mu. \tag{6.1}$$

The parameters $(\kappa;\mu)$ for proton and neutron systems are those given in Refs.[35, 37]. The proton and neutron pairing strengths are taken as:

$$G_p = \frac{23}{A},\ \ G_n = \frac{22}{A}, \tag{6.2}$$

where A is the atomic mass number. The BCS equations were solved using 92 states, both for protons and neutrons.

The projected spherical single particle basis depends on two parameters, namely the deformation d and the parameter k relating the quadrupole boson operator and the quadrupole collective coordinate. These deformation parameters were taken as in Ref.[49]. Their connection with the deformation β was in extenso studied in Refs.[40, 41, 50]. As proved in Ref.[50], the deformation parameter d and the nuclear deformation β are related by:

Nucleus	d	k	$X_{PP}=X_{NN}$ [MeV.fm^{-2}]	$X_{PN}=X_{NP}$ [MeV.fm^{-2}]	$N_{d,p}$	$N_{d,n}$
^{150}Gd	0.8	5.9	0.0120	0.0150	258	292
^{152}Gd	1.7	9.55	0.0190	0.0270	266	292
^{154}Gd	2.6	11.4	0.0175	0.0255	266	299
^{156}Gd	2.95	11.09	0.0172	0.0254	266	299
^{158}Gd	3.3	11.7	0.0181	0.0271	256	290
^{160}Gd	3.4	11.49	0.0175	0.0265	264	290

TABLE I: The strength of the dipole-dipole interaction, X_{PP} and X_{PN}, and the number of the dipole configurations for proton ($N_{d,p}$) and neutron ($N_{d,n}$), respectively.

$$d = k\beta. \tag{6.3}$$

In our calculations the parameter k was taken as given in (6.3), with β as shown in Ref. [51].

The dimension of the QRPA matrices $\mathcal{A}$ and $\mathcal{B}$ is the sum of the number of the dipole proton ($N_{d,p}$) and the number of the dipole neutron ($N_{d,n}$) configurations; these are given in Table I together with the strength of the dipole-dipole interactions, X_{PP} and X_{PN}. The other strengths are related with the mentioned ones by: $X_{NN}=X_{PP}, X_{NP}=X_{PN}$.

It is worth writing the dipole-dipole term, H_{DD}, of the model Hamiltonian, in terms of the isoscalar and isovector operators:

$$V_{1\mu}(I,I') = D_{1\mu}(p;II') - D_{1\mu}(n;II'), \;\; S_{1\mu}(I,I') = D_{1\mu}(p;II') + D_{1\mu}(n;II'). \tag{6.4}$$

The result is:

$$\begin{aligned} H_{DD} &= \frac{1}{4}\left(X_{PP}+X_{NN}-X_{PN}-X_{NP}\right)\sum_{ab;cd} V_{1\mu}(ab)V_{1,-\mu}(cd) \\ &+ \frac{1}{4}\left(X_{PP}+X_{NN}+X_{PN}+X_{NP}\right)\sum_{ab;cd} S_{1\mu}(ab)S_{1,-\mu}(cd) \\ &+ \frac{1}{4}\left(X_{PP}-X_{NN}+X_{PN}-X_{NP}\right)\sum_{ab;cd} V_{1\mu}(ab)S_{1,-\mu}(cd) \\ &+ \frac{1}{4}\left(X_{PP}-X_{NN}-X_{PN}+X_{NP}\right)\sum_{ab;cd} S_{1\mu}(ab)V_{1,-\mu}(cd). \end{aligned} \tag{6.5}$$

Since the proton-neutron interaction may lead to a system (pn) in a bound state it is reasonable to admit that $X_{PN} > X_{PP}$. In our calculations we also considered $X_{PP}=X_{NN}$ and $X_{PN}=X_{NP}$. Note that for these values the isovector interaction ($V\dot{V}$) is repulsive, while the isoscalar one ($S\dot{S}$) is attractive. Also, the last two terms of Eq. (6.5) vanish. Due to this feature one expects that the isoscalar interaction will affect the lower part of the dipole strength, while the isovector one is responsible for the higher energy range of the spectrum. The proton-neutron interaction strength was taken equal to about $1.25X_{PP}$ for ^{150}Gd and $1.45X_{PP}$ for the remaining isotopes. Thus, the strength of the isovector interaction was fixed such that the centroid of the giant resonance is placed around 13 MeV. The results are collected in Table I, while the ratio X_{pn}/X_{pp} is represented in Fig.1 as function of the atomic mass number A.

Note that dipole-dipole interaction involves the so called Schiff dipole operator. Due to this reason the $\Delta N = 3$ single particle states are correlated. Thus, it is expected that the dipole transitions are correspondingly affected.

The QRPA equations (3.9) were solved using the method described in Ref. [45]. Results for the amplitudes X and Y where further used to calculate the reduced dipole transition probability $B(E1;0^+ \to 1^-_k)$. At its turn this is employed for calculating the dipole strength distribution as function of the QRPA energies, which is plotted for the six even-even isotopes of Gd, in Figs.2 and 3. Results shown in the Fig.3 are obtained by folding the B(E1) values with Lorentzians of widths equal to 1 MeV. Results were obtained with the effective charges given by (4.4).

Since the Pygmy resonance is expected to show up below the neutron separation energy, we analyze separately the strength below 10 MeV and beyond 10 MeV. The two sets of results are collected in Tables II and III and IV, respectively. In Table II we show the peaks larger than 1e^{2}fm^2 and lying bellow 10 MeV, corresponding to the i-th dipole phonon state. For this phonon operator we depicted the maximal proton amplitude, $X_i^M(\pi,ab)$, and the

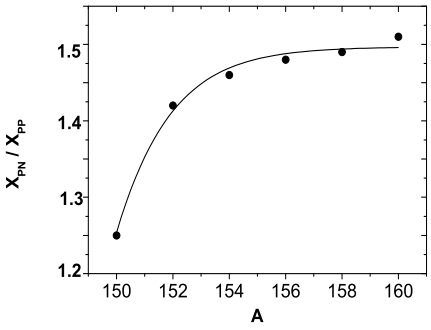

FIG. 1: The ratio of the proton-proton and proton-neutron strength interactions is plotted as function of the atomic mass number(full circle symbol). The full line curve represents the sigmoidal (Boltzmann) interpolation of the calculated ratios.

maximal neutron amplitude, $X_i^M(\nu, cd)$. The corresponding dipole configurations (ab) and (cd) are also listed. The variation of the major oscillator quantum number ΔN as well as of the total angular momentum ΔI associated to the single particle transitions $b \to a$ and $d \to c$ respectively, are listed too.

By inspection of tables II, III and IV, one notes that the listed maximal proton and neutron amplitudes have distinct relative magnitudes: i) one maximal amplitude of proton/neutron type is much larger than another maximal amplitude of neutron/proton kind; ii) the proton and neutron maximal amplitudes are of a comparable magnitude. They may have either the same or opposite phases. When the proton and neutron maximal amplitudes are equal to each other and moreover are characterized by similar single particle quantum numbers, the phonon operator is invariant to the proton and neutron permutation. Therefore, it is an isoscalar operator. If the phases of the two amplitudes are different, the phonon is of isovector type. By an abuse of language we shall conventionally call the phonon with comparable proton and neutron maximal amplitudes as isoscalar, even if they only have similar phases, and isovector if they are of opposite phases. These names reflect that they are mainly determined by the $S_1.S_1$ and $V_1.V_1$ terms of the model Hamiltonian.

In ^{150}Gd, the transitions to the 3rd , 19th and 20th phonon states are of an isovector type, while those to the 12th and 15th states have an isoscalar character. The first two transitions shown in Table II are characterized by $\Delta I = 1$ for protons and $\Delta I = 0$ for neutrons. The other transitions have $\Delta I = 1$ for both proton and neutron transitions. In ^{152}Gd three transitions are of proton type and three of neutron kind. Two of them are isovector transitions and four isoscalar. For all transitions listed in Table II $\Delta I = 1$ for protons and $\Delta I = 0$ for neutrons. Transitions to the 19th and 21st phonon states have $\Delta I = 1$ for both protons and neutrons. For ^{154}Gd one notices that the dominant transitions are those to the 31st and 32nd states and both are of isoscalar nature. Four transitions are isovector, while the rest of them are isoscalar. One remarks that two transitions, one isoscalar and one of proton two quasiparticle type, have $\Delta I = 0$ for both protons and neutrons. In ^{156}Gd one transition (to the state 19) preserves the angular momentum both for protons and neutrons and two transitions, to the states 24 and 25 respectively, which change the total angular momentum I by one unit. For ^{156}, there are six isovector and three isoscalar transitions. The dominant transition is that to the state 19, which is of isoscalar nature. In ^{158}Gd three transitions are isovector, while the rest of them are isoscalar. The dominant transitions are those to the states 9.628 MeV (isovector) and to the states of energy 9.263 MeV and 9.781 MeV respectively, which are isoscalar. For the states 26, 27 and 28, $\Delta I = 1$ for both protons and neutrons, while for the rest of transitions, one transition (proton/neutron) have $\Delta I = 1$, and the other one (neutron/proton), $\Delta I = 0$. As for ^{160}Gd, six transitions have neutron dominant components, while three are dominant proton transitions. The dominant peaks correspond to the states 21 and 27 and have an isoscalar and an isovector character, respectively. The transitions to the states 13 an 14 preserve the total angular momentum for both protons and neutrons, while those to the states 26 and 27 change I of protons and neutrons by one unit, respectively. Concluding, for ^{150,152}Gd the dominant transitions are isovector, while in ^{154,156,158,160}Gd the isoscalar transitions are dominant. The neutron oscillations concern the neutrons exceeding the saturated core, while the proton oscillations naturally affect the protons from the core.

In order to visualize the transitions composing the Pygmy resonance we plotted them in Fig. 2.

Nucleus	peak	energy	i	$(\pi; ab)$			$(\nu; cd)$			Δ N		Δ I
	$[e^2fm^2]$	[MeV]		a	b	$X_i^M(\pi; ab)$	c	d	$X_i^M(\nu; cd)$	π	ν	
	4.834	7.807	3	$\|1\ 2\ \frac{5}{2}\ \frac{1}{2}\rangle$	$\|1\ 3\ \frac{7}{2}\ \frac{3}{2}\rangle$	-0.238	$\|1\ 2\ \frac{3}{2}\ \frac{1}{2}\rangle$	$\|1\ 3\ \frac{5}{2}\ \frac{1}{2}\rangle$	0.329	1	1	1 0
^{150}Gd	3.277	9.417	12	$\|1\ 2\ \frac{5}{2}\ \frac{1}{2}\rangle$	$\|1\ 3\ \frac{7}{2}\ \frac{3}{2}\rangle$	0.106	$\|1\ 2\ \frac{3}{2}\ \frac{1}{2}\rangle$	$\|1\ 3\ \frac{5}{2}\ \frac{1}{2}\rangle$	0.874	1	1	1 0
	3.988	9.590	15	$\|1\ 2\ \frac{5}{2}\ \frac{1}{2}\rangle$	$\|1\ 3\ \frac{7}{2}\ \frac{3}{2}\rangle$	0.390	$\|1\ 2\ \frac{5}{2}\ \frac{5}{2}\rangle$	$\|1\ 3\ \frac{7}{2}\ \frac{7}{2}\rangle$	0.839	1	1	1 1
	2.561	9.741	19	$\|1\ 2\ \frac{5}{2}\ \frac{1}{2}\rangle$	$\|1\ 3\ \frac{7}{2}\ \frac{3}{2}\rangle$	-0.189	$\|1\ 2\ \frac{5}{2}\ \frac{3}{2}\rangle$	$\|1\ 3\ \frac{7}{2}\ \frac{5}{2}\rangle$	0.875	1	1	1 1
	6.553	9.836	21	$\|1\ 2\ \frac{5}{2}\ \frac{1}{2}\rangle$	$\|1\ 3\ \frac{7}{2}\ \frac{3}{2}\rangle$	0.732	$\|1\ 2\ \frac{5}{2}\ \frac{1}{2}\rangle$	$\|1\ 3\ \frac{7}{2}\ \frac{3}{2}\rangle$	-0.645	1	1	1 1
	1.013	8.036	6	$\|1\ 2\ \frac{5}{2}\ \frac{1}{2}\rangle$	$\|1\ 3\ \frac{7}{2}\ \frac{3}{2}\rangle$	0.031	$\|1\ 2\ \frac{3}{2}\ \frac{3}{2}\rangle$	$\|1\ 3\ \frac{5}{2}\ \frac{3}{2}\rangle$	0.978	1	1	1 0
	1.683	9.292	14	$\|1\ 2\ \frac{5}{2}\ \frac{3}{2}\rangle$	$\|1\ 3\ \frac{7}{2}\ \frac{3}{2}\rangle$	0.985	$\|1\ 2\ \frac{3}{2}\ \frac{1}{2}\rangle$	$\|1\ 3\ \frac{5}{2}\ \frac{1}{2}\rangle$	-0.102	1	1	1 0
^{152}Gd	2.774	9.438	16	$\|1\ 2\ \frac{5}{2}\ \frac{1}{2}\rangle$	$\|1\ 3\ \frac{7}{2}\ \frac{3}{2}\rangle$	0.131	$\|1\ 2\ \frac{3}{2}\ \frac{1}{2}\rangle$	$\|1\ 3\ \frac{5}{2}\ \frac{1}{2}\rangle$	0.915	1	1	1 0
	6.944	9.670	19	$\|1\ 2\ \frac{5}{2}\ \frac{1}{2}\rangle$	$\|1\ 3\ \frac{7}{2}\ \frac{3}{2}\rangle$	0.922	$\|1\ 2\ \frac{5}{2}\ \frac{5}{2}\rangle$	$\|1\ 3\ \frac{7}{2}\ \frac{7}{2}\rangle$	-0.269	1	1	1 1
	1.319	9.788	21	$\|1\ 2\ \frac{5}{2}\ \frac{1}{2}\rangle$	$\|1\ 3\ \frac{7}{2}\ \frac{3}{2}\rangle$	0.134	$\|1\ 2\ \frac{3}{2}\ \frac{3}{2}\rangle$	$\|2\ 1\ \frac{1}{2}\ \frac{1}{2}\rangle$	0.765	1	1	1 1
	3.864	9.990	24	$\|1\ 1\ \frac{3}{2}\ \frac{3}{2}\rangle$	$\|1\ 2\ \frac{5}{2}\ \frac{5}{2}\rangle$	0.936	$\|1\ 3\ \frac{7}{2}\ \frac{1}{2}\rangle$	$\|1\ 4\ \frac{9}{2}\ \frac{1}{2}\rangle$	0.231	1	1	1 0
	1.244	7.123	6	$\|1\ 2\ \frac{3}{2}\ \frac{1}{2}\rangle$	$\|1\ 3\ \frac{5}{2}\ \frac{1}{2}\rangle$	-0.456	$\|1\ 2\ \frac{3}{2}\ \frac{3}{2}\rangle$	$\|1\ 3\ \frac{5}{2}\ \frac{3}{2}\rangle$	0.880	1	1	0 1
	1.008	8.628	12	$\|1\ 1\ \frac{3}{2}\ \frac{3}{2}\rangle$	$\|1\ 2\ \frac{5}{2}\ \frac{3}{2}\rangle$	0.932	$\|1\ 3\ \frac{7}{2}\ \frac{1}{2}\rangle$	$\|1\ 4\ \frac{9}{2}\ \frac{1}{2}\rangle$	-0.071	1	1	0 0
^{154}Gd	5.984	8.932	13	$\|1\ 2\ \frac{5}{2}\ \frac{3}{2}\rangle$	$\|1\ 3\ \frac{7}{2}\ \frac{3}{2}\rangle$	-0.662	$\|1\ 3\ \frac{7}{2}\ \frac{1}{2}\rangle$	$\|1\ 4\ \frac{9}{2}\ \frac{1}{2}\rangle$	0.641	1	1	0 0
	7.115	9.173	16	$\|1\ 1\ \frac{3}{2}\ \frac{3}{2}\rangle$	$\|1\ 2\ \frac{5}{2}\ \frac{1}{2}\rangle$	0.191	$\|1\ 2\ \frac{3}{2}\ \frac{3}{2}\rangle$	$\|2\ 1\ \frac{1}{2}\ \frac{1}{2}\rangle$	0.735	1	1	1 1
	5.931	9.389	20	$\|1\ 2\ \frac{5}{2}\ \frac{1}{2}\rangle$	$\|1\ 3\ \frac{7}{2}\ \frac{3}{2}\rangle$	0.203	$\|1\ 3\ \frac{7}{2}\ \frac{3}{2}\rangle$	$\|1\ 4\ \frac{9}{2}\ \frac{3}{2}\rangle$	0.757	1	1	1 0
	1.298	9.521	22	$\|1\ 2\ \frac{5}{2}\ \frac{1}{2}\rangle$	$\|1\ 3\ \frac{7}{2}\ \frac{3}{2}\rangle$	0.906	$\|1\ 3\ \frac{7}{2}\ \frac{1}{2}\rangle$	$\|1\ 4\ \frac{9}{2}\ \frac{3}{2}\rangle$	-0.116	1	1	1 1
	2.168	9.750	26	$\|1\ 2\ \frac{3}{2}\ \frac{1}{2}\rangle$	$\|1\ 3\ \frac{5}{2}\ \frac{1}{2}\rangle$	0.324	$\|1\ 3\ \frac{7}{2}\ \frac{1}{2}\rangle$	$\|1\ 4\ \frac{9}{2}\ \frac{3}{2}\rangle$	0.838	1	1	0 1
	15.017	9.879	31	$\|1\ 1\ \frac{3}{2}\ \frac{3}{2}\rangle$	$\|2\ 0\ \frac{1}{2}\ \frac{1}{2}\rangle$	-0.557	$\|1\ 2\ \frac{3}{2}\ \frac{1}{2}\rangle$	$\|1\ 3\ \frac{5}{2}\ \frac{1}{2}\rangle$	-0.361	1	1	1 0
	11.759	9.961	32	$\|1\ 1\ \frac{3}{2}\ \frac{3}{2}\rangle$	$\|1\ 2\ \frac{5}{2}\ \frac{5}{2}\rangle$	0.713	$\|1\ 2\ \frac{3}{2}\ \frac{1}{2}\rangle$	$\|1\ 3\ \frac{5}{2}\ \frac{1}{2}\rangle$	0.453	1	1	1 0
	1.908	7.493	6	$\|1\ 2\ \frac{5}{2}\ \frac{3}{2}\rangle$	$\|1\ 3\ \frac{7}{2}\ \frac{1}{2}\rangle$	-0.106	$\|1\ 2\ \frac{3}{2}\ \frac{3}{2}\rangle$	$\|1\ 3\ \frac{5}{2}\ \frac{3}{2}\rangle$	0.879	1	1	1 0
	2.128	8.780	13	$\|1\ 2\ \frac{5}{2}\ \frac{3}{2}\rangle$	$\|1\ 3\ \frac{7}{2}\ \frac{3}{2}\rangle$	0.986	$\|1\ 3\ \frac{7}{2}\ \frac{3}{2}\rangle$	$\|1\ 4\ \frac{9}{2}\ \frac{1}{2}\rangle$	-0.108	1	1	0 1
	5.450	9.071	15	$\|1\ 2\ \frac{3}{2}\ \frac{1}{2}\rangle$	$\|1\ 3\ \frac{5}{2}\ \frac{1}{2}\rangle$	-0.112	$\|1\ 3\ \frac{7}{2}\ \frac{1}{2}\rangle$	$\|1\ 4\ \frac{9}{2}\ \frac{1}{2}\rangle$	0.833	1	1	1 0
^{156}Gd	5.479	9.292	18	$\|1\ 2\ \frac{3}{2}\ \frac{1}{2}\rangle$	$\|1\ 3\ \frac{5}{2}\ \frac{1}{2}\rangle$	0.132	$\|1\ 2\ \frac{3}{2}\ \frac{3}{2}\rangle$	$\|2\ 1\ \frac{1}{2}\ \frac{1}{2}\rangle$	0.782	1	1	0 1
	9.410	9.396	19	$\|1\ 2\ \frac{3}{2}\ \frac{1}{2}\rangle$	$\|1\ 3\ \frac{5}{2}\ \frac{1}{2}\rangle$	-0.219	$\|1\ 3\ \frac{7}{2}\ \frac{1}{2}\rangle$	$\|1\ 4\ \frac{9}{2}\ \frac{3}{2}\rangle$	0.834	1	1	0 0
	1.345	9.622	24	$\|0\ 3\ \frac{5}{2}\ \frac{5}{2}\rangle$	$\|0\ 4\ \frac{7}{2}\ \frac{7}{2}\rangle$	0.822	$\|1\ 3\ \frac{7}{2}\ \frac{1}{2}\rangle$	$\|1\ 4\ \frac{9}{2}\ \frac{3}{2}\rangle$	0.142	1	1	1 1
	9.975	9.705	25	$\|0\ 3\ \frac{5}{2}\ \frac{5}{2}\rangle$	$\|0\ 4\ \frac{7}{2}\ \frac{7}{2}\rangle$	0.372	$\|1\ 3\ \frac{7}{2}\ \frac{1}{2}\rangle$	$\|1\ 4\ \frac{9}{2}\ \frac{3}{2}\rangle$	-0.751	1	1	1 1
	4.526	9.745	27	$\|0\ 3\ \frac{5}{2}\ \frac{5}{2}\rangle$	$\|0\ 4\ \frac{7}{2}\ \frac{7}{2}\rangle$	0.212	$\|1\ 2\ \frac{5}{2}\ \frac{3}{2}\rangle$	$\|1\ 3\ \frac{7}{2}\ \frac{3}{2}\rangle$	0.907	1	1	1 0
	3.008	9.815	29	$\|1\ 1\ \frac{3}{2}\ \frac{3}{2}\rangle$	$\|1\ 2\ \frac{5}{2}\ \frac{5}{2}\rangle$	-0.297	$\|1\ 3\ \frac{7}{2}\ \frac{1}{2}\rangle$	$\|1\ 4\ \frac{9}{2}\ \frac{3}{2}\rangle$	0.392	1	1	1 1
	2.037	7.478	6	$\|1\ 2\ \frac{5}{2}\ \frac{3}{2}\rangle$	$\|1\ 3\ \frac{7}{2}\ \frac{1}{2}\rangle$	0.173	$\|1\ 2\ \frac{3}{2}\ \frac{3}{2}\rangle$	$\|1\ 3\ \frac{5}{2}\ \frac{3}{2}\rangle$	0.714	1	1	1 0
	2.288	8.703	13	$\|1\ 2\ \frac{5}{2}\ \frac{3}{2}\rangle$	$\|1\ 3\ \frac{7}{2}\ \frac{1}{2}\rangle$	0.986	$\|1\ 3\ \frac{7}{2}\ \frac{1}{2}\rangle$	$\|1\ 4\ \frac{9}{2}\ \frac{1}{2}\rangle$	-0.116	1	1	1 0
	3.615	8.949	14	$\|1\ 1\ \frac{3}{2}\ \frac{3}{2}\rangle$	$\|1\ 2\ \frac{5}{2}\ \frac{1}{2}\rangle$	0.691	$\|1\ 3\ \frac{7}{2}\ \frac{1}{2}\rangle$	$\|1\ 4\ \frac{9}{2}\ \frac{1}{2}\rangle$	0.595	1	1	1 0
^{158}Gd	2.236	8.955	15	$\|1\ 1\ \frac{3}{2}\ \frac{3}{2}\rangle$	$\|1\ 2\ \frac{5}{2}\ \frac{1}{2}\rangle$	0.722	$\|1\ 3\ \frac{7}{2}\ \frac{1}{2}\rangle$	$\|1\ 4\ \frac{9}{2}\ \frac{1}{2}\rangle$	-0.554	1	1	1 0
	18.241	9.263	19	$\|1\ 2\ \frac{3}{2}\ \frac{1}{2}\rangle$	$\|1\ 3\ \frac{5}{2}\ \frac{1}{2}\rangle$	0.326	$\|1\ 2\ \frac{3}{2}\ \frac{3}{2}\rangle$	$\|2\ 1\ \frac{1}{2}\ \frac{1}{2}\rangle$	0.731	1	1	0 1
	4.005	9.557	26	$\|0\ 3\ \frac{5}{2}\ \frac{5}{2}\rangle$	$\|0\ 4\ \frac{7}{2}\ \frac{7}{2}\rangle$	0.727	$\|1\ 3\ \frac{7}{2}\ \frac{1}{2}\rangle$	$\|1\ 4\ \frac{9}{2}\ \frac{3}{2}\rangle$	0.326	1	1	1 1
	14.301	9.628	27	$\|0\ 3\ \frac{5}{2}\ \frac{5}{2}\rangle$	$\|0\ 4\ \frac{7}{2}\ \frac{7}{2}\rangle$	-0.553	$\|1\ 3\ \frac{7}{2}\ \frac{1}{2}\rangle$	$\|1\ 4\ \frac{9}{2}\ \frac{3}{2}\rangle$	0.767	1	1	1 1
	19.070	9.781	28	$\|0\ 3\ \frac{5}{2}\ \frac{5}{2}\rangle$	$\|0\ 4\ \frac{7}{2}\ \frac{7}{2}\rangle$	0.359	$\|1\ 3\ \frac{7}{2}\ \frac{1}{2}\rangle$	$\|1\ 4\ \frac{9}{2}\ \frac{3}{2}\rangle$	0.397	1	1	1 1
	1.280	7.463e	5	$\|1\ 2\ \frac{5}{2}\ \frac{3}{2}\rangle$	$\|1\ 3\ \frac{7}{2}\ \frac{1}{2}\rangle$	0.557	$\|1\ 2\ \frac{3}{2}\ \frac{3}{2}\rangle$	$\|1\ 3\ \frac{5}{2}\ \frac{3}{2}\rangle$	0.797	1	1	1 0
	1.297	8.084	10	$\|1\ 1\ \frac{3}{2}\ \frac{3}{2}\rangle$	$\|1\ 2\ \frac{5}{2}\ \frac{3}{2}\rangle$	0.421	$\|1\ 3\ \frac{7}{2}\ \frac{3}{2}\rangle$	$\|1\ 4\ \frac{9}{2}\ \frac{1}{2}\rangle$	0.900	1	1	0 1
	2.251	8.638	13	$\|1\ 2\ \frac{5}{2}\ \frac{3}{2}\rangle$	$\|1\ 3\ \frac{7}{2}\ \frac{3}{2}\rangle$	0.986	$\|1\ 3\ \frac{7}{2}\ \frac{1}{2}\rangle$	$\|1\ 4\ \frac{9}{2}\ \frac{1}{2}\rangle$	-0.121	1	1	0 0
^{160}Gd	1.681	8.830	14	$\|1\ 2\ \frac{3}{2}\ \frac{1}{2}\rangle$	$\|1\ 2\ \frac{5}{2}\ \frac{1}{2}\rangle$	0.069	$\|1\ 3\ \frac{7}{2}\ \frac{3}{2}\rangle$	$\|1\ 4\ \frac{9}{2}\ \frac{3}{2}\rangle$	0.755	1	1	0 0
	1.729	8.946	16	$\|0\ 3\ \frac{5}{2}\ \frac{5}{2}\rangle$	$\|1\ 2\ \frac{5}{2}\ \frac{3}{2}\rangle$	0.886	$\|1\ 3\ \frac{7}{2}\ \frac{3}{2}\rangle$	$\|1\ 4\ \frac{9}{2}\ \frac{3}{2}\rangle$	0.288	1	1	1 0
	5.005	8.950	17	$\|0\ 3\ \frac{5}{2}\ \frac{5}{2}\rangle$	$\|1\ 2\ \frac{5}{2}\ \frac{3}{2}\rangle$	-0.463	$\|1\ 3\ \frac{7}{2}\ \frac{3}{2}\rangle$	$\|1\ 4\ \frac{9}{2}\ \frac{3}{2}\rangle$	0.526	1	1	1 0
	18.997	9.192	21	$\|1\ 2\ \frac{3}{2}\ \frac{1}{2}\rangle$	$\|1\ 3\ \frac{5}{2}\ \frac{1}{2}\rangle$	0.446	$\|1\ 2\ \frac{3}{2}\ \frac{3}{2}\rangle$	$\|2\ 1\ \frac{1}{2}\ \frac{1}{2}\rangle$	0.757	1	1	0 1
	6.646	9.511	26	$\|0\ 3\ \frac{5}{2}\ \frac{5}{2}\rangle$	$\|0\ 4\ \frac{7}{2}\ \frac{7}{2}\rangle$	0.607	$\|1\ 3\ \frac{7}{2}\ \frac{1}{2}\rangle$	$\|1\ 4\ \frac{9}{2}\ \frac{3}{2}\rangle$	0.441	1	1	1 1
	12.486	9.576	27	$\|0\ 3\ \frac{5}{2}\ \frac{5}{2}\rangle$	$\|0\ 4\ \frac{7}{2}\ \frac{7}{2}\rangle$	-0.674	$\|1\ 3\ \frac{7}{2}\ \frac{1}{2}\rangle$	$\|1\ 4\ \frac{9}{2}\ \frac{3}{2}\rangle$	0.695	1	1	1 1

TABLE II: The highest peaks contributing to the PDR are mentioned together with the corresponding energy of the i-th phonon state. Only peaks higher than $1e^2fm^2$ are mentioned. The proton (π) and neutron (ν) maximal amplitudes are also given. The states involved in the dominant single particle transitions $b \to a$ and $d \to c$ are listed. These are characterized by the variation of the major oscillator quantum number ΔN. The variations of the angular momenta involved in the single particle transitions, are also listed.

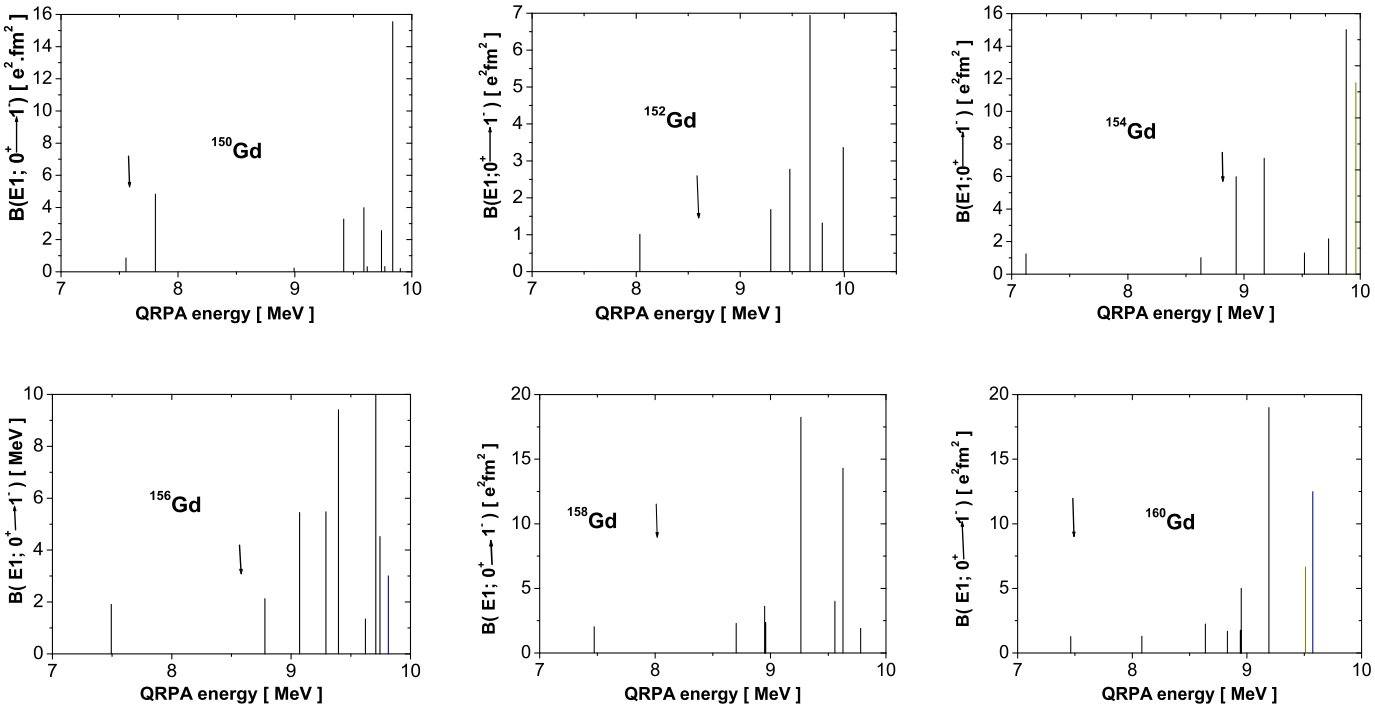

FIG. 2: The dipole strength as function of energy for $^{150-160}$Gd given in units of e^2fm^2. For ^{150}Gd the only transitions larger than $0.2e^2fm^2$, while for the rest of isotopes only those larger than $1e^2fm^2$ are plotted. The arrows indicate the neutron separation energies taken from [38].

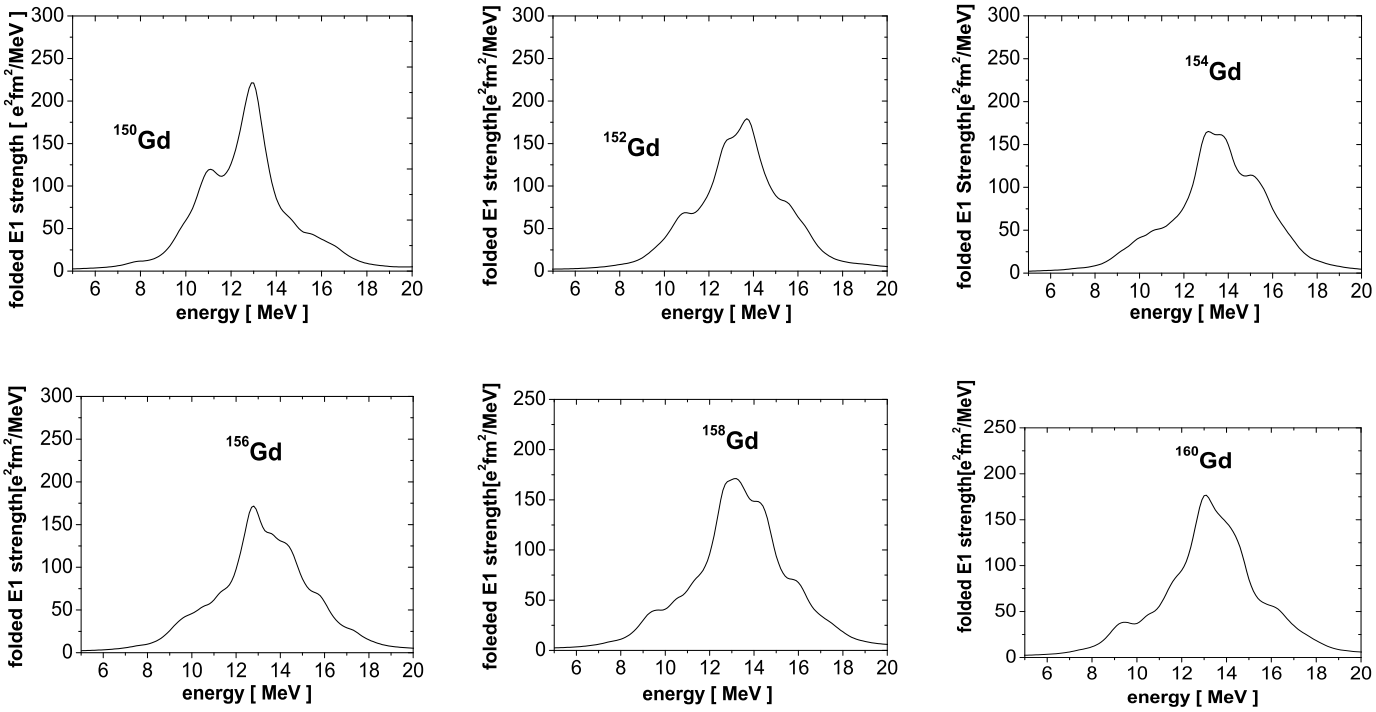

FIG. 3: The dipole strength as function of energy for the even-even isotopes $^{150-160}$Gd. The calculated strengths were folded by Lorentzians with the width of 1 MeV.

From Fig.2 it can be observed one or two dominant transitions surrounded by by many smaller transitions which results in having a dipole strength with a resonance structure. However the maximal peaks are much smaller than that determining the giant resonance (GDR) which, in fact justify the name of Pygmy resonance (PDR). Actually, the PDR is a substructure of GDR, being embedded in the left tail of it. In this context discussing the structure of PDR requires considering the main features of GDR.

Indeed, a similar analysis of the single particle transitions composing the GDR is achieved in Tables II and IV. Since there are a lot of transitions conferring a large width to the GDR we select only few of them to be commented. In ^{150}Gd one notices a dominant transition to the state 121 having an isovector character which is flanked by two isoscalar moderate transitions to the states 108 and 124, respectively. While the first two transitions (to the states 108 and 121) preserve the total angular momentum I for both protons and neutrons, for the third transition (to the state 124) that is true only for protons. In total there are four isovector and four isoscalar transitions. Also, for four transitions $\Delta I = 0$ for both the protons and the neutrons, while for the other four the vanishing ΔI holds only for one component (proton/neutron). In ^{152}Gd one listed six isoscalar transition and two isovector ones. The isoscalar transition to the state 144 is the only one which changes I neither for protons nor for neutrons. All the others change I only for one component. In ^{154}Gd we notice five isovector transitions and three of isoscalar type. The isovector transitions are dominant. The transitions to the states 115, 118 and 124 preserve I for both the protons and neutrons while for the rest of transitions the angular momentum is preserved only for one component, protons/neutrons. For ^{156}Gd we listed seven isovector transitions and three isoscalar. The dominant transitions are those to the states 120 and 134, respectively, and have an isovector character. There are two isoscalar, to the states 44 and 108, respectively, and one isovector, to the state 113, which do not change I for both protons and neutrons. The other transitions change I by one unit either for protons or for neutrons. In ^{158}Gd There are four isoscalar transitions, to the states 41, 110, 114 and 118, and 5 isovector transitions to the states 68, 123, 130, 150 and 158. The dominant transition is isoscalar and points to the state 110. For six transitions $(\Delta I(\pi), \Delta I(\nu))$ is equal to (0,0), for two equal to (1,1), one is (0,1) and one (1,0). As for ^{160}Gd there are six isoscalar and six isovector transitions among which the one to the state 118 is dominant and has an isoscalar character. In nine transitions the neutron contributions prevail over the proton ones. For six transitions $(\Delta I(\pi), \Delta I(\nu))$ is equal to (0,0), for five the mentioned I variation is (0,1) and for one that equals (1,0). One remarks the fragmentation of the dipole strength caused by the nuclear deformation. Also, the strength distribution covers a large energy interval.

The features described in detail above are reflected in Fig. 3 where the dipole strength folded with a Lorentzian with a width of 1 MeV, is plotted.

$$F_{ds}(\Gamma,\omega) = \frac{1}{2\pi}\sum_k \frac{\Gamma}{(\omega-\omega_k)^2 + \left(\frac{\Gamma}{2}\right)^2} B(E1; 0^+ \to 1_k^-). \tag{6.6}$$

One remarks that the main peak of the GDR is accompanied by a secondary one which is placed to the left side in the case of ^{150,152}Gd, while for ^{154,156,158,160}Gd in the right side of the main peak. This split of the main peak into two humps is the effect of the nuclear deformation [55, 56]. The excited states involved in the GR transitions are populated by various photoabsorbtion experiments [57–61]. The photoabsorbtion cross section is given by:

$$\sigma(\Gamma,\omega) = \frac{C}{2\pi}\sum_k \frac{\Gamma}{(\omega-\omega_k)^2 + \left(\frac{\Gamma}{2}\right)^2} \omega_k B(E1; 0^+ \to 1_k^-). \tag{6.7}$$

where C denotes a normalization constant, which in our calculation is equal to 0.014. Results of our calculations for the photoabsorbtion cross section are compared with the corresponding data in Fig.4. As seen from there the agreement of our calculation with the corresponding data is good.

Another issue treated in the present paper is that of EWSR. Calculating the B(E1) values by means of Eq. (4.4) and the QRPA excitation energies by solving Eq.(3.9), the EWSR denoted by S_l is readily obtained. We recall that the effective charges were multiplied by the factor q, listed in Table IV, which accounts for the difference in circumstances under which S_l and S_{TDK} are estimated. Results for S_l are listed in Table V. As we already mentioned this agrees with S_{TRK} given by Eq. (5.3), provided the effective charges used for calculating S_l are multiplied by the factor q listed in Table V. If, however, S_l and the right hand side of Eq. (5.3) are estimated with the same dipole operator, i.e,

Nucleus	peak	energy	i	$(\pi; ab)$			$(\nu; cd)$			Δ N		Δ I	
	$[e^2fm^2]$	[MeV]		a	b	$X_i^M(\pi; ab)$	c	d	$X_i^M(\nu; cd)$	π	ν	π	ν
	26.327	10.647	42	$\|1\ 1\ \frac{1}{2}\ \frac{1}{2}\rangle$	$\|1\ 2\ \frac{3}{2}\ \frac{3}{2}\rangle$	-0.695	$\|2\ 0\ \frac{1}{2}\ \frac{1}{2}\rangle$	$\|2\ 1\ \frac{1}{2}\ \frac{1}{2}\rangle$	0.410	1	1	1	0
	31.760	1.967	54	$\|0\ 4\ \frac{7}{2}\ \frac{3}{2}\rangle$	$\|1\ 3\ \frac{7}{2}\ \frac{3}{2}\rangle$	0.310	$\|1\ 3\ \frac{7}{2}\ \frac{1}{2}\rangle$	$\|1\ 4\ \frac{9}{2}\ \frac{1}{2}\rangle$	0.741	1	1	0	0
	25.149	11.349	49	$\|1\ 1\ \frac{3}{2}\ \frac{1}{2}\rangle$	$\|1\ 2\ \frac{5}{2}\ \frac{1}{2}\rangle$	0.867	$\|1\ 3\ \frac{7}{2}\ \frac{1}{2}\rangle$	$\|1\ 4\ \frac{9}{2}\ \frac{3}{2}\rangle$	0.273	1	1	0	1
^{150}Gd	18. 793	12.704	107	$\|1\ 2\ \frac{5}{2}\ \frac{1}{2}\rangle$	$\|2\ 1\ \frac{3}{2}\ \frac{1}{2}\rangle$	0.761	$\|1\ 2\ \frac{5}{2}\ \frac{3}{2}\rangle$	$\|2\ 1\ \frac{3}{2}\ \frac{3}{2}\rangle$	-0.462	1	1	0	0
	25.202	12.742	108	$\|0\ 4\ \frac{9}{2}\ \frac{1}{2}\rangle$	$\|1\ 3\ \frac{7}{2}\ \frac{1}{2}\rangle$	0.697	$\|0\ 4\ \frac{9}{2}\ \frac{1}{2}\rangle$	$\|1\ 3\ \frac{7}{2}\ \frac{1}{2}\rangle$	0.504	1	1	0	0
	101.438	12.989	121	$\|0\ 3\ \frac{5}{2}\ \frac{1}{2}\rangle$	$\|1\ 2\ \frac{3}{2}\ \frac{1}{2}\rangle$	-0.351	$\|0\ 4\ \frac{7}{2}\ \frac{5}{2}\rangle$	$\|1\ 3\ \frac{5}{2}\ \frac{5}{2}\rangle$	0.514	1	1	0	0
	21.412	13.088	124	$\|0\ 4\ \frac{7}{2}\ \frac{3}{2}\rangle$	$\|1\ 3\ \frac{5}{2}\ \frac{3}{2}\rangle$	0.839	$\|0\ 4\ \frac{9}{2}\ \frac{1}{2}\rangle$	$\|1\ 3\ \frac{7}{2}\ \frac{3}{2}\rangle$	0.447	1	1	0	1
	28.347	13.666	127	$\|0\ 4\ \frac{9}{2}\ \frac{3}{2}\rangle$	$\|1\ 3\ \frac{7}{2}\ \frac{3}{2}\rangle$	0.824	$\|0\ 4\ \frac{9}{2}\ \frac{1}{2}\rangle$	$\|1\ 3\ \frac{7}{2}\ \frac{3}{2}\rangle$	-0.379	1	1	0	1
	68.485	12.702	109	$\|0\ 4\ \frac{9}{2}\ \frac{1}{2}\rangle$	$\|1\ 3\ \frac{7}{2}\ \frac{1}{2}\rangle$	0.578	$\|0\ 4\ \frac{7}{2}\ \frac{1}{2}\rangle$	$\|1\ 3\ \frac{5}{2}\ \frac{3}{2}\rangle$	0.293	1	1	0	1
	21.625	13.171	126	$\|0\ 3\ \frac{7}{2}\ \frac{5}{2}\rangle$	$\|1\ 2\ \frac{5}{2}\ \frac{3}{2}\rangle$	0.567	$\|0\ 4\ \frac{9}{2}\ \frac{3}{2}\rangle$	$\|1\ 3\ \frac{7}{2}\ \frac{3}{2}\rangle$	0.499	1	1	1	0
^{152}Gd	23.975	13.506	135	$\|0\ 4\ \frac{9}{2}\ \frac{9}{2}\rangle$	$\|1\ 3\ \frac{7}{2}\ \frac{7}{2}\rangle$	-0.411	$\|1\ 3\ \frac{7}{2}\ \frac{3}{2}\rangle$	$\|2\ 2\ \frac{5}{2}\ \frac{1}{2}\rangle$	-0.588	1	1	1	1
	29.023	13.726	144	$\|0\ 4\ \frac{9}{2}\ \frac{5}{2}\rangle$	$\|1\ 3\ \frac{7}{2}\ \frac{5}{2}\rangle$	0.403	$\|0\ 4\ \frac{9}{2}\ \frac{7}{2}\rangle$	$\|1\ 3\ \frac{7}{2}\ \frac{7}{2}\rangle$	0.749	1	1	0	0
	46.881	13.768	145	$\|1\ 2\ \frac{5}{2}\ \frac{5}{2}\rangle$	$\|1\ 3\ \frac{7}{2}\ \frac{7}{2}\rangle$	0.468	$\|0\ 4\ \frac{9}{2}\ \frac{7}{2}\rangle$	$\|1\ 3\ \frac{7}{2}\ \frac{7}{2}\rangle$	0.619	1	1	1	0
	45.097	13.835	147	$\|1\ 2\ \frac{5}{2}\ \frac{5}{2}\rangle$	$\|1\ 3\ \frac{7}{2}\ \frac{7}{2}\rangle$	0.816	$\|0\ 4\ \frac{9}{2}\ \frac{7}{2}\rangle$	$\|1\ 3\ \frac{7}{2}\ \frac{7}{2}\rangle$	-0.194	1	1	1	0
	35.114	14.260	157	$\|0\ 4\ \frac{7}{2}\ \frac{7}{2}\rangle$	$\|1\ 3\ \frac{5}{2}\ \frac{5}{2}\rangle$	0.877	$\|1\ 2\ \frac{5}{2}\ \frac{1}{2}\rangle$	$\|2\ 1\ \frac{3}{2}\ \frac{3}{2}\rangle$	-0.178	1	1	1	1
	22.176	14.653	166	$\|0\ 3\ \frac{7}{2}\ \frac{3}{2}\rangle$	$\|1\ 2\ \frac{5}{2}\ \frac{1}{2}\rangle$	-0.213	$\|2\ 1\ \frac{3}{2}\ \frac{1}{2}\rangle$	$\|2\ 2\ \frac{5}{2}\ \frac{1}{2}\rangle$	-0.931	1	1	1	0
	105.442	12.794	115	$\|0\ 4\ \frac{9}{2}\ \frac{1}{2}\rangle$	$\|1\ 3\ \frac{7}{2}\ \frac{1}{2}\rangle$	-0.477	$\|0\ 4\ \frac{7}{2}\ \frac{3}{2}\rangle$	$\|1\ 3\ \frac{5}{2}\ \frac{3}{2}\rangle$	0.295	1	1	0	0
	50.478	12.983	118	$\|0\ 4\ \frac{9}{2}\ \frac{3}{2}\rangle$	$\|1\ 3\ \frac{7}{2}\ \frac{3}{2}\rangle$	-0.715	$\|1\ 3\ \frac{5}{2}\ \frac{1}{2}\rangle$	$\|2\ 2\ \frac{3}{2}\ \frac{1}{2}\rangle$	-0.168	1	1	0	0
	20.056	13.185	126	$\|0\ 3\ \frac{5}{2}\ \frac{1}{2}\rangle$	$\|1\ 2\ \frac{3}{2}\ \frac{1}{2}\rangle$	0.867	$\|1\ 3\ \frac{5}{2}\ \frac{1}{2}\rangle$	$\|2\ 2\ \frac{3}{2}\ \frac{1}{2}\rangle$	0.297	1	1	0	0
	61.574	13.556	132	$\|0\ 4\ \frac{9}{2}\ \frac{1}{2}\rangle$	$\|1\ 3\ \frac{7}{2}\ \frac{3}{2}\rangle$	0.341	$\|1\ 3\ \frac{5}{2}\ \frac{1}{2}\rangle$	$\|2\ 2\ \frac{3}{2}\ \frac{1}{2}\rangle$	-0.765	1	1	1	0
	35.282	13.501	142	$\|0\ 4\ \frac{9}{2}\ \frac{9}{2}\rangle$	$\|1\ 3\ \frac{7}{2}\ \frac{7}{2}\rangle$	-0.773	$\|0\ 4\ \frac{9}{2}\ \frac{3}{2}\rangle$	$\|1\ 3\ \frac{7}{2}\ \frac{3}{2}\rangle$	-0.325	1	1	1	0
^{154}Gd	28.367	13.948	144	$\|0\ 4\ \frac{9}{2}\ \frac{9}{2}\rangle$	$\|1\ 3\ \frac{7}{2}\ \frac{7}{2}\rangle$	-0.267	$\|0\ 4\ \frac{9}{2}\ \frac{3}{2}\rangle$	$\|1\ 3\ \frac{7}{2}\ \frac{3}{2}\rangle$	0.899	1	1	1	0
	26.639	15.092	179	$\|0\ 4\ \frac{7}{2}\ \frac{7}{2}\rangle$	$\|1\ 3\ \frac{5}{2}\ \frac{5}{2}\rangle$	0.244	$\|0\ 4\ \frac{9}{2}\ \frac{1}{2}\rangle$	$\|1\ 3\ \frac{7}{2}\ \frac{1}{2}\rangle$	-0.817	1	1	1	0
	28.740	15.672	188	$\|1\ 2\ \frac{5}{2}\ \frac{3}{2}\rangle$	$\|2\ 1\ \frac{3}{2}\ \frac{3}{2}\rangle$	0.669	$\|1\ 3\ \frac{7}{2}\ \frac{5}{2}\rangle$	$\|2\ 2\ \frac{5}{2}\ \frac{3}{2}\rangle$	-0.601	1	1	0	1
	20.636	10.504	44	$\|1\ 1\ \frac{1}{2}\ \frac{1}{2}\rangle$	$\|2\ 0\ \frac{1}{2}\ \frac{1}{2}\rangle$	0.725	$\|2\ 0\ \frac{1}{2}\ \frac{1}{2}\rangle$	$\|2\ 1\ \frac{1}{2}\ \frac{1}{2}\rangle$	0.401	1	1	0	0
^{156}Gd	27.312	12.185	99	$\|1\ 2\ \frac{5}{2}\ \frac{1}{2}\rangle$	$\|2\ 1\ \frac{3}{2}\ \frac{1}{2}\rangle$	-0.499	$\|0\ 4\ \frac{9}{2}\ \frac{9}{2}\rangle$	$\|1\ 3\ \frac{7}{2}\ \frac{7}{2}\rangle$	-0.358	1	1	0	1
	21.871	12.561	108	$\|0\ 4\ \frac{9}{2}\ \frac{1}{2}\rangle$	$\|1\ 3\ \frac{7}{2}\ \frac{1}{2}\rangle$	-0.628	$\|\ 0\ 4\ \frac{7}{2}\ \frac{3}{2}\rangle$	$\|1\ 3\ \frac{5}{2}\ \frac{3}{2}\rangle$	-0.784	1	1	0	0
	100.632	12.697	113	$\|0\ 4\ \frac{9}{2}\ \frac{1}{2}\rangle$	$\|1\ 3\ \frac{7}{2}\ \frac{1}{2}\rangle$	-0.457	$\|0\ 4\ \frac{7}{2}\ \frac{3}{2}\rangle$	$\|1\ 3\ \frac{5}{2}\ \frac{3}{2}\rangle$	0.428	1	1	0	0
	22.931	12.803	115	$\|0\ 3\ \frac{7}{2}\ \frac{5}{2}\rangle$	$\|1\ 2\ \frac{5}{2}\ \frac{3}{2}\rangle$	0.905	$\|1\ 3\ \frac{5}{2}\ \frac{3}{2}\rangle$	$\|1\ 4\ \frac{7}{2}\ \frac{3}{2}\rangle$	-0.191	1	1	1	0
	43.743	12.991	120	$\|0\ 4\ \frac{9}{2}\ \frac{3}{2}\rangle$	$\|1\ 3\ \frac{7}{2}\ \frac{3}{2}\rangle$	-0.534	$\|0\ 4\ \frac{9}{2}\ \frac{5}{2}\rangle$	$\|1\ 3\ \frac{7}{2}\ \frac{3}{2}\rangle$	0.730	1	1	0	1
	34.082	13.578	134	$\|0\ 4\ \frac{9}{2}\ \frac{1}{2}\rangle$	$\|1\ 3\ \frac{7}{2}\ \frac{3}{2}\rangle$	0.347	$\|1\ 3\ \frac{5}{2}\ \frac{1}{2}\rangle$	$\|2\ 2\ \frac{3}{2}\ \frac{1}{2}\rangle$	-0.590	1	1	1	0
	44.069	13.627	135	$\|0\ 4\ \frac{9}{2}\ \frac{1}{2}\rangle$	$\|1\ 3\ \frac{7}{2}\ \frac{3}{2}\rangle$	-0.273	$\|0\ 4\ \frac{9}{2}\ \frac{5}{2}\rangle$	$\|1\ 3\ \frac{7}{2}\ \frac{5}{2}\rangle$	0.791	1	1	1	0
	23.778	14.287	153	$\|0\ 4\ \frac{9}{2}\ \frac{9}{2}\rangle$	$\|1\ 3\ \frac{7}{2}\ \frac{7}{2}\rangle$	-0.764	$\|\ 1\ 3\ \frac{7}{2}\ \frac{3}{2}\rangle$	$\|2\ 2\ \frac{5}{2}\ \frac{3}{2}\rangle$	0.255	1	1	1	0
	24.826	14.621	162	$\|0\ 3\ \frac{7}{2}\ \frac{5}{2}\rangle$	$\|1\ 2\ \frac{5}{2}\ \frac{5}{2}\rangle$	-0.195	$\|2\ 1\ \frac{3}{2}\ \frac{1}{2}\rangle$	$\|2\ 2\ \frac{5}{2}\ \frac{3}{2}\rangle$	0.925	1	1	0	1
	24.583	10.506	41	$\|1\ 1\ \frac{1}{2}\ \frac{1}{2}\rangle$	$\|20\ \frac{1}{2}\ \frac{1}{2}\rangle$	0.703	$\|2\ 0\ \frac{1}{2}\ \frac{1}{2}\rangle$	$\|2\ 1\ \frac{1}{2}\ \frac{1}{2}\rangle$	0.541	1	1	0	0
	21.825	11.280	68	$\|1\ 1\ \frac{1}{2}\ \frac{1}{2}\rangle$	$\|1\ 2\ \frac{3}{2}\ \frac{3}{2}\rangle$	0.652	$\|1\ 2\ \frac{3}{2}\ \frac{1}{2}\rangle$	$\|1\ 3\ \frac{5}{2}\ \frac{3}{2}\rangle$	-0.362	1	1	1	1
	94.134	12.614	110	$\|0\ 4\ \frac{9}{2}\ \frac{1}{2}\rangle$	$\|1\ 3\ \frac{7}{2}\ \frac{1}{2}\rangle$	-0.443	$\|0\ 4\ \frac{7}{2}\ \frac{3}{2}\rangle$	$\|1\ 3\ \frac{5}{2}\ \frac{3}{2}\rangle$	-0.305	1	1	0	0
	22.212	12.793	114	$\|0\ 4\ \frac{9}{2}\ \frac{3}{2}\rangle$	$\|1\ 3\ \frac{7}{2}\ \frac{3}{2}\rangle$	0.280	$\|0\ 4\ \frac{7}{2}\ \frac{3}{2}\rangle$	$\|1\ 3\ \frac{5}{2}\ \frac{3}{2}\rangle$	0.840	1	1	0	0
^{158}Gd	41.379	13.104	118	$\|0\ 4\ \frac{7}{2}\ \frac{3}{2}\rangle$	$\|1\ 3\ \frac{5}{2}\ \frac{3}{2}\rangle$	0.517	$\|1\ 3\ \frac{5}{2}\ \frac{1}{2}\rangle$	$\|2\ 2\ \frac{3}{2}\ \frac{1}{2}\rangle$	0.597	1	1	0	0
	41.625	13.251	123	$\|0\ 4\ \frac{7}{2}\ \frac{3}{2}\rangle$	$\|1\ 3\ \frac{5}{2}\ \frac{3}{2}\rangle$	-0.732	$\|2\ 1\ \frac{3}{2}\ \frac{1}{2}\rangle$	$\|2\ 2\ \frac{3}{2}\ \frac{1}{2}\rangle$	0.387	1	1	0	0
	23.056	13.457	130	$\|0\ 3\ \frac{5}{2}\ \frac{1}{2}\rangle$	$\|1\ 2\ \frac{3}{2}\ \frac{1}{2}\rangle$	-0.783	$\|0\ 4\ \frac{9}{2}\ \frac{5}{2}\rangle$	$\|1\ 3\ \frac{7}{2}\ \frac{3}{2}\rangle$	0.297	1	1	0	1
	55.859	14.571	150	$\|0\ 4\ \frac{7}{2}\ \frac{1}{2}\rangle$	$\|1\ 3\ \frac{5}{2}\ \frac{3}{2}\rangle$	0.396	$\|1\ 2\ \frac{5}{2}\ \frac{3}{2}\rangle$	$\|2\ 1\ \frac{3}{2}\ \frac{3}{2}\rangle$	-0.463	1	1	1	0
	51.161	14.498	158	$\|0\ 4\ \frac{9}{2}\ \frac{9}{2}\rangle$	$\|1\ 3\ \frac{7}{2}\ \frac{7}{2}\rangle$	-0.675	$\|1\ 3\ \frac{7}{2}\ \frac{1}{2}\rangle$	$\|2\ 2\ \frac{5}{2}\ \frac{3}{2}\rangle$	0.502	1	1	1	1

TABLE III: The peaks larger than $20e^2fm^2$ and contributing to the DR, are mentioned together with the corresponding energy of the i-th phonon state. The proton (π) and neutron (ν) maximal amplitudes are also given. The states involved in the dominant single particle transitions $b \to a$ and $d \to c$ are listed. These are characterized by the variation of the major oscillator quantum number, ΔN, as well as of the total angular momentum, ΔI.

Nucleus	peak	energy	i	$(\pi;ab)$			$(\nu;cd)$			Δ N		Δ I	
	[e^{2}fm^2]	[MeV]		a	b	$X_i^M(\pi;ab)$	c	d	$X_i^M(\nu;cd)$	π	ν	π	ν
^{160}Gd	20.459	10.495	37	$\|1\ 1\ \frac{1}{2}\frac{1}{2}\rangle$	$\|2\ 0\ \frac{1}{2}\frac{1}{2}\rangle$	0.720	$\|2\ 0\ \frac{1}{2}\frac{1}{2}\rangle$	$\|2\ 1\ \frac{1}{2}\frac{1}{2}\rangle$	0.513	1	1	0	0
	31.684	12.553	107	$\|0\ 4\ \frac{9}{2}\frac{1}{2}\rangle$	$\|1\ 3\ \frac{7}{2}\frac{1}{2}\rangle$	0.264	$\|1\ 3\ \frac{5}{2}\frac{1}{2}\rangle$	$\|2\ 2\ \frac{3}{2}\frac{1}{2}\rangle$	0.591	1	1	0	0
	29.042	12.803	114	$\|0\ 4\ \frac{9}{2}\frac{3}{2}\rangle$	$\|1\ 3\ \frac{7}{2}\frac{3}{2}\rangle$	0.675	$\|0\ 4\ \frac{7}{2}\frac{3}{2}\rangle$	$\|1\ 3\ \frac{7}{2}\frac{5}{2}\rangle$	-0.459	1	1	0	1
	27.099	12.930	116	$\|0\ 4\ \frac{9}{2}\frac{3}{2}\rangle$	$\|1\ 3\ \frac{7}{2}\frac{3}{2}\rangle$	0.424	$\|0\ 4\ \frac{7}{2}\frac{3}{2}\rangle$	$\|1\ 3\ \frac{5}{2}\frac{3}{2}\rangle$	0.773	1	1	0	0
	63.631	13.015	118	$\|1\ 2\ \frac{5}{2}\frac{5}{2}\rangle$	$\|1\ 3\ \frac{7}{2}\frac{5}{2}\rangle$	-0.411	$\|0\ 4\ \frac{7}{2}\frac{3}{2}\rangle$	$\|1\ 3\ \frac{5}{2}\frac{3}{2}\rangle$	-0.507	1	1	0	0
	25.175	13.232	122	$\|0\ 4\ \frac{7}{2}\frac{3}{2}\rangle$	$\|1\ 3\ \frac{5}{2}\frac{3}{2}\rangle$	0.718	$\|1\ 3\ \frac{7}{2}\frac{5}{2}\rangle$	$\|1\ 4\ \frac{9}{2}\frac{7}{2}\rangle$	0.470	1	1	0	1
	24.723	13.306	125	$\|0\ 4\ \frac{7}{2}\frac{3}{2}\rangle$	$\|1\ 3\ \frac{5}{2}\frac{3}{2}\rangle$	-0.357	$\|1\ 3\ \frac{7}{2}\frac{5}{2}\rangle$	$\|1\ 4\ \frac{9}{2}\frac{7}{2}\rangle$	0.807	1	1	0	1
	25.030	13.675	136	$\|0\ 3\ \frac{5}{2}\frac{1}{2}\rangle$	$\|1\ 2\ \frac{3}{2}\frac{1}{2}\rangle$	0.205	$\|2\ 1\ \frac{3}{2}\frac{1}{2}\rangle$	$\|2\ 2\ \frac{5}{2}\frac{3}{2}\rangle$	-0.845	1	1	0	1
	25.513	13.785	138	$\|1\ 1\ \frac{3}{2}\frac{1}{2}\rangle$	$\|1\ 2\ \frac{3}{2}\frac{3}{2}\rangle$	0.611	$\|1\ 3\ \frac{7}{2}\frac{3}{2}\rangle$	$\|2\ 2\ \frac{5}{2}\frac{3}{2}\rangle$	-0.651	1	1	1	0
	22.048	14.035	146	$\|0\ 4\ \frac{9}{2}\frac{5}{2}\rangle$	$\|1\ 3\ \frac{7}{2}\frac{5}{2}\rangle$	-0.674	$\|0\ 4\ \frac{9}{2}\frac{5}{2}\rangle$	$\|1\ 3\ \frac{7}{2}\frac{5}{2}\rangle$	0.580	1	1	0	0
	21.230	14.261	152	$\|0\ 3\ \frac{7}{2}\frac{3}{2}\rangle$	$\|1\ 2\ \frac{5}{2}\frac{3}{2}\rangle$	0.317	$\|1\ 2\ \frac{5}{2}\frac{3}{2}\rangle$	$\|2\ 1\ \frac{3}{2}\frac{3}{2}\rangle$	0.852	1	1	0	0
	45.745	14.674	163	$\|0\ 3\ \frac{7}{2}\frac{5}{2}\rangle$	$\|1\ 2\ \frac{5}{2}\frac{5}{2}\rangle$	0.728	$\|1\ 2\ \frac{3}{2}\frac{1}{2}\rangle$	$\|2\ 1\ \frac{3}{2}\frac{3}{2}\rangle$	0.228	1	1	0	1

TABLE IV: The same as in Table III but for ^{160}Gd.

the Schiff momentum, the result for S_l should be compared with S_{corr} given by Eq. (**??**).The quality of agreement for the sum rule is appraised by the relative deviation, r.d. $(= |S_l - S_{corr}|/S_l)$. From Table V we see that r.d. is very small, which reflects a quite good agreement for the EWSR.

The area of the surface below the cross section shown in Fig. 4 is the total cross section:

$$\sigma_t = \int \sigma(\Delta,\omega)d\omega = C\sum_k \omega_k B(E1;0^+ \to 1_k^-) = CS_l. \tag{6.8}$$

Inserting the EWSR given in Table V in the above equation the total cross section is readily obtained. The result are

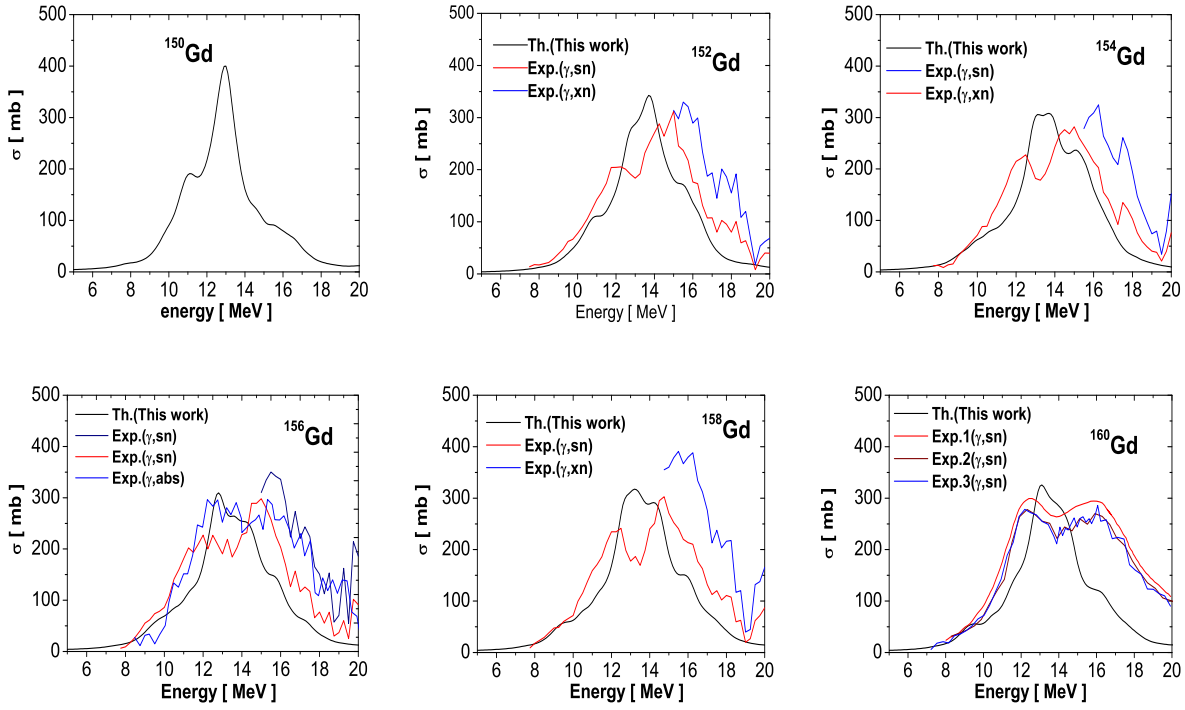

FIG. 4: The dipole photoabsorbtion cross section as function of energy for even-even $^{150-160}$Gd. The Lorentzian folding function has a width of 1MeV and the normalization constant is 0.014. The dimension is mb.Experimental data are taken from Refs.[57–61]. The error bars for experimental data were omitted.

Nucleus	S_l(EWSR) [MeV.e^{2}b]	S_{corr} [MeV.e^{2}b]	r.d. [%]	S_{TRK} [MeV.e^{2}b]	q	PSR [%]
^{150}Gd	156.470	157.433	0.60	205.232	1.145	1.98
^{152}Gd	170.673	170.984	0.18	207.413	1.102	1.15
^{154}Gd	167.257	169.218	1.17	209.199	1.118	3.10
^{156}Gd	164.152	167.690	2.15	211.106	1.134	2.69
^{158}Gd	175.622	175.268	0.20	218.496	1.115	2.77
^{160}Gd	169.963	174.649	2.70	214.477	1.124	2.97

TABLE V: The two members of the sum rule equation, S_l(EWSR) and S_{corr}, the relative deviation (r.d.=$|S_{corr} - S_l|/S_l$, the TRK sum rule S_{TRK}, the ratio q(=S_{TRK}/S_l) and the contribution of the PDR transitions to the total sum rule, PSR, are listed for the six isotopes of Gd.

Nucleus	σ_t[MeVe^2b]	
	Th.	Exp.
^{150}Gd	2.19	-
^{152}Gd	2.39	-
^{154}Gd	2.34	-
^{156}Gd	2.30	2.07±0.07 [57]
^{158}Gd	2.46	-
^{160}Gd	2.38	2.87±0.20 [60]

TABLE VI: The calculated total photoabsorbtion cross sections are compared with the corresponding available experimental data.

listed in Table VI, where the available experimental data are also given. From this comparison we may say that the calculations of the photoabsorbtion cross section, shown in Fig.4, are consistent with those concerning the EWSR.

VII. SUMMARY AND CONCLUSIONS

In the previous sections we developed a formalism for the microscopic description of the Pygmy Dipole and Giant Dipole resonances. The main ingredients, specific to the present approach, are the projected spherical single particle basis, which allows for an unified description of spherical, transitional and deformed nuclei, and the use of the Schiff dipole moment for the two body dipole-dipole interaction. The model Hamiltonian consists of the spherical shell model single particle term, the pairing interaction for alike nucleons and the dipole-dipole interaction. This is successively subject to the BCS and QRPA treatment. The results of the QRPA approach are used to calculate the B(E1) values characterizing the dipole transitions from the ground state, 0^+, to the dipole states 1^-_k, with k labelling the roots of the QRPA equations.

For the PDR region, [0,10] MeV, the dipole strength was plotted as function of the excitation energy. From there one sees that the strength distribution reclaims a resonance structure. Table II shows that for ^{150,152,156}Gd the largest B(E2) values are associated with the isovector states while for ^{154,158,160}Gd the isoscalar transitions are dominant. Except for ^{154}Gd where $(\Delta I(\pi), \Delta I(\nu)$ =(0,1), for all the others the transitions change I by one unit

Nucleus	k	$B(E1;0^+ \to 1^-_k)$[W.u.]	type	k	$B(E1;0^+ \to 1^-_k)$[W.u.]	type
^{150}Gd	21	3.60	IV	3	2.66	IV
^{152}Gd	19	3.78	IV	24	2.10	IS
^{154}Gd	31	8.10	IS	32	6.35	IS
^{156}Gd	25	5.34	IV	19	5.04	IV
^{158}Gd	28	10.13	IS	19	9.69	IS
^{160}Gd	21	10.00	IS	27	6.57	IV

TABLE VII: The largest two B(E1) values selected from Table II. Also, the label k for the state populated by the mentioned transition is mentioned.

for both the protons and the neutrons.The major single particle transitions participating to the collective transition, are characterized by $\Delta N = 1$ despite the fact the Schiff effect is included. This is true also for the energy interval [10,20] MeV. The $\Delta N = 3$ transitions become dominant for states of energies larger than 20 MeV, where a local resonance structure may appear. However, in order to make a definite statement, this energy region should be carefully investigated by both experimentalists and theoreticians. The PDR transitions bring only a few percents (1.15-3.1) contribution to the total EWSR. Concluding, the dominant transitions of the PDR-kind are to phonon states describing oscillations of the neutron excess in phase or anti-phase with the oscillations of protons from the saturated core.

We may ask ourselves whether the PDR is formed of collective transitions. To answer this question, in Table VII we listed the largest two B(E1) values in W.u., for each isotope. We notice that the biggest peaks appear in ^{154,158,160}Gd and amounts about 8-10 W.u. which means that the corresponding transitions may be called as moderate collective. However, although for ^{150}Gd the largest B(E1) values are only of few W.u., since the corresponding maximal phonon amplitudes are relatively small, many dipole configurations are needed in order to saturate the normalization restriction given by the second equations (3.8). Moreover these transitions are of isovector type, which means that the protons and neutrons contributions to the transition probabilities add coherently, given the fact that the neutron effective charge is negative. Concluding, we met situations when despite the transition collective nature, the reduced transition probability is only of few W.u.. Therefore, to be collective does not necessarily mean a large B(E1) value. Also, we notice that the largest B(E1) values are associated with the transitions characterized by $(\Delta I(\pi), \Delta I(\nu))$= (1,1), excepting ^{154}Gd and ^{160}Gd where the mentioned pair of angular momentum variation are (1,0) and (0,1) respectively. Even for these two isotopes the contribution of protons/neutrons prevail over that of neutrons/protons if the considered transition flips the total angular momentum, I, by one unit.

The PDR is placed on the left tail of the GDR for which our results are as follows. As for the energy interval [10,20] MeV,enveloping the discrete B(E1) values by Lorentzians of a width equal to 1 MeV, one obtains the continuous distribution of the dipole strength with energy, shown in Fig 3. The involved transitions forming The GDR, have either an isovector or an isoscalar character, i.e. they describe proton and neutron oscillations, which are either in phase or out of phase. The nuclear deformation induces a split of the dipole strength, which is diminished by the r^3term. The r^3 term from the Schiff momentum suppresses the transition matrix elements, which results in needing an increasing factor q for the effective charges (4.4) in order to obey the TRK sum rule. This small violation of the TRK sum rule is caused by that the sum rule uses the standard dipole momentum, while for the dipole transition matrix elements, the Schiff momentum is employed. Indeed, using the Schiff momentum also for the TRK sum rule, this is corrected to S_{cor} which agrees well with S_l, as seen from Table V. Once the B(E1) transition probabilities are calculated, one easily obtains the photoabsorbtion cross section which is plotted in Fig.4, where the experimental data are also shown. The agreement between our results and experimental data is reasonable good. Integrating the cross section over the whole excitation energy interval one obtains the total cross section which is collected in Table VI. For two isotopes, ^{156,160}Gd, the experimental data for total cross section are known. One notices that the agreement between our our calculation and experimental data is quite good which reflects a positive consistency of the calculations of the cross section shown in Fig. 4 and the EWSR. We mention again that the Schiff correction diminishes the matrix elements of the standard dipole operator and by this wash out a part of the effect caused by the non-conservation of the center of mass momentum. This effect was fully eliminated in Ref.[18]. Another symmetry which is taken care here is that against rotation transformations, the considered isotopes being deformed. This is achieved by using a projected spherical single particle basis which results in having a contribution from all K-components of the involved wave functions to the cross section as well as to the EWSR.

Concluding, the proposed formalism allows a unified description of dipole resonances PDR and GDR for spherical and deformed nuclei.

[1] M. Goldhaber and E. Teller, Physical Review 74,9, 1046 (1948).
[2] D. M. Brink, Talk presented at the workshop on " Chaos and Collectivity in Many Body Systems at the PMIPKS, Drezden, Germany, March 5-8, 2008.
[3] N. Lo Iudice and F. Palumbo,Phys. Rev. Lett. **41**, 1532 (1978).
[4] A. Faessler, Nucl. Phys. **85**, 653 (1966).
[5] V. Marhun-Rewani, W. Greiner and J. A. Marhun, Phys. Lett.**57 B**,109 (1975).
[6] E. G. Lanza,et. al., Prog. Part. Nucl. Phys, **129**, 104006 (2023).
[7] A. Bracco. J. Phys.:Conf. Series **312**, 92005 (2011).
[8] P. G. Reinhard and W. Nazarewicz, Phys. Rev. C **81** 051303(R) (2010).
[9] M. Arnold and S. Goriely, Phys. Reports **384**, 1 (2003).
[10] A. Krugmann *et. al.*, EPJ Web of Conferences **66**, 02060 (2014).

[11] D. H. Youngblood, Y.-W. Lui, H. L. Clark, B. Hohn, Y. Tokimoto and X. Chen, Phys. Rev. **C 69**, 034315 (2004).
[12] T. Aumann, Eur. Phys. J. **A 26**, 441 (2005).
[13] J. Suhonen et. al., Phys. Lett. **B 668**,277 (2008).
[14] A. P. Tonchev et. al., J, Phys.:Conf. Series **312**, 092058 (2011).
[15] Nguen Van Giai and H. Sagawa, Nucl. Phys. **A 371**, 1 (1981).
[16] N. N. Arsenyev, A. P. Severyukhin, V. V. Voronov and N. Van Giai, EPJ Web of Conf.**194**, 04002 (2018).
[17] V. Yu. Ponomarev *et al.*, Nucl. Phys. **A 569**, 333c (1994).
[18] E. Guliyev, H. Quliyev and A. A. Kuliev, J. Phys. G; Nucl. Part. Phys. **47**, 115107 (2020).
[19] K. Yoshida and T. Nakatsukasa, Phys. Rev. **C 83**, 021304(R) (2011).
[20] N. Auerbach, Ch. Stoyanov, M. R. Anders and S. Shlomo, Phys. Rev. **C 89**, 014335 (2014).
[21] H. Quliev, Z. Zenginerler,E. Guliev, A. A. Kuliev, AIP Conference Proceedings **1815**, 060020 (2017).
[22] J. Enders, *et. al.* , preprint, 12 May 2004.
[23] D. Vretenar et. al., Nucl. Phys. **A 692**, 496 (2001).
[24] E. Litvinova, P. Ring and V. Tselyaev, Phys. Rev. **C78**, 014312 (2008).
[25] V. Baran, B. Frecus, M. Colonna and M. Di Toro, Phys. Rev. **C85**, 051601(R) (2012).
[26] V. Baran, M. Colonna, M. Di Toro, A. Croitoru, D. Dumitru, Phys. Rev. **C 88**,044610 (2013).
[27] A. A. Raduta, D. S. Delion and N. Lo Iudice, Nucl. Phys. **A 564** (1993) 185.
[28] A. A. Raduta, N. Lo Iudice and I. I. Ursu, Nucl. Phys. **A584** (1995) 84.
[29] A. A. Raduta, A. Escuderos and E. Moya de Guerra, Phys. Rev. **C 65** (2002) 024312.
[30] A. A. Raduta, A. Escuderos, A. Faessler, E. Moya de Guerra and P. Sarriguren, Phys. Rev. **C69** (2004) 064321.
[31] A.A. Raduta, A. Faessler and D. S. Delion, Nucl. Phys. **A 564** (1993) 185; Phys. Lett.**B 312** (1993) 13.
[32] A. A. Raduta, D. S. Delion and A. Faessler, Nucl. Phys. **A 617**, 176 (1997).
[33] A. A. Raduta and R. Budaca, Ann. Phys. [NY], **347**, 141 (2014).
[34] A. A. Raduta, C. M.Raduta and R. Poenaru,Phys. Rev **C 106**, 044301 (2022).
[35] S. G. Nilsson, Mat. Fys. Medd. K. Dan. Vid. Selsk. **29**, no. 16 (1955).
[36] L. I. Schiff, Phys. Rev. 132, 2194 (1963).
[37] P. Ring and P. Schuck, *The nuclear many-body problem, Springer, Berlin, Heidelberg, New York,p. 76.*
[38] P. Ring and P. Schuck, *The nuclear many-body problem, Springer, Berlin, Heidelberg, New York,p. 38.*
[39] M. E. Rose, Elementary Theory of Angular Momentum (Wiley, New York, 1957).
[40] C. M. Raduta, A. A. Raduta and I. I. Ursu, Phys. Rev. **C 84**,064322 (2011).
[41] A. A. Raduta, C. M. Raduta and A. Escuderos, Phys. Rev. **C 71**, 024307(2005).
[42] E. Baranger, Ch. Wan Lee, Nucl. Phys. 22, 17 (1961)
[43] H. J. Lipkin, Phys. Rev. 110, 1395 (1958).
[44] A. A. Raduta, R. Budaca and Al. H. Raduta, Phys. Rev. **A 79** 023202 (2009).
[45] T.Ullah, D. Rowe, Nucl. Phys. **A 163**, 257 (1971).
[46] W. Thomas, Naturwissenshaften 13 627 (1925)
[47] F. Reiche and W. Thomas, Z. Phys. 34, 510 (1925).
[48] W. Kuhn, Z. Phys. 33, 408 (1925).
[49] A. A. Raduta and A. Faessler, J. Phys. G; Nucl. Part. Phys. **31**,873 (2005).
[50] N. Lo Iudice, A. A. Raduta and D. S. Delion, Phys. Rev. C50, 127 (1994).
[51] G. A. Lalazissis, S.Roman and P. Ring, Atomic Data and Nuclear Data Tables 71,1 (1999).
[52] P. Carlos *et. al.*, Nucl. Phys **A 225**, 171 (1974).
[53] Kenichi Yoshida and Takashi Nakatsukasa, Phys. Rev. **88**, 034309 (2013).
[54] L.M. Donaldson *et. al.*, Phys. Lett. **B 276**, 133, (20180.
[55] V. Rezwani *et. al.* , Proc. Int. Conf. on nuclear structure studies, Sendai (Jap.), Sept. !972.
[56] M. Danos and W. Greiner, Phys. Rev. **138 B**, 876 (1965).
[57] G. M. Gurevich *et al.*, Nucl. Phys. **A 31**, 257 (1981).
[58] O. V. Vasiliev*et al.*, Sov. J. Nucl. Phys. **13**, 259 (1971).
[59] B. L. Berman *et al.*,Phys. Rev. **189**, 1576 (1969).
[60] V. V. Varlamov *et al.*, Izv. Aka. Nauk. Ross. Aka. NaukSeri. Fizich.**67**, 656 (2003).
[61] V. V. Varlamov *et al.*, Memoirs of Phys. Fac. Moscow State Univ. **1**, 1910202 (2019).

Toward a new approach for the Pygmy Dipole Resonance in even-even nuclei. Application to the isotopes ^{144,148,150,152,154}Sm.

A. A. Raduta[a),b)], C. M. Raduta [a)] and Al. H. Raduta [a)]
[a)] *Department of Theoretical Physics, Institute of Physics and Nuclear Engineering, Bucharest, POBox MG6, Romania and*
[b)] *Academy of Romanian Scientists, 54 Splaiul Independentei, Bucharest 050094, Romania*

A many body Hamiltonian consisting in a spherical shell model mean field term, a pairing interaction for alike nucleons and a dipole-dipole interaction, with the dipole operator involving a cubic term in the radial coordinate, is studied within a quasiparticle random phase approximation (QRPA) and applied numerically to five even-even isotopes of Sm. The resulting wave functions are further used to calculate the B(E1) values which at their turn are employed to calculate the photo absorption cross section, the integrated moments of the cross section and the energy weighted sum rule (EWSR). The calculated cross section and its integrated moments are compared with the available data and a good agreement is pointed out. One distinguishes two regions corresponding to the Pygmy Dipole Resonance (PDR), 1-10 MeV, and to the Giant Dipole Resonance (GDR), 10-20 MeV respectively, these being separately studied. The peaks belonging to each of the two ranges are in detail analyzed. The PDR states are located around the neutron separation energy and are mainly formed of collective isoscalar and neutron collective states. The PDR states describe oscillations of the neutrons excess against the protons from the isospin saturated core. The character of the states from the GDR region, isoscalar or isovector, is also pointed out. The PDR states carry only 0.8-2.7% of the total EWSR and 0.4-5.9% of the total E1 strength. The dependence of the dipole strength on nuclear deformation is evidenced. A comment on the cross section split into two branches for deformed isotopes, is included. The r-cubic term and the nuclear deformation have opposite effect on the dipole strength. Also it diminishes the effect of the non-conservation of the center of mass momentum. The famous Thomas Reiche Kuhn sum rule formula is generalized to the case of the Schiff dipole momentum. The new sum rule is well satisfied. The projected spherical single particle basis used in our formalism allows for an unified description of the spherical transitional and deformed isotopes.

I. INTRODUCTION

Since the pioneering paper of Goldhaber and Teller [1] describing the giant dipole resonance (GDR) as a linear out of phase oscillation of neutrons and proton respectively showed up [2], many papers have been devoted to the study of the relative motion of protons and neutrons [3–5]. One of the hot subject of the last decades is that of Pygmy dipole resonance (PDR), which appears at an energy lower than the GDR peak, around the neutron emission energy threshold. It is commonly accepted that such a resonance is determined by the neutron excess oscillation against the proton from an isospin saturated core [6–8].

The presence of the PDR in nuclei with neutron excess could be related with the symmetry energy parameters. Several attempts have been made to use the PDR data to constrain the symmetry energy and extract a relation with the neutron skin thickness in neutron rich nuclei. The neutron skin thickness is defined as the difference between the root mean square of neutron and proton radii: $r_{skin} = r^n_{rms} - r^p_{rms}$. There exists a strong correlation between neutron skin thickness and the dipole polarizability defined as:

$$\alpha_D = \frac{8\pi e^2}{9} m_{-1}(E1), \tag{1.1}$$

where $m_{-1}(E1)$ denotes the sum of the inverse energy weighted dipole strengths [9][1]. The product $\alpha_D \mathcal{J}$, with $\mathcal{J}$ standing for the symmetry energy at saturation density, is related with the neutron skin thickness r_{skin} and the slope of the symmetry energy at the saturation density, L [10]. Therefore, a precise measurement of α_D would allow to determine a relation between the symmetry energy $\mathcal{J}$ and the slope L, which of course improves our knowledge about the symmetry energy.

Pygmy resonance in neutron rich nuclei is an important topic of study at the new generation of radioactive ion beam facilities [11, 12]. Furthermore, important nuclear-structure effects have to be taken into account in order to

---

[1] The standard definition is used: $m_{-1}(E1) = \sum_k E_k^{-1} |\langle 1^-_k \mu | D_{1\mu} | 0 \rangle|^2$. Here $D_{1\mu}$ denotes the transition dipole operator while E_k is the excitation energy corresponding to the electric dipole state $|1^-_k\rangle$.

interpret results obtained in the next generation of neutrinoless double-beta ($0\nu\beta\beta$) decay experiments [13] [2].

Knowledge of the nuclear matrix elements, governed by the PDR, for example, will be indispensable for reliably deducing the effective Majorana mass.

The knowledge of the electromagnetic transition strength is very important for the calculation of the neutron capture rates in the r-process (rapid neutron capture process), a phenomenon which competes with the β decay and is responsible for producing about half of the heavy elements. The Pygmy resonance taking place near the neutron threshold has also important astrophysical implications. Indeed, the reaction rates of (γ,n) and (n,γ) reactions in explosive nucleosynthesis of certain neutron deficient nuclei, may be significantly enhanced by the PDR [11].

Experimentally the PDR are studied by: a) isovector probes like i) Relativistic Coulomb excitation; ii) Nuclear Resonance Fluorescence technique, (γ,γ');iii) Coulomb excitations by (p,p') scattering [14]; b) isoscalar probes like: (α,α')[15]; (^{17}O,^{17}O'); (^{68}Ni,^{68}Ni' γ). The PDR states split into two parts, one belonging to an energy range between 4 and 6 MeV, which is excited in $(\alpha,\alpha'\gamma)$ as well as (γ,γ') experiments and one part at higher energy, excited only in (γ,γ'). This phenomenon is known under the name of isospin splitting or of isospin mixing.

Many theoretical approaches have been used to reveal various properties of the PDR. To save the space here we mention only few of them. Thus, the isoscalar dipole strength distribution was studied within a self-consistent RPA approach in Ref. [16] . Also, in Ref. [17] starting with the Skyrme mean field calculation, some properties of the electric dipole strength in Ca isotopes are studied by taking into account the coupling of one and two phonon terms in the wave functions of the excited states. Calculation performed within Hartree Fock Bogoliubov (HFB) plus quasiparticle random phase approximation (QRPA) with Skyrme interaction for Nd and Sm isotopes, the summed dipole strength dependence on nuclear deformation has been studied [18]. In Ref.[19] it was shown that the isoscalar dipole strength distribution contributes to the Schiff moment. The PDR in ^{154}Sm and even-even Gd isotopes was also studied in Refs.[20, 21], respectively. The spectral statistics and the fine structure of the Pygmy dipole resonance in the isotones with N=82 has been studied in Ref.[22]. The relativistic random phase approximations (RRPA) was used for describing some features of the PDR[23]. Solving the self-consistent Landau-Vlasov equation, the dependence of the PDR properties on the symmetry energy has been explored. Also, the existence of a isoscalar dipole mode below the GDR has been pointed out [24, 25]. The toroidal, compression and vortical dipole modes were studied in Ref.[26] for the semi-magic and double magic Sn isotopes, and their dependence on the convection and magnetic current densities respectively, was evidenced. It was shown that the toroidal mode resides in the region of the Pygmy dipole resonance. The toroidal and compression states were also analyzed within a QRPA formalism with Skyrme interaction, for ^{24}Mg [27]. The effect of pairing and nuclear deformation on the Pygmy resonance was considered in Ref.[28] and it was concluded that for low energy dipole and toroidal modes, the branch $K^\pi = 1^-$ dominates over the $K^\pi = 0^-$ one. H. Quliev et al.[29] described the split of the photoabsorption cross section into K=0 and K=$\pm$ components in the deformed even isotopes of Nd.

In the present paper we propose a formalism for describing the properties of the PDR states. The main ingredients of our approach consist of using a projected spherical single particle basis as well as of a Schiff dipole momentum in the dipole-dipole interaction. The paper is organized as follows: In section 2 we introduce the single particle basis states, which is used for treating a many body Hamiltonian presented in Section 3, through a QRPA method. The electric dipole transition probability is considered in Section 4. Section 5 is devoted to the description of the energy weighted sum rule (EWSR), while Section 6 presents the results of a numerical application to the isotopes ^{144,148,150,152,154}Sm. Section 7 summarizes the main conclusions.

II. PROJECTED SINGLE PARTICLE BASIS

The angular momentum projected single particle basis, defined in Ref.[30], seems to be suitable for the description of the single particle motion in a deformed mean field generated by the particle-core interaction. Such a projected spherical single particle basis has been used to study the collective M1 states in deformed nuclei [30–32] as well as the rate of double beta process [33–36].

To fix the necessary notations and moreover for the sake of a self-contained presentation, we describe briefly the main ideas underlying the construction of the projected single particle basis.

---

[2] The neutrinos-oscillation experiment Super-Kamiokande showed that neutrino has a non-zero mass, which means that it is a Majorana particle. The fact that neutrino is massive particle could be confirmed if the $0\nu\beta\beta$ decay were detected. Since the inverse of the half life of this process is proportional with the nuclear matrix element and the neutrino effective mass (i.e. the sum of the electron, μ and τ-like neutrino masses), quantitative information about the effective mass might be obtained only with reliable nuclear matrix elements.

The single particle mean field is determined by a particle-core Hamiltonian:

$$\tilde{H} = H_{sm} + H_{core} - M\omega_0^2 r^2 \sum_{\lambda=0,2} \sum_{-\lambda\leq\mu\leq\lambda} \alpha^*_{\lambda\mu} Y_{\lambda\mu}, \tag{2.1}$$

where H_{sm} denotes the spherical shell model Hamiltonian, while H_{core} is a harmonic quadrupole boson (b^+_μ) Hamiltonian associated to a phenomenological core. The interaction of the two subsystems is accounted for by the third term of the above equation, written in terms of the shape coordinates $\alpha_{00}, \alpha_{2\mu}$. The quadrupole coordinates are related to the quadrupole boson operators by the canonical transformation:

$$\alpha_{2\mu} = \frac{1}{k\sqrt{2}}(b^\dagger_{2\mu} + (-)^\mu b_{2,-\mu}), \tag{2.2}$$

where k is an arbitrary C number. The monopole shape coordinate is to be determined from the volume conservation condition.

Averaging $\tilde{H}$ on a given eigenstate of H_{sm}, denoted as usual by $|nljm\rangle$, one obtains a deformed quadrupole boson Hamiltonian, which admits the axially symmetric coherent state

$$\Psi_g = exp[d(b^+_{20} - b_{20})]|0\rangle_b, \tag{2.3}$$

as eigenstate. $|0\rangle_b$ stands for the vacuum state of the boson operators, while d is a real parameter which simulates the nuclear deformation. On the other hand, averaging $\tilde{H}$ on Ψ_g, one obtains a single particle mean field operator for the single particle motion, similar to the Nilsson Hamiltonian. Concluding, by averaging the particle-core Hamiltonian with a factor state, the rotational symmetry is broken and the mean field mentioned above may generate, by diagonalization, a deformed basis for treating the many body interacting systems. However, this standard procedure is tedious since the final many body states should be projected over the angular momentum.

Our procedure defines first a spherical basis for the particle-core system, by projecting out the angular momentum from the deformed state

$$\Psi^{pc}_{nlj} = |nljm\rangle\Psi_g. \tag{2.4}$$

The projected states are obtained, in the usual manner, by acting on these deformed states with the projection operator

$$P^I_{MK} = \frac{2I+1}{8\pi^2}\int D^{I*}_{MK}(\Omega)\hat{R}(\Omega)d\Omega. \tag{2.5}$$

We consider the subset of projected states :

$$\Phi^{IM}_{nlj}(d) = \mathcal{N}^I_{nlj}P^I_{MI}[|nljI\rangle\Psi_g] \equiv \mathcal{N}^I_{nlj}\Psi^{IM}_{nlj}(d), \tag{2.6}$$

which are orthonormalized to unity and form a basis for the particle-core system. This basis exhibits useful properties, which have been presented in some of our previous publications.

To the projected spherical states, one associates the "deformed" single particle energies defined as the average values of the particle-core Hamiltonian $H' = \tilde{H} - H_{core}$:

$$\epsilon^I_{nlj} \;=\; \langle\Phi^{IM}_{nlj}(d)|H'|\Phi^{IM}_{nlj}(d)\rangle. \tag{2.7}$$

Since the core contribution to this average value does not depend on the quantum numbers of the single particle energy levels, it produces a constant shift for all energies. For this reason such a term is omitted in (2.7). The deformation dependence of the new single particle energies is similar to that shown by the Nilsson model [37]. Therefore, the average values ϵ^I_{nlj} may be viewed as approximate single particle energies in deformed Nilsson orbits [37]. We may account for the deviations from the exact eigenvalues by considering, at a later stage, when a specific treatment of the many body system is performed, the exact matrix elements of the two body interaction. The dependence of single particle energies on deformation parameter d is shown in Fig.1 for protons and neutrons respectively, in the major shell with N=5 and N=6.

It is worth to mention that if the volume conservation is ignored, the single particle energies depend linearly on the deformation parameter d. Is the volume conservation condition the restriction which causes the bending of energy curve. Although the energy levels are similar to those of the Nilsson model, the quantum numbers in the two schemes are different. Indeed, here we generate from each j a multiplet of $(2j+1)$ states distinguished by the quantum number I, which plays the role of the Nilsson quantum number Ω, and runs from 1/2 to j. Moreover, the energies

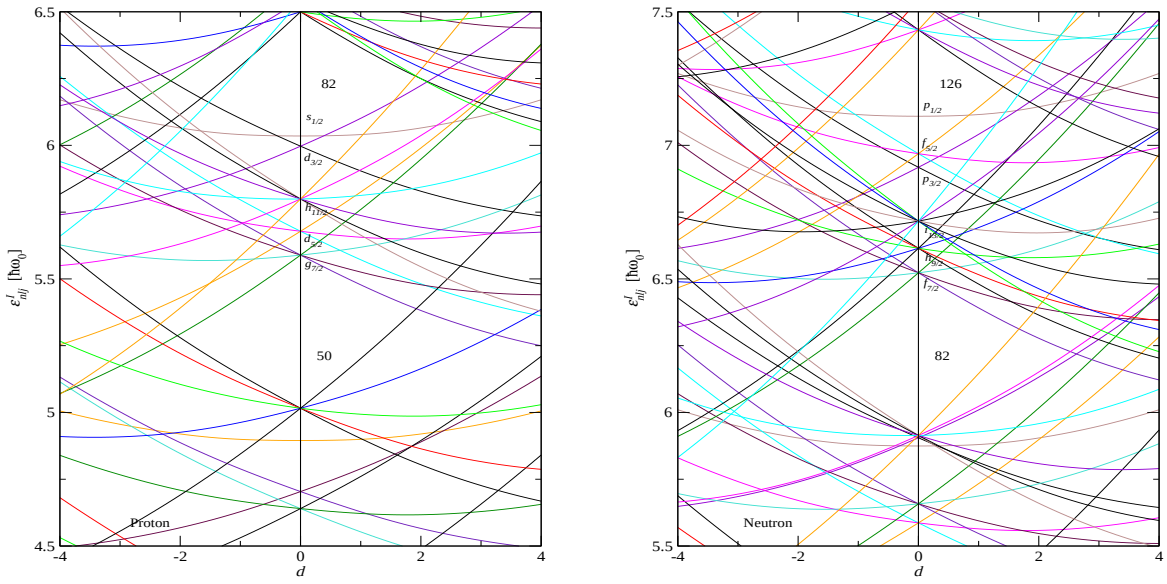

FIG. 1: Color online. Proton and neutron single-particle energies in the region of N=5 and N=6 shells respectively, given by Eq.(2.7), where the shell model parameters are $\kappa = 0.0637$ and $\mu = 0.60$ for protons, and $\mu = 0.42$ for neutrons were used. The canonical transformation constant is fixed to $k = 10$.

corresponding to the quantum numbers K and $-K$ are equal to each other. On the other hand, for a given I there are $2I + 1$ degenerate sub-states, while the Nilsson states are only double degenerate. As explained in Ref. [30], the redundancy problem can be solved by changing the normalization of the model functions:

$$\langle \Phi_\alpha^{IM} | \Phi_\alpha^{IM} \rangle = 1 \Longrightarrow \sum_M \langle \Phi_\alpha^{IM} | \Phi_\alpha^{IM} \rangle = 2. \tag{2.8}$$

Due to this weighting factor the particle density function is providing the consistency result that the number of particles which can be distributed on the (2I+1) sub-states is at most 2, which agrees with the Nilsson model. Here α stands for the set of shell model quantum numbers nlj. Due to this normalization, the states Φ_α^{IM} used to calculate the matrix elements of a given operator should be multiplied with the weighting factor $\sqrt{2/(2I+1)}$.

The projected states might be viewed as eigenstates of an effective rotational invariant fermionic one-body Hamiltonian $H_{\rm eff}$, with the corresponding energies given by Eq.(2.7):

$$H_{\rm eff} \Phi_\alpha^{IM} = \epsilon_\alpha^I(d) \Phi_\alpha^{IM}. \tag{2.9}$$

As shown in Ref. [30], in the vibrational limit, $d \to 0$, the projected spherical basis goes to the spherical shell model basis, and ϵ_{nlj}^I to the eigenvalues of H_{sm}.

A fundamental result obtained in Ref. [36] for the product of two single particle states, which comprises a product of two core components, deserves to be mentioned. Therein we have proved that the matrix elements of a two body interaction corresponding to the present scheme are very close to the matrix elements corresponding to spherical states projected from a deformed product state with one factor being a product of two spherical single particle states, and a second factor consisting of a unique collective core wave function. The small discrepancies of the two types of matrix elements could be washed out by using slightly different strengths for the two body interaction in the two methods. Due to this property the basis (2.6) might be used for studying any two-body interaction.

As for the matrix elements of a one-body operator T_μ^k the result is:

$$\begin{aligned} &\langle \Phi_{nlj}^I || T^k || \Phi_{n'l'j'}^{I'} \rangle = f_{nljI}^{n'l'j'I'}(d) \langle nlj || T^k || n'l'j' \rangle, \quad \text{with} \\ &f_{nljI}^{n'l'j'I'}(d) = \mathcal{N}_{nlj}^I(d) \mathcal{N}_{n'l'j'}^{I'}(d) \hat{j}\hat{I}' \sum_J C_{I\ 0\ I}^{j\ J\ I} C_{I'\ 0\ I'}^{j'\ J\ I'} W(jkJI'; j'I) (N_J^g)^{-2}. \end{aligned} \tag{2.10}$$

This expression is used to calculate the reduced matrix elements of the dipole moment operator. $\mathcal{N}^I_{nlj}(d)$ denotes the norm of the projected spherical single particle state, while N^g_J is the norm of the core projected state. Also, the Rose's convention is used for the reduced matrix elements [38]. Finally, we mention that if we used a Nilsson basis instead of a projected spherical single particle basis, the final state resulting from a specific many body treatment have to be projected over angular momentum, since in the laboratory frame the rotational symmetry holds. But the angular momentum projection from a many body state is always a tedious task.

III. THE MODEL HAMILTONIAN

We suppose that the states describing the nuclei that might be excited in a giant or a Pygmy resonance are described by a many body Hamiltonian, written in the projected spherical basis as:

$$H = \sum_{\tau,\alpha,I,M} \frac{2}{2I+1}(\epsilon_{\tau\alpha I} - \lambda_{\tau\alpha}) c^\dagger_{\tau\alpha IM} c_{\tau\alpha IM} \tag{3.1}$$
$$- \sum_{\tau,\alpha,I,I'} \frac{G_\tau}{4} P^\dagger_{\tau\alpha I} P_{\tau\alpha I'} - \sum_{\tau ab;\tau' cd;\mu} X_{\tau,\tau'} D_{1\mu}(\tau; ab) D_{1,-\mu}(\tau'; cd)(-)^\mu,$$

where $c^\dagger_{\tau\alpha IM}(c_{\tau\alpha IM})$ denotes the creation (annihilation) operator of one nucleon of the type $\tau(=\pi,\nu)$ in the state Φ^{IM}_α, with α being an abbreviation for the set of quantum numbers nlj. The Hamiltonian H contains the mean field term, the pairing interaction and the Schiff dipole-dipole interaction [39] for alike nucleons.

To simplify the notations, hereafter the set of quantum numbers $\alpha(=nlj)$ will be omitted. The two body interactions are separable with the factors defined by the following expressions:

$$P^\dagger_{\tau I} = \sum_M \frac{2}{2I+1} c^\dagger_{\tau IM} \widetilde{c^\dagger_{\tau IM}}, \tag{3.2}$$

$$D_{1\mu}(\tau; II') = \tag{3.3}$$
$$\sum_{M,M'} \frac{\sqrt{2}}{\hat{I}} \langle \tau; IM | (r - \frac{3}{5}\frac{r^3}{b^2}) Y_{1\mu} | \tau; I'M' \rangle \frac{\sqrt{2}}{\hat{I}'} c^\dagger_{\tau;IM} c^\dagger_{\tau;I'M'} \equiv d_1(\tau; II') \left(c^\dagger_{\tau;I} c_{\tau;I'} \right)_{1\mu},$$

where:

$$d_1(\tau; II') = \frac{2}{\hat{1}\hat{I}'} \mathcal{N}^I_{nlj}(d) \mathcal{N}^{I'}_{n'l'j'}(d) \tag{3.4}$$
$$\times \sum_J C^{j\ J\ I}_{I\ 0\ I} C^{j\ J\ I'}_{I'\ 0\ I'} W(j1JI'; j'I) \left(N^{(g)}_J(d) \right)^{-2} \langle nlj || \left(r - \frac{3}{5}\frac{r^3}{b^2} \right) Y_{1\mu} || n'l'j' \rangle.$$

The dipole operator involves the oscillator length denoted by $b = \sqrt{\frac{\hbar}{M\omega}}$. Note that the matrix element of the Schiff dipole operator is a product of two factors, one carrying the deformation dependence and one being a matrix element corresponding to the standard spherical shell model states.

We may ask ourselves, why do we use the Schiff dipole operator instead of the standard form, linear in r, showing up naturally as the first order expansion of the Coulomb interaction between the charge of the target nucleus and the electric field generated by the projectile. To answer this question we first notice that the corrective term is of an opposite phase than the standard dipole term and by this induces a screening effect on the transition matrix elements. On the other hand this term is the one which generates $\Delta N = 3$ transitions which, as we shall see later, might conctribute to the considered resonances. It is conspicuous that the Hamiltonian (3.2) does not commute with the center of mass linear momentum, and consequently this magnitude is not conserved. However, the contribution to the H energies, of the spurious components of the wave function, due to the center of mass linear momentum non-conservation, is small, of the order of $1/A$ with A denoting the atomic mass number [40, 41]. This small contribution is still diminished by the presence of the cubic term in the expression of the Schiff dipole operator. Two of the present team (AAR and AlHR) used a Schiff-type dipole transition operator for the description of the photoabsorption cross-section spectra in the medium atomic clusters of Na [42]. There in, a good agreement with the experimental data was pointed out.

Within the quasiparticle representation, defined by the Bogoliubov-Valatin transformation:

$$a^\dagger_{\tau IM} = U_{\tau I} c^\dagger_{\tau IM} - s_{IM} V_{\tau I} c_{\tau I-M}, \ \ s_{IM} = (-)^{I-M},$$
$$U^2_{\tau I} + V^2_{\tau I} = 1, \ \ \tau = p, n, \tag{3.5}$$

the first two terms of H are replaced by the independent quasiparticles (qp) term, $\sum E_{\tau I} a^{\dagger}_{\tau IM} a_{\tau IM}$, while the dipole-dipole interaction is expressed in terms of the dipole two *qp* and the *qp* density operators:

$$\begin{aligned}
A^{\dagger}_{1\mu}(\tau; II') &= \sum C^{I\ I'\ 1}_{m\ m'\ \mu} a^{\dagger}_{\tau;Im} a^{\dagger}_{\tau;I'm'}, \\
A_{1\mu}(\tau; II') &= \left(A^{\dagger}_{1\mu}(\tau; II')\right)^{\dagger}, \\
B^{\dagger}_{1\mu}(\tau; II') &= \sum C^{I\ I'\ 1}_{m\ -m\ \mu} a^{\dagger}_{\tau;Im} a_{\tau;I'm'} (-)^{I'-m'}, \\
B_{1\mu}(\tau; II') &= \left(B^{\dagger}_{1\mu}(II')\right)^{\dagger}.
\end{aligned} \tag{3.6}$$

In the quasiparticle (qp) representation and with the above introduced notation for two qp and qp density dipole operator, the Schiff dipole operator becomes:

$$\begin{aligned}
D_{1\mu}(\tau; II') = \sum_{E_{\tau I} < E_{\tau I'}} & d_1(\tau; II') \left[\xi^{(-)}(\tau, II') \left(A^{\dagger}_{1\mu}(\tau; II') - (-)^{1-\mu} A_{1,-\mu}(\tau; II')\right)\right. \\
+ \ \left. \eta^{(-)}(\tau, II') \left(B^{\dagger}_{1\mu}(\tau; II') - (-)^{1-\mu} B_{1,-\mu}(\tau; II')\right)\right], \\
\xi^{(-)}(\tau, II') = U_{\tau I} V_{\tau I'} - U_{\tau I'} V_{\tau I}, \ \ & \eta^{(-)}(\tau, II') = U_{\tau I} U_{\tau I'} - V_{\tau I} V_{\tau I'}.
\end{aligned}$$

Using the quasiparticle representation for the model Hamiltonian, a boson-like commutation relations for the operators $A^{\dagger}_{1\mu}$ and $A_{1\mu}$, and vanishing commutators for the operators $A^{\dagger}_{1\mu}$ and $B_{1\mu}$ as well as for $B^{\dagger}_{1\mu}$ and $B_{1\mu}$, one can define the phonon operator:

$$\Gamma^{\dagger}_{1\mu} = \sum_{\tau; II'} \left[X(\tau; II') A^{\dagger}_{1\mu}(\tau; II') + Y(\tau; II')(-)^{1-\mu} A_{1,-\mu}(\tau; II')\right], \tag{3.7}$$

such that the

$$\left[H, \Gamma^{\dagger}_{1\mu}\right] = \omega \Gamma^{\dagger}_{1\mu}, \ \left[\Gamma_{1\mu}, \Gamma^{\dagger}_{1\mu'}\right] = \delta_{\mu,\mu'}. \tag{3.8}$$

The first relation (3.8) leads to the quasiparticle random phase approximation (QRPA) equation:

$$\begin{pmatrix} \mathcal{A} & \mathcal{B} \\ -\mathcal{B} & -\mathcal{A} \end{pmatrix} \begin{pmatrix} X(\tau; II') \\ Y(\tau; II')) \end{pmatrix} = \omega \begin{pmatrix} X(\tau; II') \\ Y(\tau; II') \end{pmatrix}. \tag{3.9}$$

To simplify the notations we abbreviate the set of quantum numbers τI by a and the two quasiparticle energies $E_a + E_b$ by E_{ab}. Thus, the QRPA matrices acquire a compact form:

$$\begin{aligned}
\mathcal{A}_{ab;a'b'} &= E_{ab}\delta_{aa'}\delta_{bb'} - \frac{X_{\tau,\tau'}}{2} d_1(ab)\xi^{(-)}(ab) d_1(a'b')\xi^{(-)}(a'b'), \\
\mathcal{B}_{ab;a'b'} &= \frac{X_{\tau,\tau'}}{2} d_1(ab)\xi^{(-)}(ab) d_1(a'b')\xi^{(-)}(a'b').
\end{aligned}$$

The equation (3.9) determines the amplitudes X and Y up to a multiplicative factor which is to be determined by the second equation (3.8), which can be written as:

$$\sum_{\substack{a,b \\ E_a < E_b}} \left(X(ab)^2 - Y(ab)^2\right) = 1. \tag{3.10}$$

Since the dipole-dipole interaction is separable, the compatibility condition for the homogeneous linear equations provides a dispersion equation for ω. Also, the QRPA amplitudes have the analytical expressions given in Appendix A.

IV. ELECTRIC DIPOLE TRANSITIONS

The dipole transition operator is:

$$E_{1\mu} = \sqrt{\frac{4\pi}{3}} e \left(r - \frac{3}{5}\frac{r^3}{b^2}\right) Y_{1\mu}. \tag{4.1}$$

In the quasiparticle representation, for a system of Z protons and N neutrons, this operator acquires the form:

$$E_{1\mu} = \sqrt{\frac{4\pi}{3}}\left[e^{(p)}_{eff}\sum_{E_a<E_b} d_1(p;ab)\xi^{(-)}(p,ab)\left(A^{\dagger}_{1\mu}(p,ab)-(-)^{1-\mu}A_{1,-\mu}(p,ab)\right)\right.$$
$$\left. + \; e^{(n)}_{eff}\sum_{E_a<E_b} d_1(n;ab)\xi^{(-)}(n,ab)\left(A^{\dagger}_{1\mu}(n,ab)-(-)^{1-\mu}A_{1,-\mu}(n,ab)\right)\right], \tag{4.2}$$

where $e^{(p)}_{eff}$ and $e^{(n)}_{eff}$ denote the effective charge for proton and neutrons, respectively. The reduced dipole transition probability from the QRPA ground state $|0\rangle$ to the dipole state $|1_k,\mu\rangle$ corresponding to the k-th root of the QRPA equations has the expression:

$$B(E1;0^+\to 1^-_k) = \left(\langle 0||E_1||1_k\rangle\right)^2 = 4\pi \tag{4.3}$$
$$\times \left[e^{(p)}_{eff}\sum_{E_a<E_b} d_1(p;ab)\xi^{(-)}(p,ab)\left(X_k(p,ab)+Y_k(p,ab)\right)\right.$$
$$\left. + \; e^{(n)}_{eff}\sum_{E_a<E_b} d_1(n;ab)\xi^{(-)}(n,ab)\left(X_k(n,ab)+Y_k(n,ab)\right)\right]^2.$$

The effective charges which take care of the center of mass momentum conservation as well as of the polarization effect induced by the charged particles motion are:

$$e^{(p)}_{eff} = \frac{N}{A}, \;\; e^{(n)}_{eff} = -\frac{Z}{A}. \tag{4.4}$$

V. THE ENERGY WEIGHTED SUM RULE (EWSR)

Here we evaluate the sum of the weighted reduced dipole transition probabilities:

$$S_l = \sum_k \omega_k B(E1;0^+\to 1^-_k) = 3\sum_{k,\mu}\omega_k|\langle 1_k\mu|E_{1\mu}|0\rangle|^2$$
$$= 3\sum_{n,\mu}\omega_k\langle 0|E_{1,-\mu}(-)^{\mu}|1_n\mu\rangle\langle 1_n\mu|E_{1\mu}|0\rangle$$
$$= \frac{3}{2}\sum_{\mu}\langle 0|\left[E_{1\mu},[H,E_{1,-\mu}(-)^{\mu}]\right]|0\rangle. \tag{5.1}$$

Here ω_k (k$\neq 0$) denotes the k-th QRPA energy, which corresponds to the eigenstate $|1_k\mu\rangle$. H is the model Hamiltonian defined by Eq.(3.2). Note that to the commutators involved in Eq.(5.1) only one term of H does contribute, namely the kinetic energy $\sum_{i=1}^{A}\frac{p_i^2}{2M}$, with M denoting the nucleon mass. Let us denote the last term of Eq.(5.1) by S_r. By direct and cumbersome manipulations one arrives at the following expression:

$$S_r = \frac{27\hbar^2}{2M} \tag{5.2}$$
$$\times \left\{(e^p_{eff})^2\left[Z-2\sum_{i=1}^{Z}\langle 0|\frac{r_i^2}{b^2}|0\rangle+\frac{33}{25}\sum_{i=1}^{Z}\langle 0|\frac{r_i^4}{b^4}|0\rangle\right]\right.$$
$$\left. \times \;(e^n_{eff})^2\left[N-2\sum_{i=1}^{N}\langle 0|\frac{r_i^2}{b^2}|0\rangle+\frac{33}{25}\sum_{i=1}^{N}\langle 0|\frac{r_i^4}{b^4}|0\rangle\right]\right\}.$$

Note that if instead of the Schiff dipole momentum the standard one was used, then in the last expression of S_r only the first term would survive, which results in getting the famous sum rule of Thomas-Reiche-Kuhn (TRK)[47–49].

$$S_{TRK} = \frac{27\hbar^2}{2M}\frac{ZN}{A}. \tag{5.3}$$

This sum rule is model independent and is obtained by an exact evaluation of the double commutators from Eq. (5.1). When $S_l = S_{TRK}$, one says that the EWSR is satisfied. The accuracy of the sum rule obedience is actually a measure of the adopted approximation consistency. In this paper we shall analyze the contribution of the major humps in the E1 strength distribution to the EWSR.

The last two terms from Eq.(5.3) are due to the cubic term in the radial coordinate. These can be calculated either based on microscopic ground or phenomenologically. Here we adopt the first option and we start by noticing that:

$$\begin{aligned}\langle o|r_\tau^2|0\rangle &= \sum_{k,mu}\langle o|(r_\tau)_{1,-\mu}(-1)^\mu|1_k,\mu\rangle\langle 1_k,\mu|(r_\tau)_{1\mu}|0\rangle, \\ \langle o|r_\tau^4|0\rangle &= \left(\sum_{k,mu}\langle o|(r_\tau)_{1,-\mu}(-1)^\mu|1_k,\mu\rangle\langle 1_k,\mu|(r_\tau)_{1\mu}|0\rangle\right)^2, \quad \tau = p,n.\end{aligned} \tag{5.4}$$

Inserting the matrix elements for the proton and neutron dipole operators, the expression of S_r becomes:

$$\begin{aligned}S_{cor} &= \frac{27\hbar^2}{2M}\left\{\frac{ZN}{A} - \frac{8\pi}{3b^2}\frac{N^2}{A^2}\sum_k\left[\sum_{E_a<E_b} d(p;ab)\xi^{(-)}(p,ab)\left(X_k(p,ab)+Y_k(p,ab)\right)\right]^2\right. \\ &- \frac{8\pi}{3b^2}\frac{Z^2}{A^2}\sum_k\left[\sum_{E_a<E_b} d(n;ab)\xi^{(-)}(n,ab)\left(X_k(n,ab)+Y_k(n,ab)\right)\right]^2 \\ &+ \frac{16\pi^2}{9b^4}\frac{N^2}{A^2}\frac{33}{25}\sum_k\left[\sum_{E_a<E_b} d(p;ab)\xi^{(-)}(p,ab)\left(X_k(p,ab)+Y_k(p,ab)\right)\right]^4 \\ &+ \left.\frac{16\pi^2}{9b^4}\frac{Z^2}{A^2}\frac{33}{25}\sum_k\left[\sum_{E_a<E_b} d(n;ab)\xi^{(-)}(n,ab)\left(X_k(n,ab)+Y_k(n,ab)\right)\right]^4\right\}.\end{aligned} \tag{5.5}$$

where the factor $d(\tau, ab)$ is obtained from Eq.(3.5) restricting in the last factor, the Schiff momentum to the linear term in the radial coordinate. Note that the above expression is fully consistent with the dipole strength. Indeed, in both cases the transition operator is the same, i.e.,the Schiff momentum.

VI. NUMERICAL RESULTS

A. Parameters

The formalism presented in the previous sections was applied to five even-even isotopes of Sm, ^{144,148,150,152,154}Sm. The spherical shell model single particle basis is defined using the parameters given in Ref.[37]:

$$\hbar\omega_0 = 41A^{-1/3},\ C = -2\hbar\omega_0\kappa,\ D = -\hbar\omega_0\mu. \tag{6.1}$$

The parameters $(\kappa;\mu)$ for proton and neutron systems are those given in Refs.[37, 43]. The proton and neutron pairing strengths are taken as:

$$G_p = \frac{23}{A},\ \ G_n = \frac{22}{A}, \tag{6.2}$$

where A is the atomic mass number. The BCS equations were solved using 92 states both for protons and neutrons. Increasing the dimension of the single particle space, the final results concerning the QRPA energies and transition probabilities remain unchanged.

The projected spherical single particle basis depends on two parameters, namely the deformation d and the parameter k relating the quadrupole boson operator and the quadrupole collective coordinate. The deformation parameter was taken as in Ref.[32], while k was fixed such that the single particle energy spacings be optimally described. Their connection with the nuclear deformation β was in extenso studied in Refs.[36, 44, 45]. As shown in Ref.[45] the deformation parameter d and the nuclear deformation β are related by:

$$d = k\beta. \tag{6.3}$$

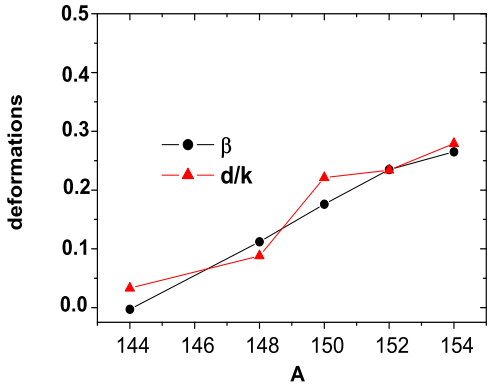

FIG. 2: Color online. The ratio between the deformation parameter d and canonicity parameter k as well as the nuclear deformation β [50], versus the atomic number A.

Nucleus	$X_{PP} = X_{NN}$ [MeV.fm^{-2}]	$X_{PN} = X_{NP}$ [MeV.fm^{-2}]	$N_{d,p}$	$N_{d,n}$
^{144}Sm	0.0129	0.0179	264	256
^{148}Sm	0.0110	0.0130	258	298
^{150}Sm	0.0160	0.0220	266	290
^{152}Sm	0.0190	0.0230	266	290
^{154}Sm	0.0185	0.0255	256	290

TABLE I: The strength of the dipole-dipole interaction, X_{PP} and X_{PN}, and the number of the dipole configurations for proton ($N_{d,p}$) and neutron ($N_{d,n}$), respectively.

This equation is approximatively obeyed by the deformations used in the present paper. This is illustrated in Fig. 2.

The dimension of the QRPA matrices $\mathcal{A}$ and $\mathcal{B}$ is the sum of the number of the dipole proton ($N_{d,p}$) and the number of the dipole neutron ($N_{d,n}$) configurations; these are given in Table I together with the strength of the dipole-dipole interactions, X_{PP} and X_{PN}. The other strengths are related with the mentioned ones by: $X_{NN} = X_{PP}, X_{NP} = X_{PN}$.

It is worth writing the dipole-dipole term, H_{DD}, of the model Hamiltonian, in terms of the isoscalar and isovector operators:

$$V_{1\mu}(I,I') = D_{1\mu}(p;II') - D_{1\mu}(n;II'), \quad S_{1\mu}(I,I') = D_{1\mu}(p;II') + D_{1\mu}(n;II'). \tag{6.4}$$

The result is:

$$\begin{aligned} H_{DD} &= \frac{1}{4}\left(X_{PP} + X_{NN} - X_{PN} - X_{NP}\right) \sum_{ab;cd} V_{1\mu}(ab) V_{1,-\mu}(cd) \\ &+ \frac{1}{4}\left(X_{PP} + X_{NN} + X_{PN} + X_{NP}\right) \sum_{ab;cd} S_{1\mu}(ab) S_{1,-\mu}(cd) \\ &+ \frac{1}{4}\left(X_{PP} - X_{NN} + X_{PN} - X_{NP}\right) \sum_{ab;cd} V_{1\mu}(ab) S_{1,-\mu}(cd) \\ &+ \frac{1}{4}\left(X_{PP} - X_{NN} - X_{PN} + X_{NP}\right) \sum_{ab;cd} S_{1\mu}(ab) V_{1,-\mu}(cd). \end{aligned} \tag{6.5}$$

Since the proton-neutron interaction may lead to a system (pn) in a bound state it is reasonable to admit that $X_{PN} > X_{PP}$. In our calculations we also considered $X_{PP} = X_{NN}$ and $X_{PN} = X_{NP}$. Note that for these values the isovector interaction ($V\dot{V}$) is repulsive, while the isoscalar one ($S\dot{S}$) is attractive. Also, the last two terms of Eq. (6.5) vanish. Due to this feature one expects that the isoscalar interaction will affects the lower part of the strength, while the isovector one is responsible for the higher energy range of the spectrum. The proton-neutron interaction strength

was taken equal to about $1.2X_{PP}$ for ^{148}Sm and ^{152}Sm, and $1.38X_{PP}$ for the other isotopes. Thus, the strength of the isovector interaction was fixed so that the centroid of the giant resonance is placed around 13 MeV.

Note that dipole-dipole interaction involves the so called Schiff dipole operator. Due to this reason the $\Delta N = 3$ single particle states are correlated. Thus, it is expected that the dipole transitions are correspondingly affected.

B. Solving the QRPA equations

The QRPA equations (3.9) were solved using the method described in Ref. [46]. Results for the amplitudes X and Y where further used to calculate the reduced dipole transition probability $B(E1; 0^+ \to 1^-_k)$. At its turn this is employed for calculating the dipole strength distribution, and the photoabsorption cross section as function of the QRPA energies. Results for PDR and GDR will be separately described.

C. The Pygmy Dipole Resonance

We begin with analyzing the results obtained for the energy interval 0-10 MeV. which are collected in Table III. Therein, we show the peaks larger than $1e^2fm^2$ and lying bellow 10 MeV, corresponding to the i-th dipole phonon state. For this phonon operator we depicted the maximal proton amplitude, $X^M_i(\pi, ab)$ and the maximal neutron amplitude, $X^M_i(\nu, cd)$. The corresponding dipole configurations (ab) and (cd) are also listed. The variation of the major oscillator quantum number ΔN as well of the total angular momentum I, ΔI, associated to the single particle transitions $b \to a$ and $d \to c$ respectively, are listed too. The contribution of the transitions $0^+ \to 1^-_k$, with $\omega_k < 10$ MeV, to the total energy weighted sum rule (EWSR) is given in Table.VII

By inspection of tables III, one notes that the listed maximal proton and neutron amplitudes have distinct relative magnitudes: i) one maximal amplitude of proton/neutron type is much larger than another maximal amplitude of neutron/proton kind; ii) the proton and neutron maximal amplitudes are of a comparable magnitude. They may have either the same or opposite phase. When the proton and neutron maximal amplitudes are equal to each other and moreover are characterized by similar single particle quantum numbers, the depicted phonon state is invariant to the proton and neutron permutation. Therefore, it is an isoscalar state. If the phases of the two amplitudes are different, the state is of isovector type. By an abuse of language we conventionally call the phonon with comparable proton and neutron maximal amplitudes as isoscalar even if they only have similar phases and isovector if they are of opposite phases. These names reflect that they are mainly determined by the $S_1.S_1$ and $V_1.V_1$ terms of the model Hamiltonian.

^{144}**Sm**: As shown in Table III, the transition to the first phonon state is of an isoscalar nature, while that to the 21-st phonon state is predominantly of collective neutron kind. We call the latest transition as being collective, since many dipole configuration participate to the process. That is necessary in order to saturate the normalization to unity of the single phonon state norm.

^{148}**Sm**: There exist two isovector transitions, to the 18th and 19th phonon state respectively, and one to the state 13, describing a collective neutron oscillation.

^{150}**Sm**: One notices two transitions of collective neutron nature, those to the 6th and the 20th phonon state, respectively, one to a 2qp proton state (17th), two isoscalar transitions to the states 23 and 26 and one isovector transition to the state 24.

^{152}**Sm**: There are two phonon states of proton nature (one of 2 qp kind and one collective), namely those determined by the 15-th and 24-th phonon operators respectively, while those of energies equal to 7.72 MeV and 9.397 MeV respectively, have a neutron character. Moreover, one finds two isoscalar transitions to the states of energy 9.746 MeV and 9.756 MeV and three isovector transitions to the 19th, 29th and 30th phonon state.

^{154}**Sm**: In this case, the situation stands as follows. There is one transition to a collective neutron state at 7.381 MeV, two transitions to the isovector states at 9.231 MeV and 9.743 MeV and four isoscalar transitions to the states of energy 8.998 MeV, 9.328 MeV, 9.697 MeV and 9.893 MeV.

Concluding, the peaks of the Pygmy resonance are determined by proton and neutron $\Delta N = 1$ transitions. For most of them the neutron oscillations prevail over the proton ones. However, there are situations where the proton maximal and neutron maximal amplitudes are comparable in magnitude. Some of the corresponding phonon states have an isoscalar character, but there are also transitions to isovector states. Except for ^{148}Sm, in all considered isotopes the highest peaks are of an isoscalar nature.

On the last column of Table VII, the contribution of the Pygmy transitions to the total EWSR, is presented. One sees that the Pygmy resonance brings only a few percents to the total EWSR.

The dipole strengths for the PDR transitions are pictorially presented in Fig. 3. From there one sees that the Pygmy transitions exhibit, indeed, a resonance structure. While for the spherical isotope,^{144}Sm, most of the strength

Nucleus	k	$B(E1;0^+ \to 1_k^-)$[W.u.]	type	k	$B(E1;0^+ \to 1_k^-)$[W.u.]	type
^{144}Sm	1	7.06	IS	21	1.60	IV
^{148}Sm	2	3.55	IS	18	7.82	IV
^{150}Sm	24	2.22	IV	26	6.20	IS
^{152}Sm	19	3.68	IV	26	7.63	IS
^{154}Sm	20	6.69	IS	26	6.65	IS

TABLE II: The largest two B(E1) values selected from Table III. Also, the label k for the state populated by the mentioned transition is mentioned.

is concentrated in one transition for the other isotopes there are two major transitions surrounded by some other which are smaller in magnitude. The split of the main strength into two fragments is an effect of the nuclear deformation.

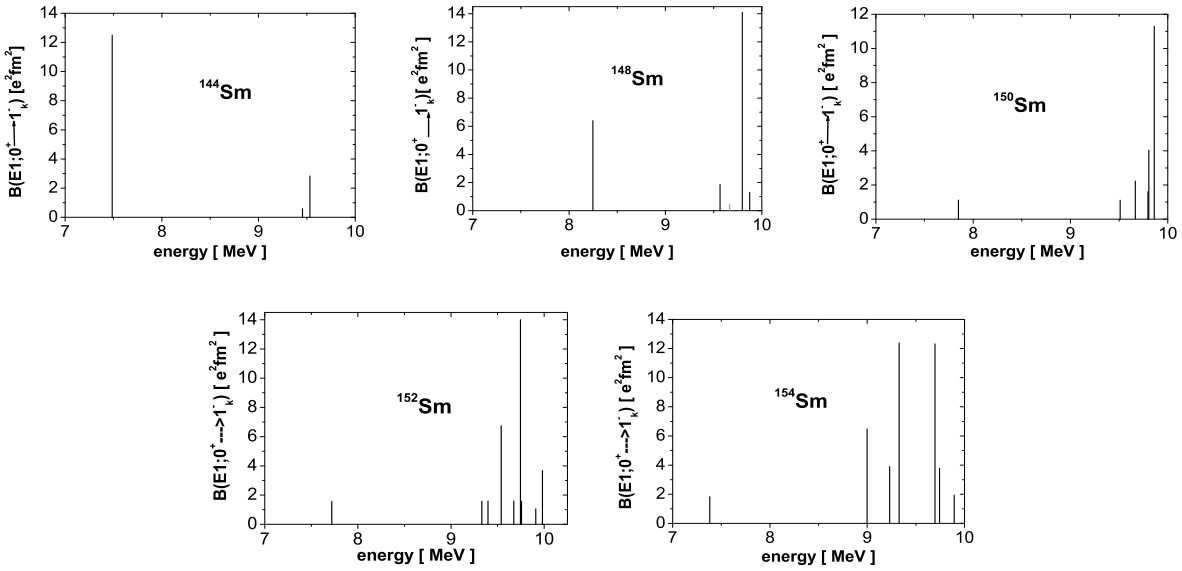

FIG. 3: The dipole strength as function of energy for ^{144,148,150,152,154}Sm, in the PDR energy region.

D. Collectivity

In order to appraise whether a transition from PDR is collective or not, in Table.II we collected the largest two B(E1) values from each isotope, expressed in W. u.. One notes that there are transitions which are moderate collective and they have either an isoscalar or an isovector nature. In ^{150}Sm, one notices two transitions of 2 qp type, one of neutron (k=6) and one of proton (k=17) nature. Both transitions are characterized by a B(E1) equal to 0.61 W.u. Also in ^{152}Sm one finds two proton-like transitions to the states k=15 and k=27 respectively, whose B(E1) values amounts of 0.85 and 0.86 W.u., respectively. Concluding, for each nucleus one identifies two collective transitions, the rest of them being mostly of 2qp type, i.e. non-collective.

E. The giant dipole resonance

The data for the peaks with energy larger than 10 MeV and magnitudes larger than 20 e^2fm^2 are collected in Table IV. In this energy region, our calculations indicate a bulk of transitions defining the dipole giant dipole resonance (GDR). To the giant resonance many transitions contribute, but we selected the largest peaks defining the GDR centroid, namely those larger than 20 e^2fm^2. The pictures for each of considered isotopes are as follows.

^{144}**Sm**: There are one isovector transition to the state of energy 10.790 MeV and one isoscalar to the 78th phonon state. All the remaining transitions are either to a collective or to a two quasiparticle proton state.

^{148}**Sm**: One sees three isoscalar transitions to the states labelled by 38, 122 and 138, respectively, three isovector transitions to the 46th, 52nd, 102nd phonon states respectively, to one collective neutron state, (58), and one collective proton state, (140).

^{150}**Sm**: The GDR is determined by three isoscalar transitions (108, 111, 155) and four isovector transitions (107, 129, 130, 167).

^{152}**Sm**: One notices three isoscalar transitions to the states 42, 113 and 129 respectively, and four isovector transitions to the states 102, 114, 121 and 160, respectively.

^{154}**Sm**: Here, one find five isoscalar transitions to the states 45, 112, 130, 152 and 167 respectively, and five isovector transitions to the phonon states labeled by 66, 115, 122, 129 and 135, respectively.

In Fig. 4, in the spherical nuclei ^{144}Sm and ^{148}Sm, we notice a peak lying close to and 11 MeV. Its position, magnitude and the corresponding dominant single particle transitions are also mentioned in Table III. Thus, in ^{144}Sm this peak is based on the isovector transition to the state placed at an energy of 10.79 MeV and an isoscalar transition to the state of energy 11.262 MeV. In ^{148}Sm, the peak is formed of the isoscalar transition to the state at 10.612 MeV and two isovector transitions to the phonon states 46 and 52, respectively. In the heavier isotopes this peak does not show up, since the single particle energy spacings are modified by the nuclear deformation and thus, the transitions of higher energies become favored. Another consequence of the nuclear deformation is the appearance of an additional split for the GDR [51–53]. Moreover, the split in the dipole distribution determined by the nuclear deformation is less pregnacollectivnt in the case where the transition operator is of a Schiff type than in the case of a standard dipole moment. Thus, one could say that the nuclear deformation and the Schiff correction have an opposite effect on the dipole strength distribution. Indeed, as shown in Fig. 4, the depth of the minimum which separates the two peaks is very damped. The two peak structure of the GDR, which is seen in deformed nuclei, was interpreted [20, 21] as being determined by the K=0 and K=1 dipole transitions, respectively. It is worth commenting on how this feature is reflected in our formalism. According to the defining equation (2.6), the projected spherical state is a weighted sum of all K components with K smaller than the projected angular momentum I. However, the dominant component is that having K=I. Since the K transition is caused by the K component of the dipole transition operator, it results that the angular momentum of the initial state is modified with K-units, i.e. $\Delta I = K$. In this context, in Tables III and IV we listed ΔI for the states associated with the maximal amplitudes of the QRPA phonon operator. For deformed single particle basis the phonon operator has a definite K quantum number which results in having a separate contribution of the K=1 and K=0 transitions. This implies that for a given phonon state, the proton and neutron transitions take place by modifying the K good quantum number by the same amount, i.e. either $\Delta K = 1$ or $\Delta K = 0$. In Table III and IV we notice that there are, indeed, transitions with $(\Delta_\pi, \Delta I_\nu)$= (1,1) or (0,0). However, there are many transitions where the mentioned doublet is either (0,1) or (1,0). Consequently, working with a projected spherical single particle basis, one can not separate the K=0 and K=1 contributions to the photoabsorption cross section.

The split of the major peaks of the GDR is shown in Table V where the largest two strengths are listed together with the corresponding transition nature and the ordering label of the excited state involved.

The two branches of the photoabsorption cross section are obtained in distinct experiments, namely (γ, n) and $(\gamma, 2n)$, respectively [55].

The peaks attached to the GDR are determined by proton and neutron $\Delta N = 1$ transitions, some being of isovector and some of isoscalar nature. The GDR transitions are dominantly proton oscillations of isovector nature, although there are also transitions of neutron IS character.

It is worth mentioning that the position of the GDR centroid given here in Fig. 4 agrees with those given in Ref.[55]. Also, the GDR centroid is close to those presented in Ref.[56] in Fig. 8, the upper panel.

Results for the dipole strength distribution and the photoabsorption cross section as function of the excitation energy are presented in Figs 4 and 5, respectively. The calculations are based on the following defining equations. The dipole strengths were folded by a Lorenz function of width $\Gamma = 1$ MeV.

$$F_{ds}(\Gamma,\omega) = \frac{1}{2\pi}\sum_k \frac{\Gamma}{(\omega-\omega_k)^2+\left(\frac{\Gamma}{2}\right)^2} B(E1;0^+\to 1_k^-)[e^2fm^2/MeV]. \tag{6.6}$$

The photoabsorption cross section is given by:

$$\sigma(\Gamma,\omega) = C\sum_k \frac{\Gamma}{(\omega-\omega_k)^2+\left(\frac{\Gamma}{2}\right)^2} \omega_k B(E1;0^+\to 1_k^-)[mb]. \tag{6.7}$$

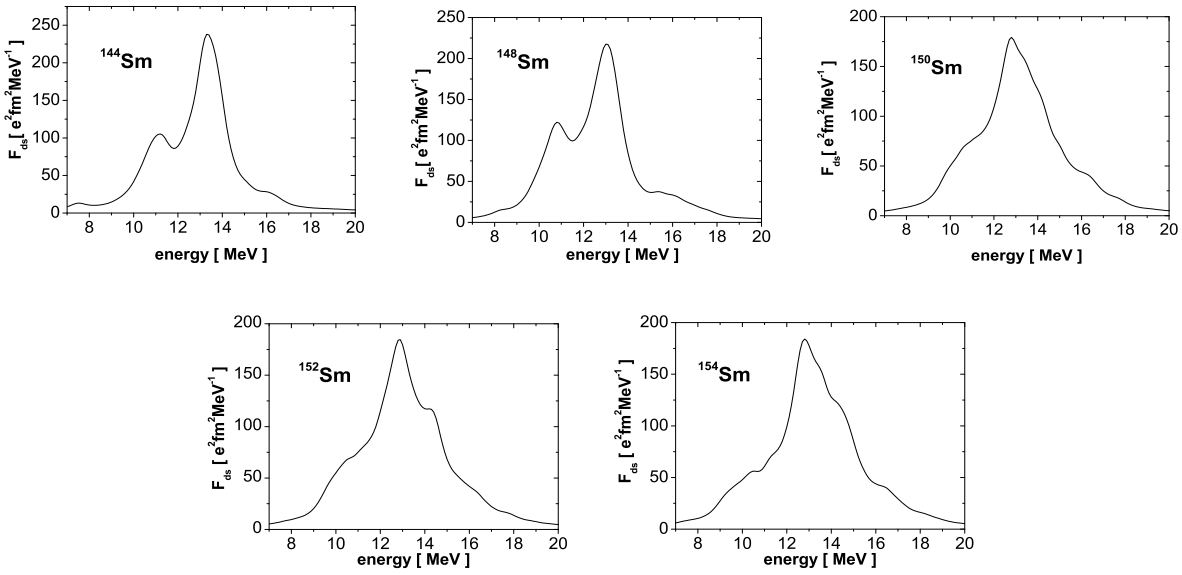

FIG. 4: The dipole strength as function of energy for ^{144,148,150,152,154}Sm. The calculated strengths were folded by Lorentzianes with the width of 1 MeV.

where C denotes a normalization factor which, in this paper has the value[54]:

$$C = 0.02e^{-2}, \tag{6.8}$$

while the width is taken equal to 3 MeV.

The area of the surface below the cross section, shown in Fig. 5, is the total cross section:

$$\sigma_0 = \int \sigma(\Gamma, \omega)d\omega = C\sum_k \omega_k B(E1; 0^+ \to 1_k^-) = CS_l[\text{MeVmb}]. \tag{6.9}$$

Extended to the n-th moment of the integrated cross sections, this defining relation looks like:

$$\sigma_n = \int \omega^{n+1}\sigma(\Gamma, \omega)d\omega. \tag{6.10}$$

The integral over ω can be easily performed. In this paper we present the results for:

$$\begin{aligned} \sigma_{-2} &= C\sum_k \omega_k^{-1} B(E1; 0^+ \to 1_k^-)[\text{MeV}^{-1}\text{mb}], \\ \sigma_{-1} &= C\sum_k B(E1; 0^+ \to 1_k^-)[\text{mb}]. \end{aligned}$$

The three moments, $\sigma_{-2}, \sigma_{-1}, \sigma_0$, predicted by our calculations are given in Table VI. Note that for the two plots one used different width for the enveloping Lorentzian, namely 1 MeV for the strength function and 3 MeV or the cross section. The reason for this option consists of that we wanted to show how the substructure details are stumped by growing the Lorentzian width. For ^{154}Sm the calculated cross section was compared with the corresponding experimental data taken from [57]. Since the experimental data exhibit uncertainties of about 10%, one may assert that our calculations agree with the experimental data, reasonable well. It is conspicuous that the moments of the integrated cross section do not depend on the Lorentzian width. Three of these integrated moments of the cross section, namely σ_0, σ_{-1} and σ_{-2} are compared with the experimental data from Refs.[55, 57] in Table VI. Therein, the sum of the PDR transition strengths and the sum of the dipole strengths for the whole interval of 0-20 MeV are also given. The agreement, evidenced by Table VI, between predictions and the experimental data is quite good.

Nucleus	peak	energy	i	$(\pi;ab)$			$(\nu;cd)$			ΔN		Δ I	
	[e^{2}fm^2]	[MeV]		a	b	$X_i^M(\pi;ab)$	c	d	$X_i^M(\nu;cd)$	π	ν	π	ν
	12.497	7.482	1	$\|1\ 1\ \frac{1}{2}\frac{1}{2}\rangle$	$\|1\ 2\ \frac{3}{2}\frac{3}{2}\rangle$	0.208	$\|\ 1\ 2\ \frac{3}{2}\frac{3}{2}\rangle$	$\|2\ 1\ \frac{1}{2}\frac{1}{2}\rangle$	0.309	1	1	1	1
	0.584	9.455	19	$\|1\ 1\ \frac{1}{2}\frac{1}{2}\rangle$	$\|1\ 2\ \frac{3}{2}\frac{3}{2}\rangle$	0.037	$\|\ 0\ 4\ \frac{7}{2}\frac{3}{2}\rangle$	$\|1\ 3\ \frac{5}{2}\frac{3}{2}\rangle$	0.796	1	1	1	1
^{144}Sm	2.833	9.531	21	$\|1\ 1\ \frac{1}{2}\frac{1}{2}\rangle$	$\|12\ \frac{3}{2}\frac{3}{2}\rangle$	-0.079	$\|0\ 4\ \frac{7}{2}\frac{3}{2}\rangle$	$\|1\ 3\ \frac{5}{2}\frac{3}{2}\rangle$	0.582	1	1	1	1
	6.394	8.247	2	$\|1\ 1\ \frac{1}{2}\frac{1}{2}\rangle$	$\|\ 1\ 2\ \frac{3}{2}\frac{3}{2}\rangle$	-0.183	$\|1\ 2\ \frac{3}{2}\frac{3}{2}\rangle$	$\|1\ 3\ \frac{5}{2}\frac{1}{2}\rangle$	-0.425	1	1	1	1
	1.855	9.566	13	$\|1\ 1\ \frac{3}{2}\frac{3}{2}\rangle$	$\|\ 1\ 1\ \frac{5}{2}\frac{5}{2}\rangle$	0.095	$\|1\ 2\ \frac{3}{2}\frac{1}{2}\rangle$	$\|1\ 3\ \frac{5}{2}\frac{1}{2}\rangle$	0.638	1	1	1	0
^{148}Sm	14.102	9.798	18	$\|1\ 1\ \frac{3}{2}\frac{3}{2}\rangle$	$\|1\ 2\ \frac{5}{2}\frac{5}{2}\rangle$	-0.543	$\|1\ 2\ \frac{5}{2}\frac{1}{2}\rangle$	$\|1\ 3\ \frac{7}{2}\frac{3}{2}\rangle$	0.590	1	1	1	1
	1.307	9.874	19	$\|1\ 1\frac{3}{2}\frac{3}{2}\rangle$	$\|1\ 2\ \frac{5}{2}\frac{5}{2}\rangle$	0.795	$\|1\ 2\ \frac{3}{2}\frac{1}{2}\rangle$	$\|1\ 3\ \frac{5}{2}\frac{3}{2}\rangle$	-0.340	1	1	1	1
	1.118	7.849	6	$\|12\ \frac{5}{2}\frac{1}{2}\rangle$	$\|13\ \frac{7}{2}\frac{3}{2}\rangle$	0.048	$\|1\ 2\ \frac{3}{2}\frac{3}{2}\rangle$	$\|1\ 3\ \frac{5}{2}\frac{3}{2}\rangle$	0.956	1	1	1	0
	1.107	9.511	17	$\|1\ 2\ \frac{5}{2}\frac{3}{2}\rangle$	$\|1\ 3\ \frac{7}{2}\frac{3}{2}\rangle$	0.988	$\|1\ 2\ \frac{3}{2}\frac{1}{2}\rangle$	$\|1\ 3\ \frac{5}{2}\frac{1}{2}\rangle$	-0.092	1	1	0	0
^{150}Sm	2.233	9.666	20	$\|0\ 3\ \frac{5}{2}\frac{5}{2}\rangle$	$\|0\ 4\ \frac{7}{2}\frac{7}{2}\rangle$	-0.120	$\|1\ 2\ \frac{3}{2}\frac{3}{2}\rangle$	$\|2\ 1\ \frac{1}{2}\frac{1}{2}\rangle$	0.785	1	1	1	1
	1.618	9.796	23	$\|1\ 1\ \frac{5}{2}\frac{1}{2}\rangle$	$\|1\ 3\ \frac{7}{2}\frac{3}{2}\rangle$	0.307	$\|1\ 3\ \frac{7}{2}\frac{3}{2}\rangle$	$\|1\ 4\ \frac{9}{2}\frac{1}{2}\rangle$	0.880	1	1	1	1
	4.041	9.805	24	$\|1\ 2\ \frac{5}{2}\frac{1}{2}\rangle$	$\|1\ 3\ \frac{7}{2}\frac{3}{2}\rangle$	0.767	$\|1\ 3\ \frac{7}{2}\frac{3}{2}\rangle$	$\|1\ 4\ \frac{9}{2}\frac{1}{2}\rangle$	-0.400	1	1	1	1
	11.288	9.861	26	$\|1\ 1\ \frac{3}{2}\frac{3}{2}\rangle$	$\|2\ 0\ \frac{1}{2}\frac{1}{2}\rangle$	0.556	$\|1\ 3\ \frac{7}{2}\frac{1}{2}\rangle$	$\|1\ 4\ \frac{9}{2}\frac{1}{2}\rangle$	0.619	1	1	1	0
	1.559	7.720	6	$\|1\ 1\ \frac{3}{2}\frac{3}{2}\rangle$	$\|1\ 2\ \frac{5}{2}\frac{3}{2}\rangle$	-0.050	$\|1\ 2\ \frac{3}{2}\frac{3}{2}\rangle$	$\|1\ 3\ \frac{5}{2}\frac{3}{2}\rangle$	0.941	1	1	0	0
	1.577	9.330	15	$\|1\ 2\ \frac{5}{2}\frac{3}{2}\rangle$	$\|1\ 3\ \frac{7}{2}\frac{3}{2}\rangle$	0.986	$\|1\ 3\ \frac{7}{2}\frac{1}{2}\rangle$	$\|1\ 4\ \frac{9}{2}\frac{1}{2}\rangle$	0.125	1	1	0	0
^{152}Sm	1.591	9.397	16	$\|1\ 2\ \frac{5}{2}\frac{3}{2}\rangle$	$\|1\ 3\ \frac{7}{2}\frac{3}{2}\rangle$	0.089	$\|1\ 3\ \frac{7}{2}\frac{1}{2}\rangle$	$\|1\ 4\ \frac{9}{2}\frac{1}{2}\rangle$	0.805	1	1	0	0
	6.747	9.539	19	$\|0\ 3\ \frac{5}{2}\frac{5}{2}\rangle$	$\|0\ 4\ \frac{7}{2}\frac{7}{2}\rangle$	-0.238	$\|1\ 2\ \frac{3}{2}\frac{3}{2}\rangle$	$\|1\ 3\ \frac{5}{2}\frac{1}{2}\rangle$	0.696	1	1	1	1
	1.601	9.674	24	$\|1\ 2\ \frac{5}{2}\frac{1}{2}\rangle$	$\|1\ 3\ \frac{7}{2}\frac{3}{2}\rangle$	0.798	$\|0\ 4\ \frac{7}{2}\frac{5}{2}\rangle$	$\|1\ 3\ \frac{7}{2}\frac{3}{2}\rangle$	-0.180	1	1	1	1
	13.996	9.746	26	$\|1\ 1\ \frac{3}{2}\frac{3}{2}\rangle$	$\|2\ 0\ \frac{1}{2}\frac{1}{2}\rangle$	0.613	$\|1\ 2\ \frac{3}{2}\frac{1}{2}\rangle$	$\|1\ 3\ \frac{5}{2}\frac{1}{2}\rangle$	0.631	1	1	1	0
	1.574	9.756	27	$\|0\ 4\ \frac{7}{2}\frac{3}{2}\rangle$	$\|1\ 3\ \frac{7}{2}\frac{1}{2}\rangle$	0.959	$\|1\ 2\ \frac{3}{2}\frac{1}{2}\rangle$	$\|1\ 3\ \frac{5}{2}\frac{1}{2}\rangle$	0.234	1	1	1	0
	1.063	9.910	29	$\|1\ 1\ \frac{3}{2}\frac{3}{2}\rangle$	$\|2\ 0\ \frac{1}{2}\frac{1}{2}\rangle$	0.466	$\|1\ 2\ \frac{3}{2}\frac{1}{2}\rangle$	$\|1\ 3\ \frac{5}{2}\frac{1}{2}\rangle$	-0.433	1	1	1	0
	3.670	9.981	30	$\|1\ 1\ \frac{3}{2}\frac{3}{2}\rangle$	$\|1\ 2\ \frac{5}{2}\frac{5}{2}\rangle$	0.857	$\|1\ 2\ \frac{5}{2}\frac{5}{2}\rangle$	$\|1\ 3\ \frac{7}{2}\frac{7}{2}\rangle$	-0.188	1	1	1	1
	1.823	7.381	6	$\|1\ 1\ \frac{3}{2}\frac{3}{2}\rangle$	$\|1\ 2\ \frac{5}{2}\frac{3}{2}\rangle$	-0.064	$\|1\ 2\ \frac{3}{2}\frac{3}{2}\rangle$	$\|1\ 3\ \frac{5}{2}\frac{3}{2}\rangle$	0.839	1	1	0	0
	6.481	8.998	16	$\|1\ 2\ \frac{5}{2}\frac{3}{2}\rangle$	$\|1\ 3\ \frac{7}{2}\frac{3}{2}\rangle$	0.687	$\|1\ 3\ \frac{7}{2}\frac{1}{2}\rangle$	$\|1\ 4\ \frac{9}{2}\frac{1}{2}\rangle$	0.640	1	1	0	0
	3.903	9.231	18	$\|0\ 4\ \frac{7}{2}\frac{5}{2}\rangle$	$\|1\ 3\ \frac{7}{2}\frac{3}{2}\rangle$	-0.262	$\|1\ 2\ \frac{3}{2}\frac{3}{2}\rangle$	$\|2\ 1\ \frac{1}{2}\frac{1}{2}\rangle$	0.698	1	1	1	0
^{154}Sm	12.384	9.328	20	$\|1\ 1\ \frac{3}{2}\frac{3}{2}\rangle$	$\|2\ 0\ \frac{1}{2}\frac{1}{2}\rangle$	0.325	$\|1\ 3\ \frac{7}{2}\frac{3}{2}\rangle$	$\|1\ 4\ \frac{9}{2}\frac{3}{2}\rangle$	0.741	1	1	1	0
	12.320	9.697	26	$\|1\ 2\ \frac{3}{2}\frac{1}{2}\rangle$	$\|1\ 3\ \frac{5}{2}\frac{1}{2}\rangle$	0.431	$\|1\ 3\ \frac{7}{2}\frac{1}{2}\rangle$	$\|1\ 4\ \frac{9}{2}\frac{3}{2}\rangle$	0.818	1	1	0	1
	3.781	9.743	27	$\|1\ 2\ \frac{3}{2}\frac{1}{2}\rangle$	$\|1\ 3\ \frac{5}{2}\frac{1}{2}\rangle$	-0.326	$\|1\ 3\ \frac{5}{2}\frac{3}{2}\rangle$	$\|1\ 3\ \frac{7}{2}\frac{3}{2}\rangle$	0.828	1	1	0	0
	1.940	9.893	31	$\|0\ 3\ \frac{7}{2}\frac{7}{2}\rangle$	$\|0\ 4\ \frac{9}{2}\frac{9}{2}\rangle$	0.892	$\|1\ 2\ \frac{3}{2}\frac{1}{2}\rangle$	$\|1\ 3\ \frac{5}{2}\frac{1}{2}\rangle$	0.146	1	1	1	0

TABLE III: The highest peaks contributing to the PDR, are mentioned together with the corresponding energy of the i-th phonon state. Only peaks higher than 0.5e^{2}fm^2 are mentioned. The proton (π) and neutron (ν) maximal amplitudes are also given.The states involved in the dominant single particle transitions $b \to a$ and $d \to c$ are listed. These are characterized by the variation of the major oscillator quantum number ΔN. The difference between angular momenta characterizing the states involved in the single particle transitions, ΔI, are also listed. The notation $|nljI\rangle$ stands for Φ^{IM}_{nlj} (2.6), where the quantum number M is omitted. The dipole strength corresponds to the effective charges (4.4).

F. The Energy Weighted Sum Rule

Another issue treated in the present paper is that of EWSR. Calculating the B(E1) values by means of Eq. (4.4) and the QRPA excitation energies by solving Eq.(3.9), the EWSR denoted by S_l is readily obtained. We recall that the effective charges were multiplied by the factor q, listed in Table VII, which accounts for the difference in circumstances under which S_l and S_{TDK} are estimated. Results for S_l are listed in Table VII. As we already mentioned this agrees with S_{TRK} given by Eq. (5.3), provided the effective charges used for calculating S_l are multiplied by the factor q listed in Table VII. If, however, S_l and the right hand side of Eq. (5.2) are estimated with the same dipole operator, i.e, the Schiff momentum, the result for S_l should be compared with S_{corr} given by Eq. (5.4). The quality of agreement for the sum rule is appraised by the relative deviation, r.d. ($= |S_l - S_{corr}|/S_l$). From Table VI we see that r.d. is very small, which reflects a quite good agreement for the EWSR. Energy weighted sum rule values (EWSR), S_l , and the relative deviation (r.d.) of S_l from the corrected TRK, S_{corr} , are also presented.

Nucleus	peak	energy	i	$(\pi;ab)$			$(\nu;cd)$			Δ N		Δ I	
	[e^{2}fm^2]	[MeV]		a	b	$X_i^M(\pi;ab)$	c	d	$X_i^M(\nu;cd)$	π	ν	μ	ν
	21.294	10.790	54	$\|1\ 1\ \frac{1}{2}\ \frac{1}{2}\rangle$	$\|2\ 0\ \frac{1}{2}\ \frac{1}{2}\rangle$	-0.467	$\|0\ 4\ \frac{9}{2}\ \frac{5}{2}\rangle$	$\|1\ 3\ \frac{7}{2}\ \frac{3}{2}\rangle$	0.647	1	1	0	1
	42.292	11.262	78	$\|1\ 1\ \frac{3}{2}\ \frac{3}{2}\rangle$	$\|2\ 0\ \frac{1}{2}\ \frac{1}{2}\rangle$	-0.594	$\|1\ 2\ \frac{5}{2}\ \frac{3}{2}\rangle$	$\|1\ 3\ \frac{5}{2}\ \frac{1}{2}\rangle$	-0.508	1	1	1	1
	25.386	12.569	126	$\|1\ 2\ \frac{3}{2}\ \frac{1}{2}\rangle$	$\|1\ 3\ \frac{5}{2}\ \frac{1}{2}\rangle$	0.823	$\|1\ 3\ \frac{7}{2}\ \frac{7}{2}\rangle$	$\|1\ 4\ \frac{9}{2}\ \frac{9}{2}\rangle$	0.094	1	1	0	1
	52.867	13.136	143	$\|0\ 4\ \frac{9}{2}\ \frac{7}{2}\rangle$	$\|1\ 3\ \frac{7}{2}\ \frac{5}{2}\rangle$	0.517	$\|1\ 3\ \frac{5}{2}\ \frac{3}{2}\rangle$	$\|2\ 2\ \frac{5}{2}\ \frac{3}{2}\rangle$	-0.081	1	1	1	0
	117.5220	13.250	147	$\|0\ 3\ \frac{7}{2}\ \frac{7}{2}\rangle$	$\|1\ 2\ \frac{5}{2}\ \frac{5}{2}\rangle$	-0.623	$\|2\ 1\ \frac{3}{2}\ \frac{1}{2}\rangle$	$\|2\ 2\ \frac{5}{2}\ \frac{1}{2}\rangle$	-0.075	1	1	1	0
	30.973	13.454	154	$\|0\ 4\ \frac{9}{2}\ \frac{9}{2}\rangle$	$\|1\ 3\ \frac{7}{2}\ \frac{7}{2}\rangle$	-0.970	$\|2\ 1\ \frac{3}{2}\ \frac{1}{2}\rangle$	$\|2\ 1\ \frac{5}{2}\ \frac{1}{2}\rangle$	-0.035	1	1	1	0
^{144}Sm	31.859	13.597	143	$\|0\ 4\ \frac{7}{2}\ \frac{7}{2}\rangle$	$\|1\ 3\ \frac{5}{2}\ \frac{5}{2}\rangle$	-0.967	$\|2\ 1\ \frac{3}{2}\ \frac{1}{2}\rangle$	$\|2\ 2\ \frac{5}{2}\ \frac{1}{2}\rangle$	-0.034	1	1	1	0
	21.625	13.694	161	$\|0\ 3\ \frac{7}{2}\ \frac{3}{2}\rangle$	$\|1\ 2\ \frac{5}{2}\ \frac{1}{2}\rangle$	-0.975	$\|2\ 1\ \frac{3}{2}\ \frac{1}{2}\rangle$	$\|2\ 2\ \frac{5}{2}\ \frac{1}{2}\rangle$	-0.027	1	1	1	0
	31.292	13.837	165	$\|1\ 2\ \frac{5}{2}\ \frac{1}{2}\rangle$	$\|2\ 1\ \frac{3}{2}\ \frac{1}{2}\rangle$	-0.902	$\|2\ 1\ \frac{3}{2}\ \frac{1}{2}\rangle$	$\|2\ 2\ \frac{5}{2}\ \frac{1}{2}\rangle$	-0.031	1	1	0	0
	63.940	13.862	166	$\|1\ 2\ \frac{5}{2}\ \frac{3}{2}\rangle$	$\|2\ 1\ \frac{3}{2}\ \frac{1}{2}\rangle$	0.904	$\|21\ \frac{3}{2}\ \frac{1}{2}\rangle$	$\|2\ 2\ \frac{5}{2}\ \frac{1}{2}\rangle$	0.044	1	1	1	0
	25.613	10.612	38	$\|1\ 1\ \frac{1}{2}\ \frac{1}{2}\rangle$	$\|2\ 0\ \frac{1}{2}\ \frac{1}{2}\rangle$	0.672	$\|2\ 0\ \frac{1}{2}\ \frac{1}{2}\rangle$	$\|2\ 1\ \frac{3}{2}\ \frac{3}{2}\rangle$	0.452	1	1	0	1
	39.336	10.751	46	$\|1\ 1\frac{3}{2}\ \frac{3}{2}\rangle$	$\|2\ 0\ \frac{1}{2}\ \frac{1}{2}\rangle$	0.666	$\|2\ 0\ \frac{1}{2}\ \frac{1}{2}\rangle$	$\|2\ 1\ \frac{3}{2}\ \frac{3}{2}\rangle$	-0.350	1	1	1	1
^{148}Sm	37.224	10.906	52	$\|0\ 3\ \frac{5}{2}\ \frac{5}{2}\rangle$	$\|0\ 4\ \frac{7}{2}\ \frac{7}{2}\rangle$	0.645	$\|1\ 2\ \frac{5}{2}\ \frac{3}{2}\rangle$	$\|2\ 1\ \frac{3}{2}\ \frac{1}{2}\rangle$	-0.506	1	1	1	1
	20.295	11.196	58	$\|0\ 4\ \frac{7}{2}\ \frac{3}{2}\rangle$	$\|1\ 3\ \frac{7}{2}\ \frac{3}{2}\rangle$	0.199	$\|1\ 2\ \frac{5}{2}\ \frac{5}{2}\rangle$	$\|2\ 1\ \frac{3}{2}\ \frac{3}{2}\rangle$	0.751	1	1	0	1
	40.9576	12.480	102	$\|0\ 4\ \frac{7}{2}\ \frac{3}{2}\rangle$	$\|1\ 3\ \frac{5}{2}\ \frac{1}{2}\rangle$	0.827	$\|0\ 4\ \frac{9}{2}\ \frac{5}{2}\rangle$	$\|1\ 3\ \frac{7}{2}\ \frac{3}{2}\rangle$	-0.262	1	1	1	1
	94.929	12.931	122	$\|0\ 4\frac{9}{2}\ \frac{7}{2}\rangle$	$\|1\ 3\ \frac{7}{2}\ \frac{5}{2}\rangle$	-0.646	$\|0\ 4\ \frac{9}{2}\ \frac{1}{2}\rangle$	$\|1\ 3\ \frac{7}{2}\ \frac{3}{2}\rangle$	-0.292	1	1	1	1
	64.708	13.273	138	$\|1\ 2\frac{5}{2}\ \frac{3}{2}\rangle$	$\|2\ 1\ \frac{3}{2}\ \frac{1}{2}\rangle$	-0.744	$\|1\ 3\ \frac{7}{2}\ \frac{5}{2}\rangle$	$\|1\ 4\ \frac{9}{2}\ \frac{5}{2}\rangle$	-0.311	1	1	1	0
	33.743	13.347	140	$\|0\ 4\frac{9}{2}\ \frac{9}{2}\rangle$	$\|1\ 3\ \frac{7}{2}\ \frac{7}{2}\rangle$	-0.963	$\|0\ 4\ \frac{9}{2}\ \frac{1}{2}\rangle$	$\|1\ 3\ \frac{7}{2}\ \frac{1}{2}\rangle$	-0.069	1	1	1	0
	82.002	12.722	107	$\|0\ 3\ \frac{7}{2}\ \frac{5}{2}\rangle$	$\|1\ 2\ \frac{5}{2}\ \frac{3}{2}\rangle$	-0.418	$\|1\ 3\ \frac{7}{2}\ \frac{5}{2}\rangle$	$\|1\ 4\ \frac{9}{2}\ \frac{5}{2}\rangle$	0.503	1	1	1	0
	24.732	12.768	108	$\|0\ 4\ \frac{9}{2}\ \frac{1}{2}\rangle$	$\|1\ 3\ \frac{7}{2}\ \frac{1}{2}\rangle$	0.204	$\|1\ 3\ \frac{7}{2}\ \frac{5}{2}\rangle$	$\|1\ 4\ \frac{9}{2}\ \frac{5}{2}\rangle$	0.805	1	1	0	0
^{150}Sm	29.487	12.873	111	$\|0\ 3\ \frac{5}{2}\ \frac{1}{2}\rangle$	$\|1\ 2\ \frac{3}{2}\ \frac{1}{2}\rangle$	0.515	$\|1\ 3\ \frac{7}{2}\ \frac{1}{2}\rangle$	$\|2\ 2\ \frac{5}{2}\ \frac{1}{2}\rangle$	0.186	1	1	0	0
	33.039	13.406	129	$\|0\ 4\ \frac{7}{2}\ \frac{3}{2}\rangle$	$\|1\ 3\ \frac{5}{2}\ \frac{3}{2}\rangle$	0.267	$\|0\ 4\ \frac{9}{2}\ \frac{3}{2}\rangle$	$\|1\ 3\ \frac{7}{2}\ \frac{1}{2}\rangle$	-0.725	1	1	0	1
	21.877	13.450	130	$\|0\ 4\ \frac{7}{2}\ \frac{3}{2}\rangle$	$\|1\ 3\ \frac{5}{2}\ \frac{3}{2}\rangle$	-0.171	$\|0\ 4\ \frac{9}{2}\ \frac{3}{2}\rangle$	$\|1\ 3\ \frac{7}{2}\ \frac{3}{2}\rangle$	0.912	1	1	0	0
	23.096	14.270	155	$\|0\ 4\ \frac{9}{2}\ \frac{9}{2}\rangle$	$\|1\ 3\ \frac{7}{2}\ \frac{7}{2}\rangle$	0.947	$\|0\ 4\ \frac{9}{2}\ \frac{7}{2}\rangle$	$\|1\ 3\ \frac{7}{2}\ \frac{7}{2}\rangle$	0.256	1	1	1	0
	27.899	14.976	167	$\|0\ 3\ \frac{5}{2}\ \frac{1}{2}\rangle$	$\|1\ 2\ \frac{3}{2}\ \frac{3}{2}\rangle$	-0.227	$\|1\ 3\ \frac{5}{2}\ \frac{1}{2}\rangle$	$\|2\ 2\ \frac{3}{2}\ \frac{1}{2}\rangle$	0.913	1	1	1	0
	22.273	10.512	42	$\|1\ 1\ \frac{1}{2}\ \frac{1}{2}\rangle$	$\|2\ 0\ \frac{1}{2}\ \frac{1}{2}\rangle$	0.559	$\|2\ 0\ \frac{1}{2}\ \frac{1}{2}\rangle$	$\|2\ 1\ \frac{1}{2}\ \frac{1}{2}\rangle$	0.492	1	1	0	0
	29.284	12.386	102	$\|1\ 2\ \frac{1}{2}\ \frac{1}{2}\rangle$	$\|2\ 1\ \frac{3}{2}\ \frac{1}{2}\rangle$	0.594	$\|0\ 4\ \frac{9}{2}\ \frac{9}{2}\rangle$	$\|1\ 3\ \frac{7}{2}\ \frac{7}{2}\rangle$	-0.536	1	1	0	1
	32.998	12.744	113	$\|0\ 3\ \frac{5}{2}\ \frac{1}{2}\rangle$	$\|1\ 2\ \frac{3}{2}\ \frac{1}{2}\rangle$	0.401	$\|1\ 3\ \frac{5}{2}\ \frac{1}{2}\rangle$	$\|2\ 2\ \frac{5}{2}\ \frac{1}{2}\rangle$	0.679	1	1	0	0
	23.276	12.762	114	$\|0\ 3\ \frac{5}{2}\ \frac{1}{2}\rangle$	$\|1\ 2\ \frac{3}{2}\ \frac{1}{2}\rangle$	0.509	$\|1\ 3\ \frac{5}{2}\ \frac{1}{2}\rangle$	$\|2\ 2\ \frac{5}{2}\ \frac{1}{2}\rangle$	-0.717	1	1	0	0
^{152}Sm	30.272	13.013	121	$\|0\ 4\ \frac{9}{2}\ \frac{3}{2}\rangle$	$\|1\ 3\ \frac{7}{2}\ \frac{3}{2}\rangle$	0.932	$\|2\ 1\ \frac{3}{2}\ \frac{1}{2}\rangle$	$\|2\ 2\ \frac{5}{2}\ \frac{1}{2}\rangle$	-0.135	1	1	0	0
	37.263	13.354	129	$\|0\ 4\ \frac{7}{2}\ \frac{3}{2}\rangle$	$\|1\ 3\ \frac{5}{2}\ \frac{3}{2}\rangle$	0.299	$\|21\ \frac{3}{2}\ \frac{1}{2}\rangle$	$\|2\ 2\ \frac{5}{2}\ \frac{1}{2}\rangle$	0.845	1	1	0	0
	50.479	14.403	160	$\|0\ 4\ \frac{9}{2}\ \frac{9}{2}\rangle$	$\|1\ 3\ \frac{7}{2}\ \frac{7}{2}\rangle$	-0.262	$\|0\ 4\ \frac{9}{2}\ \frac{1}{2}\rangle$	$\|1\ 3\ \frac{7}{2}\ \frac{1}{2}\rangle$	0.858	1	1	1	0
	30.209	10.455	45	$\|1\ 1\ \frac{1}{2}\ \frac{1}{2}\rangle$	$\|20\ \frac{1}{2}\ \frac{1}{2}\rangle$	0.720	$\|2\ 0\ \frac{1}{2}\ \frac{1}{2}\rangle$	$\|2\ 1\ \frac{1}{2}\ \frac{1}{2}\rangle$	0.448	1	1	0	0
	21.300	11.252	66	$\|1\ 1\ \frac{1}{2}\ \frac{1}{2}\rangle$	$\|1\ 2\ \frac{3}{2}\ \frac{3}{2}\rangle$	-0.641	$\|1\ 2\ \frac{5}{2}\ \frac{5}{2}\rangle$	$\|1\ 3\ \frac{5}{2}\ \frac{5}{2}\rangle$	0.255	1	1	1	0
	47.1158	12.602	112	$\|0\ 4\ \frac{9}{2}\ \frac{1}{2}\rangle$	$\|1\ 3\ \frac{7}{2}\ \frac{1}{2}\rangle$	0.279	$\|0\ 4\ \frac{7}{2}\ \frac{3}{2}\rangle$	$\|1\ 3\ \frac{5}{2}\ \frac{3}{2}\rangle$	0.640	1	1	0	0
	85.650	12.715	115	$\|0\ 4\ \frac{9}{2}\ \frac{1}{2}\rangle$	$\|1\ 3\ \frac{7}{2}\ \frac{1}{2}\rangle$	-0.347	$\|0\ 4\ \frac{7}{2}\ \frac{3}{2}\rangle$	$\|1\ 3\ \frac{5}{2}\ \frac{3}{2}\rangle$	0.616	1	1	0	0
^{154}Sm	60.647	13.021	122	$\|0\ 3\ \frac{5}{2}\ \frac{1}{2}\rangle$	$\|1\ 2\ \frac{3}{2}\ \frac{1}{2}\rangle$	0.441	$\|0\ 4\ \frac{9}{2}\ \frac{5}{2}\rangle$	$\|1\ 3\ \frac{7}{2}\ \frac{3}{2}\rangle$	-0.664	1	1	0	1
	33.213	13.452	129	$\|0\ 3\ \frac{5}{2}\ \frac{1}{2}\rangle$	$\|1\ 2\ \frac{5}{2}\ \frac{1}{2}\rangle$	0.591	$\|1\ 3\ \frac{5}{2}\ \frac{1}{2}\rangle$	$\|2\ 2\ \frac{3}{2}\ \frac{1}{2}\rangle$	-0.579	1	1	0	0
	20.651	13.467	130	$\|0\ 3\ \frac{5}{2}\ \frac{1}{2}\rangle$	$\|1\ 2\ \frac{5}{2}\ \frac{1}{2}\rangle$	0.804	$\|1\ 3\ \frac{5}{2}\ \frac{1}{2}\rangle$	$\|2\ 2\ \frac{3}{2}\ \frac{1}{2}\rangle$	0.419	1	1	0	0
	22.059	13.678	135	$\|0\ 4\ \frac{9}{2}\ \frac{1}{2}\rangle$	$\|1\ 3\ \frac{7}{2}\ \frac{3}{2}\rangle$	-0.178	$\|0\ 4\ \frac{9}{2}\ \frac{5}{2}\rangle$	$\|1\ 3\ \frac{7}{2}\ \frac{5}{2}\rangle$	0.883	1	1	1	0
	25.702	14.249	152	$\|1\ 2\ \frac{3}{2}\ \frac{3}{2}\rangle$	$\|1\ 3\ \frac{5}{2}\ \frac{3}{2}\rangle$	-0.387	$\|0\ 4\ \frac{9}{2}\ \frac{3}{2}\rangle$	$\|1\ 3\ \frac{7}{2}\ \frac{3}{2}\rangle$	-0.693	1	1	0	0
	23.619	14.793	167	$\|0\ 4\ \frac{9}{2}\ \frac{9}{2}\rangle$	$\|1\ 3\ \frac{7}{2}\ \frac{7}{2}\rangle$	0.905	$\|1\ 3\ \frac{7}{2}\ \frac{5}{2}\rangle$	$\|2\ 2\ \frac{5}{2}\ \frac{3}{2}\rangle$	0.184	1	1	1	1

TABLE IV: The peaks larger than $20e^2fm^2$ and contributing to the GR, are mentioned together with the corresponding energy of the i-th phonon state. The proton (π) and neutron (ν) maximal amplitudes are also given. The states involved in the dominant single particle transitions $b \to a$ and $d \to c$ are listed. These are characterized by the variation of the major oscillator quantum number ΔN. Also the angular momentum variations ΔI for the states involved in the single particle transitions are listed for protons (π) and neutrons (ν), respectively.The dipole strength corresponds to the effective charges (4.4).

Nucleus	k	$B(E1;0^+\rightarrow 1^-_k)[e^2fm^2]$	energy	type	k	$B(E1;0^+\rightarrow 1^-_k)[e^2fm^2]$	energy[MeV]	type	gap[MeV]
^{144}Sm	147	117.26	13.250	IS	166	63.94	13.862	IS	0.612
^{148}Sm	122	94.92	12.931	IS	138	64.71	13.273	IS	0.342
^{150}Sm	107	82.00	12.722	IV	167	27.89	14.976	IV	2.254
^{152}Sm	113	33.00	12.744	IS	160	50.48	14.403	IV	1.659
^{154}Sm	115	85.65	12.715	IV	152	25.70	14.249	IS	1.534

TABLE V: The largest two B(E1) values selected from Table IV, for the energy interval 10-20 MeV. Also, the label k for the state populated by the mentioned transition is given. The type of the transition $0^+\rightarrow 1^-_k$ and the gap between the two largest peaks are also given.

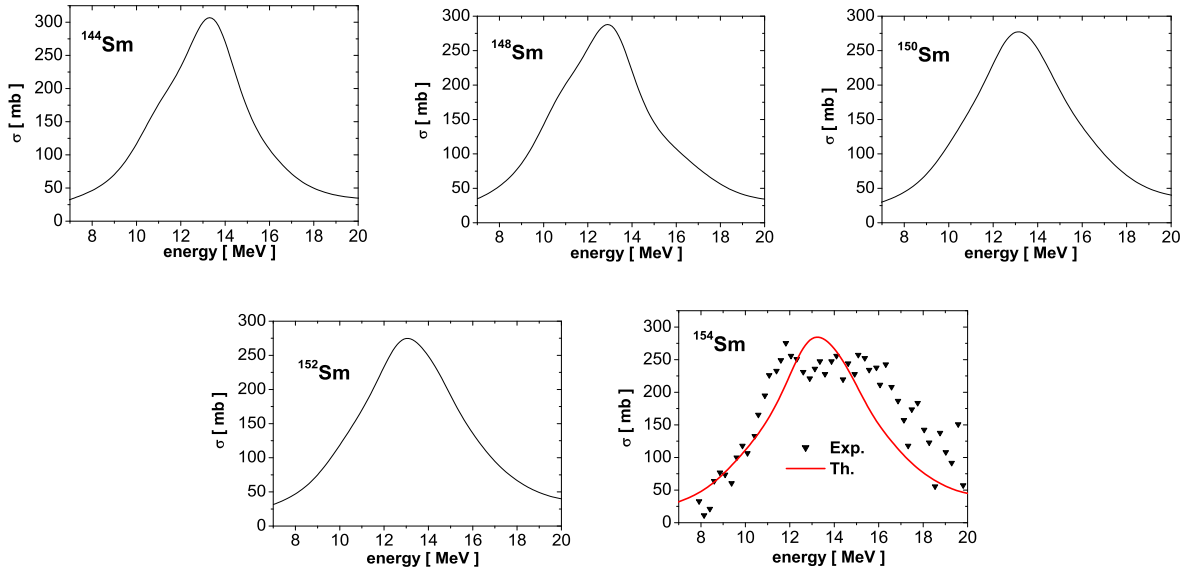

FIG. 5: Color online. The photoabsorption cross section as function of energy for ^{144,148,150,152,154}Sm. The calculated strengths were folded by Lorentzianes with the width of 3 MeV. The experimental data shown for ^{154}Sm were taken from Ref.[57].

VII. SUMMARY AND CONCLUSIONS

In the previous sections we developed a formalism for the microscopic description of the Pygmy dipole resonance. The main ingredients, specific to the present approach, are the projected spherical single particle basis, which allows for an unified description of spherical, transitional and deformed nuclei, and the use of the Schiff dipole moment for the two body dipole-dipole interaction. The model Hamiltonian consists in the spherical shell model single particle

	$\sum_{PDR}(BE1)[e^2b]$	$\sum_{total}(BE1)[e^2b]$	σ_0[MeVb]		σ_{-1}[mb]		$\sigma_{-2}[MeV^{-1}b]$	
			Th.	Exp.	Th.	Exp.	Th.	Exp.
^{144}Sm	0.036	7.879	2.078	2.00±0.14$^{a)}$	157.57	131±15$^{a)}$	12.19	8.7±0.8$^{a)}$
^{148}Sm	0.185	7.672	1.996	1.94±0.10$^{a)}$	153.44	134±10$^{a)}$	12.00	9.5±0.7$^{a)}$
^{150}Sm	0.237	7.620	1.998	2.00±0.14$^{a)}$	152.40	141±15$^{a)}$	11.82	10.3±0.9$^{a)}$
^{152}Sm	0.336	7.764	1.959	2.05±0.10$^{a)}$	152.27	144±10$^{a)}$	12.51	10.6±0.7$^{a)}$
^{154}Sm	0.437	7.440	1.914	1.94±0.06$^{b)}$	148.80	145±10$^{a)}$	11.69	10.8±0.7$^{a)}$
				2.07±0.10$^{a)}$				

TABLE VI: The sum of the B(E1) values for the PDR energy interval 0-10 MeV and the GDR energy interval 0-20 MeV respectively, are given. The zero (σ_0), the first (σ_{-1}) and the second (σ_{-2}) moments of the integrated cross sections are also listed. The experimental data are taken from $^{a)}$[55] and $^{b)}$[57]

Nucleus	S_l(EWSR) [MeV.e^{2}b]	S_{corr} [MeV.e^{2}b]	r.d. [%]	S_{TRK} [MeV.e^{2}b]	q	PSR [%]
^{144}Sm	149.82	159.59	0.50	197.47	1.318	0.8
^{148}Sm	153.81	156,65	1.80	201.50	1.310	1.6
^{150}Sm	160.26	160.00	0.16	203.44	1.269	1.6
^{152}Sm	159.09	159.98	0.56	205.33	1.291	2.2
^{154}Sm	163.62	162.85	0.47	207.16	1.266	2.7

TABLE VII: The two members of the sum rule equation, S_l and S_{corr}, the relative deviation (r.d.=$|S_{corr} - S_l|/S_l$), the TRK sum rule S_{TRK}, the ratio q(=S_{TRK}/S_l) and the contribution of the PDR transitions to the total sum rule, PSR, are listed for the five isotopes of Sm.

term, the pairing interaction for alike nucleons and the dipole-dipole interaction. This is subject successively to the BCS and QRPA treatment. The results of the QRPA approach are used to calculate the B(E1) values characterizing the dipole transitions from the ground state, 0^+, to the dipole states 1^-_k, with k labeling the roots of the QRPA equations. Enveloping these discrete values by Lorentzianes of a width equal to 1 MeV, one obtains a continuous distribution of the dipole strength with energy, shown in Figs 4. One distinguishes two energy domains: one with energy smaller than 10 MeV, which includes the neutron separation energy and one defined by the interval 10-20 MeV which comprises the giant dipole resonance. The first region is occupied by the PDR, while the second by the GDR. We studied the microscopic support of the principal peaks from the two regions, respectively. Thus, we have seen that the dominant transition of the PDR-kind are to two quasiparticle states of proton nature associated with phonon states describing oscillations of the neutron excess in anti-phase with the proton oscillations. There are transitions where the oscillations of the two subsystems are in phase, suggesting an isoscalar nature. All transitions are characterized by $\Delta N = 1$. The PDR transitions bring only a few percents (0.8-2.7) contribution to the total EWSR. Concerning the GDR, all transitions are also of $\Delta N = 1$ type, having an isovector or an isoscalar character. The GDR transitions yield a change of the total angular momentum by $(\Delta I_\pi, \Delta I_\nu)$ equal to (1,1), (0.0), (0,1), (1,0), respectively. It seems that the first two cases are associated with the two peaks seen in the deformed isotopes. The last two transition types are caused by the rotation symmetry restoration which results in diminishing the depth of the minimum placed between the two peaks. According to [55] the first peak is populated in a (γ, n) while the second one in a $(\gamma, 2n)$ reactions. The states composing the two resonances are characterized by their isovector or isoscalar nature and, of course, by their energies. In fact this is the reason they may be populated by different nuclear reactions.

The nuclear deformation induces a split of the dipole strength, which is diminished by the r-cubic term. Indeed, the r-cubic term from the Schiff momentum suppresses the transition matrix elements, which results in needing an increasing factor q for the effective charges (4.4) in order to obey the TRK sum rule. This small violation of the TRK sum rule is caused by that the sum rule uses the standard dipole momentum, while for the dipole transition matrix elements, the Schiff momentum is employed. Indeed, using the Schiff momentum also for the TRK sum rule, this is corrected to S_{cor} which agrees well with S_l, as seen from Table VII.

Results for photoabsorptin cross section in ^{154}Sm are compared with experimental data in Fig. 5 and one concluded that the agremment is resonable good. As for integrated cross section momenta $\sigma_0, \sigma_{-1}, \sigma_2$, the results of the present work and the experimental data from [55] are given in Table VI, where a good agrement is evidenced.

The r-cubic term of the Schiff dipole moment diminishes the matrix elements of the standard dipole moment and therefore supresses the contamination of energies and wave functions due to the non-conservation of the center of mass momentum. These spurious components have the relative magnitude of the order of 1/A [40], with A denoting the atomic mass number, and by this they have a small contribution for heavy nuclei. However, this symmetry was fully restored in Ref. [21]. Another symmetry which is brocken for deformed isotopes of Sm, is that caused by the rotation transformations. This is restored in this paper by using a projected spherical single particle basis. The effect consists of that the cross section cannot be separated into two branches one determined by the K=0 component while the other one by the K=0 wave function. Indeed, within a restored rotation symmetry picture, there are notable contriution due to the single particle transitions characterized by $(\Delta I_\pi, \Delta I_\nu)$ equal to either (0,1) or (1,0), which results in flattening the minimum separating the two mentioned branches. The largest two strengths are listed in Table V, where it is shown that there is a gap between the two peaks, which is larger for the more deformed isotopes.

Concluding, we may say that the present formalism describes in an unified fashion the main features of the Pygmy and Giant resonance of the spherical, transitional and deformed isotopes of Sm. Comparison with the available experimental data suggests a good agreement.

Acknowledgments

This work was supported by UEFISCU through the project PCE- 16/2021.

VIII. APPENDIX A

In what follows we shall write the dispersion equation for the QRPA energies as well as for the phonon forward and backward amplitudes. For this purpose it is useful to introduce the notations:

$$\begin{aligned}
\mathcal{X}_p &= X_1 \sum_{\substack{a,b \\ E_{p,a}<E_{p,b}}} \frac{E_{p,ab} d_1(p,ab)^2 \xi^{(-)}(p,ab)^2}{E_{p,ab}^2-\omega^2}, \qquad (A.1)\\
\mathcal{Y}_p &= X_1 \sum_{\substack{a,b \\ E_{n,a}<E_{n,b}}} \frac{E_{n,ab} d_1(n,ab)^2 \xi^{(-)}(n,ab)^2}{E_{n,ab}^2-\omega^2},\\
\mathcal{C}_p &= X_1 \sum_{\substack{a,b \\ E_{p,a}<E_{p,b}}} \frac{E_{p,ab} d_1(p,ab)^2 \xi^{(-)}(p,ab)^2}{(E_{p,ab}^2-\omega^2)^2},\\
\mathcal{C}_n &= X_1 \sum_{\substack{a,b \\ E_{n,a}<E_{n,b}}} \frac{E_{n,ab} d_1(n,ab)^2 \xi^{(-)}(n,ab)^2}{(E_{n,ab}^2-\omega^2)^2},\\
\mathcal{D} &= \frac{\sqrt{2}}{\sqrt{\omega}} \left[\mathcal{C}_p \mathcal{X}_p^{-2} + \frac{\mathcal{C}_n {\mathcal{X}_n}^{-2}}{4X_{np}} \left(\mathcal{X}_p^{-1} - X_{pp} \right)^2 \right]^{-1/2}.
\end{aligned}$$

The dispersion equations is:

$$1 - X_{pp}\mathcal{X}_p - X_{nn}\mathcal{X}_n - 3X_{pn}X_{np}\mathcal{X}_p\mathcal{X}_n = 0. \qquad (A.2)$$

The phonon amplitudes are:

$$\begin{aligned}
X(p,ab) &= \frac{1}{2}\frac{d_1(p,ab)\xi(p,ab)}{E_{p,ab}-\omega}\mathcal{X}_p^{-1}\mathcal{D},\\
Y(p,ab) &= -\frac{1}{2}\frac{d_1(p,ab)\xi(p,ab)}{E_{p,ab}+\omega}\mathcal{X}_p^{-1}\mathcal{D}, \qquad (A.3)\\
X(n,ab) &= \frac{1}{4}\frac{d_1(n,ab)\xi(n,ab)}{E_{n,ab}-\omega}\frac{{\mathcal{X}_n}^{-1}}{X_{np}}\left(\mathcal{X}_p^{-1}-X_{pp}\right)\frac{1}{2}\mathcal{D},\\
Y(n,ab) &= -\frac{1}{4}\frac{d_1(n,ab)\xi(n,ab)}{E_{n,ab}+\omega}\frac{{\mathcal{X}_n}^{-1}}{X_{np}}\left(\mathcal{X}_p^{-1}-X_{pp}\right)\frac{1}{2}\mathcal{D}.
\end{aligned}$$

The QRPA energies can be obtained by solving either Eq. (3.9) [46] or the dispersion equation (A.2). One can check that the above amplitudes satisfy the normalization equation.

$$\sum_{\substack{\tau,ab \\ E_{\tau,a}<E_{\tau,b}}} \left[X(\tau,ab)^2 - Y(\tau,ab)^2 \right] = 1. \qquad (A.4)$$

[1] M. Goldhaber and E. Teller, Physical Review 74,9, (1948) 1046.
[2] D. M. Brink, Talk presented at the workshop on " Chaos and Collectivity in Many Body Systems at the PMIPKS, Drezden, Germany, March 5-8, 2008.
[3] N. Lo Iudice and F. Palumbo,Phys. Rev. Lett. 41, (1978) 1532.
[4] A. Faessler, Nucl. Phys. **85** (1966) 653 .
[5] V. Marhun-Rewani, W. Greiner and J. A. Marhun, Phys. Lett.**57 B** (1975) 109.

[6] E. G. Lanza, L, Pellegri, A. Vitturi, M.V. Andres,, Prog. Part. Nucl. Phys, **129** (2023) 104006.
[7] A. Bracco. J. Phys.:Conf. Series **312**, (2011) 92005 .
[8] A. Bracco, E.G. Lanza and A. Tamii, Prog. Part. Nucl. Phys.**106** (2019) 360.
[9] O. Bohigas, A. M. Lane, J. Martotell, Phys. Rep. **51** (1979) 267.
[10] P. G. Reinhard and W. Nazarewicz, Phys. Rev. C **81**(2010) 051303.
[11] M. Arnold and S. Goriely, Phys. Reports **384**, (2003) 1.
[12] T. Aumann, Eur. Phys. J. **A 26** (2005) 441.
[13] S. Fukuda *et al.*, Phys. Rev. Lett.**86**(2001) 5651.
[14] A. Krugmann *et. al.*, EPJ Web of Conferences **66**, (2014) 02060.
[15] D. H. Youngblood, Y.-W. Lui, H. L. Clark, B. Hohn, Y. Tokimoto and X. Chen, Phys. Rev. **C 69** (2004) 034315.
[16] Nguen Van Giai and H. Sagawa, Nucl. Phys. **A 371** (1981) 1 .
[17] N. N. Arsenyev, A. P. Severyukhin, V. V. Voronov and N. Van Giai, EPJ Web of Conf.**194** (2018) 04002.
[18] K. Yoshida and T. Nakatsukasu, Phys. Rev. **C 83** (2011) 021304(R).
[19] N. Auerbach, Ch. Stoyanov, M. R. Anders aand S. Shlomo, Phys. Rev. **C 89** (2014) 014335.
[20] H. Quliev, Z. Zenginerler,E. Guliev, A. A. Kuliev, AIP Conference Proceedings **1815** (2017) 060020 .
[21] E. Guliyev, H. Quliyev and A. A. Kuliev, J. Phys. G; Nucl. Part. Phys. **47** (2020) 115107.
[22] J. Enders, *et. al.* , preprint, 12 May 2004.
[23] D. Vretenar et. al., Nucl. Phys. **A 692** (2001) 496.
[24] V. Baran, B. Frecus, M. Colonna and M. Di Toro, Phys. Rev. **C85** (2012) 051601(R).
[25] V. Baran, M. Colonna, M. Di Toro, A. Croitoru, D. Dumitru, Phys. Rev. **C 88** (2013) 044610.
[26] J. Kvasil *et al.*, Phys. Scr. 154 (2013) 014019.
[27] V. O Nesterenko *et al..*, Phys. Rev. Lett. 120 (2018) 182501.
[28] A. Repko *et al.*, Eur. Phys. J. **A 53** (2017) 221.
[29] H. Qulyev *et al.*, Nucl. Phys. **A 1014** (2021) 122239.
[30] A. A. Raduta, D. S. Delion and N. Lo Iudice, Nucl. Phys. **A 564** (1993) 185.
[31] A. A. Raduta, N. Lo Iudice and I. I. Ursu, Nucl. Phys. **A584** (1995) 84.
[32] A. A. Raduta, A. Escuderos and E. Moya de Guerra, Phys. Rev. **C 65** (2002) 024312.
[33] A. A. Raduta, A. Escuderos, A. Faessler, E. Moya de Guerra and P. Sarriguren, Phys. Rev. **C69** (2004) 064321.
[34] A. A. Raduta, A. Faessler and D. S. Delion, Nucl. Phys. **A 564** (1993) 185; Phys. Lett.**B 312** (1993) 13.
[35] A. A. Raduta, D. S. Delion and A. Faessler, Nucl. Phys. **A 617** (1997) 176.
[36] A. A. Raduta, C. M. Raduta and A. Escuderos, Phys. Rev. **C 71** (2005) 164.
[37] S. G. Nilsson, Mat. Fys. Medd. K. Dan. Vid. Selsk. **29** no. 16 (1955) 1.
[38] M. E. Rose, *Elementary Theory of Angular Momentum* (Wiley, New York, 1957).
[39] L. I. Schiff, Phys. Rev. 132 (1963) 2194.
[40] E. Baranger, Ch. Wan Lee, Nucl. Phys. **22** (1961) 17.
[41] H. J. Lipkin, Phys. Rev. 110 (1958) 1395.
[42] A. A. Raduta, R. Budaca abd Al. H. Raduta, Phys. Rev. **A 79** (2009) 023202.
[43] P. Ring and P. Schuck, *The nuclear many-body problem, Springer*, Berlin, Heidelberg, New York,p. 76.
[44] C. M. Raduta, A. A. Raduta and I. I. Ursu, Phys. Rev. **C 84** (2011) 064322.
[45] N. Lo Iudice, A. A. Raduta and D. S. Delion, Phys. Rev. C50 (1994) 127.
[46] T.Ullah, D. Rowe, Nucl. Phys. **A 163** (1971) 257.
[47] W. Thomas, Naturwissenshaften **13** (1925) 627
[48] F. Reiche and W. Thomas, Z. Phys. 34 (1925) 510 .
[49] W. Kuhn, Z. Phys. **33** (1925) 408 .
[50] G. A. Lalazissis, S.Roman and P. Ring, Atomic Data and Nuclear Data Tables **71** (1999) 1.
[51] L.M. Donalson *et. al.*, Phys. Lett. **B 276** (20180 133.
[52] V. Rezwani *et. al.* , Proc. Int. Conf. on nuclear structure studies, Sendai (Jap.), Sept. !972.
[53] M. Danos and W. Greiner, Phys. Rev. **138 B** (1965) 133.
[54] P. Ring and P. Schuck, *The nuclear many-body problem*, Springer, Berlin, Heidelberg, New York,p. 294.
[55] P. Carlos *et. al.*, Nucl. Phys **A 225** (1974) 171.
[56] Kenichi Yoshida and Takashi Nakatsukasa, Phys. Rev. **88** (2013) 034309.
[57] G. M. Gurevich *et al.*,Nucl. Phys. **A 351** (1981) 257.